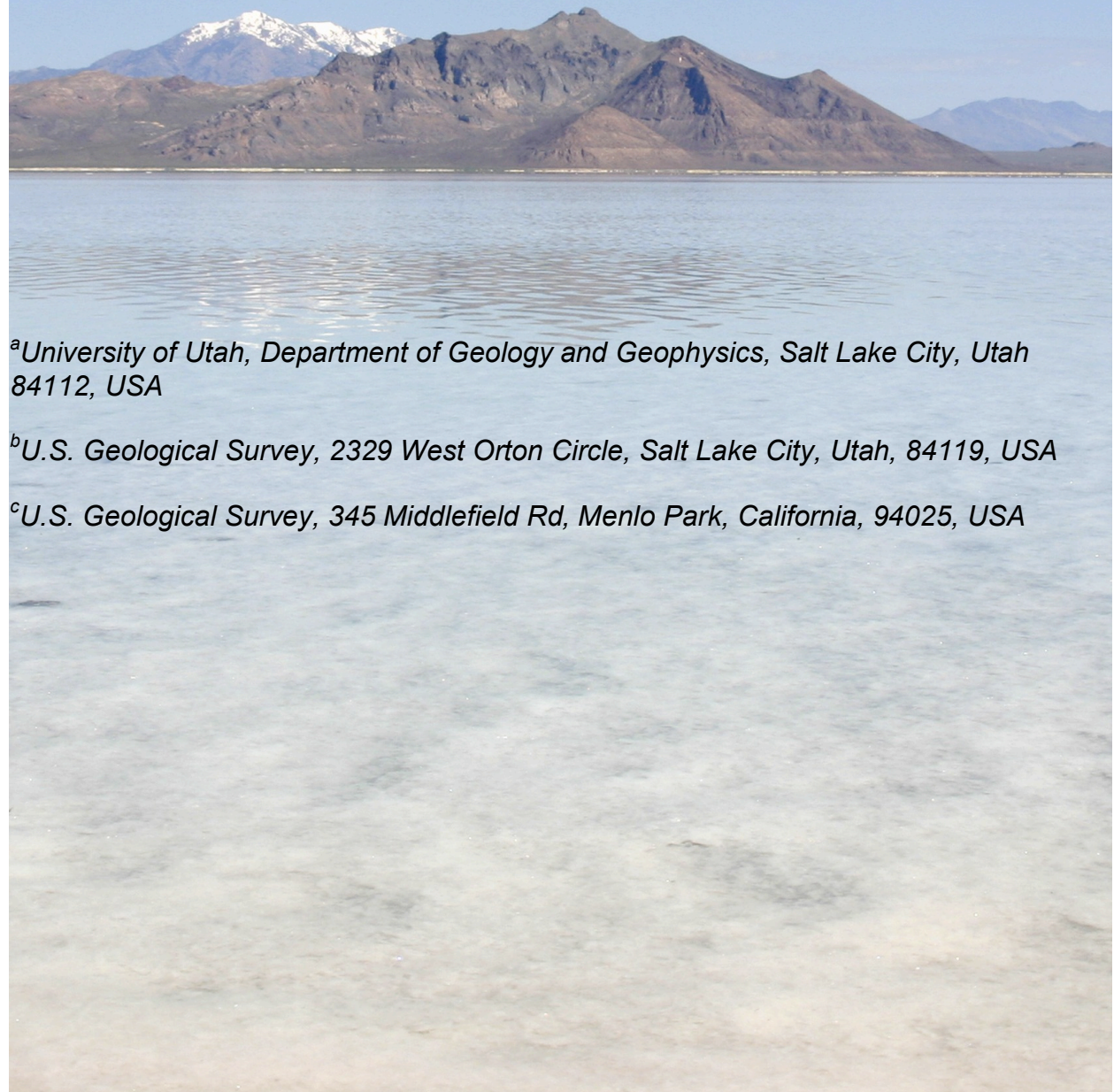


Estimation of selenium removal fluxes from the south arm of the Great Salt Lake, Utah: Final Report 04-07-08

By William P. Johnson^a, David L. Naftz^b, Ximena Diaz^a, Kimberly Beisner^a, Wade Oliver^a, Christopher Fuller^c



^a*University of Utah, Department of Geology and Geophysics, Salt Lake City, Utah 84112, USA*

^b*U.S. Geological Survey, 2329 West Orton Circle, Salt Lake City, Utah, 84119, USA*

^c*U.S. Geological Survey, 345 Middlefield Rd, Menlo Park, California, 94025, USA*

Executive Summary

Measurements were made during the period March 2006 through September 2007 to examine the existing distribution of selenium in the water and sediment of the south arm of the Great Salt Lake, and to measure Se fluxes between water, sediment, and the atmosphere at the Great Salt Lake. Results of these measurements are summarized in six sections below.

Great Salt Lake Characteristics

The average selenium (Se) concentration from May 2006 to July 2007 for unfiltered acidified (RA) samples was $0.64 \pm 0.28 \mu\text{g/L}$, whereas the filtered acidified (FA) samples showed an average Se concentration of $0.49 \pm 0.25 \mu\text{g/L}$ for the same period. Differences between total and dissolved Se concentrations showed that a significant but minor fraction of Se was carried in particulate phases, more so in the deep brine layer relative to the shallow brine layer, but in either layer, the Se mass was dominantly dissolved rather than particulate. In terms of temporal variation, increases in the measured total (RA) and dissolved (FA) Se concentrations were observed in both the deep and shallow brine layers during the period of the investigation (Figure 7), constituting a net increase ranging between 0.16 and 0.34 $\mu\text{g/L}$ over the period of the investigation (Naftz et al., 2007).

Volatilization

The average concentration of volatile Se in the water column was 3.0 ng/L, but this measured concentration varied over two orders of magnitude spatially and temporally. The measured volatile Se concentrations increased with depth for paired measurements in the shallow brine layer. Comparison of measured to estimated volatile Se flux showed reasonable agreement, indicating that Se flux to the atmosphere could be integrated from measured volatile Se concentrations, wind speeds, and water temperatures. The resulting estimated annual volatile Se flux to the atmosphere from the Great Salt Lake is 2108 Kg/yr. This estimate is considered accurate to within a factor of 1.5 (within a 68% confidence interval), yielding a potential range between 1380 to 3210 Kg/yr. The large range in estimated flux results from the spatial and temporal variability of volatile Se concentrations. Despite the variability, the results demonstrate that Se volatilization is the major mechanism of Se removal from the Great Salt Lake.

Downward Sedimentation

Downward sedimentation fluxes were highest where influenced by the Bear River inflow, and were lowest in the shallow brine layer at sites located near the northwest-southeast axis of the south arm. Notably, sediment accumulation rates in the deep brine layer were much greater than corresponding shallow layer sediment accumulation rates, suggesting that re-suspension accounted for most of the sediment accumulation at depth. The influence of re-suspension on sediment accumulation in the Great Salt Lake was also indicated by ^7Be analyses in sediment cores.

Permanent (Net) Sedimentation

The permanent Se removal flux via sedimentation was estimated at 520 Kg/yr, based on ^{210}Pb profiles from ten sediment cores in the south arm. This estimated

sedimentation flux is considered accurate within a range of uncertainty between 45 and 990 Kg/yr.

Re-suspension – Re-solubilization

Temperature readings from six depths at two sites in the south arm demonstrate periodic equilibration events consistent with temporary displacement of the deep brine layer via seiche transmission in the lake. This observation suggests that anoxic sediments are periodically and ephemerally placed into contact with oxic shallow brine layer, potentially leading to re-solubilization of Se from the anoxic sediment. Short term (24 hour) batch studies indicate that Se re-solubilization during these ephemeral events yields negligible change in Se concentration in the water column. Longer term contact between oxic shallow brine and anoxic sediment may occur via shrinkage of the deep brine layer. Longer term (week to month) batch studies indicate that a significant mass (e.g. 25 Kg) may be contributed by these longer term events.

Mass Balance

The combined sedimentation and volatilization fluxes total to about 2650 Kg/yr (based on the geometric means). Comparison of volatilization to sedimentation flux demonstrates that sedimentation is NOT the major mechanism of removal of Se from the Great Salt Lake. Rather, volatilization is demonstrated to be the major mechanism of Se removal from the Great Salt Lake. These measured loss fluxes balance (more than) the measured annual load (1,500 Kg/yr) during the study period. The observed increase in total Se concentration during the period of the study indicates that most Se loads to the lake are not yet measured, and that continued monitoring of Se concentrations is needed. However, it should be noted that the inefficiency of in-lake mixing processes complicates comparison of measured Se concentrations to measured Se loads and removal fluxes.

Table of Contents

Executive Summary	2
1. Introduction	5
2. Methods	6
2.1 Water column.....	6
2.2 Sediments.....	7
2.2.1 Sediment traps.....	7
2.2.2 Cores.....	8
2.2.3 Bed sediment samples.....	10
2.2.4 Freeze-drying, extraction, and chemical analyses	11
2.3 Analysis	11
2.3.1 Major and minor elements.....	11
2.3.2 Total Se analysis.....	12
2.3.3 Water.....	12
2.3.4 Sediments	13
2.3.5 Volatile Se analysis	13
2.3.6 Wind velocity, atmospheric temperature, lake elevation, lake surface area	16
2.3.7 Total dissolved gas pressure, hydrostatic pressure, barometric pressure... ..	19
2.3.8 Thermistor analysis	19
2.3.9 TOC analysis.....	21
2.3.10 Isotope analysis	21
2.3.11 Sediments	21
3. Results	23
3.1 Great Salt Lake characteristics.....	23
3.1.1 Water.....	23
3.1.2 TOC	24
3.1.3 Bed sediment	24
3.2 Volatile selenium flux.....	25
3.2.1 Volatile Se concentrations.....	25
3.2.2 Volatilization flux estimates	25
3.2.3 Direct measurement of volatilization flux.....	26
3.2.4 Integration of the volatile Se flux	28
3.3 Sedimentation fluxes	31
3.3.1 Downward sedimentation flux	31
3.4 Permanent sedimentation or net sedimentation	33
3.4.1 Mass accumulation rates.....	33
3.4.2 Downward sedimentation vs. net sedimentation	34
3.4.3 Estimation of Se removal by sedimentation	34
3.4.4 Sediment trace element analysis	39
3.5 Re-suspension – Re-solubilization.....	40
3.5.1 Temperature stratification.....	40
3.5.2 Seiche	41
3.5.3 Mechanism of temperature equilibration events.....	41
3.5.4 Batch equilibration tests	42
3.6 Mass balance.....	45
3.7 Variability	48
4. References.....	50

1. Introduction

Characterization of the existing distribution of selenium (Se) in the water and sediment of the south arm of the Great Salt Lake, and measurement of Se fluxes between water, sediment, and the atmosphere at the Great Salt Lake are motivated by the goal of setting a Se standard for the open waters of the Great Salt Lake.

The open waters of the Great Salt Lake are protected for their current beneficial uses (Class 5) through the application of the narrative criteria clause. Existing EPA-promulgated numeric standards for inland lakes cannot be applied to the Great Salt Lake due to its highly individual nature, i.e. large, terminal, hypersaline, and meromictic (i.e. multiple, stable layers).

The development of an open water standard for Se requires a working knowledge of the biological significance of existing Se concentrations in the Great Salt Lake, as well as a working understanding of the likely changes in these concentrations over time given existing and proposed loads to the system. This “working knowledge” has been previously represented in a conceptual model (Johnson et al., 2006) that accounts for Se in various “stocks” in the system (e.g. water, sediment, biota) and the “flow” of Se between stocks (e.g., precipitation and settling, volatilization, and bioconcentration).

The conceptual model serves as the basis for five investigations conducted during the period April 2006 to October 2007. These investigations involved: 1) Characterization of Se concentrations and effects in avian species associated with the south arm of the Great Salt Lake; 2) Characterization of Se concentrations and effects in brine shrimp, seston, and benthic organisms in the south arm of the Great Salt Lake; 3) Characterization of Se uptake kinetics in brine shrimp; 4) Determination of annual Se loads to the south arm of the Great Salt Lake; 5) Characterization of the distribution of Se in water and sediment and determination of selenium removal fluxes via sedimentation and volatilization in the south arm of the Great Salt Lake. This report describes findings of the 5th investigation.

2. Methods

2.1 Water column

Aqueous chemical conditions were characterized in the field at 19 locations across the main body of the Great Salt Lake (Figure 1). Four of these stations (2267, 2565, 2767 and 3510) were characterized at 7 to 13 depths (varying by station), ranging from 0.2 to 8 m depth below lake surface. The remaining stations were characterized at three depths (3, 6 & 8 m). Aqueous characteristics included temperature, conductivity, pH, oxidation-reduction potential (ORP), and dissolved oxygen (DO), as measured using a Hydrolab Troll 9000 (In-Situ Inc., Fort Collins, CO).

Samples for major and trace element analysis were collected in acid-rinsed polyethylene bottles from four stations (2267, 2565, 2767 and 3510). At two stations (2267 & 2767), samples were collected from two depths representing the shallow brine layer (0.2 m (both sites) and 4 m (2267) or 2.5 m (2767)). At the remaining two stations (2565 & 3510), samples were collected from three depths representing the shallow and deep brine layers and the interface between them (0.2, 8, and 6.5 m, respectively). Replicate samples (4 x 250 mL) were collected from each location using a peristaltic pump with acid-rinsed C-flex tubing (Cole-Parmer's Masterflex, Vernon Hills, IL). Two of the replicates were filtered (0.45 μm pore size, capsule-type filter). All four replicates were stored on ice, acidified (trace metals grade nitric acid, 2 mL, 7.7 N), and transferred to a refrigerator. One each of the filtered-acidified and raw-acidified samples were sent to a contract lab (Frontier Geoscience, Seattle, WA) for total Se analysis as described below. The other replicates were stored at 4°C for major and trace elements analyses (Al, As, Ba, Ca, Cd, Co, Cr, Cu, Fe, K, Li, Mg, Mn, Mo, Na, Ni, Pb, S, Sb, Sc, Sr, Ti, Tl, U, V, Zn) via inductively coupled plasma mass spectrometry (ICP-MS) as described below.

At the 19 locations in Figure 1, analyses were performed for volatile Se concentrations and total dissolved gas pressure, at multiple depths (representing deep and shallow brine layers). Semi-monthly samples were taken at those locations and multiple depths in the south arm of the Great Salt Lake to explore temporal variations in volatile Se concentrations. Collection of volatile Se using the purge and cryo-focusing trap process was performed in-situ at the respective sampling sites on the lake in order to avoid any degradation of the water sample (as described in the Analyses section).

Direct measurements of volatilization of Se were taken at two primary (3510 and 2267) and one secondary (2565) location in the south arm of the Great Salt Lake. The flux measurements were taken concurrently with characterizations of the parameters used in estimating volatile Se flux: surface water temperature, wind velocity, and volatile Se concentration, in order to assess the accuracy of the predictive model.

At an additional twelve locations in the deep brine layer (Figure 1), samples were taken for total organic carbon (TOC) analysis (GS1, GS3, GS4, GS5, GS8, GS9, GS11, GS12, GS14, GS15, GS18, GS20).

At sites 2565 and 3510 (Figure 1), temperature was measured at 6 depths spanning the interface between the deep and shallow brine layers. Temperature was measured using thermistors (StowAway®, TidbiT™, model #89419) attached to the sediment trap cables. For site 2565, thermistor distances above the anchor were 1.75, 2.10, 2.45, 2.81, 3.15 and 3.51 meters. In August 2006, the chain at the base of the site 2565 trap was shortened by one meter to decrease the distance of each thermistor above the base by 1 meter. For site 3510, thermistor distances above the anchor were 1.86, 2.21, 2.61, 3.02, 3.38 and 3.73 meters. At both sites (2565 and 3510), thermistor spacing was increased (on September 28, 2006) to 0.5 m to yield distances above the anchor of 1.0, 1.5, 2.0, 2.5, 3.0 and 3.5 meters (Figure 2a). Thermistor readings were taken at 6-minute intervals, and were downloaded approximately monthly with an optical reader device that connects to a computer. Once the data had been offloaded from the thermistors, Boxcar® software was used to view the data and export data files to Excel.

2.2 Sediments

2.2.1 Sediment traps

2.2.1.1 Description

The sediment traps used for sampling in the Great Salt Lake consist of balanced pairs of detachable cylindrical acrylic sampling traps (72 mm internal diameter, 450 mm length) mounted in stainless steel holders located above their center of gravity to keep them vertical (Figure 2). The holders were attached to a stainless steel cable strung between a cement anchor and a buoy.

The traps were deployed at three sites representing three distinct locations in the main body of the Great Salt Lake (Figure 1). Site 2267 was located near the mouth of the Bear River, the largest contributor of flow to the lake (70% of inflows). Sites 2565 and 3510 represent northern and southern basins in the main body of the lake. At site 2267, the top of a sediment trap pair was placed at 2.8 m below the lake surface (Figure 2b), where the water depth was 4.1 m. At sites 2565 and 3510, where the water depths were 8.1 and 8.4 m, respectively, the trap pair tops were placed at two depths, approximately 3.7 m and 7 m below the lake surface (Figure 2c), corresponding to the shallow and deep brine layers, respectively.

2.2.1.2 Collection and processing of trap sediments

Sediments from sediment traps were collected approximately monthly starting March 3, 2006 for sites 2267 and 2565, and starting June 27, 2006 for site 3510.

After retrieving the sediment traps from the water, most of the water was drained using a peristaltic pump. The remaining water was swirled to make slurry, which was collected in 1-L polyethylene bottles and kept on ice until transfer to a refrigerator.

Processing involved filtering the slurry onto a Millipore vacuum filtration system (1.2 µm pore size, glass microfibre filter). The filter cake was freeze-dried, digested and analyzed by ICP-MS as described below. Salinity corrections for the filter cake mass were performed as described below for the core segments.

2.2.2 Cores

2.2.2.1 Collection and sub-sampling

Historical and contemporary sedimentation rates and sediment Se concentrations were investigated by analysis of sediment cores taken at various sites in the South Arm of the Great Salt Lake in order to estimate permanent Se removal by sedimentation.

Shallow cores (~6 cm) were taken at 20 sites (yielding quantifiable sedimentation rates in 13 sites) during June, 2007 across the south arm of the Great Salt Lake. A preliminary linear sedimentation rate was determined in each core based on ^{210}Pb decay at intervals of 0-1 cm and 4-5 cm using the CF-CS (constant flux-constant sedimentation) method (described below). Though these rates did not account for compaction of sediment, they were useful for determining relative differences in sedimentation rates, and were used as a guide to select the five additional deep coring sites occupied in 2007.

Deep core sediments were collected at sites 2267, 2565 and 3510 during July, 2006 and at sites DD-C, DD-Q, DD-I, DD-L, and DD-R during July, 2007 (Figure 2d). Each of the 2007 cores was sliced into a minimum of 10 1-cm increments. At site 2267 (total water depth of 4.1 m), one gravity core of 88 cm in length was recovered. The top ten centimeters were sliced in 2-cm intervals, whereas the remainder of the core was sliced in 3-cm intervals. At site 2565 (total water depth of 8.1 m), two gravity cores (32 and 35 cm) were collected. Both were sliced in 2-cm intervals. For site 3510 (total water depth of 8.4 m), two core samples were collected. A box corer was used to collect a 12.5-cm sediment core. This device was used to avoid compaction of this shallow sediment, in order to provide the best possible determination of age as a function of depth (and sedimentation rate). This sample was sectioned in-situ in 1-cm intervals. The core slices were placed into individual plastic containers and were stored on ice until transfer to a freezer. Also at site 3510, a gravity coring device was used to collect a 38-cm long core, which was sliced in 2-cm intervals. The 2007 cores were collected with a gravity core device, cut into 1-cm slices and processed in a similar manner as the 2006 cores.

All deep core slices were freeze-dried as described below and ground using a ceramic mortar and pestle. After grinding, the samples were homogenized by mechanical mixing and divided into four fractions.

The homogenized core slices were divided into four fractions. One fraction was analyzed for sedimentation rate using the CF-CS method for more precise determination of sediment mass accumulation rates (MAR) in these cores (at the USGS, Menlo Park, CA). In the CF-CS method, the natural logarithm of unsupported ^{210}Pb (dpm/g) in each 1-cm increment is plotted against the cumulative dry mass (g/cm^2) of sediment. The decay constant for ^{210}Pb divided by the slope of the linear trendline on the above plot yields the sediment MAR in $\text{g}/\text{cm}^2/\text{yr}$.

In eight cores, the second fraction was sent to the contract lab (LET Incorporated, Columbia, MO) for Se analysis. To reflect contemporary Se removal by sedimentation,

only the top 2 cm of sediment were included in calculating the average Se concentration for each core.

Lab results for Se concentration in the above-mentioned cores required correction for salt content. The mass of salt and additional selenium deposited on the sample from the saline pore water during the drying process was removed using the following equation and solving for $[Se_{sed}]$:

$$[Se_{sed}] = \frac{[Se_{dry}] - \frac{Mass_{water} \times \%Salinity}{Mass_{dry}} \times [Se_{salt}]}{\frac{Mass_{dry} - (Mass_{water} \times \%Salinity)}{Mass_{dry}}}$$

where $[Se_{dry}]$ is the concentration of selenium in the dry sample, $Mass_{water}$ is the mass of pore water in the sample found by subtracting the dry weight from the wet weight, % Salinity is the percent salinity of the pore water, $Mass_{dry}$ is the total dry mass of the sample, $[Se_{salt}]$ is the selenium concentration in the salt calculated from the percent salinity and a 0.5 $\mu\text{g/L}$ aqueous concentration, and $[Se_{sed}]$ is the selenium concentration in the sediment corrected for salt content.

In the three cores taken in 2006, a third fraction was analyzed for minor and major elements by ICP-MS at the University of Utah as described below. The fourth fraction was archived at room temperature.

2.2.2.2 Estimating Selenium Removal by Sedimentation

Annual Se removal by sedimentation was estimated from core analysis results. Holocene sediment thicknesses were estimated by David Dinter (University of Utah) and Steven Colman (USGS, Woods Hole, MA) by analysis of 30 Chirp (variable frequency) and Geopulse high-resolution seismic reflection transects (Dinter, 2007; Colman, 2002), as shown in the Results section. These Holocene thickness contours were plotted in ArcGIS along with the shallow core results in order to develop contours delineating qualitative zones of very high to very low contemporary sedimentation rates. Average MAR in each zone was determined by comparison of sedimentation zones to the MARs from the eight deep cores. The Se concentrations in the top 2 cm of the eight deep cores provided average contemporary sediment selenium concentrations for each zone.

With Se concentration, mass accumulation rate, and area known for each of the sedimentation zones described above, the following equation was used to determine the permanent Se removal by sedimentation for each zone:

$$\text{Se Removed} \left(\frac{Kg_{Se}}{yr} \right) = \text{Se Conc.} \left(\frac{\mu g}{g_{sed}} \right) \times \text{MAR} \left(\frac{g_{sed}}{cm^2 yr} \right) \times \text{Area} (Km^2) \times 10 \left(\frac{cm^2}{Km^2} \frac{Kg_{Se}}{\mu g_{Se}} \right),$$

The sum of the sedimentation fluxes in each of the zones yielded the total mass of Se removed by sedimentation over the entire south arm.

2.2.3 Bed sediment samples

2.2.3.1 Collection and treatment

Thirty bed sediment samples were collected at 15 locations (ranging from 6.8 to 9.4 m in depth) in the main body of the Great Salt Lake using an Eckman dredge on May 31, June 2, 26 and 27, 2006 (Figure 1, GS sites). The sediment surface was typically coated with what appeared to be an organic-rich ooze. Hence, 10 ooze layer samples (top 1-2 cm) were taken at 12 locations (GS1, GS4, GS5, GS8, GS9, GS11, GS12, GS14, GS18, GS20) (two locations did not have an ooze layer: GS3 & GS15), using a plastic spoon to scoop this surface off the collected sediment. Eight samples corresponded to composite sediments (mixture of ooze and underlying mineral sediment). The remaining 12 sediment samples corresponded to the mineral layer. Composite, ooze, and mineral layer samples were collected in glass jars and kept on ice until transfer to a refrigerator.

Each sample was subdivided in the laboratory and stored in pure water-rinsed plastic centrifuge tubes in a freezer. Bed sediment subsamples were sent to a contract lab (LET Incorporated, Columbia, MO) for Se analysis using proprietary digestion procedures. Bed sediment subsamples were also analyzed for major and trace elements (including Se) via ICP-MS at the University of Utah as described below. Prior to analysis, bed samples were thawed to allow drainage of water, and then were freeze-dried, digested and analyzed as described below. Se and TOC concentrations were corrected for salinity as described in section 2.2..2.1.

2.2.3.2 Batch tests

Batch equilibration tests were performed to determine whether significant Se would be re-solubilized from anoxic bed sediment upon equilibration with shallow brine layer water (e.g. via re-suspension or displacement of the deep brine layer). Shallow brine layer water (15 g) collected from site 2267 in December 2006 was equilibrated with anoxic bed sediment (7.5 g) in a 50-ml plastic centrifuge tube. The equilibration test was performed for sub-samples from all 15 bed sediment sampling sites. In order to avoid direct addition of atmospheric oxygen to the sample, the bed sediment container was opened and a sub-sample was added to the shallow brine layer water in a nitrogen glove bag. In order to examine the influence of the availability of oxygen on Se re-mobilization into the shallow brine layer, two batch equilibration replicates were performed for each bed sediment sample; one with nitrogen, and the other with air, in the centrifuge tube headspace (25 ml). The centrifuge tubes were placed upright on a shaking table (130 rpm) for 24 hours. Following equilibration, centrifuge tubes were centrifuged at 5500 rpm for 3 minutes, and supernatant was removed and acidified to pH < 2 by addition of 0.8% nitric acid by volume. Batch equilibration tests were repeated over week and month time scales to determine if selenium release over longer periods of exposure with shallow brine water would be significant. Air was used for the

headspace of these longer term samples since no statistically significant difference was observed for air versus nitrogen headspace replicates in the 24 hour batch experiment. In the longer term samples, the headspace (vapor) was replaced once per day, and samples were shaken in upright tubes on a shaking table (130 rpm) for 5 minutes per day. Major and trace element concentrations were analyzed via ICP-MS. Equivalent batch experiments were performed on exposed shore zone sediments; however, these results are described in the report concerning Se loads to the south arm of the Great Salt Lake.

2.2.4 Freeze-drying, extraction, and chemical analyses

Sediment samples were freeze-dried under vacuum using a liquid nitrogen trap. Wet and dry weights were recorded. Salt content was corrected based on water weight and salinity.

Extraction of metals from freeze-dried sediment (approximately 0.5 g) was performed serially in trace metal grade nitric acid (3 mL, 15.8 N) and trace metal grade hydrochloric acid (5 mL, 12 N) using a Savillex 60-mL teflon closed reactor heated by microwave oven at 50% power for 2.5 min per reactor. The extraction solution was collected in a 50-mL centrifuge tube and made up to a volume of 50 mL with milliQ water. The mixture was centrifuged at 5000 rpm for 30 minutes. The supernatant was collected in a pure water-rinsed centrifuge tube while the sediments were collected in a glass Petri dish and dried at 110°C prior to weighing. For each 10th sample, a duplicate was treated via the extraction procedure and analyzed independently.

Elemental analyses of the extraction solutions were carried out using ICP-MS at the University of Utah Center for Water, Ecosystems, and Climate Sciences (CWECS) laboratory facility.

Sediments were analyzed for Se and 29 other major and minor elements (Ag, Al, As, Ba, Be, Ca, Cd, Co, Cr, Cu, Fe, K, Li, Mg, Mn, Mo, Na, Ni, P, Pb, S, Sb, Sc, Sr, Ti, Tl, V, U, Zn) using ICP-MS. Although Hg is another element of interest, it cannot be reliably measured in most aquatic systems using ICP-MS.

For sediment samples greater than 4 grams, a representative split was sent to a commercial analytical laboratory (LET Incorporated, Columbia, MO) for Se analysis.

2.3 Analysis

2.3.1 Major and minor elements

2.3.1.1 Water

ICP-MS analyses in water were carried out in an Agilent 7500 ce. Interferences were minimized by collision or reaction with gas in a collision cell. Se, As and Cr were analyzed using hydrogen gas in the collision cell, while analyses for the rest used helium as a collision cell gas. Indium (7 µg/L equivalent concentration) was used as

internal standard. General conditions used in the ICP-MS for water sample analyses are presented in [Table 1a](#).

Dilution of Great Salt Lake samples was required to prevent salt accumulation and consequent decrease of ICP-MS signal. Major elements (Ba, Ca, Cl, K, Li, Mg, Na, S) were diluted 100:1 or 900:1 prior to being analyzed. Minor elements, including Se, were diluted 50:1 or 30:1 prior to being analyzed. Methanol (3%) and HNO₃ (ultra high purity, 0.1%) was used as a dilution matrix. A synthetic Great Salt Lake matrix was used in the preparation of standards and quality control samples. The chemical recipe for this solution is given in [Table 1b](#).

Quality control was carried out using the US EPA Multi-Media, Multi-Concentration, Inorganic Analytical Service for Superfund (ILM05.3) for ICP-MS, released in February 2004 and upgraded in January 2007 ([Table 1c](#)). The samples used for QA/QC (quality assurance/quality control) included an initial calibration blank (ICB), initial calibration verification (ICV), CRQL check standard (CRI), continuing calibration verification (CCV), continuing calibration blank (CCB), and interference check sample (ICS). For each 10 samples, a duplicate, spike, spike duplicated, serial dilution, CCV, and CCB were run.

The limit of determination (LoD) for all elements except Se were calculated as three times the standard deviation of counts for all of the CCBs divided by the slope of the calibration curve and multiplied by the dilution. For Se, for which the CCBs showed decreasing trends throughout each run, three CCBs were run sequentially following each set of nine samples and two CCVs. For each group of triplicate CCBs the standard deviation was calculated. The LoD was calculated from the average of all the triplet standard deviations by multiplying by three and multiplying by the dilution.

2.3.1.2 Sediments

As described below, sediment samples were freeze-dried, digested and analyzed by ICP-MS for 30 elements. Solution samples were diluted 20:1 using 3% methanol and 0.1% HNO₃ (ultra high purity) as a dilution matrix. The same matrix was used in the preparation of standards and quality control samples. The same QA/QC protocol used for analyses of water samples was used for sediment samples.

2.3.2 Total Se analysis

2.3.3 Water

2.3.3.1 Hydride generation

Frontier Geoscience (Seattle, WA) analyzed total Se in water by a hydride generation and atomic fluorescence spectrometry (HG-AFS).

2.3.4 Sediments

2.3.4.1 Hydride generation

Total Se in sediments was analyzed at LET Inc. (Columbia, MO) laboratory by hydride generation – atomic absorption spectrometry on acid-digested samples. Maximum detection limit for Se was 0.4 mg/Kg.

2.3.4.2 ICP-MS

Sediment samples were freeze-dried, digested and analyzed for total Se by ICP-MS at the CWECS laboratory facility. Samples were diluted 20:1 and analyzed as described above. Maximum detection limit for Se was 0.01 mg/Kg.

2.3.5 Volatile Se analysis

2.3.5.1 Water

2.3.5.1.1 Purge and cryo trap system

Collection of volatile Se from the water involved a cryo-focusing trap system (Figure 3a) following concepts used by researchers at the University of Pau in France (Amouroux and Donard, 1996).

The system consisted of a reactor (a modified desiccator) with a diffuser connected to a helium line. The reactor sparges 7 liters of hypersaline water. The vapor swept from the reactor moved via Teflon tubing to a glass water trap (-55°C, dry ice/ethanol) to remove water from the flowing vapor. The vapor then entered a glass trap (-196°C, liquid nitrogen) to trap the volatile compounds collected from the water. Studies demonstrate that the entire volume of water can be sparged at a helium flow rate of 300 mL/min for approximately 15 minutes. After collection, nitric acid was added to the glass trap to oxidize volatile Se compounds and convert them to their stable aqueous species. The closed trap was digested in a water bath at 75°C for 3 hours, and the solution was analyzed for Se by ICP-MS at the University of Utah CWECS laboratory facility.

The purge and cryo-focusing trap system was calibrated with dimethyl selenide (DMeSe) (AlfaAesar, 99% purity), which is reported to be the most stable volatile Se compound in seawater (Amouroux et al., 2000). This system was tested in the laboratory using Great Salt Lake water spiked with pure dimethyl selenide. The analyzed spiked dimethyl selenide concentrations were equivalent to the expected value (within the 95% confidence limit) based on the calibration curve (Figure 3b). Since measurements of pure water yield apparent volatile Se concentrations of 0.04 ± 0.01 ng/L, the practical detection limit for volatile Se using the purge and trap system is 0.04 ng/L. These results demonstrate that the system can quantify volatile Se concentrations in the nanogram per liter (ng/L or ppt) range. This resolution is 100 to 1000 times greater than typical analyses used for aquatic contaminants. It should be noted that the

regressed recovery of volatile Se was 25% due to losses in the system. Therefore, measured values were corrected for 25% recovery according to the regression on [Figure 3b](#). The losses yielding the 25% recovery likely include partitioning to stainless steel, ceramic, glass and teflon surfaces in the chamber and tubing, and to epoxy sealant in holding the lid of the chamber (which was a modified dessiccator). Between samples, the entire system was thoroughly cleaned by rinsing five times with nitric acid (4 L, 2%) and deionized water (4 L). Tests demonstrated that volatile Se concentrations returned to background concentrations after cleaning. The calibration curve was used to correct the values measured in the field.

Laboratory tests were run using pure water and Great Salt Lake shallow brine water with and without spiking of DMeSe to determine the analytical. This error was determined to be 13%, which includes the error associated with the ICP-MS analyses.

2.3.5.2 Fluxes calculations, different temperatures and wind velocities

2.3.5.2.1 Models

To estimate the volatile Se flux from the Great Salt Lake to the atmosphere, several models are available in the literature. These models have been used for estimating fluxes in fresh and sea water.

The general equation for mass transfer flux for a volatile compound between two phases is defined in terms of the overall mass transfer velocity ($k_{ph1/ph2}$) and the concentration gradient between the phases ([Schwarzenbach et al., 2003](#)). An expression for the volatile Se flux in the Great Salt Lake is given below with the assumption that mass transfer is kinetically controlled in the water phase, as opposed to mass transfer in the vapor phase being the kinetically limiting process.

$$Flux = ak_w \left(C_{water}^{VSe} - C_{water}^{VSe,eq} \right) = ak_w \left(C_{water}^{VSe} - \frac{C_{air}^{VSe}}{K'_{H_{GSL}}} \right) \text{ (mol/m}^2\text{/yr)}$$

where: a is a unit correction factor (= 0.24); k_w is the water transfer velocity in the air-water interface (cm/h); C_{water}^{VSe} is the concentration of volatile Se in water (mol/m³); $C_{water}^{VSe,eq}$ is the equilibrium concentration of volatile Se in water (mol/m³); C_{air}^{VSe} is the concentration of volatile Se in air (mol/m³); $K'_{H_{GSL}}$ is the dimensionless Henry's constant for volatile Se for the Great Salt Lake.

In our case, concentrations of volatile Se in the water have been measured. Concentrations of volatile Se in the air can potentially be measured; however, in the estimations below we assume this concentration to be zero.

2.3.5.2.1.1 Dimensionless Henry's constant correction

The dimensionless Henry's constant ($K'_{H_{GSL}}$) and the water mass transfer velocity in the air-water interface (k_w) were determined using empirical models from the literature. These models are based on wind velocity, water temperature, viscosity and diffusivity of the volatile species. The viscosity, diffusivity, and dimensionless Henry's constant each require corrections for the salinity of the Great Salt Lake, which is 3-5 times greater than that of the ocean.

An equation to estimate the dimensionless Henry's constant for DMeSe as a function of temperature was developed by Guo et al. (2000), whereas a salinity correction was provided by Schwarzenbach et al. (2003), yielding:

$$K'_{H_{GSL}} = 0.0248 \exp(0.0418T) * 10^{K^s [\text{salt}]_{\text{tot}}}$$

where K^s is the salinity constant, and $[\text{salt}]_{\text{tot}}$ is the total molar concentration of salt. Dimethyl selenide (DMeSe) is the most important volatile Se compound found in air; and in fresh and saline waters (Atkinson et al., 1990; Neumann, 2003; Tessier et al., 2003), and therefore is an appropriate species on which to base our estimations. The K^s for DMeSe was not available from the literature, whereas a value for dimethyl sulfide (DMeS) was available, and was used on the basis of its similarity to DMeSe (Amouroux, 1995).

2.3.5.2.1.2 Water transfer velocity - Estuarine model

To calculate the water transfer velocity, an approximation used in the Hudson estuary by Clark et al. (1995), corrected for the Schmidt number according to the boundary layer model (Schwarzenbach et al., 2003). This so-called Estuarine model is as follows:

$$k_w(\text{cm/h}) = \left(\frac{Sc}{600}\right)^{-1/2} (2 + 0.24u_{10}^2) \text{ for } u_{10} > 5 \text{ m/s}$$

$$k_w(\text{cm/h}) = \left(\frac{Sc}{600}\right)^{-2/3} (2 + 0.24u_{10}^2) \text{ for } u_{10} \leq 5 \text{ m/s}$$

where Sc is the Schmidt number, and u_{10} is the wind velocity measured 10 m over the surface of the lake.

Saltzman et al. (1993) defined a Schmidt number for DMeS as a function of water temperature ($^{\circ}\text{C}$) and corrected for the sea water salinity (via coefficients) as follows:

$$Sc_{DMeS}^{\text{sea water}} = 2674.0 - 147.12T + 3.726T^2 - 0.038T^3$$

2.3.5.2.1.3 Water transfer velocity - modified Liss and Merlivat model

An alternative approach is provided by the modified Liss and Merlivat model (Livingstone and Imboden, 1993; Liss and Merlivat, 1986), the results of which largely corroborate the Estuarine model. This model, which was also corrected for the Schmidt number according to the boundary layer model (Schwarzenbach et al., 2003), defined three wind velocity regimes:

$$k_w(\text{cm/h}) = \left(\frac{Sc}{600}\right)^{-2/3} (0.65 * 3.6) \quad \text{for } u_{10} < 4.2 \text{ m/s}$$

$$k_w(\text{cm/h}) = \left(\frac{Sc}{600}\right)^{-1/2} (0.79u_{10} - 2.68) * 3.6 \quad \text{for } 4.2 \text{ m/s} < u_{10} < 13 \text{ m/s}$$

$$k_w(\text{cm/h}) = \left(\frac{Sc}{600}\right)^{-1/2} (1.64u_{10} - 13.69) * 3.6 \quad \text{for } u_{10} > 13.6 \text{ m/s}$$

2.3.5.2.1.4 Diffusive flux

The diffusive flux can be calculated assuming that diffusion is the limiting mass transfer process, as follows:

$$J = D_e \frac{\Delta C}{\Delta x}$$

where: J is the diffusive flux (g/cm²/yr); D_e is the effective diffusion coefficient (cm/s), ΔC is the concentration gradient (ng/L); and, Δx is the difference in depth (m).

The diffusion coefficient for DMeSe can be calculated using the diffusion coefficient for DMeS as function of temperature, corrected for sea water, according to Saltzman et al. (1993):

$$D_{DMeSe} \approx D_{DMeS} = 0.0192 \exp(-18.1/RT)$$

where: R is the gas constant (kJ/mole K) and T is the temperature (K)

2.3.6 Wind velocity, atmospheric temperature, lake elevation, lake surface area

2.3.6.1 Wind velocity and atmospheric temperature

Wind velocity and atmospheric temperature data from January 2006 to August 2007 were obtained from the MesoWest station at Hat Island. Weekly surface water temperatures were obtained using AVHRR (advanced very high resolution radiometer). The AVHRR is a scanner mounted on National Oceanic and Atmospheric Administration (NOAA) polar-orbiting satellites for measuring visible and infrared radiation reflected from vegetation, cloud cover, shorelines, water, snow, and ice. (ESRI Support Center, <http://support.esri.com/index.cfm?fa=homepage.homepage>). The data

were obtained for the period January 2006 to December 2006, from the Department of Meteorology at the University of Utah. Comparisons were made between the AVHRR data (January 2006 to December 2006) and thermistor measurements in Gunnison Bay (January 2006 to August 2007) to ensure that the AVHRR data correctly represented water surface temperature during the period of study (Figure 3c)

The estimated error for wind velocity measurement is 2.5 m/s (Horel, 2007). The estimated error for temperature measurement from an AVHRR is 0.5 – 1°C (Crosman and Horel, 2006).

2.3.6.2 Lake elevation and lake surface area

Lake elevation data were obtained from the USGS gage at the Saltair boat harbor. Surface area of the lake, used to calculate the cumulative volatile Se flux from the lake, was corrected for lake elevation (in 0.5-ft intervals) according to the data summarized by Baskin (2005). Water-surface elevations reported at the USGS Great Salt Lake gages are considered to be accurate within +/- 0.10 foot of the datum in use (<http://ut.water.usgs.gov/gsl%20corr/gslcorrection.htm>).

2.3.6.3 Direct measurements of volatilization

Direct measurements of volatilization of Se were taken at two primary locations (3510 and 2267) and one secondary location (2565) in the south arm of the Great Salt Lake. The flux measurements were taken concurrently with characterizations of the parameters used in estimating volatile Se flux: surface water temperature, wind velocity, and volatile Se concentration, in order to assess the accuracy of the predictive model.

An emission isolation flux chamber (St. Croix Sensory, Inc.) was used to collect volatilized Se from the surface of the lake (Figure 4a). The bottom of the stainless steel chamber is a cylinder that circumscribes a capture area for volatile compounds. Helium gas was released from a compressed helium tank and swept through the chamber (while it floated on the lake surface) to drive volatile gases coming from the lake into a cryo-trap. The sweep rate was set to approximately 3 L/min to prevent accumulation of volatilized Se (and other gases) within the chamber. A constant sweep rate was used in lieu of variable rate matching environmental conditions because studies have shown that high sweep rates can induce convection in the water column and subsequently bias flux results high (Card et al., 2002). A sweep rate of 3 L/min corresponds to approximately 1 chamber volume being swept every 6 min and is consistent with the manufacturer's recommendations.

The gas mixture in the chamber was then pumped (Universal 44XR Single Pump, SKC West Inc.) at an equivalent rate through Teflon tubing to a glass finger-trap in acetone/dry ice slush (-20°C) to remove any water vapor. Downstream of the water trap, volatile Se was cryo-focused onto glass wool in a finger-trap held at -170°C by liquid nitrogen and a Watlow PID temperature controller connected to a temperature sensor (PT-103-AM Platinum RTD, Lakeshore Cryotronics, Inc.) and cartridge heater (3039-002, Cryogenic Control Systems, Inc.). Figure 4b depicts the apparatus used to hold the glass finger-trap in the liquid nitrogen. Designed with the assistance of Dr. Kip

Solomon (University of Utah) and Erwin McPherson (University of Utah), the device was placed in a Dewar flask filled with liquid nitrogen. The “heat” of the liquid nitrogen was conducted through the brass rod to the copper block and tube surrounding the finger-trap. The length of brass rod necessary for optimal temperature controller performance was determined experimentally to be 1 cm, at which point the cartridge heater embedded in the copper block was activated approximately 25% of the time. The stainless steel shield prevented any direct contact between the liquid nitrogen and the copper block and tube.

After a substantial sampling time (typically between 1.5 and 3 hours), the sample in the cryo-trap was acidified with 5 mL of 14% nitric acid to stabilize volatile Se compounds as oxidized aqueous species. The sealed trap was then digested in a water bath at 75°C for 3 hours and analyzed for Se by ICP-MS at the University of Utah CC-ICP-MS facility. The resulting measured concentration was then converted to a mass of Se and divided by the area under the flux chamber (0.13 m²) and the period of sampling in order to yield a flux rate.

Wind velocity measurements used for developing predicted fluxes were taken at 3 meters above the water surface using a Kestrel 1000 Wind Meter. These measurements were then projected to a height of 10 meters by the method described by Wind Energy Department of Risoe National Laboratory and Det Norske Veritas (2001) for use in flux prediction calculations. Surface water temperature and volatile Se concentration measurement techniques are described in sections 2.1 and 2.4.5.1, respectively.

To ensure that the sampling system was operating properly, tests were performed to quantify the background level of Se, examine response of the system to qualitative changes in volatilization rate, and verify reproducibility of measurements. Three flux samples were taken in the laboratory by placing the chamber over a nitric acid-washed pan filled with pure water (Milli-Q) to determine the background “flux” that is measured in a pure sample. All background samples were low, with a mean of 1.60 ng/m²h and a maximum of 2.67 ng/m²h. To test response of the system, two more samples were taken at Saltair marina for 30 minutes each. During the first sampling, a diffuser hanging 1 m below the surface bubbled helium through the water column into the flux chamber to produce a high flux rate. For the second sample the diffuser was turned off, producing a low flux rate. Analyses yielded an order of magnitude higher flux rate for the first sample relative to the second, indicating that the system responded appropriately. Finally, reproducibility was demonstrated by two 2-hour samples taken during the same day at site 2267. The results showed similar Se flux rates with a slightly higher flux rate corresponding to the sample that was taken under conditions of increased surface chop.

The effect on measured flux of sweep rate, sweep gas composition (helium versus nitrogen), and concentration of dissolved volatile Se was also investigated. In the laboratory, a stainless steel basin was filled with 50 L of Great Salt Lake water and spiked with various masses of DMeSe to yield concentrations from about 2 to 27 ng/L. Seven liters of this water was analyzed for volatile Se concentration using the purge and cryo-trap system described above. Other input variables were held constant with a steady water temperature and no wind. The flux of volatile Se from the solution

remaining in the stainless steel basin was measured using the system described above. Sweep rates were 2 and 3 L/min for helium, and were 2,3, and 6 L/min for nitrogen. All 5 flux measurements were higher than those observed on the Great Salt Lake, consistent with the higher dissolved volatile Se concentration in the chamber relative to the lake (Table 1d). The measured fluxes were also highly reproducible regardless of whether nitrogen or helium gas was used, and the values did not change as a result of changing sweep rate. The influence of concentration is discussed in the results section.

A recovery test was performed in the laboratory in order to quantify the response of the direct measurement system to the introduction of a known mass of Se. A DMSe spike solution was prepared to a concentration of approximately 125 $\mu\text{g/L}$. Drops of the spike solution were placed on a glass Petri dish and immediately set inside a large cylindrical Pyrex basin. The flux chamber was then fitted tightly over the basin and a 1-hour direct measurement was performed as the drops of spike solution evaporated into the flux chamber headspace. No outside heat was applied to speed evaporation. Three recovery tests were performed with 50, 100, and 150 μL of spike solution. The mass of spiked Se was verified independently by analysis of equivalent volumes of spike solution by ICP-MS using the digestion procedure described above. The results of the flux recovery tests are discussed below.

2.3.7 Total dissolved gas pressure, hydrostatic pressure, barometric pressure

2.3.7.1 Water

Total dissolved gas pressures were measured at 12 locations (GS1, GS3, GS4, GS5, GS8, GS9, GS11, GS12, GS14, GS15, GS18, GS20) and 6 depths (between 1.5 and 8 m) in the main body of the Great Salt Lake (Figure 1) by using a total dissolved gas (TDG) sensor (In-Situ Inc., Fort Collins, CO). The TDG probe needed at least 7 minutes for stabilization. The probe was zeroed at the lake surface before starting to measure the total dissolved gas pressure. TDG measurements were achieved each two months from May 31 to November 17, 2006. Hydrostatic and barometric pressure were measured at the same locations, depths and times given above, using a Hydrolab Troll 9000 (In-Situ Inc., Fort Collins, CO).

All TDG measurements made during spring, 2006 were well below hydrostatic pressure indicating insignificant exsolution of gas (including volatile Se), or exsolution of gas in discrete zones not corresponding to the TDG sites. The TDG measurements were discontinued in summer, 2006.

2.3.8 Thermistor analysis

2.3.8.1 Lake Mixing

2.3.8.1.1 Thermal mixing

Temperature equilibration events in the water column may represent genuine mixing of the deep and shallow brine layers. Complete mixing or homogenization of the water column should yield an intermediate temperature between the two temperatures of the stratified column.

The expected intermediate temperature can be determined from an energy balance, under the assumption that despite density and temperature differences among water column strata, the specific heats of these strata are equal. Since heat energy lost by one layer must equal the heat energy gained by the other layer, the intermediate temperature can be determined from the mass (m), specific heat (c), and temperature difference between the initial (T_1 and T_2) and final (T_3) temperatures for both strata:

$$m_1c(T_1 - T_3) = m_2c(T_3 - T_2)$$

Substituting density and volume for masses of the two water column strata, and considering a water column with a given cross sectional area with heights h_1 and h_2 for the strata:

$$\rho_1h_1(T_1 - T_3) = \rho_2h_2(T_3 - T_2)$$

The intermediate temperature can be determined as follows:

$$T_3 = \frac{\rho_1h_1T_1 + \rho_2h_2T_2}{\rho_1h_1 + \rho_2h_2}$$

For example, on June 14 the temperature of the deep brine layer was 16°C and the temperature of the shallow brine layer was 21°C and the thermal mixing of these two layers would yield:

$$T_3 = \frac{1.10 \frac{\text{g}}{\text{cm}^3} (6 \text{ m})(21^\circ\text{C}) + 1.16 \frac{\text{g}}{\text{cm}^3} (2 \text{ m})(16^\circ\text{C})}{1.10 \frac{\text{g}}{\text{cm}^3} (6 \text{ m}) + 1.16 \frac{\text{g}}{\text{cm}^3} (2 \text{ m})}$$

$$T_3 = 19.7^\circ\text{C}$$

2.3.8.2 Seiche periodicity

A seiche is a prolonged oscillating wave in a body of water initiated by atmospheric effects such as wind. The period of an internal seiche is related to the length of the lake (l) and the physical characteristics of the layers within the lake. In the Great Salt Lake, the layering (density stratification) is defined by salinity (deep and shallow brine layers) rather than temperature. The characteristics of the layers, epilimnion (e) and hypolimnion (h), are thickness (z) and density (ρ) (Wetzel, 2001).

$$t = \frac{2l}{\sqrt{\frac{g(\rho_h - \rho_e)}{\frac{\rho_h}{z_h} + \frac{\rho_e}{z_e}}}}$$

2.3.9 TOC analysis

2.3.9.1 Water

Water samples for total organic carbon (TOC) analysis were collected in acid-rinsed amber glass 250-mL bottles from the deep brine layer at 12 stations (GS1, GS3, GS4, GS5, GS8, GS9, GS11, GS12, GS14, GS15, GS18, GS20) (Figure 1). Samples were collected from each location using a peristaltic pump with acid-rinsed C-flex tubing (Cole-Parmer's Masterflex, Vernon Hills, IL), stored on ice and transferred to a refrigerator. TOC analysis were carried out at the U of U CW ECS laboratory facility using a TOC-5000 (Shimadzu, Columbia, MD) where water samples were analyzed sequentially for total carbon (TC) and inorganic carbon (IC), the TOC being the difference between TC and IC. In both analyses, the carbon contained in the sample was converted in CO₂ and analyzed by an infrared CO₂ analyzer. For the TC, the sample was heated at 680°C, while for the IC, the sample was acidified with H₃PO₄ (25%). QC samples included a duplicate, spike, check standard, spike standard, and a blank.

2.3.9.2 Sediments

TOC analyses in 31 bed sediment samples were carried out by LET Inc. (Columbia, MO) by using a LECO combustion carbon analyzer, based on National Soil Center Method 4H2. Sediment samples were heated in the combustion chamber in an atmosphere of pure oxygen, which converted the organic carbon in the sample into carbon dioxide gas. The quantity of carbon dioxide gas evolved from the sample was measured by an infrared CO₂ analyzer and automatically converted into a percent carbon value for the sample.

2.3.10 Isotope analysis

2.3.11 Sediments

Subsections of the freeze-dried sediment cores were analyzed at the U.S. Geological Survey (Menlo Park, CA) for ²¹⁰Pb, ²²⁶Ra, ²³⁴Th, ⁷Be, and ¹³⁷Cs activities for determination of sediment accumulation rates. Wet and dry weights were recorded to determine water content of sediment. Sediment bulk density was assumed to be 2.6 g/cm³. Sediment dry weights were corrected for salt content of sediment porewater assuming a salinity of 171 g/L (17.1 %). The assumed salinity value was based on averaging measured salinity values of the deep brine layer obtained during late Summer and Fall, 2006.

Activities of total ²¹⁰Pb, ²²⁶Ra, ²³⁴Th, ⁷Be, and ¹³⁷Cs were measured simultaneously by gamma spectrometry based on previously published methods (Van Metre et al., 2006; Fuller et al., 1999). Subsamples of dried sediment samples were sealed in 7-mL

scintillation vials and counted using a high-resolution intrinsic germanium well detector. The upper 3 cm of the core was counted within two weeks of collection for determining ^7Be and unsupported ^{234}Th (half lives 53 and 24 days, respectively) as indicators of recent sediment deposition and reworking by mixing or resuspension processes.

^{210}Pb activity as a function of depth in the sediment provides an estimate of the sedimentation rate. ^{210}Pb in core sediments results from the decay of two isotopes: ^{222}Rn (referred to as unsupported lead) and the long-lived ^{226}Ra (referred to as supported lead). ^{222}Rn decays in the atmosphere to ^{210}Pb , and is deposited onto the lake surface where it becomes associated with settling particles and it is deposited in the accumulating sediment. ^{210}Pb has a half-life of 22.3 years; hence, the rate of ^{210}Pb decrease with depth corresponds to the rate of burial. However, another source of ^{210}Pb is present in the sediment (^{226}Ra) and must be accounted for.

The supported ^{210}Pb activity, defined by its long-lived progenitor, ^{226}Ra activity, was determined on each interval from the 352 KeV and 609 KeV gamma emission lines of ^{214}Pb and ^{214}Bi daughters of ^{226}Ra , respectively. Supported ^{234}Th activity was determined by re-analyzing the samples 5 months later, after decay of unsupported ^{234}Th activity. Self-absorption of the 46 KeV ^{210}Pb and 63 KeV ^{234}Th gamma emission lines was corrected using the attenuation factor for each counting vial that was calculated via an empirical relationship between self absorption and bulk density (Cutshall et al., 1983). Self-absorption of the ^{214}Pb , ^{214}Bi , 474 KeV ^7Be and the 661.5KeV ^{137}Cs gamma emission lines was negligible. Detector efficiency for each isotope was determined from NIST traceable standards. NIST and IAEA reference materials were used to check detector calibration. The reported uncertainty in the measured activity was calculated from the random counting error of samples and background spectra at the one standard deviation level, and was typically within $\pm 10\%$. The measured activities of replicate analyses of material from the same interval agreed to within $\pm 15\%$.

Sedimentation rate was determined using the constant flux–constant sedimentation rate (CF-CS), method of Appleby and Oldfield (1992). The CF-CS method assumes a steady state accumulation of sediments and a constant unsupported ^{210}Pb activity per gram of depositing sediment particles.

3. Results

3.1 Great Salt Lake characteristics

3.1.1 Water

3.1.1.1 Spatial, depth, and temporal variation

Total Se concentrations in water samples (raw acidified) showed similar results among the four sites sampled (Figure 5), as represented by the data collected for May, 2006. This similarity was apparent in all other months sampled (Table 2); however, important differences with depth and over time were observed, as described below.

The average Se concentration from May 2006 to July 2007 for unfiltered acidified (RA) samples was 0.64 ± 0.28 $\mu\text{g/L}$, whereas the filtered acidified (FA) samples showed an average Se concentration of 0.49 ± 0.25 $\mu\text{g/L}$ for the same period of time. The geometric means for Se were 0.60 ± 0.31 $\mu\text{g/L}$ and 0.45 ± 0.21 $\mu\text{g/L}$ for all RA and FA water samples, respectively, for the same period of time. The medians for RA and FA water samples were 0.64 and 0.46 $\mu\text{g/L}$, respectively (Table 2d), indicating a limited number of outliers. Quartile analysis for outliers indicates that the value obtained for site 2767 during June, 2007 (2.77 $\mu\text{g/L}$) corresponds to an extreme outlier, although it does reflect the trend of increasing total Se concentration during the period of the study (described below). Table 2 includes arithmetic and geometric means, median, standard deviation, and lowest and highest values for Se, calculated for each site (2267, 2767, 2565 and 3510).

In terms of depth, the major changes in water chemistry coincided with transition to the deep brine layer, where dissolved oxygen (DO), oxidation-reduction potential and pH decreased, conductivity increased and temperature increased or decreased depending on season (Figure 6).

Total Se (RA) concentrations also changed dramatically upon transition from the shallow to the deep brine layer (Figure 7c), either increasing or decreasing with no apparent relationship to season. In contrast, the vast majority of dissolved Se (FA) concentrations decreased upon transition from the shallow to the deep brine layer. These results indicate that particulate phases (if defined as RA minus filtered acidified, or FA) bear a significant but minor fraction of the Se mass in these samples.

Results for trace metals other than Se are shown in Table 3 and Figure 8. Notably, total As concentrations averaged 147 ± 6.3 $\mu\text{g/L}$ (with a geometric mean of 147 $\mu\text{g/L}$ and a median of 147 $\mu\text{g/L}$) in the shallow brine layer (Table 3 a & b). Total As concentration in the deep brine layer was 163 ± 16.7 $\mu\text{g/L}$ (with a geometric mean of 163 $\mu\text{g/L}$ and a median of 162 $\mu\text{g/L}$) (Table 3 c & d). Elements such as Al, Fe, Mn, Mo, and Pb showed significantly higher concentrations in the deep brine layer relative to the shallow brine layer (Figure 8 a & b). Particulate concentrations of some trace metals (Pb, Mo, Cu, Fe, Co, Ni, Zn, Ti, V) tended to be higher in the deep brine layer relative to

the shallow brine layer (Figure 9), possibly reflecting the formation of sulfide particulates and increased adsorption under the reduced conditions in the deep brine layer.

In terms of temporal variation, increases in the measured total (RA) and dissolved (FA) Se concentrations (measured at Frontier Geosciences, Inc.) were observed in both the deep and shallow brine layers during the period of the investigation (Figure 7a-d), constituting a net increase ranging between 0.16 and 0.34 $\mu\text{g/L}$ among the four sites in the Great Salt Lake (Naftz et al., 2007).

In contrast to the results using hydride generation (252 samples – May 2006 to July 2007), the total and dissolved Se concentrations analyzed via ICP-MS at the University of Utah (132 samples – September 2006 to July 2007) showed slight to insignificant increases during the course of the study (Figure 7e & 7f, Table 2e – 2g). This contrast may result from the lesser number of samples (and/or lesser period) analyzed via ICP-MS and by the large scatter in the data.

3.1.2 TOC

3.1.2.1 Spatial and temporal variations

Concentrations of total organic carbon (TOC) in the deep brine layer showed no spatial trend, as shown for June, 2006 (Figure 10). The lack of a spatial trend was observed for all other months. The TOC concentration remained constant over the sampling period, demonstrating no temporal variation (TOC averaging approximately 95 mg/L) (Figure 10).

3.1.3 Bed sediment

3.1.3.1 Se concentrations

3.1.3.1.1 Spatial variation

Total Se concentrations in bed sediment samples showed no spatial variation in either the ooze or mineral layer, or in the composite of the two (Figure 11).

At 7 of 10 sites where ooze was present, the Se concentration in the mineral layer was greater than the corresponding Se concentration in the ooze. The average Se concentration in the ooze layer was 1.29 ± 0.41 mg/Kg, whereas the average Se concentration in the mineral layer was 1.59 ± 0.59 mg/Kg.

TOC concentrations in bed sediment showed no spatial trend for any of the sediment samples retrieved (ooze, mineral layer, and composite) (Figure 12). Average TOC concentrations in the ooze and mineral layers were not significantly different, $6.16 \pm 4.1\%$ versus $4.75 \pm 2.2\%$, respectively.

Se concentrations were slightly correlated to TOC in the bed sediments (Figure 13). The correlation was most significant (but still weak) in the mineral layer samples ($r^2 =$

0.43) (Figure 13). Se concentrations in the ooze and composite samples showed no correlation with TOC concentrations.

3.2 Volatile selenium flux

3.2.1 Volatile Se concentrations

3.2.1.1 Spatially and with depth

Concentrations of volatile Se showed no spatial trend in the main body of the lake (Figure 14). Volatile Se concentrations increased with depth in the shallow brine layer (Figure 15a), for all sampling periods and sites where multiple depths were measured in the shallow brine layer. Volatile Se concentrations for depths below 5 to 6.5 m apparently decreased with depth, for all sampling periods and sites where multiple depths were measured (Figure 15b).

3.2.1.2 Temporal

The average volatile Se concentrations in water were reduced during the winter and elevated during spring, summer, and fall (Figure 16a and Table 4 a-c), coincident with warmer temperatures and increased primary productivity. During the course of the investigation, average concentrations (across the entire lake and entire water column) of volatile Se ranged from 2.4 ± 2.6 ng/L in September 2006 to 0.31 ± 0.47 ng/L in early December 2006 and 6.9 ± 6.9 ng/L in July 2007. This temporal trend is also reflected in the two-depth plots and three-depth plots shown in Figure 15a for the shallow brine. The same temporal trend occurred in the deep brine layer (Figure 15b).

The decrease in volatile Se concentrations in the shallow brine layer during winter 2006 corresponded to decreased temperature, and decreased primary productivity, which can be expected since phyto- and zoo-plankton are the expected main producers of volatile Se (Amouroux and Donard, 1996).

The average volatile Se concentration from September 2006 to August 2007 was 3.0 ± 4.4 ng/L. This value represents 0.6% of the average total Se concentration in the water column. Although this fraction seems negligible, its significance depends on the residence time of volatile Se in the lake. For example, water vapor represents only 0.001% of the global water budget whereas the great importance of water vapor (clouds) in transferring water across the surface of earth is undeniable, and arises from the short residence time of water in the vapor phase. The flux of Se from the lake to the overlying atmosphere must be known in order to assess its significance.

3.2.2 Volatilization flux estimates

Recalling that a near-surface volatile Se concentration gradient was observed (Figure 15), a diffusive flux was calculated assuming that diffusion is the limiting mass transfer

process. The estimated diffusive flux was calculated for temperatures and concentration gradients observed in the lake (Table 5). The average diffusive flux yielded 3.9×10^{-12} g Se/cm²/yr, which translates to 7.3×10^{-2} Kg/yr. This extremely small flux would represent the quiescent lake, which we believe is far too conservative a condition for this shallow large surface area lake. Furthermore, such a low volatilization flux is not consistent with observed Se concentrations in the Great Salt Lake, as described below.

The estimated water transfer velocities corresponding to wind-driven mixing (both models) are shown in Table 6a. The volatile Se fluxes were estimated using an average volatile Se concentration of 3 ng/L, and the water transfer velocities corresponding to wind velocities of 5 and 25 miles per hour. Assuming a negligible volatile Se concentration in the overlying air, the corresponding volatile Se fluxes from the lake are shown in Table 6a.

The estimated volatile Se fluxes range from 4.2×10^{-8} or 2.4×10^{-8} g Se/cm²/yr under cold, low-wind conditions to 8.2×10^{-7} or 5.6×10^{-7} g Se/cm²/yr under hot, high-wind conditions. This flux can be converted to a mass transfer rate by multiplying the known surface area of the lake (1842 km²) (Baskin, 2005). The estimated Se mass transfer rates via volatilization range from 766 or 450 Kg/yr under cold, low-wind conditions to 15,030 or 10,395 Kg/yr under hot, high-wind conditions.

3.2.3 Direct measurement of volatilization flux

The results of measured volatile Se fluxes from Great Salt Lake are shown in Table 6b along with the corresponding predicted flux rates (Estuarine model) and input variables (wind velocity, surface water temperature, surface volatile Se concentration). Measured fluxes ranged from 2 to 20 ng/m²h in the ten samples taken on the Great Salt Lake with average wind velocities of 1 to 4 m/s, water temperatures of 12 to 28°C, and volatile Se concentrations of 0.04 to 4.6 ng/L.

The measured volatile Se fluxes were highly sensitive to near-surface volatile Se concentrations. For example, despite similar wind and wave conditions, samples 1C and 2C yielded volatile Se fluxes of 2.08 and 20.13 ng/m²h corresponding to measured near-surface volatile Se concentrations of 0.05 and 1.43 ng/L respectively.

Measured volatile Se fluxes did not change appreciably with changes in wind speed under the relatively calm conditions examined. For example, in two samples taken on 5/24/2007 to show reproducibility, measured flux rates were 10.7 and 8.0 for average wind velocities at 10 meters above the water surface of 5.1 and 6.7 m/s respectively. Though counterintuitive, the surface roughness during the first sample was significantly higher than the second resulting in the slightly higher flux rate for the first (assumes constant volatile Se concentration and water temperature). This observation is consistent with the fact that surface matrix effects, rather than wind speed, dominate liquid-to-atmosphere fluxes on liquid surfaces (Schmidt, 2007). Although increasing wind can increase surface roughness of a water body, the extent of convection also depends on wind direction and surrounding geography.

3.2.3.1 Correlation between measured and predicted fluxes

In order to account for the background Se flux measured by the system, the average background flux (1.6 ng/m²h) was subtracted from each measured flux value. This assumes the background flux rate is constant as opposed to the system measuring a constant background mass (and therefore not dependent on the time of sample). The implications of this assumption are insignificant, however, because subtracting the average background mass recovered gives an almost identical result to subtracting the background flux. In the majority of measurements, the background correction was small relative to the measured value.

The majority of measured flux rates fell significantly below their corresponding predicted flux values (Figure 16b). This was most clearly seen under the higher predicted flux condition driven by the higher volatile Se concentration of sample 3C (Table 6b). Measured flux in this sample was an order of magnitude below the predicted flux (9.28 and 105.89 ng/m²h respectively). The low measured flux relative to predicted flux indicated inefficiency in the flux measurement or inadequacy of the model to reflect volatilization in the Great Salt Lake.

To explore possible inefficiencies in the flux measurements, DMSe recovery was examined in tests (described above) involving addition of small drops DMSe spike solution under the chamber. Results ranged from 7% to 24% of the input mass of Se (Table 6c). The cause of low mass recovery is unknown, but a likely possibility is the adsorption of DMSe vapor to surfaces, which appears to be especially significant in absence of other vapors (e.g. water) that may compete with DMSe for surfaces. Inefficiency via loss of DMSe to surfaces is supported by calibration tests for the purge and cryo-trap system (described in Appendix A) which show a consistent 25% recovery that is attributed to partitioning of Se, primarily in the vapor phase, to various surfaces in the system. The loss of DMSe from the aqueous phase to surfaces appears to be low relative to loss from the vapor phase, as indicated by measurements of aqueous DMSe concentrations under controlled conditions (described below). The apparent lower recovery of the direct flux measurement system relative to the purge and cryo-trap system is consistent with the much larger surface area in former relative to the latter. Another possible contributor to the low recovery in the direct flux measurement system is the lack of water vapor due to addition of small drops (50 to 150 μ L) to the system. The presence of water vapor in the purge and cryo-trap system may contribute to the higher recoveries observed in that system.

Inefficiencies in the direct flux measurements were explored under controlled conditions that reflected the presence of water vapor in the system under field conditions. Fifty liters of GSL water was spiked with DMSe in a stainless steel container (described above) and the flux was measured over this container. Figure 16c (and Table 1d) show the measured flux determined under controlled laboratory conditions (zero wind, constant temperature). Volatile Se concentrations ranged from zero in the background samples to 27 ng/L and were independently verified by the purge and cryo-trap system described in Appendix A. Measured fluxes exhibited a strong 1/10 linear direct relationship with the predicted fluxes under these controlled conditions, indicating that the flux measurement system was 10% efficient in measuring the actual DMSe flux. We

conclude, that the 1/10 relationship between measured and predicted fluxes under controlled conditions is due to systemic inefficiency in the direct flux measurement, likely resulting from partitioning of volatile Se to surfaces in the vapor phase.

To account for measurement inefficiency determined above, corrections were applied to the flux measurements taken on the GSL. In each sample, the measured flux rate after background subtraction was multiplied by 10 to correct for the 1/10 measurement inefficiency observed under controlled laboratory conditions. [Figure 16d](#) shows the corrected flux rates from the GSL. The majority of corrected measured fluxes are close to, but higher than the predicted fluxes. Two points (samples 1B and 2C) are significantly higher than their corresponding predicted fluxes. No obvious differences in conditions were observed during these two samples to cause this discrepancy.

The high measured flux (after correction) relative to the predicted flux could result from a number of factors. One possibility is the underestimation of flux by the predictive model, which could potentially result from influences of the high salinity of the GSL. The air-water transfer velocity (k_w) is inversely proportional to the Schmidt Number (Sc) to a power between $\frac{1}{2}$ and $\frac{2}{3}$. Sc is a dimensionless ratio of kinematic viscosity to molecular diffusivity, both of which are influenced by salinity. Unfortunately, the rate of change in each of these parameters as a function salinity at levels of the GSL could not be determined; hence, we can only suggest that the hyper salinity of the GSL may play a role in the discrepancy between measured and predicted fluxes.

Another possibility is that the corrected measured fluxes are biased high relative to the actual flux rates from the GSL. At higher flux rates, accumulation of volatilized Se in the vapor phase in the chamber may occur, leading to a lower concentration gradient between the water and vapor phases, and resulting in inhibited flux. Since a majority of the laboratory flux tests using GSL water spiked with DMSe simulate higher flux conditions, the measured flux rate may have been inhibited to a greater extent than that which occurred in the lower flux conditions in the field. The result would be a slight over-correction of the field flux measurements from the 1/10 relationship between measured and observed fluxes in the laboratory. However, the laboratory tests under controlled conditions negate this possibility; since the measured flux rate was constant despite changes in sweep rate ([see Methods and Table 1d](#)).

A third possibility is that the differences between measured and predicted fluxes are magnified because of the relatively narrow range of fluxes that could be measured on the GSL. If multiple flux measurements could have been made under more turbulent conditions (i.e. higher flux), the discrepancy may have been reduced in significance.

Though the exact cause of the discrepancy is unclear, the proximity of measured fluxes to predicted fluxes within the limited dataset of direct measurements leads us to conclude that a correction of the predicted fluxes is not warranted. The predictive model is an appropriate means of estimating annual removal of Se from the GSL by volatilization.

3.2.4 Integration of the volatile Se flux

The annual Se flux is obtained by integration of calculated volatile Se fluxes using recorded wind and temperature data. The volatile Se flux estimates from the Estuarine model were integrated over time using measured wind velocities (10 m above lake surface), water temperatures (at lake surface), and lake surface areas for the 1-year period of study. The integration assumed an instantaneous response of volatile selenium flux to changes in wind velocity and water temperature. The measured parameter values are shown for the period of study in [Figure 17a](#).

The volatile Se concentrations were discretely sampled and were temporally and spatially variable (areally and with depth). Flux estimates were based on volatile Se concentrations at depths of 0.2 to 0.5 m from the surface. Although these data are limited, they indicate decreased volatile Se concentration during winter ([Figure 17b](#)), and so were fitted using a sinusoidal function shown in [Figure 17b](#), according to the following equation:

$$C_{water}^{VSe} = 10^{\{A+B \cdot \sin[(t-C)\pi/D]\}} \text{ (ng Se/L)}$$

where A,B,C, and D are constants.

The concentration values span nearly two orders of magnitude; therefore the geometric mean is the better descriptor of the data than the arithmetic mean. The geometric mean (μ_g) is the n^{th} root of the product of n values, as follows:

$$\mu_g = \sqrt[n]{x_1 \cdot x_2 \cdot \dots \cdot x_n}$$

The geometric standard deviation (σ_g) is determined from the geometric mean as follows:

$$\sigma_g = \exp\left(\sqrt{\frac{\sum_{i=1}^n (\ln X_i - \ln \mu_g)^2}{n}}\right)$$

The geometric standard deviation is the ratio of the geometric mean to the 84th percentile (or inverse ratio to the 16th percentile) of the distribution of values, thereby describing 68% of the data (1st standard deviation).

The constants A through D were adjusted to yield the geometric mean (0.938 ng/L) and the geometric standard deviation (5.5) of the data for the period where volatile Se concentrations were actually measured (measurements were not taken between December 15th, 2006 and April 15th, 2007, due to logistical reasons). The corresponding values of the constants are shown in the equation below.

$$C_{water}^{VSe} = 10^{\{-0.5815+1.5741 \cdot \sin[(t-30)\pi/185]\}}$$

During integration, the following data frequencies were used for the lake area, temperature, and wind data: daily average for lake area, weekly average for water

temperature and 1.5-hour intervals for wind speed. The cumulative integrated flux is shown as a function of time in [Figure 17c](#).

Integration of the volatile Se flux yielded **2108** Kg of volatile Se lost to the atmosphere in 1 year.

3.2.4.1 Propagation of error in the calculation of the volatile Se flux

To determine error associated with the integrated flux, the estimated error for each parameter required to estimate flux was propagated. The individual errors were associated with near-surface water temperature, wind velocity, and volatile Se concentration ([Table 6d](#)), as described below.

The near-surface water temperature was incorporated into the Schmidt number shown below:

$$Sc_{DMeS}^{sea\ water}(T) = 2674.0 - 147.12T + 3.726T^2 - 0.038T^3$$

The error for this polynomial function was calculated using the derivative of the function, where:

$$\Delta Sc_{DMeS}^{sea\ water}(T) = 147.12\Delta T + 3.726 * 2\Delta T * T + 0.038 * 3\Delta T * T^2$$

where ΔSc is the error for the Sc number, ΔT is the error associated with measurement of the near-surface water temperature (± 0.5 °C).

The wind velocity (u_{10}) was incorporated into the air/water transfer velocity (k_w), shown below:

$$k_w(cm/h) = \left(\frac{Sc(T)}{600}\right)^{-1/2} (2 + 0.24u_{10}^2) \text{ for } u_{10} > 5 \text{ m/s}$$

$$k_w(cm/h) = \left(\frac{Sc(T)}{600}\right)^{-2/3} (2 + 0.24u_{10}^2) \text{ for } u_{10} \leq 5 \text{ m/s}$$

The error propagation for these functions can be calculated as follows:

for $u_{10} > 5$ m/s

$$\Delta k_w(cm/h) = \left(\frac{2}{600}\right)^{-1/2} * \frac{\Delta Sc}{2 * Sc^{3/2}} + \left(\frac{0.24}{600}\right)^{-1/2} * \left(\frac{\Delta Sc}{2 * Sc} + \frac{2 * \Delta u_{10}}{u_{10}}\right) * Sc^{-1/2} * u_{10}^2$$

for $u_{10} \leq 5$ m/s

$$\Delta k_w (cm/h) = \left(\frac{2}{600}\right)^{-2/3} * \frac{2 * \Delta Sc}{3 * Sc^{5/3}} + \left(\frac{0.24}{600}\right)^{-2/3} * \left(\frac{2 * \Delta Sc}{3 * Sc} + \frac{2 * \Delta u_{10}}{u_{10}}\right) * Sc^{-2/3} * u_{10}^2$$

where Δu_{10} is the error associated to wind velocity (± 2.5 m/s) and Δk_w is the calculated error for the air/water transfer velocity.

The concentration of volatile Se (C_{water}^{VSe}) was incorporated into the expression for volatile Se flux to the atmosphere as shown below:

$$Flux = a k_w (C_{water}^{VSe}) * Area$$

where Area is the area of the South Arm of the Great Salt Lake.

The error associated with the volatile Se flux can therefore be determined as follows:

$$\Delta Flux = Flux * \left(\frac{\Delta k_w}{k_w} + \frac{\Delta (C_{water}^{VSe})}{(C_{water}^{VSe})} + \frac{\Delta Area}{Area} \right)$$

where $\Delta C_{water}^{VSe,eq}$ is the error associated with volatile Se concentration (factor of 5.9) and $\Delta Area$ is the error due to the variation in the lake area (± 427 acres per 0.1 stage inaccuracy).

The estimated error associated with k_w is approximately 100%, whereas estimated $\Delta Area$ was only a factor of 1E-3 relative to Area. By far the largest contributor to $\Delta Flux$ is ΔC_{water}^{VSe} for which the geometric standard deviation is 5.9.

The uncertainty range for the volatile Se flux was estimated using confidence intervals. The 95% (2σ) and the 68% (1σ) confidence intervals (Figures 17d and 17e) for the near-surface volatile Se concentration were determined using the logarithms of the volatile Se concentration data obtained from the sinusoidal function (expected data) and the measured data. The anti-log transformed arithmetic mean (of the log transformed data) yielded the geometric mean of the arithmetic data. The ratios of the arithmetic (anti-log transformed) confidence intervals to the geometric mean yielded the geometric standard deviation around this mean. Values of 2σ (geometric) ranged from 2.0 to 3.8 (2.6 average) for the 95% confidence interval; and values of σ (geometric) ranged from 1.4 to 1.8 (1.5 average) for the 68% confidence interval (Figures 17d and 17e).

The geometric standard deviation represents a factor describing the range around the geometric mean. The resulting estimated volatile Se fluxes therefore range (around the mean of 2108 Kg Se/yr) from 820 Kg Se/yr to 5450 Kg Se/yr within the 95% confidence interval, and from 1380 Kg Se/yr to 3210Kg Se/yr within the 68% confidence interval.

3.3 Sedimentation fluxes

3.3.1 Downward sedimentation flux

The mass of sediment that accumulated in the traps over the period of deployment represents the downward sedimentation flux at that location over the period of deployment.

Sedimentation fluxes showed significant spatial variations (Figure 18 a-c and Table 7a). The sediment trap at shallow site (2267) yielded an average downward sediment flux of 2.95 g/cm²/yr for the period 03/23/06 to 06/26/07, which is an order of magnitude higher than any of the other average sediment fluxes measured during that period. The next-highest apparent sedimentation rates occurred at the two deep sites (2565 & 3510, Tables 7b & 7d), which were 0.53 and 0.35 g/cm²/yr, respectively. The shallow sediment traps at sites 2565 and 3510 (Tables 7c & 7e) yielded very low downward sedimentation rates (0.035 and 0.068 g/cm²/yr) that were approximately an order of magnitude below those of the corresponding deep traps.

The high sedimentation rates at shallow site (2267) correspond to its location in a relatively narrow channel between the Promontory Point and Fremont Island near the outlet of the Bear River. The observed peak sedimentation rate in spring corresponds to peak discharge from the Bear River. For this reason, results from this trap are not considered representative of the rest of the lake.

The high sedimentation rates in the deep traps relative to the shallow traps at Sites 2565 and 3510 likely reflect re-suspension and lateral focusing of sediment from the lake bottom, since it is unlikely that it represents increased sediment generation at intermediate depths. Had the material in the deep traps originated from shallower water, it would have also been collected in the shallow traps. This observation indicates significant re-suspension and lateral focusing of lake-bottom sediment. The topic of re-suspension will be further described below.

In terms of temporal variation, all sites showed higher sedimentation rates in spring and early summer relative to late summer and fall (Figure 18 a-c and Table 7a).

The average Se downward fluxes mirror the spatial trends in downward sediment fluxes (Figure 18 and Table 7), where the average downward Se flux at shallow site 2267 (1.44×10^{-6} g Se/cm²/yr) was one to two orders of magnitude larger than those at the deep sites (2565 & 3510, Tables 7b & 7d), which were 1.53×10^{-7} and 3.88×10^{-8} g Se/cm²/yr, respectively. The downward Se flux obtained at the shallow sediment traps at sites 3510 and 2565 yielded 3.18×10^{-8} g Se/cm²/yr and 4.30×10^{-8} g Se/cm²/yr (Tables 7e & 7c).

Regarding temporal variations, peak downward Se fluxes did not correspond to peak sedimentation fluxes (Figure 18), and did not show an apparent correspondence to season. However, the limited data would not be expected to yield a clear trend.

Collected sediment included mineral particles and organic material (e.g. phyto- and zoo-plankton, and brine shrimp). Based on visual inspection, mineral particles dominated the matrix at site 2267, whereas accumulated sediments at the other sites appeared to have mostly organic material. A notable exception occurred at site 2565 in April, 2006 when the matrix was dominated by mineral particles and the sedimentation flux was relatively high.

The downward sedimentation rates will be compared to net sedimentation rates below.

3.4 Permanent sedimentation or net sedimentation

3.4.1 Mass accumulation rates

Mass accumulation rates (MAR) were determined from ^{210}Pb and ^{226}Ra activity changes with depth in the sediment cores. Figure 19 presents a ^{226}Ra profile for site 3510, which is relatively constant in the core profile, whereas the total ^{210}Pb profile decreases with depth. Figure 20 shows the corresponding unsupported ^{210}Pb (^{210}Pb minus ^{226}Ra) profile for site 3510, which decreases exponentially with depth (cumulative sediment mass). This profile was used to calculate the net sedimentation rate as well as the date of the sediment profile.

The slope of the linear regression of Figure 20 determines the MAR. As an example, the permanent sedimentation rate for site 3510 was calculated to be $0.043 \text{ g/cm}^2/\text{yr}$. The MARs in the cores ranged from 0.010 to $0.049 \text{ g/cm}^2/\text{yr}$ with an average of $0.032 \text{ g/cm}^2/\text{yr}$ and two failing to yield sufficient ^{210}Pb activity for use in MAR estimation (Table 9).

Sediment chronologies are shown as a function of depth for site 3510 in Figure 21a. The zone of near-constant ^{210}Pb activity between 0 and 3 cm may reflect a period of increased accumulation or mixing of the sediment due to physical processes, such as episodic re-suspension and re-deposition. Re-suspension is confirmed by the presence of ^7Be at 2 cm depth in the sediment (Figure 21b), indicating that all of the sediment in this interval was exposed to the water column within the past year.

Since the half-life of ^{137}Cs is 26 years, it can be used to confirm the dates obtained with unsupported ^{210}Pb . However, in this case the two methods disagreed. Figure 22 shows poor agreement between unsupported ^{210}Pb and ^{137}Cs , consistent with ^{137}Cs remobilization via desorption of ^{137}Cs from clays by cation exchange for ammonium ions produced during diagenesis. Subsequent diffusion of dissolved ^{137}Cs results in deeper penetration of the radionuclide, and upward migration of the activity maximum (Anderson et al., 1987), which is demonstrated in Figure 22.

In core samples from sites 2267 and 2565, the unsupported ^{210}Pb activities were too low to estimate MAR (Figures 23 & 24). In core 2267, unsupported ^{210}Pb was detected in the upper-most (0-2 cm) interval; whereas no measurable unsupported ^{210}Pb was observed in core 2565. The ^{210}Pb data may be indicative of very low sediment accumulation rates ($< 2 \text{ cm}/100 \text{ years}$ at 2267; and likely much lower at 2565). ^{137}Cs was undetectable by 8 and 6 cm in depth in cores 2267 and 2565, respectively (Figures 25 & 26). The greater depth of measurable ^{137}Cs compared to unsupported ^{210}Pb in these cores is consistent with diagenetic remobilization of ^{137}Cs . ^7Be was detected in the surface interval (0-2 cm) in cores 2267 and 2565, suggesting some resuspension of this interval occurred during the past year. However, the much lower ^7Be activities in these cores relative to core 3510 indicate that resuspension occurs to a much lesser extent in these cores relative to core 3510.

3.4.2 Downward sedimentation vs. net sedimentation

A representative downward sedimentation flux from the shallow sediment traps at sites 2565 and 3510 can be considered to be representative of the main body of the Great Salt Lake. Representative sedimentation fluxes cannot be obtained from site 2267 due to its proximity to the Bear River. Nor can such a flux be obtained from the deep sediment traps at sites 2565 and 3510, due to the influence of re-suspension and lateral focusing. The average sedimentation rate for these two shallow sediment traps is $0.016 \text{ g/cm}^2/\text{yr}$. This value is lower than the net sedimentation rate from the core at site 3510 ($0.043 \text{ g/cm}^2/\text{yr}$), indicating that the net sedimentation rate does not reflect through-fall from the surface. This discrepancy indicates that re-suspension and lateral transport of newly deposited sediment to permanent deposition zones is significant, in agreement with the ^7Be results.

Regarding downward Se sedimentation rate, the single significant value for the shallow sediment trap at site 3510 was $1.19 \times 10^{-8} \text{ g Se/cm}^2/\text{yr}$. This value is smaller than the net Se sedimentation rate from the core at site 3510 ($4.2 \times 10^{-8} \text{ g Se/cm}^2/\text{yr}$). Based on relative overall sedimentation rates, one might have expected the downward Se sedimentation rate to exceed the net Se sedimentation rate at site 3510 (reflecting re-suspension). However, lateral redistribution of Se is expected to occur as a result of re-suspension in the deep brine layer. Recall that Se accumulation in the deep traps at site 3510 was $1.4 \times 10^{-8} \text{ g Se/cm}^2/\text{yr}$, which matches the order of the net Se sedimentation rate ($4.2 \times 10^{-8} \text{ g Se/cm}^2/\text{yr}$).

3.4.3 Estimation of Se removal by sedimentation

Assignment of Se concentration, MAR, and area to qualitative sedimentation zones indicates that about 520 Kg of Se are removed annually by sedimentation. Results of shallow core sedimentation rates overlain on Holocene isopach contours developed by Dr. David Dinter (University of Utah) and Steven Colman (USGS, Menlo Park, CA) are shown on the map in [Figure 27a](#). The geophysical measurements used in the development of these contours are described in Colman et al. (2002). Quantifiable shallow core linear sedimentation rates ranged from 0.02 to 0.67 cm/yr. The linear sedimentation rate for core DD-I was determined to be 95 cm/yr, but is considered an outlier since it is 2 orders of magnitude greater than the remaining 12 quantifiable cores. Seven cores showed negligible ^{210}Pb activity and are interpreted to indicate very low sedimentation rates at these locations (DD-A, DD-D, DD-G, DD-H, DD-K, DD-O, DD-S).

In general, Holocene thickness and sedimentation rates were high along the fault slightly west of the shore of western Antelope Island. East of this line, Holocene thickness decreased dramatically. West of the fault, the sedimentation rates and Holocene thicknesses fell more slowly and continued to decline to the western shore of the south arm of the Great Salt Lake (Dinter, 2007). The contours bounding the zones developed to reflect different sedimentation rates are shown in [Figure 27b](#). In the south basin of the south arm of the GSL, Holocene sediment thicknesses matched relatively well with shallow core results making development of the sedimentation zones straightforward. Areas with sediment thicknesses 2 meters and below consistently

showed insufficient ^{210}Pb to determine a linear sedimentation rate, indicating very low sedimentation. Areas near thicker Holocene sediment (>8 m) such as DD-C and DD-R showed the highest sedimentation rates (0.67 and 0.25 cm/yr respectively). This agreement did not, however, extend to the northwest basin of the south arm. Two shallow cores (DD-I and DD-H) and one deep core (2565) fell within this basin. Holocene sediment thicknesses indicate medium to high sedimentation rates over much of the area for the past ~10,000 years. However, cores DD-H and 2565 did not contain sufficient ^{210}Pb for a sedimentation rate determination. Though the shallow core results for core DD-I indicate that it may be an outlier, the MAR determined from the long core at this location is of similar magnitude to other cores. The discrepancy between Holocene isopach contours and shallow core results may be due to the northwest basin's proximity to the Southern Pacific Railroad (SPRR) causeway. The sedimentation regime of this basin has likely been altered since construction. Since the shallow cores more closely represent contemporary sedimentation, Thiessen polygons were developed for the basin bounded on the west by the SW-NE trending Carrington Fault (Colman, 2002). The Thiessen polygon surrounding core DD-I was designated as a "very high" sedimentation zone. The polygons surrounding cores DD-H and 2565 were designated as "very low" sedimentation zones and grouped together. Overall, the qualitative "very low" sedimentation zone had the largest area, with areas decreasing with each increasing step in sedimentation rate.

The average Se concentration in each sedimentation zone was determined by averaging the Se concentrations in the 0-2 cm interval (e.g. Figure 27c) for all cores falling within each zone. The average salinity corrected Se concentrations from 0-2 cm in the 8 cores are shown in Table 8. The concentrations ranged from 0.79 to 3.02 $\mu\text{g/g}$ with an average of 2.01 $\mu\text{g/g}$. Though an MAR for cores 2565 and 2267 could not be determined, the Se concentrations in the upper 2 cm of these cores were still used because they represent the Se concentration of the most recent sediment deposited in these locations. The Holocene thickness-based "very high SE" sedimentation zone did not contain any cores, and so was assigned a Se concentration based on that in the "high" sedimentation zone, as described below.

Average mass accumulation rate (MAR) in each zone was determined by interpretation of the MAR results from the deep cores (Table 9). MARs in the "medium," "high," and "very high NW" zones were found by averaging the cores that fell within them. The MAR for the "low" sedimentation zone was calculated by averaging the two cores with sufficient ^{210}Pb activity (DD-Q and 3510) with a sedimentation rate of zero for core 2267 (based on insufficient ^{210}Pb indicating very low sedimentation rate) – yielding an average MAR of 0.018 $\text{g/cm}^2/\text{yr}$. The "very low" sedimentation zone did not contain any cores with sufficient ^{210}Pb activity to estimate a MAR. Therefore, the representative MAR for this zone was estimated to be a factor of 2 below the value for the "low" sedimentation zone. The MAR for the "very high SE" sedimentation zone was estimated as 0.049 $\text{g/cm}^2/\text{yr}$, 25% higher than the "high" zone value. This value is also consistent with the representative MAR for the "very high NW" zone.

Table 10 show the Se concentration, MAR, area, and calculated mass of Se removed annually within each sedimentation zone. Results indicate that about 520 Kg of Se are permanently removed from the Great Salt Lake by sedimentation each year.

3.4.3.1 Estimating uncertainty in Se removal by sedimentation

In order to estimate uncertainty in the mass of Se removed by sedimentation, an uncertainty was determined for each step in the sedimentation removal calculation. These steps involved determining the representative sediment Se concentration for each qualitative sedimentation zone, the representative mass accumulation rate (MAR) for each zone, and the area of each zone. For the Se concentration and MAR determinations above, 2.6 in-diameter cores were used to represent the 5 zones with a total area of 2080 Km². The strength of this extrapolation (i.e. the greater number of cores in each zone, the stronger the confidence in the value) is incorporated into the uncertainty calculations as described below.

3.4.3.1.1 Estimating uncertainty in Se concentration

Uncertainty in the annual Se mass removed by sedimentation was determined by estimating uncertainty for, and propagating uncertainty through, each step in the Se removal calculation. These steps involved determining the representative sediment Se concentration, mass accumulation rate (MAR), and the area for each qualitative sedimentation zone. For the Se concentration and MAR determinations above, 2.6 in-diameter cores were used to represent the 6 zones with a total area of 2083 Km². The strength of this extrapolation (i.e. the greater number of cores in each zone, the stronger the confidence in the value) is incorporated into the uncertainty calculations as described below.

Uncertainty in representative Se concentration for each zone was determined. Eight cores were used to describe the area of the south arm of the Great Salt Lake. In each core, the top 2 cm were sliced into 1 or 2 slices and analyzed for Se content. These concentrations were corrected for salinity as described above. Since uncertainty was not determined by the laboratory for Se concentrations in these samples, and since no replicate analyses were made, the uncertainty was estimated as 2 times the reporting limit (RL) for each core slice, and the uncertainties for each slice were propagated into an uncertainty in Se concentration for the core as shown, for example, for core DD-Q:

$$\sigma_{DD-Q} = \sqrt{\sigma_{0-1cm}^2 + \sigma_{1-2cm}^2} = \sqrt{0.4^2 + 0.4^2} = 0.57 \text{ mg/Kg}$$

where σ_{DD-Q} is the estimated uncertainty of the average Se concentration in the top 2 cm of the core and σ_{x-y} is the uncertainty in the Se concentration in the slice of the core from depths 0 to 1 or 1 to 2 cm.

The Se concentrations in the top 2 cm of cores that fall within a single sedimentation zone were averaged together to find the representative Se concentration for that zone. For example, the “low” sedimentation zone calculation of uncertainty in Se concentration is:

$$\sigma_{\text{low}^{\text{Avg}}} = \sqrt{\sigma_{2267}^2 + \sigma_{DD-Q}^2 + \sigma_{3510}^2}$$

$$\sigma_{\text{low}^{\text{Avg}}} = \sqrt{0.8^2 + 0.57^2 + 1.13^2} = 1.50 \text{ mg/Kg}$$

where $\sigma_{\text{low}^{\text{Avg}}}$ is the uncertainty associated with averaging the Se concentration values that fall within the “low” sedimentation zone.

The uncertainty in the sediment Se concentration for the entire lake is estimated as the relative standard deviation of all cores:

$$RSD_{\text{Lake}} = \frac{\sigma}{\bar{x}} \times 100\% = \frac{0.86}{2.01} \times 100\% = 43\%$$

where RSD_{Lake} , σ , and \bar{x} are the relative standard deviation, standard deviation, and mean of the 8 cores respectively. This is used as the background uncertainty of the entire dataset because it represents the uncertainty if the sedimentation zones described above had not been developed. These zones, though qualitative in nature, were developed to increase confidence in the estimation of Se removal by recognizing the spatial variation in sedimentation rates as controlled by lake bottom topography.

The RSD for each zone was developed from RSD_{Lake} by comparing the number of cores contributing information for the area. The 8 cores in the 2083 Km^2 lake yield an area/core ratio of 260 Km^2 of lake area per core. Division of RSD_{Lake} by this value, and multiplication of the quotient by the ratio of the zone area to the number of cores in that zone yielded the RSD for each zone. The RSD for the qualitative “low” sedimentation zone (420.9 Km^2) is shown below as an example:

$$RSD_{\text{low}^{\text{ext}}} = \frac{43\% \text{ RSD}_{\text{Lake}}}{260.4 \text{ Km}^2/\text{core}} \times \frac{404.6 \text{ Km}^2}{3 \text{ cores}} = 22\%$$

The high area/core ratio in the “low” zone relative to that of the entire lake serves to decrease the uncertainty from the background of 43%; whereas a zone with a lower area/core ratio would have a higher RSD than 43%. This process is applied to all of the sedimentation zones, with the exception of the “very high SE” zone because no cores fell within it. The uncertainty of the “high” sedimentation zone is applied to the “very high” zone.

To combine the uncertainties associated with Se concentration to those associated with extrapolation to larger areas, the RSDs are converted back to standard deviations, which are then combined as shown above. This error propagation process was repeated for each core and sedimentation zone.

Uncertainty in mass accumulation rate for each zone was determined by a similar method as Se concentration. However, due to the method of analysis of ^{210}Pb decay (use of the slope of the trendline of the natural logarithm of unsupported ^{210}Pb), standard deviation errors for unsupported ^{210}Pb could not be propagated directly through to the final MAR value for each core. In order to determine the error associated

with the MAR determination in each core, a Monte Carlo method was implemented by randomly generating an unsupported ^{210}Pb value in each core slice using the laboratory reported unsupported ^{210}Pb value as the mean and the 1-sigma uncertainty as the standard deviation. This was performed in Microsoft Excel using the NORMINV function paired with RAND(), which generates a random value between 0 and 1. The NORMINV function reads the RAND() value as a percentile based on the defined mean and standard deviation. For example, a mean of 2 and a standard deviation of 1 would be input as NORMINV(RAND(),2,1). If the RAND() value was 0.16, the output of the function would be 1 standard deviation below the mean (16th percentile) yielding a value of 1. This approach was applied to each core slice to randomly generate a new unsupported ^{210}Pb profile, from which the slope of the linear trendline (using the SLOPE function) of the natural logarithm was determined and converted into an MAR. The process was repeated 10,000 times for each core. The uncertainty in MAR for each core was then defined by the standard deviation of the 10,000 MAR results. Figure 27d shows the convergence of the standard deviation of MAR as a function of the number of MAR values included. The standard deviations from different sized populations (10, 20, 50, 100, etc.) were determined for 10 different randomly chosen populations among the 10,000 MAR results. From this plot we observe that the range in estimated standard deviations converges to a constant after several hundred values; hence, we conclude that 10,000 repetitions is sufficient for representing the uncertainty in MAR for each core.

The process described for Se concentration above, propagating the uncertainty for each core to the average of the cores within a zone and then incorporating the uncertainty due to the extrapolation, was also followed for MAR uncertainty. Two cores (2565 and 2267) did not have an associated standard deviation because no MAR could be reported. In core 2565 representing the “very low” sedimentation zone, an uncertainty of 100% or 0.009 g/cm²/yr was assigned. This uncertainty was assigned in order to incorporate the interpreted MAR of the core (0 g/cm²/yr) with the assigned MAR for the zone (0.009 g/cm²/yr). Though an MAR of zero is assigned to core 2267, an uncertainty of 0.009 was assigned to this as well to be consistent with the uncertainty for 2565. The RSD of the “high” sedimentation zone (12.5%) was assigned to the “very high SE” sedimentation zone because no cores fell within this zone.

Uncertainty in the areal extent of each sedimentation zone was determined. The uncertainty associated with the areal extent of the lake is 1.73 Km² due to a 0.03 m stage inaccuracy in the USGS gage for lake elevation. This uncertainty was translated into uncertainties for the areal extent of each sedimentation zone by the equation:

$$\sigma_{\text{zone area}} = \text{Area}_{\text{zone}} \times \frac{\sigma_{\text{lake area}}}{\text{Area}_{\text{lake}}}$$

where $\sigma_{\text{zone area}}$ is the uncertainty in the areal extent of each zone and $\sigma_{\text{lake area}}$ is the uncertainty in the area of the entire lake, 1.73 Km².

With uncertainties established for the sediment Se concentration, MAR, and area in each zone, the uncertainty of the mass of Se removed by sedimentation was calculated.

The uncertainty was converted into a relative standard deviation for each factor in calculating the mass of Se removed:

$$RSD = \frac{\sigma}{\bar{x}}$$

where RSD is the relative standard deviation, σ is the uncertainty, and \bar{x} is the average value within each zone. This process was done for Se concentration, MAR, and areal extent for each sedimentation zone.

The RSDs were then propagated through to the mass of Se removed in each zone and converted back into an uncertainty:

$$RSD_{\text{mass removed}} = \sqrt{RSD_{[Se]}^2 + RSD_{MAR}^2 + RSD_{area}^2}$$

$$\sigma_{\text{mass removed}} = RSD_{\text{mass removed}} \times \text{Mass}_{\text{Se removed}}$$

where $\sigma_{\text{mass removed}}$ represents the uncertainty in the mass of Se removed for a particular sedimentation zone. [Table 11a](#) shows the RSD and $\sigma_{\text{mass removed}}$ values for each sedimentation zone.

Since the masses of Se removed in each zone are summed to determine the mass removed for the lake, the $\sigma_{\text{mass removed}}$ values for each scenario are propagated to define the uncertainty range:

$$\sigma_{\text{total mr}} = \sqrt{\sigma_{\text{"very low" mr}}^2 + \sigma_{\text{"low" mr}}^2 + \sigma_{\text{"medium" mr}}^2 + \sigma_{\text{"high" mr}}^2 + \sigma_{\text{"very high" mr}}^2}$$

where “mr” stands for mass removed and $\sigma_{\text{total mr}}$ is the uncertainty of the total mass removed. The result is a possible range between about 45 and 990 Kg Se per year, with about 520 Kg representing the mean estimate. [Table 11b](#) shows the propagation of uncertainty from the $RSD_{\text{mass removed}}$ for each zone to the final range of uncertainty of Se mass removed by sedimentation.

3.4.4 Sediment trace element analysis

Trace element concentrations as a function of depth at site 3510, show maxima at a depth of several cm ([Figure 28](#)). In contrast, trace elements concentrations at the two other sites analyzed show maximum values near the surface ([Figures 29 & 30](#)). The trace elements that show increased concentrations near the sediment surface are those expected from mining activities and urban development. These increases in the top 10 cm correspond to development of the basin (past 100 years), according to the chronology from site 3510. However, diagenetic changes may have influenced the concentration-depth profiles such that historical trends may not be accurately recorded ([Callendar, 2000](#)).

3.5 Re-suspension – Re-solubilization

3.5.1 Temperature stratification

3.5.1.1 Seasonal trends

Temperature in the water column of the Great Salt Lake varies seasonally with highest temperatures observed in summer and lowest in the winter (Figures 31a & b). At sites 2565 and 3510 (Figure 1) the water column is stratified due to the presence of the deep brine layer. During the summer the deep brine layer was cooler than shallow brine layer and reversed in the winter when the deep brine layer was warmer than the shallow brine layer (Figures 31a & b).

Periodic events punctuate the record of temperature stratification when temperatures equilibrate to a single value across the measured depth of the water column (Figure 31c). At least eight of these equilibration events occurred during the 6-month period of observation from June to December 2006. From January through June 2007 at least six temperature equilibration events were recorded. Five of the events at site 2565 during that 6-month period occurred within a ten day period during the month of April (Figure 31c). Equilibration events ranged in duration from 12 to 24 hours. All significant equilibration events were associated with wind speeds greater than about 30 mph (e.g., Figures 32 a & b), signaling that wind speed drove the equilibration process. The wind direction may also influence the temperature equilibration process as indicated by the muted response at site 3510 relative to site 2565 to the increase in wind speed on October 16th. A change in wind direction from 250 to 360 (or zero) degrees yielded a strong temperature equilibration response at site 3510 (Figure 32b), indicating that this northerly wind yielded great influence at site 3510 relative to the westerly wind. The different responses of the two sites are likely related to their being located in two different sub-basins in the south arm of the Great Salt Lake, as shown by the bathymetric map (Figure 1).

3.5.1.2 Lake Mixing

3.5.1.3 Langmuir circulations

Temperature equilibration events in the water column may represent genuine mixing of the deep and shallow brine layers. One means of achieving this vertical mixing is Langmuir circulation (Wetzel, 2001), which involves helical advection within the water column in response to wind shear. The diagnostic feature of Langmuir circulation is longitudinal streaks oriented with the dominant wind direction.

At wind velocities of 2-7 m/s or greater, streaks of aerated water and floating materials are observed at the water surface (Wetzel, 2001). The spacing between streaks is proportional to the depth over which helical circulation occurs (mixing depth). Assuming symmetric helical cells, mixing depth is equal to half of the distance between adjacent streaks.

3.5.2 Seiche

An internal seiche may result from the wind loading of water in response to atmospheric pressure changes. The loading of water forces the displacement of water at depth, producing an internal wave that may be transmitted across the water body. In a stratified system, deeper layers of the water column may be temporarily displaced in the zone of the internal wave. Displacement of the anoxic deep brine layer may put oxic shallow water in contact with sediment that was previously anoxic. This change in redox potential may cause the release of trace metals back into the water column.

3.5.3 Mechanism of temperature equilibration events

Langmuir circulation is a candidate mechanism to drive actual mixing of the water column. The maximum depth of the water column in the south arm of the Great Salt Lake is about 9 m. In order to mix the water column to this depth, the spacing between Langmuir circulation-produced surface streaks would need to be 18 m. Streaks associated with Langmuir circulations have been observed on the Great Salt Lake in this study and have been previously documented (Stommel, 1951). Although to our knowledge no quantitative measurements of streak spacing have been performed on the Great Salt Lake, observed streak spacing was qualitatively consistent with magnitude needed to mix the deep brine layer. Such mixing depths have been observed in lakes of much smaller areal extent. Maximum mixing depth observed at Lake George, NY was between 10 and 15 m (Langmuir, 1938).

If the temperature equilibration events represent true mixing of the entire water column, one would expect the final temperature to reflect mixing of the initially stratified water column temperatures. The final temperature calculated using the thermal mixing approach for an equilibration event on June 14, 2006, yields 19.7°C. The measured temperature during this event remained near 21°C (Figure 32a), suggesting that actual mixing of the entire water column did not occur.

The nature of the temperature equilibration events, in terms of time passed during equilibration and re-stratification of temperature; can also be used to deduce the mechanism. The response of temperature was rapid, with equilibration often occurring over periods less than an hour. For example, on June 14, 2006 at site 2565, the temperature of the deepest thermistor increased from 17°C to 21°C (temperature of shallow thermistors) over the 70-minute period from 02:27 to 03:39 MDT (Figure 32a). The termination of temperature equilibration and return to stratified temperature conditions also occurred over short time periods (Figures 32 a & b).

Another clue to the mechanism of temperature equilibration is provided by the observation that equilibrated temperature was always that of the shallow brine layer regardless of which layer (shallow or deep brine) was warmer. This observation indicates that temperature equilibration occurred via displacement of the deep brine layer, which is an effect that is consistent with a seiche-driven internal wave. Historical evidence of surface seiche activity has been documented on the south arm of the Great Salt Lake (Lin, 1977). Increase in the lake level at the north end of the lake (Promontory Point) corresponds with a decrease in lake level at the south end of the

lake (Silver Sands) following a strong wind event (Figure 33a). Ranges in the magnitude of the lake level change associated with a seiche event vary with distance across the lake (Figure 33b).

Evidence of surface seiche activity on the lake was recorded at the USGS Saltair Gauge for both temperature equilibration events discussed above. Gauge elevation increased from 0.5 ft to 1 ft after a wind event, and elevation oscillated after initial surge about the initial lake elevation value (Figures 31c, 34a and 34b). The duration of the period over which lake elevation oscillated significantly was similar to the duration of the period over which temperatures responded and periodically equilibrated to the shallow brine temperature. Furthermore, the timing of individual complete temperature equilibration events corresponded to peaks in the lake elevation oscillations, demonstrating a strong relationship between lake elevation oscillation and temperature equilibration. This indicates that loading of water at the surface of the lake induced an internal seiche that displaced the deep brine layer as it passed.

Assuming that the period of an internal seiche corresponds to the period of temperature equilibration, a comparison can be made between the estimated period of an internal seiche and the period of temperature equilibration. The observed duration of temperature equilibration events was sometimes long; for example, the June 14, 2006 equilibration event included a 24-hour period of complete equilibration. This long period of equilibration is similar to what is predicted by the expression for the period of a uninodal internal seiche, which is 25.6 hours for a 40-Km length corresponding to the basin south of the submerged ridge of the Carrington fault. Obviously the actual seiche may not be uninodal, and so the estimated period is based only on a simplified approximation. Another aspect of the temperature equilibration events that is suggestive transmission of an internal wave is the oscillation between complete equilibration and partial stratification that was observed during the temperature equilibration events discussed above. For example, during October 17 and 18th, 2006, site 3510 showed several of these oscillations that corresponded approximately to a 6-hour period. This period was far smaller than the estimated period of an idealized seiche; however, the oscillatory nature of these events was consistent with the transmission of an internal wave.

3.5.4 Batch equilibration tests

Total Se concentrations in bed sediment samples were analyzed at LET and the University of Utah, and results showed good correlation (Figure 35a). The average Se concentration for the 30 samples analyzed was 1.0 ± 0.30 mg/Kg (LET) and 1.24 ± 0.22 mg/Kg (University of Utah).

Following 24 hours of contact between the bed sediments and the shallow brine water, the resultant Se concentration in water varied among the sediment samples, with the highest concentrations found in samples with air headspace.

Percent Se solubilized (of extractable) varied spatially with no discernable pattern (Figure 35b). The average percent Se solubilized in the samples with nitrogen gas headspace was $1.18 \pm 0.68\%$, whereas the average percent Se solubilized in the

samples with air headspace was $1.16 \pm 1.36\%$. The maximum percent solubilized was from site GS 11 composite with air headspace at 6.07% (Figure 36).

Solubilization of Se into the water column due to equilibration of anoxic sediment with shallow brine layer may occur periodically, in response to wave-induced sediment re-suspension and seiche-driven displacement of the deep brine layer. The significance of these events to Se concentration is demonstrated by an example scenario based on observed sediment re-suspension into the sediment traps. Since approximately 1 g of sediment is periodically re-suspended into the sediment traps (3.6 cm radius), a 3.6-cm column of water can be expected to equilibrate with 1 g of sediment. Assuming that the equilibrated column of water is 4 m in height, the resulting additional Se concentration from equilibration with anoxic sediment is:

$$Se_{add} \left(\frac{ig_{solubilized}}{L} \right) = \left(\frac{1.31 ig_{extracted}}{g_{sed}} \right) \left(\frac{0.1476 ig_{solubilized}}{2.4340 ig_{extracted}} \right) \left(\frac{1 g}{\pi(0.036 m)^2 (4 m)} \right) \left(\frac{m^3}{1000 L} \right)$$

$$Se_{add} = 0.0049 \frac{ig_{solubilized}}{L}$$

Where: Se_{add} is the additional Se concentration in the water column ($\mu\text{g/L}$); Se_{sed} is the concentration of Se in the sediment ($\mu\text{g/g}$); Se_{ratio} is the amount of Se solubilized in the batch test divided by the amount of Se extracted during sediment digestion ($\mu\text{g}/\mu\text{g}$); w is the weight of sediment in deep sediment trap (g); r is the internal radius of a sediment trap tube (m); and h is the height of the water column over which the Se from the sediment is mixed (m).

The resultant additional Se concentration from site GS 11 is 0.0049 $\mu\text{g/L}$, which is a negligible value compared to aqueous Se concentrations measured in the lake. Site GS 11 represents the greatest potential for additional concentration based on batch test measurements. The average additional Se concentration contribution for samples with either air or nitrogen headspace is 0.0009 $\mu\text{g/L}$. Reduction of the equilibrated water column length by a factor of 10 (0.4 m) would still yield negligible additional Se concentration. The contribution from re-suspension is therefore not likely to significantly increase the concentration of Se of the water column.

Solubilization of Se into the water column may also occur in response to shrinking of the deep brine layer, since anoxic sediment present under the deep brine layer may be put into direct contact with oxic shallow brine water when the extent of the deep brine layer decreases. Lake level decreased from 4198.0 ft in June, 2006 to 4196.5 ft in September, 2006 (Table 12). During this period, the thickness of the shallow brine layer remained constant (as measured at sites 2565 and 3510); whereas the deep brine layer thickness decreased by 1.5-ft (Figure 6). This decrease in deep brine layer extent corresponds to exposure of 23,775 acres of anoxic sediment to oxic shallow brine layer water, based on bathymetric data (Baskin, 2005). The thickness of the deep brine layer depends on the dynamics of the bi-directional flow through the Pacific Railroad causeway. Loving et al. (2002) pointed out the parameters that affect the thickness of the deep brine layer in the following equation to calculate the altitude of the deep brine interface:

$$\text{Altitude of the interface} = ES - \Delta H * \frac{\rho_s}{\rho_n - \rho_s}$$

where: ES is the south arm lake elevation, ΔH is the head difference between the south and north arm surface elevations; and ρ_n , ρ_s are the densities in the north and south arm, respectively.

Se flux from the sediment may be influenced by the conditions of the overlying water (Byron and Ohlendorf, 2006). Anoxic conditions (DBL) would favor low redox values that would promote Se retention in the sediment while oxygenated conditions would have the opposite effect and release Se into the overlying water (Massecheleyn and Patrick, 1993).

The potential solubilization of Se from anoxic sediment into shallow brine layer water was examined in batch tests where 15 g shallow brine layer water were equilibrated with 7.5 g anoxic sediment (including pore water, taken from the top two cm) for periods ranging from one week to one month, (with daily shaking for 5 min). Samples from 8 different Great Salt Lake locations consisting of 8 composite samples and one ooze sample were tested.

Se mass released from sediment to water varied spatially with no distinct spatial pattern (Figure 37a). The amount of Se released during the week long experiment was $0.05 \pm 0.03 \mu\text{g}$. Se mass released in the batch test samples over a month of equilibration was $0.06 \pm 0.03 \mu\text{g}$ per 7.5 g sediment. The corresponding percent Se solubilized (of extractable) was $2.40 \pm 1.09\%$ for the week long test and $3.01 \pm 1.06\%$ for the month long test (Figure 37b).

The corresponding Se input to the lake (Kg_{Se}) over a period of a month can be calculated if one assumes a maximum depth in the sediment from which Se is solubilized. Here, we assumed this depth to be 2 cm, which yields a 1.44 cm^2 area (for 7.5 g sediment) for a sediment bulk density of 1.6 g/cm^3 :

$$\text{Kg}_{\text{Se}} = \frac{0.06 \text{ } \mu\text{g}_{\text{solubilized}}}{2.34 \text{ cm}^2} (23,775 \text{ acres}) \left(\frac{4.05\text{E}7 \text{ cm}^2}{1 \text{ acre}} \right) \left(\frac{\text{Kg}}{10^9 \text{ } \mu\text{g}} \right)$$

$$\text{Kg}_{\text{Se}} = 24.7 \text{ Kg}$$

Although this 24.7 kg load is not dominant, it is significant. Furthermore, there may be multiple such loads annually, and the estimate is based on batch equilibration tests reflecting a 2:1 ratio of water to sediment conducted over a period of one month; whereas the larger water:sediment ratios and longer equilibration times in the field may yield larger Se inputs.

Results for trace metals other than Se are given in Table 13. Several elements show negative % solubilized (of extractable) indicating that the element may have precipitated out of the water into the sediment due to change in oxidation state.

3.6 Mass balance

The total Se mass in the Great Salt Lake calculated for May 2006 was 4780 Kg. Of that, 3190 Kg (66.6%) was dissolved ($< 0.45 \mu\text{m}$) and 1596 Kg (33.4%) was bound to particulates ($> 0.45 \mu\text{m}$). In July 2007, the total Se mass in the lake water column was 7680 Kg, of which 6230 Kg (81.2%) was dissolved, and 1440 Kg (18.8%) was bound to particulates. These example values demonstrate that about 20% to 30% of Se mass in the water column of the Great Salt Lake was associated with particulates. For the sake of mass balance, we consider the total Se concentration, thereby including dissolved and particulate forms in our analysis below.

According to the loading report (Naftz et al., 2007), about 1,480 Kg Se/yr are introduced to the south arm of the Great Salt Lake annually (dissolved plus particulate). Given the present volume of the Great Salt Lake, a Se concentration of $15 \mu\text{g/L}$ would result from just 100 years of loading if Se were conservative. Clearly, given the $\sim 10,000$ year history of the lake, removal mechanisms (e.g., sedimentation, volatilization, and brine shrimp harvest) have influenced the observed concentration towards the present observed average concentration of $0.49 \mu\text{g/L}$.

The most significant contribution from the resolubilization-resuspension analysis was 25 Kg from shrinkage of the deep brine layer. Whether this represents a new load is debatable; however, we include it in our mass balance calculation below as a new load since this magnitude is inconsequential.

The brine shrimp industry removed 16.6 million pounds of cysts and *Artemia* biomass over the 2006-2007 season (Marden, 2007). A characteristic industry estimate is 23% dry yield for the commercial harvest (Marden, 2007). The range of average tissue selenium concentrations were $1.18 \mu\text{g/g dw}$ (Marden, 2007) to $5.7 \mu\text{g/g dw}$ (Conover, 2007). The resulting range in Se mass flux via the brine shrimp harvest is from 9.9 to 48 Kg/yr.

The fluxes of Se out of the south arm of the Great Salt Lake were estimated to be: 1) a permanent sedimentation flux of 520 Kg/year (arithmetic mean); 2) an integrated volatilization flux of 2108 Kg/yr (geometric mean); and, 3) Se flux via brine shrimp harvest of 28 Kg/yr in 2006-2007 (intermediate value from above). These loss fluxes total to 2656 Kg/yr. The mean volatile and mean permanent sedimentation Se fluxes are 79% and 20%, respectively, of the overall Se removal flux based on the above estimates (Figure 38). The loss flux (2656 Kg/yr) exceeds the estimated loading ($1,480 + 25 \approx 1500$ Kg/yr). The flux estimation indicates that the annual Se losses more than balance the Se loads, with the larger loss mechanism being volatilization. The results demonstrate that sedimentation is a relatively minor mechanism of Se removal from the Great Salt Lake, and that most Se removal occurs via volatilization.

Given that two parameters (sedimentation and volatilization fluxes) vary over three values (low, medium, high) for a 68% confidence interval, there are eight (2^3) possible scenarios that can represent the range of possible conditions. To simplify, we show the percentage distribution corresponding to particular scenarios, where the low or high values of both parameters (sedimentation and volatilization fluxes) coincide (Table 14a and Figure 38).

Assuming that the Se loss flux basically balances the loads (about 1500 Kg/yr), then the residence time of Se in the Great Salt Lake ranges from about 3 to 5 years, based on the observed range of 4780 Kg to 7680 Kg Se mass in the Great Salt Lake during the course of the study.

As shown in Figure 7, and as described in the loading report (Naftz et al., 2007), the aqueous Se concentration in the Great Salt Lake increased by an amount ranging from 0.16 to 0.34 $\mu\text{g/L}$ during the period of observation (May 2006 to July 2007). This observation was based on Se concentrations analyzed using hydride generation (Frontier Geosciences), which was the primary analytical method used in this project. Below, we discuss these concentration trajectories relative to expectations from mass balance. We also consider the concentration trajectories determined using collision cell ICP-MS (University of Utah).

The concentration trajectories of total Se (dissolved plus particulate) over the course of the study were explored by integrating the total Se concentration over time via the following mass balance:

$$[\text{Se}]_t = [\text{Se}]_{t-1} + \frac{[\text{Se}_{load} - \text{Se}_{volatilization} - \text{Se}_{\text{permanent sedimentation}} - \text{Se}_{\text{brine shrimp harvesting}}]}{\text{Volume}}$$

where $[\text{Se}]_t$ and $[\text{Se}]_{t-1}$ represent the total Se concentration in $\mu\text{g/L}$ for the present and previous time steps, respectively; Se_i ($i = \text{load or removal process}$) represents the mass flux (loading or removal) per unit time; and Volume represents the volume of the lake. The mass balance was determined from May 19, 2006 to August 1, 2007 using daily values of fluxes (loads and removal processes). The daily values for loads and volatilization were determined as described in Naftz et al. (2007) and this report, respectively; whereas the daily values for permanent sedimentation and brine shrimp harvest were determined by division of the annual values by 365. Daily values of surface area and volume of the Great Salt Lake, for the same period, were obtained from the USGS National Water Information System (<http://waterdata.usgs.gov/nwis>).

The trend in total Se concentration, without inclusion of removal processes (Figure 39), showed an increase during the time period of the investigation, with the final estimated total Se concentration (0.64 $\mu\text{g/L}$) nearly matching the measured value in July, 2007 (0.75 $\mu\text{g/L}$ = average of the four sites). Addition of the removal processes (volatilization, permanent sedimentation and brine shrimp harvesting), yielded decreases in the estimated total Se concentration during the time period of the investigation (Figure 39). For the mean fluxes of volatilization and permanent sedimentation, the final estimated total Se concentration was (0.32 $\mu\text{g/L}$), which was low (by about 0.43 $\mu\text{g/L}$) relative to the measured value in July, 2007 (Figure 39). For the low fluxes of volatilization and permanent sedimentation, the final estimated total Se concentration was (0.47 $\mu\text{g/L}$) somewhat below (about 0.28 $\mu\text{g/L}$) the measured value in July, 2007. These results suggest that the actual volatilization flux is in the low end of the spectrum of estimated values.

Assuming conservative behavior of Se, Naftz et al. (2007) calculated the existence of an unmeasured load of approximately 1350 Kg/yr (1500 Kg during the 15-month period of study). Potential source(s) of the unmeasured Se load that were previously described by Naftz et al. (2007) include: (1) submarine groundwater discharge; (2) wet and dry atmospheric deposition falling directly on the lake surface; (3) lake sediment release into the overlying water column; and (4) poorly characterized exchange with the north arm, as described in the report regarding Se loads to the Great Salt Lake.

For all measurements made during this flux study, the dissolved volatile Se concentrations increased with depth, demonstrating that the dissolved volatile Se flux was outward (to the atmosphere) for all measured periods. However, this observation does not preclude the possibility that the total Se concentration increased with depth, since the dissolved volatile Se concentration comprises only 0.1% of the total aqueous Se concentration. Furthermore, it is possible that the near-surface Se concentration gradient differs during precipitation events, which could not be measured due to logistical limitations.

Estimated values of atmospheric Se deposition for several global sites are presented in Table 15. A highly speculative literature-based estimate of dry deposition for the Great Salt Lake ($162.67 \mu\text{g}/\text{m}^2/\text{yr}$) was developed by averaging estimated dry deposition at the Great Lakes and Chesapeake Bay. This estimated dry deposition flux yields an estimated atmospheric load of 300 Kg/yr.

When atmospheric deposition (300 Kg/yr) was included in the trajectory simulations using the low values of the estimated volatilization and sedimentation fluxes, the final estimated Se concentration was $0.68 \mu\text{g}/\text{L}$ (Figure 40), which was approximately $0.07 \mu\text{g}/\text{L}$ below the measured value. This suggests that the observed trajectories can be explained by a combination of unmeasured loads and removal fluxes that correspond to the low end of the estimated range.

As mentioned before, data from ICP-MS analysis of Se analyzed at the University of Utah (Figure 7e and 7f) did not show the strong increase in Se concentration during the course of the study that was demonstrated in the HG-AF analyses. The difference in the observed trends may represent analytical errors associated with the different methods used. In hydride generation, the analyte is removed from the confounding matrix (via exsolution as a gas) prior to analyses, whereas in collision cell ICP-MS, the analyte is removed from its confounding matrix (via kinetic attenuation of the non-analyte ions) just prior to detection. The data quality for both methods is high (Figure 42), showing good to excellent spike recoveries (Figure 42, top). Notably, the spike concentrations used to evaluate the ICP-MS data quality were much more challenging (0.03 to $2.0 \mu\text{g}/\text{L}$ range) than the spike concentrations used for HG-AFS (1.0 to $30 \mu\text{g}/\text{L}$ range). The lesser number of samples analyzed via ICP-MS, and somewhat greater scatter in results, yield lower confidence in the ICP-MS trend relative to the HG-AF trends.

The concentration trajectories of trace metals (other than Se) may provide perspective regarding the Se trajectories. Elements such as As, Sb, Mo, U, Ba and Mn showed total (RA) and dissolved (FA) concentrations that were slightly higher in summer-fall and

lower in winter-spring (Figures 42 and 43). Al and Fe showed dramatic increases in total (RA) concentration during winter-spring (Figures 42 and 43). These observations indicate that the trends in the trace elements may be influenced by both evaporative concentration and geochemical processes. The apparent cyclical nature of the trace element concentrations contrasts against the apparent monotonic increase in Se concentration during the course of the study. Clearly additional monitoring of Se concentrations is warranted to determine longer term trend in Se concentration.

3.7 Variability

The mass balance section necessarily simplified the characteristics of the Great Salt Lake in order to allow the development of a simple mass balance. In reality, the Great Salt Lake is neither vertically nor areally homogenous.

Data presented above speak to the vertical heterogeneity, that is, the density stratification of the lake. The denser Deep Brine Layer of the Great Salt Lake is anoxic, and is therefore geochemically distinct from the oxic Shallow Brine Layer. The dynamics of the Deep Brine Layer, and its influence on Se, as well as other trace metal and metalloid cycling, needs to be better understood. The evolution of the Deep Brine Layer from its origin at the north arm to its apparent assimilation via mixing at the south end of the lake needs to be investigated in order to understand the time and space scales over which anoxia occurs, and over which oxidized trace metals and metalloids are reduced to other forms. With this understanding, it may be possible to design strategies to mitigate negative influences of the Deep Brine Layer on the cycling of particular trace metals (e.g. Hg).

The measured volatile Se concentrations in the water column demonstrate vertical variation, where a distinct increase in volatile Se concentration with depth was observed in the Shallow Brine Layer (Table 5 and Figure 15a); whereas no such trend was observed in the Deep Brine Layer (Table 5 and Figure 15b). This trend may implicate phytoplankton as the generators of volatile Se. The trend seems to be more clearly established for the shallow sites (2267 and 2767), possibly suggesting the bioherms as an important source of volatile Se, or possibly suggesting the importance of proximity to labile carbon sources such as the Bear and Weber rivers and Farmington Bay.

The measured downward sedimentation fluxes (Table 7 and Figure 18) demonstrate that areal variability exists with respect to downward sedimentation in the Great Salt Lake. Site 2267 in the Bear River Strait showed downward sedimentation values that were one to two orders of magnitude higher than sites 3510 and 2565. Temporal variability is also evident with orders of magnitude higher downward sedimentation fluxes during spring and summer relative to fall and winter. The higher downward sedimentation flux in the Bear River Strait is likely due to its proximity to the Bear River, which is the presumed source of the corresponding particulates.

As shown in the Naftz et al. (2007) report, the total Se concentration increased over the course of the study. This increase was also observed in the dissolved ($< 0.45 \mu\text{m}$) concentrations, with an average increase of $0.35 \mu\text{g/L}$ (Figure 41a). Areal variability is demonstrated in this data, where sites 2267 and 2767 show greater increases in Se

concentration (dissolved and total) relative to sites 2565 and 3510. The latter two sites have deep brine layers, which could potentially act as an Se sink; whereas the former two sites are located nearest to major load points (Bear and Weber Rivers, and Farmington Bay causeway), which may locally enhance Se loading. Notably, particulate-associated Se concentration trajectories did not show an increase over the course of the study ([Figure 41b](#)).

Although suspension of consideration of the above-described variability in the south arm of the Great Salt Lake was useful for ease of implementation of the mass balance, the observed variability provides clues to important processes that control the cycling of Se in the system, and warrant further investigation. Furthermore, the period of observation was merely 15 months and fortunately coincided with a transition to reduced runoff. However, a more complete understanding of the system will be achieved with continued observation, including transition to periods of increased runoff.

4. References

- Amouroux, D. (1995) Ph.D. Thesis, University of Bordeaux I, Bordeaux, France.
- Amouroux, D., Tessier, E. and Donard, O.F.X. (2000) Volatilization of organotin compounds from estuarine and coastal environments, *Environ. Sci. Technol.* **34**: 988-995
- Amouroux, D. and Donard, O.F.X. (1996) Maritime emission of selenium to the atmosphere in eastern Mediterranean seas, *Geophysical Research Letters*, **23**(14): 1777-1780
- Anderson, R.A., Schiff, S.L., and Hesslein, R.H. (1987). Determining sediment accumulation and mixing rates using ^{210}Pb , ^{137}Cs and other tracers: Problems due to postdepositional mobility or coring artifacts. *Canadian Journal of Fisheries and Aquatic Sciences*, **44**:231-250.
- Appleby, P.G. and Oldfield, F. (1992). Application of ^{210}Pb to sedimentation studies. Chapter 21. IN: Ivanovich, M., and Harmon. R.S., Ed., Uranium-series Disequilibrium: Application to Earth, Marine, and Environmental Sciences, Second edition. Clarendon Press, Oxford, pp. 731-778
- Atkinson, R., Aschmann, S.A., Hasegawa, D., Thompson-Eagle, E.T. and Frankenberger, W.T., Jr. (1990). Kinetics of the atmospherically important reactions of dimethyl selenide, *Environmental Science and Technology*, **24**:1326-1332
- Baker J.E., Burdige D., Church, T.M., Cutter G., Dickhut, R.M., Leister, D.L., Ondov, J.M. and Scudlark J.R. (1994) The Chesapeake Bay Atmospheric Deposition Study. Phase II Final Report, July 1990-December 1991,
- Baskin, R.L. (2005) Calculation of area and volume for the south part of the Great Salt Lake, Utah. U.S. Department of Interior, U.S. Geological Survey, Open-File Report 2005 - 1327
- Byron, E.R. and Ohlendorf H.M. (2006) Selenium flux and speciation from lake sediment as influenced by quality of overlying water: evaluating restoration alternatives for the Salton Sea. Abstracts - AGU Conference, San Francisco.
- Callendar E. (2000) Geochemical effects of rapid sedimentation in aquatic systems: minimal diagenesis and the preservation of historical metal signatures, *J. of Paleolimnology* **23**: 243–260.
- Card, T., Schmidt, C.E., Witherspoon, J. and Koe, L. (2002) Theoretical and Practical Considerations in the Use of Wind Tunnel for Odor Emission Measurement, Paper No. 42654, 95th Annual Meeting of the Air and Waste Management Association, Baltimore, MD, June, 2002.

- Clark, J.F., Schlosser, P., Simpson, H.J., Stute, M., Wanninkhof, R. and Ho, D.T. (1995). Relationship between the gas transfer velocities and wind speeds in the tidal Hudson River determined by the dual tracer technique. IN: Air-water gas transfer, Jähne, B. and Monahan E.C., Eds., AEON Verlag, Hanau, Germany, pp. 785-800
- Cole, G.A. (1983) Textbook of limnology. 3rd ed. Mosby, St. Louis.
- Colman S.M., K.R. Kelts, D.A. Dinter (2002) Depositional history and neotectonics in Great Salt Lake, Utah, from high-resolution seismic tomography. *Sedimentary Geology*, **148**: 61-78.
- Conover, M.R., Luft, J. and Perschon, C. (2007) Concentration and effects of selenium in California gulls breeding on the Great Salt Lake. Final report: 2006-2007 data.
- Crosman, E. and Horel, J. (2006) Remote sensing of the temperature of the Great Salt Lake, submitted to *Journal of Geophysical Research - Oceans*.
- Cutter, G.A. and Cutter, L.S. (1998) Metalloids in the high latitude North Atlantic Ocean: Sources and internal cycling, *Marine Chemistry*, 61:25-36
- Cutter, G.A. and Cutter, L.S. (2001) Source and cycling of selenium in the western and equatorial Atlantic Ocean. *Deep-Sea Research II*, 48:2917-2931
- Cutshall, N.H., Larsen, I.L., and Olsen, C.R. (1983). Direct analysis of ²¹⁰Pb in sediment samples: self-absorption corrections. *Nuc. Inst. and Methods*, **306**:309-312.
- Dinter, David (2007) Personal communication (Lecturer, Department of Geology & Geophysics, University of Utah). Suggested Core Sample Locations in the Great Salt Lake Based on Long-term Holocene Depositional Rates Estimated from Chirp and Geopulse Seismic Reflection Profiles. May 9, 2007.
- EPA (2007) Multi-Media, Multi-Concentration, Inorganic Analytical Service for Superfund (ILM05.3), EPA Publication 540-FS-07-004
- Fuller, C.C., vanGeen, A., Baskaran, M., and Anima, R. (1999). Sediment chronology in San Francisco Bay defined by ²¹⁰Pb, ²³⁴Th, ¹³⁷Cs, and ^{239,240}Pu. *Marine Chemistry*, **64**:7-27.
- Guo L., Jury W.A., Frankenberger W.T. (2000) Measurement of the Henry's constant of dimethyl selenide as a function of temperature, *Journal of Environmental Quality* **29** (5): 1715-1717.
- Horel, J. (2007) Personal communication (Meteorology Professor, University of Utah).
- Langmuir, I. (1938) Surface motion of water induced by wind. *Science*, **87**: 119-123.
- Lin, A. (1977) Final Report on Wind Tides of the Great Salt Lake, Submitted to Utah Geological and Mineralogical Survey.

- Liss, P.S., and Merlivat, L. (1986) Air-sea gas exchange rates: Introduction and synthesis. IN: P. Buat-Ménard, Ed., The role of air-sea exchanges in geochemical cycling, D. Reidel Publishing Company, pp. 113-127
- Livingstone, D.M. and Imboden, D.M. (1993) The non-linear influence of wind variability on gas transfer in lakes. *Tellus Ser. B*, **45**:275-295
- Loving, B.L., Waddell, K.M. and Miller, C.W. (2002) Water and salt balance of Great Salt Lake, Utah, and simulation of water and salt movement through the causeway, 1963-98. In: Great Salt Lake: An overview of change, Gwynn, J.W. (Ed), DNR Special Publication, Utah Geological Survey, 143-165.
- Masscheleyn, P.H. and Patrick, W.H. (1993) Biogeochemical processes affecting selenium cycling in wetlands. *Environmental Toxicology and Chemistry*. **12**:2235-2243.
- Marden, B. (2007) Synoptic survey of the pelagic zone: Selenium in water, seston, and *Artemia*. Preliminary results.
- Naftz, D.L., Johnson, W.P., Freeman, M., Beisner, K., Diaz, X. (2007) Estimation of selenium loads entering the South Arm of Great Salt Lake, Utah: Preliminary results.
- Neumann, P.M., De Souza, M.P., Pickering, I.J. and Terry, N. (2003) Rapid microalgal metabolism of selenate to volatile dimethylselenide, *Plant, Cell and Environment*, **26**:897-905.
- Saltzman, E.S. and King, D.B. (1993) Experimental determination of the diffusion coefficient of dimethyl sulfide in water, *J. Geophys. Res.* **98**(C9):16481-16486
- Schmidt, C.E. (2007) Personal communication (Designer of the USEPA Flux Chamber)
- Schwarzenbach, R.P., Gschwend, P.M. and Imboden, D.M. (2003) Environmental Organic Chemistry, 2nd. Ed., Wiley-Interscience, Hoboken, NJ, pp. 159-163, 887-921
- Stommel, H. (1951) Streaks on natural water surfaces, *Weather*, **6**:72-74.
- Sweet C.W., Weiss A. and Vermette, S.J. (1998) Atmospheric deposition of trace metals at three sites near the Great Lakes. *Water, Air and Soil Pollution*, **103**:423-439
- Tessier E, Amouroux, D. and Donard, O.F.X. (2003) Biogenic volatilization of trace elements from European Estuaries, Chapter 12. IN: Biogeochemistry of environmentally important trace elements, Cai, Y. and Braids, O.C. (Eds), American Chemical Society, Washington, pp. 151-165
- Van Metre, P.C., Horowitz, A.J., Mahler, B.J., Foreman, W.T., Fuller, C.C., Burkhardt, M.R., Elrick, K.A., Furlong, E.T., Skrobialowski, S., Smith, J.J., Wilson, J.T., and Zaugg, S.D. (2006) The impact of hurricanes Katrina and Rita on the chemistry of bottom sediments in Lake Pontchartrain, Louisiana, USA. *Environmental Science and Technology*, **40**:6895-6902

Wetzel, R.G. (2001) Limnology. 3rd ed. Saunders, Philadelphia.

Wind Energy Department of Risoe National Laboratory and Det Norske Veritas (2001)
Guidelines for Design of Wind Turbines, Copenhagen. ISBN 87-550-2870-5

TABLES

Table 1a. ICP-MS conditions for water sample analysis

Condition	Value
RF power (W)	1550
Plasma gas flowrate (L/min)	15.0
Hydrogen flowrate (mL/min)	5.0
Helium flowrate (mL/min)	6.5
Carrier flowrate (L/min)	0.73
Make-up gas (L/min)	0.21
Auxiliary gas (L/min)	1.0
Sample pump (rps)	0.1
Sample depth (mm)	8.0
Tuning solution:	
⁷ Li mean (cps)	30,000
⁸⁹ Y mean (cps)	29,000
²⁰⁵ Th mean (cps)	64,000
% RSD for each cps	< 3%
Sample nebulizer tubing:	
Material	Tygon
Internal diameter (mm)	1.02
Internal standard tubing:	
Material	Tygon
Internal diameter (mm)	0.91

Table 1b Great Salt Lake synthetic solution recipe

Salt	Concentration (mol/g_{solution})	Concentration g/L	Grams in 100mL milliQ W	Salt Purity	Salt brand
NaCl	1.99E-03	116.7884	11.6788	99.999%	Sigma- Aldrich
MgCl ₂	1.46E-04	13.9657	1.3966	99.99%	Sigma
MgSO ₄	3.73E-05	4.4874	0.4487	99.99+%	Aldrich
K ₂ SO ₄	3.21E-05	5.5877	0.5588	99.99%	Aldrich
CaSO ₄	4.88E-06	0.6306	0.0631	99.99+%	Aldrich

Table 1c. Quality control summary (EPA, 2007)

QC Operation	Frequency
Instrument Calibration	Daily or each time instrument is set up.
Initial Calibration Verification (ICV)	Following each instrument calibration for each wavelength or mass used.
Initial Calibration Blank (ICB)	Following each instrument calibration, immediately after the Initial Calibration Verification (ICV).
Continuing Calibration Verification (CCV)	For each wavelength or mass used, at a frequency of 10% or every two hours of a run, whichever is more frequent, and at the beginning and end of each run.
Continuing Calibration Blank (CCB)	10% or every two hours of a run, whichever is more frequent, and at the beginning and end of each run. Performed immediately after the last Continuing Calibration Verification (CCV).
CRQL Check Standard (CRI)	Every 20 analytical samples and at the beginning and end of each run, but not before the ICV. Performed before the Interference Check Sample.
Interference Check Sample (ICS)	For ICP-AES, every 20 analytical samples and at the beginning and end of each run, immediately after the CRI. For ICP-MS, at the beginning of the run.
Serial Dilution for ICP	For each matrix type or for each SDG, whichever is more frequent.
Preparation Blank	For each SDG or each sample preparation and analysis procedure per batch of prepared samples.
Laboratory Control Sample	For each SDG or each sample preparation and analysis procedure per batch of prepared samples, except aqueous mercury and cyanide.
Spike Sample	For each matrix type or for each SDG, whichever is more frequent.
Post Digestion/Distillation Spike	Each time Spike Sample Recovery is outside QC limits.
Duplicate Sample Analysis	For each matrix type or for each SDG, whichever is more frequent.
ICP-MS Tune	Prior to calibration.
Method Detection Limit Determination	Prior to contract, annually thereafter, and after major instrument maintenance.
Inter-element Corrections	Prior to contract, quarterly thereafter, and after major instrument adjustment.
Linear Range Analysis	Prior to contract, and quarterly thereafter.

Table 1d. Results of measured volatile Se fluxes under controlled laboratory conditions with variable sweep rate and sweep gas composition.

Sample ID	Sweep Gas	Sweep Rate	Wind	Water Temp.	Vol [Se]	Measured Flux
		L/min	m/s	oC	ng/L	ng/m²h
GT1	N2	2	0	19	2.24	5.72
GT2	N2	3	0	19	21.50	32.26
GT3	N2	6	0	19	17.45	24.65
GT4	He	3	0	19	27.36	43.11
GT5	He	2	0	19	21.90	29.51
GT7	N2	2	0	19	21.90	31.80
1X	He	3	0	19	0	2.67
2X	He	3	0	19	0	1.25
3X	He	3	0	19	0	0.87

Table 2a. Total (RA) and dissolved (FA) selenium concentrations in water, site 2267.

Site	Sampling date	Depth (m)	FA (µg/L)	RA (µg/L)	
2267	26-May-06	0.2	0.311	0.404	
	26-May-06	4	0.341	0.524	
	19-Jun-06	0.2	0.267	0.311	
	19-Jun-06	4	0.278	0.405	
	28-Jul-06	0.2	0.425	0.469	
	28-Jul-06	4	0.38	0.461	
	29-Aug-06	0.2	0.685	0.785	
	29-Aug-06	3.8	0.647	0.948	
	28-Sep-06	0.2	0.483	0.664	
	28-Sep-06	3.5	0.456	0.594	
	01-Nov-06	0.2	0.532	0.57	
	01-Nov-06	3.9	0.494	0.896	
	21-Nov-06	0.2	0.307	0.414	
	21-Nov-06	3.7	0.292	0.466	
	07-Dec-06	0.2	0.366	0.63	
	07-Dec-06	3.5	0.64	0.732	
	20-Mar-07	0.2	0.477	0.664	
	20-Mar-07	4	0.572	0.714	
	26-Apr-07	0.2	0.49	0.759	
	26-Apr-07	4	0.702	0.865	
	23-May-07	0.2	0.526	0.644	
	23-May-07	4	0.607	0.658	
	26-Jun-07	0.2	0.816	0.681	
	26-Jun-07	4	0.702	0.729	
	24-Jul-07	0.2	0.669	0.705	
	24-Jul-07	3.5	0.622	0.751	
		Arithmetic average		0.50	0.63
		Geometric mean		0.48	0.61
		Median		0.49	0.66
		Standard deviation		0.16	0.16
		Geometric standard deviation		0.21	0.33
		Lowest value		0.27	0.31
	Highest value		0.82	0.95	

Table 2b. Total (RA) and dissolved (FA) selenium concentrations in water, site 2565.

Site	Sampling date	Depth (m)	FA (µg/L)	RA (µg/L)	
2565 shallow	26-May-06	0.2	0.418	0.496	
	19-Jun-06	0.2	0.245	0.396	
	29-Jul-06	0.2	0.361	0.476	
	29-Sep-06	0.2	0.391	0.646	
	2-Nov-06	0.2	0.768	0.805	
	22-Nov-06	0.2	0.291	0.416	
	6-Dec-06	0.2	0.417	0.509	
	20-Mar-07	0.2	0.361	0.656	
	26-Apr-07	0.2	0.54	0.658	
	23-May-07	0.2	0.547	0.64	
	26-Jun-07	0.2	0.436	0.764	
	25-Jul-07	0.2	0.708	0.651	
	Arithmetic average			0.46	0.59
	Geometric mean			0.43	0.58
	Median			0.42	0.64
	Standard deviation			0.16	0.13
	Geometric standard deviation			1.38	1.25
	Lowest value			0.25	0.40
	Highest value			0.77	0.81
2565 deep	26-May-06	6.5	0.366	0.504	
	26-May-06	7.5	0.25	0.594	
	19-Jun-06	6.5	0.205	0.446	
	19-Jun-06	8	0.219	0.973	
	29-Jul-06	6.5	0.25	0.25	
	29-Jul-06	7.5	0.291	0.311	
	29-Sep-06	6.5	0.401	0.484	
	29-Sep-06	7.5	0.25	0.25	
	2-Nov-06	6.5	0.584	0.643	
	2-Nov-06	8	0.334	0.553	
	22-Nov-06	6.5	0.25	0.25	
	22-Nov-06	7.5	0.25	0.25	
	6-Dec-06	6.5	0.377	0.502	
	6-Dec-06	7.5	0.273	0.417	
	20-Mar-07	6.5	0.463	0.682	
	20-Mar-07	7.5	0.43	0.961	
	26-Apr-07	6.5	0.507	0.825	
	26-Apr-07	8	0.532	0.865	
	23-May-07	6.5	0.632	0.709	
	23-May-07	7.5	0.404	0.809	
	26-Jun-07	6.5	0.433	0.616	
	26-Jun-07	7.5	0.645	1.05	
	25-Jul-07	6	0.574	0.864	
	25-Jul-07	7	0.601	0.746	
	Arithmetic average			0.40	0.61
	Geometric mean			0.37	0.55
	Median			0.39	0.61
	Standard deviation			0.14	0.25
	Geometric standard deviation			1.43	1.58
	Lowest value			0.21	0.25
Highest value			0.65	1.05	

Table 2c. Total (RA) and dissolved (FA) selenium concentrations in water, site 3510.

Site	Sampling date	Depth (m)	FA (µg/L)	RA (µg/L)	
3510 shallow	23-May-06	0.2	0.461	0.605	
	20-Jun-06	0.2	0.363	0.479	
	27-Jul-06	0.2	0.335	0.437	
	1-Sep-06	0.2	0.586	0.779	
	29-Sep-06	0.2	0.452	0.534	
	4-Nov-06	0.2	0.559	0.665	
	21-Nov-06	0.2	0.334	0.522	
	7-Dec-06	0.2	0.452	0.623	
	19-Mar-07	0.2	0.59	0.671	
	1-May-07	0.2	0.843	0.8	
	31-May-07	0.2	0.591	0.746	
	27-Jun-07	0.2	0.506	0.613	
	25-Jul-07	0.2	0.62	0.642	
	Arithmetic average			0.51	0.62
	Geometric mean			0.50	0.61
	Median			0.51	0.62
	Standard deviation			0.14	0.11
	Geometric standard deviation			1.29	1.19
	Lowest value			0.33	0.44
	Highest value			0.84	0.80
3510 deep	23-May-06	6.5	0.409	0.642	
	23-May-06	8.5	0.292	0.716	
	20-Jun-06	7	0.348	0.477	
	20-Jun-06	8.5	0.243	0.654	
	27-Jul-06	7	0.248	0.411	
	27-Jul-06	8.5	0.35	0.417	
	1-Sep-06	6.5	0.745	0.777	
	1-Sep-06	8.5	0.461	1.14	
	29-Sep-06	6.5	0.431	0.526	
	29-Sep-06	8	0.25	0.251	
	4-Nov-06	6.5	0.408	0.576	
	4-Nov-06	8	0.349	0.548	
	21-Nov-06	6.5	0.478	0.723	
	21-Nov-06	8	0.549	0.551	
	7-Dec-06	6.5	0.378	0.47	
	7-Dec-06	8	0.25	0.523	
	19-Mar-07	6.5	0.544	0.674	
	19-Mar-07	8	0.681	0.812	
	1-May-07	6.5	0.622	0.806	
	1-May-07	8.5	0.468	0.718	
	31-May-07	7	0.569	0.916	
	31-May-07	8.3	0.593	0.718	
	27-Jun-07	7	0.571	0.712	
	27-Jun-07	8.1	0.453	0.723	
	25-Jul-07	6.5	0.662	0.736	
	25-Jul-07	8	0.618	0.76	
	Arithmetic average			0.46	0.65
	Geometric mean			0.44	0.63
	Median			0.46	0.69
	Standard deviation			0.15	0.18
Geometric standard deviation			1.40	1.35	
Lowest value			0.24	0.25	
Highest value			0.75	1.14	

Table 2d. Total (RA) and dissolved (FA) selenium concentrations in water, site 2767.

Site	Sampling date	Depth (m)	FA (µg/L)	RA (µg/L)
	23-May-06	0.2	0.333	0.439
	23-May-06	3	0.364	0.412
	20-Jun-06	0.2	0.284	0.582
	20-Jun-06	3	0.319	0.418
	27-Jul-06	0.2	0.346	0.439
	27-Jul-06	3	0.33	0.449
	29-Aug-06	0.2	0.713	0.925
	29-Aug-06	2.7	0.762	0.844
	27-Sep-06	0.2	0.431	0.513
	27-Sep-06	2.2	0.538	0.626
	03-Nov-04	0.2	0.445	0.657
	20-Nov-06	0.2	0.281	0.46
	20-Nov-06	2.5	0.363	0.545
	07-Dec-06	0.2	0.432	0.464
	07-Dec-06	2.5	0.528	0.572
	19-Mar-07	0.2	0.626	0.677
	19-Mar-07	3	0.574	0.795
	02-May-07	0.2	0.546	0.699
	02-May-07	2.8	0.558	0.705
	31-May-07	0.2	0.545	0.625
	31-May-07	2.8	0.594	0.58
	28-Jun-07	0.2	0.522	0.845
	28-Jun-07	3	0.507	0.808
	24-Jul-07	0.2	0.662	0.68
	24-Jul-07	2.5	2.77	3.11
	Arithmetic average		0.57	0.71
	Geometric mean		0.50	0.64
	Median		0.52	0.63
	Standard deviation		0.48	0.52
	Geometric standard deviation		0.24	0.29
	Lowest value		0.28	0.41
2767	Highest value		2.77	3.11
Arith. average over total samples			0.49	0.64
Geometric mean over total samples			0.45	0.60
Median over total samples			0.46	0.64
Standard deviation over total samples			0.25	0.28
Geometric standard deviation over total samples			0.21	0.31
Lowest value			0.21	0.25
Highest value			2.77	3.11

Table 2e. Total (RA) and dissolved (FA) selenium concentrations in water, sites 2267 & 2565. Analysis via ICP-MS at the U of Utah.

Site	Sampling date	Depth (m)	FA (µg/L)	RA (µg/L)	
2267	8/29/06	0.2	0.27	0.60	
	8/29/06	3.8	0.45	0.60	
	11/1/06	0.2	0.34	0.24	
	11/1/06	3.9	0.20	0.40	
	12/7/06	0.2	0.14	0.21	
	12/7/06	3.5	0.18	0.33	
	3/20/07	0.2	0.37	0.56	
	3/20/07	4.0	0.50	0.46	
	4/27/07	0.2	0.30	0.30	
	5/24/07	0.2	0.30	0.30	
	6/27/07	0.2	0.30	0.58	
	7/25/07	0.2	0.30	0.46	
	8/24/07	0.2	0.55	0.65	
	Arithmetic average			0.32	0.44
	Geometric mean			0.30	0.41
	Median			0.30	0.46
	Standard deviation			0.12	0.15
Lowest value			0.14	0.21	
Highest value			0.55	0.65	
2565 shallow	11/1/06	0.2	0.43	0.36	
	12/6/06	0.2	0.09	0.27	
	3/20/07	0.2	0.47	0.60	
	4/27/07	0.2	0.30	0.30	
	5/24/07	0.2	0.32	0.30	
	6/28/07	0.2	0.30	0.30	
	7/26/07	0.2	0.41	0.30	
	8/22/07	0.2	0.47	0.34	
	Arithmetic average			0.35	0.34
	Geometric mean			0.32	0.33
	Median			0.36	0.30
	Standard deviation			0.13	0.10
	Lowest value			0.09	0.27
Highest value			0.47	0.60	
2565 deep	11/1/06	6.5	0.65	1.03	
	11/1/06	8.0	2.67	3.40	
	12/6/06	6.5	1.07	1.09	
	12/6/06	7.5	3.72	2.27	
	3/20/07	6.5	0.50	0.50	
	3/20/07	7.5	0.71	1.15	
	4/27/07	8.0	0.40	0.40	
	5/24/07	7.5	0.40	0.40	
	6/27/07	7.5	0.40	0.40	
	7/26/07	7.0	0.40	0.40	
	8/22/07	7.8	0.40	0.40	
	Arithmetic average			1.03	1.04
	Geometric mean			0.71	0.76
	Median			0.50	0.50
	Standard deviation			1.12	0.97
	Lowest value			0.40	0.40
	Highest value			3.72	3.40

Table 2f. Total (RA) and dissolved (FA) selenium concentrations in water, site 3510. Analysis via ICP-MS at the U of Utah.

Site	Sampling date	Depth (m)	FA (µg/L)	RA (µg/L)	
3510 shallow	9/1/06	0.2	0.41	0.60	
	11/3/06	0.2	0.35	0.56	
	12/7/06	0.2	0.15	0.26	
	3/19/07	0.2	0.42	0.77	
	5/2/07	0.2	0.30	0.32	
	6/1/07	0.2	0.30	0.45	
	6/28/07	0.2	0.65	0.61	
	7/26/07	0.2	0.37	0.48	
	8/22/07	0.2	0.83	0.79	
	Arithmetic average			0.42	0.54
	Geometric mean			0.38	0.51
	Median			0.37	0.56
	Standard deviation			0.20	0.18
	Lowest value			0.15	0.26
	Highest value			0.83	0.79
3510 deep	9/1/06	6.5	0.65	1.69	
	9/1/06	8.5	1.61	3.15	
	11/3/06	6.5	0.42	1.85	
	12/7/06	6.5	0.96	1.19	
	12/7/06	8.0	2.26	2.97	
	3/19/07	6.5	0.71	1.15	
	3/19/07	8.0	0.60	1.04	
	5/2/07	8.5	0.40	0.40	
	6/1/07	8.3	0.40	0.40	
	6/28/07	8.1	0.40	0.40	
	7/26/07	8.0	0.40	0.40	
	8/22/07	8.0	0.40	0.40	
	Arithmetic average			0.77	1.25
	Geometric mean			0.63	0.93
	Median			0.51	1.09
Standard deviation			0.59	0.99	
Lowest value			0.40	0.40	
Highest value			2.26	3.15	

Table 2g. Total (RA) and dissolved (FA) selenium concentrations in water, site 2767. Analysis via ICP-MS at the U of Utah.

Site	Sampling date	Depth (m)	FA (µg/L)	RA (µg/L)	
	8/29/06	0.2	0.41	0.41	
	8/29/06	2.7	0.55	0.67	
	11/3/06	0.2	0.31	0.45	
	12/6/06	0.2	0.36	0.41	
	12/6/06	2.5	0.09	0.16	
	3/19/07	0.2	0.58	0.69	
	3/19/07	3	0.57	0.74	
	5/3/07	0.2	0.30	0.30	
	6/1/07	0.2	0.30	0.30	
	6/29/07	0.2	0.54	0.60	
	7/25/07	0.2	0.30	0.30	
	8/24/07	2.5	0.30	0.91	
	8/24/07	0.2	0.30	0.45	
	Arithmetic average			0.38	0.49
	Geometric mean			0.35	0.45
	Median			0.31	0.45
	Standard deviation			0.14	0.21
Lowest value			0.09	0.16	
2767	Highest value			0.58	0.91
Arith. average over total samples			0.55	0.70	
Geometric mean over total samples			0.43	0.54	
Median over total samples			0.40	0.45	
Standard deviation over total samples			0.58	0.67	
Lowest value			0.09	0.16	
Highest value			3.72	3.40	

Table 3a. Arithmetic average results (all water column sites and samples) for major and minor elements in shallow brine layer analyzed by ICP-MS. Total (RA) and dissolved (FA) results.

Element	Unit	Average for FA shallow brine	Average for RA shallow brine	Highest value FA/RA	Lowest value FA/RA
Li	mg/L	20.34 ± 0.80	20.79 ± 0.63	21.45 / 21.19	19.02 / 19.26
Na	mg/L	44891.18 ± 2004.37	46026.82 ± 1561.48	48231 / 47052	41841 / 42876
Mg	mg/L	4637.86 ± 205.44	4746.85 ± 160.21	4972.50 / 4847.40	4326.30 / 4397.40
S	mg/L	3377.62 ± 118.42	3415.25 ± 94.62	3522.60 / 3460.50	3188.70 / 3174.30
Cl	mg/L	85588.36 ± 2926.50	85968.00 ± 2384.21	89127 / 87183	81045 / 80154
K	mg/L	2603.86 ± 106.01	2654.35 ± 72.15	2685.60 / 2691.00	2402.10 / 2457.90
Ca	mg/L	270.23 ± 9.02	275.76 ± 5.78	283.14 / 283.68	258.93 / 265.14
Al	mg/L	14.52 ± 8.08	94.90 ± 35.61	26.45 / 127.80	4.65 / 21.86
Ti	µg/L	327.45 ± 14.10	338.75 ± 6.61	343.60 / 347.10	308.25 / 328.70
V	µg/L	6.06 ± 0.15	6.22 ± 0.08	6.54 / 6.37	6.02 / 6.15
Cr	µg/L	12.01 ± 0.97	12.23 ± 0.76	12.79 / 12.89	9.87 / 10.43
Mn	µg/L	20.97 ± 4.73	24.86 ± 3.54	25.63 / 26.81	13.95 / 17.94
Fe	µg/L	32.54 ± 18.61	95.50 ± 20.51	83.50 / 116.25	16.59 / 44.82
Co	µg/L	3.57 ± 0.03	3.62 ± 0.04	3.63 / 3.71	3.54 / 3.56
Ni	µg/L	4.42 ± 0.21	4.47 ± 0.12	4.78 / 4.65	4.13 / 4.17
Cu	µg/L	15.33 ± 1.52	15.50 ± 0.85	18.05 / 17.20	13.30 / 14.20
Zn	µg/L	15.20 ± 8.13	19.37 ± 16.82	31.85 / 64.50	4.68 / 6.58
As	µg/L	145.22 ± 9.98	147.44 ± 6.30	156.20 / 154.60	132.45 / 131.60
Sr	µg/L	2469.09 ± 107.58	2536.41 ± 58.01	2589.50 / 2598.00	2310.00 / 2428.00
Mo	µg/L	44.75 ± 3.20	46.13 ± 1.92	51.20 / 50.15	42.29 / 43.95
Cd	µg/L	2.60 ± 0.21	2.65 ± 0.33	2.80 / 3.08	2.12 / 1.88
Sb	µg/L	15.43 ± 0.71	15.67 ± 0.64	16.33 / 16.63	14.50 / 14.98
Ba	µg/L	124.67 ± 1.97	130.71 ± 2.64	126.85 / 133.70	120.50 / 126.80
Tl	µg/L	1.78 ± 0.04	1.77 ± 0.02	1.84 / 1.79	1.71 / 1.73
Pb	µg/L	3.41 ± 0.28	3.66 ± 0.24	3.98 / 4.01	3.04 / 3.10
U	µg/L	9.34 ± 0.41	9.55 ± 0.19	9.93 / 9.87	8.87 / 9.33

Table 3b. Geometric mean and median (all water column sites and samples) for major and minor elements in shallow brine layer analyzed by ICP-MS. Total (RA) and dissolved (FA) results

Element	Units	Geometric mean -Shallow		Median - Shallow	
		FA	RA	FA	RA
Li	mg/L	19.8	20.1	19.76	19.84
Na	mg/L	43707.9	44514.9	43245.00	43830.00
Mg	mg/L	4502.2	4583.3	4440.15	4509.00
S	mg/L	3302.8	3324.2	3296.70	3310.20
Cl	mg/L	83832.7	83887.4	83785.50	83245.50
K	mg/L	2541.8	2575.2	2553.75	2580.75
Ca	mg/L	268.3	272.8	268.02	270.59
Al	mg/L	12.3	85.6	12.12	98.58
Ti	µg/L	324.6	335.9	328.60	333.68
V	µg/L	6.1	6.2	6.07	6.18
Cr	µg/L	11.6	11.9	11.57	12.00
Mn	µg/L	17.9	21.9	17.89	21.40
Fe	µg/L	30.4	80.8	27.97	87.58
Co	µg/L	3.6	3.6	3.56	3.61
Ni	µg/L	4.4	4.4	4.41	4.46
Cu	µg/L	15.6	15.5	15.50	15.69
Zn	µg/L	13.9	16.4	14.38	14.51
As	µg/L	143.8	147.3	144.60	147.33
Sr	µg/L	2431.3	2519.7	2463.25	2521.25
Mo	µg/L	45.8	47.0	45.54	46.75
Cd	µg/L	2.5	2.5	2.54	2.59
Sb	µg/L	15.3	15.8	15.4	15.7
Ba	µg/L	123.7	129.6	124.5	129.1
Tl	µg/L	1.8	1.8	1.77	1.76
Pb	µg/L	3.5	3.6	3.59	3.64
U	µg/L	9.3	9.5	9.3425	9.46

Table 3c. Arithmetic average results for major and minor elements in deep brine layer (all water column sites and samples) analyzed by ICP-MS. Total (RA) and dissolved (FA) results

Element	Unit	Average for FA deep brine	Average for RA deep brine	Highest value FA/RA	Lowest value FA/RA
Li	mg/L	25.84 ± 5.61	26.15 ± 5.82	35.84 / 37.36	20.08 / 20.56
Na	mg/L	55920.38 ± 11944.08	56787.75 ± 12591.38	78561 / 81567	43812 / 44604
Mg	mg/L	5857.31 ± 1315.12	5927.74 ± 1369.95	8297.10 / 8518.50	4465.8 / 4574.7
S	mg/L	4255.99 ± 925.75	4207.50 ± 883.04	5979.60 / 5762.70	3282.3 / 3301.2
Cl	mg/L	106984.13 ± 23324.56	105842.25 ± 22193.84	152370 / 145620	81810 / 82656
K	mg/L	3275.10 ± 667.25	3309.98 ± 683.16	4508.10 / 4631.40	2577.6 / 2667.6
Ca	mg/L	293.48 ± 21.34	299.89 ± 22.80	325.26 / 335.52	268.74 / 278.19
Al	mg/L	344.48 ± 940.88	899.50 ± 1248.80	2673.00 / 3491.50	6.68 / 15.71
Ti	µg/L	374.11 ± 46.87	397.17 ± 67.83	475.55 / 538.50	328.95 / 330.75
V	µg/L	5.96 ± 1.89	7.41 ± 1.92	10.34 / 11.59	4.28 / 6.17
Cr	µg/L	14.78 ± 3.34	14.90 ± 3.29	20.34 / 20.43	10.84 / 11.26
Mn	µg/L	54.73 ± 34.96	64.75 ± 44.88	124.45 / 147.40	22.61 / 26.74
Fe	µg/L	227.75 ± 566.46	592.99 ± 706.55	1629.50 / 2040.00	17.04 / 48.79
Co	µg/L	3.64 ± 0.34	3.88 ± 0.41	4.47 / 4.76	3.40 / 3.54
Ni	µg/L	5.55 ± 1.67	5.52 ± 1.36	9.08 / 8.29	4.44 / 4.34
Cu	µg/L	16.21 ± 5.08	19.26 ± 6.29	27.13 / 31.97	11.33 / 15.02
Zn	µg/L	18.54 ± 8.66	18.32 ± 8.43	31.72 / 29.84	7.66 / 8.36
As	µg/L	163.69 ± 18.59	163.16 ± 16.65	206.80 / 192.95	149.55 / 146.65
Sr	µg/L	2816.38 ± 247.83	2797.75 ± 228.39	3199.00 / 3143.50	2509 / 2492
Mo	µg/L	33.54 ± 13.85	39.92 ± 9.41	49.28 / 52.00	13.29 / 29.43
Cd	µg/L	3.25 ± 0.55	3.08 ± 0.64	4.15 / 4.06	2.45 / 2.24
Sb	µg/L	16.43 ± 0.95	16.27 ± 1.22	17.75 / 17.76	15.01 / 14.55
Ba	µg/L	135.02 ± 13.80	145.30 ± 17.38	165.21 / 173.73	123.16 / 124.81
Tl	µg/L	1.91 ± 0.27	1.88 ± 0.12	2.56 / 2.02	1.73 / 1.71
Pb	µg/L	4.23 ± 3.56	6.90 ± 4.51	12.98 / 16.20	2.42 / 3.61
U	µg/L	9.51 ± 0.34	9.67 ± 0.35	9.89 / 10.14	8.88 / 9.11

Table 3d. Geometric mean and median (all water column sites and samples) for major and minor elements in deep brine layer analyzed by ICP-MS. Total (RA) and dissolved (FA) results

	Units	Geometric mean-Shallow		Median - Shallow	
		FA	RA	FA	RA
Li	mg/L	25.8	26.2	25.3	25.6
Na	mg/L	55920.4	56787.8	54871.2	55664.2
Mg	mg/L	5857.3	5927.7	5734.7	5798.3
S	mg/L	4256.0	4207.5	4172.3	4130.0
Cl	mg/L	106984.1	105842.3	104908.9	103906.3
K	mg/L	3275.1	3310.0	3218.3	3252.6
Ca	mg/L	293.5	299.9	292.8	299.1
Al	mg/L	344.5	899.5	21.5	297.4
Ti	µg/L	374.1	397.2	371.8	392.6
V	µg/L	6.0	7.4	5.7	7.2
Cr	µg/L	14.8	14.9	14.5	14.6
Mn	µg/L	54.7	64.7	46.0	53.1
Fe	µg/L	227.7	593.0	44.0	281.3
Co	µg/L	3.6	3.9	3.6	3.9
Ni	µg/L	5.5	5.5	5.4	5.4
Cu	µg/L	16.2	19.3	15.6	18.5
Zn	µg/L	18.5	18.3	16.7	16.6
As	µg/L	163.7	163.2	162.9	162.4
Sr	µg/L	2816.4	2797.8	2806.8	2789.7
Mo	µg/L	33.5	39.9	30.8	39.0
Cd	µg/L	3.3	3.1	3.2	3.0
Sb	µg/L	16.4	16.3	16.4	16.2
Ba	µg/L	135.0	145.3	134.5	144.4
Tl	µg/L	1.9	1.9	1.9	1.9
Pb	µg/L	4.2	6.9	3.5	5.9
U	µg/L	9.5	9.7	9.5	9.7

Table 4a. Volatile selenium concentration in the Great Salt Lake

Date	Site	Depth (m)	[Se] (ng/L)	[Se] (pmol/L)
9/1/06	3510	0.2	1.1	10.1
9/1/06	3510	1.5	1.9	17.5
9/1/06	3510	8.5	0.6	5.2
9/11/06	GS-5	7.5	6.4	58.5
9/12/06	GS-11	8	1.8	16.3
9/12/06	GS-20	7	0.3	2.4
9/12/06	3510	0.2	5.3	48.4
9/27/06	2267	0.2	0.1	1.0
9/27/06	2267	3.5	3.3	30.6
9/27/06	2767	0.2	1.1	9.6
9/27/06	2767	2.2	1.4	12.4
9/28/06	2565	0.2	9.2	84.3
9/28/06	2565	8	1.7	15.4
9/28/06	3510	0.2	1.5	13.6
9/28/06	3510	8	0.2	1.7
September	Average		2.4	21.8
	Standard deviation		2.6	24.0
	Lowest value		0.1	1.0
	Highest value		9.2	84.3
11/1/06	2565	6.5	3.0	27.2
11/3/06	3510	0.2	6.4	58.9
11/3/06	3510	6.5	0.4	3.7
11/16/06	GS-9	2.5	3.1	28.2
11/16/06	GS-5	2	2.4	21.8
11/17/06	GS-20	2.5	0.4	3.4
11/17/06	GS-18	7.7	1.8	16.6
11/17/06	GS-14	7	0.6	6.0
11/17/06	GS-12	5	3.4	31.6
11/20/06	3510	3	1.7	15.5
11/20/06	3510	7	0.0	0.2
11/20/06	2767	2	1.3	11.6
11/21/06	2267	1	1.7	15.2
11/21/06	2565	8	0.6	5.9
11/21/06	2565	0.2	1.3	12.0
November	Average		1.9	17.2
	Standard deviation		1.6	15.0
	Lowest value		0.0	0.2
	Highest value		6.4	58.9

Table 4b. Volatile selenium concentration in the Great Salt Lake

Date	Site	Depth (m)	[Se] (ng/L)	[Se] (pmol/L)
12/6/06	2565	0.5	0.0	0.4
12/6/06	2565	4	0.0	0.4
12/6/06	2767	0.5	0.0	0.4
12/6/06	2767	2.5	1.2	10.6
12/7/06	3510	0.5	0.2	1.6
12/7/06	3510	8	0.0	0.4
12/7/06	2267	0.5	0.0	0.4
12/7/06	2267	3	1.0	8.9
December	Average		0.3	2.9
	Standard deviation		0.5	4.3
	Lowest value		0.0	0.4
	Highest value		1.2	10.6
5/1/07	3510	0.2	7.1	65.4
5/1/07	3510	3	0.0	0.4
5/1/07	3510	4.5	0.0	0.4
5/1/07	3510	6.5	0.0	0.4
5/1/07	3510	8.5	0.3	2.3
5/10/07	2565	0.2	0.3	2.6
5/10/07	2565	3	1.9	17.8
5/10/07	2565	6.5	9.1	83.3
5/10/07	2565	7.5	0.5	4.6
May	Average		2.1	19.7
	Standard deviation		3.5	31.8
	Lowest value		0.0	0.4
	Highest value		9.1	83.3
6/1/07	3510	0.5	0.0	0.4
6/1/07	3510	4	8.5	78.3
6/1/07	3510	5	0.9	8.3
6/1/07	3510	6.5	3.0	27.4
6/1/07	3510	8	0.0	0.4
6/27/07	3510	0.2	0.0	0.4
6/27/07	3510	3	1.6	15.0
6/27/07	3510	5	4.3	39.7
6/27/07	3510	7	0.1	0.8
6/27/07	3510	8	0.2	2.2
June	Average		1.9	17.3
	Standard deviation		2.8	25.3
	Lowest value		0.0	0.4
	Highest value		8.5	78.3

Table 4c. Volatile selenium concentration in the Great Salt Lake

Date	Site	Depth (m)	[Se] (ng/L)	[Se] (pmol/L)
7/2/07	2267	0.2	1.6	14.8
7/2/07	2267	1	1.7	15.4
7/2/07	2267	2	4.1	37.5
7/2/07	2267	3.5	22.7	208.1
7/26/07	2267	0.2	4.6	41.9
7/26/07	2267	1.5	6.1	56.0
7/26/07	2267	2.5	7.8	71.3
7/26/07	2267	3.5	17.0	156.1
7/27/07	2565	0.2	0.1	0.6
7/27/07	2565	3	2.2	20.2
7/27/07	2565	5	7.7	70.2
7/27/07	2565	6.5	13.3	122.3
7/27/07	2565	7.5	0.6	5.1
July	Average		6.9	63.0
	Standard deviation		6.9	63.4
	Lowest value		0.1	0.6
	Highest value		22.7	208.1
8/24/07	2767	0.2	4.5	41.7
8/24/07	2767	1	2.3	21.1
8/24/07	2767	2	0.8	7.7
8/30/07	3510	0.2	3.4	31.0
8/30/07	3510	3	10.0	91.7
8/30/07	3510	5	17.8	163.5
8/30/07	3510	7	0.4	3.6
8/30/07	3510	8	0.0	0.4
August	Average		4.9	45.1
	Standard deviation		6.1	56.2
	Lowest value		0.0	0.4
	Highest value		17.8	163.5
Average over total samples			3.0	27.4
Geometric mean			0.9	8.2
Standard deviation over total samples			4.4	39.9
Lowest value over total samples			0.0	0.2
Highest value over total value			22.7	208.1

Table 5. Volatile selenium diffusive flux

Date	Site	Depth (m)	ngSe/L	T(°C)	D _{DMS} (cm ² /s)	J (g Se/cm ² /yr)	Flux (Kg/yr)
9/1/06	3510	0.2	0.37	22.15	1.2E-05	5.4E-13	9.9E-03
		1.5	0.55				
9/27/06	2267	0.2	0.14	16.4	1.0E-05	7.2E-13	1.3E-02
		3.5	0.87				
9/27/06	2767	0.2	0.36	16.4	1.0E-05	1.1E-13	2.1E-03
		2.2	0.43				
12/6/06	2767	0.5	0.04	8.48	8.4E-06	4.5E-13	8.3E-03
		2.5	0.38				
12/6/06	2565	0.5	0.02	8.48	8.4E-06	4.7E-14	8.6E-04
		4	0.09				
12/7/06	2267	0.5	0.09	8.48	8.4E-06	2.6E-13	4.7E-03
		3	0.34				
5/10/07	2565	0.2	0.18	17.87	1.1E-05	4.4E-13	8.2E-03
		3	0.56	16.28	1.0E-05	1.5E-12	2.7E-02
		6.5	2.17	13.78			
6/1/07	3510	0.5	0.091	20.55	1.1E-05	1.8E-13	3.4E-03
		5	0.322	19.36	1.1E-05	1.1E-12	2.0E-02
		6.5	0.794	18.51			
6/27/07	3510	0.2	0.05	24.71	1.3E-05	6.3E-13	1.2E-02
		3	0.49	23.59	1.2E-05	1.2E-12	2.2E-02
		5	1.10	23.04			
7/2/07	2267	0.2	0.484	25.53	1.3E-05	7.8E-14	1.4E-03
		1	0.499	25.53	1.3E-05	2.2E-12	4.1E-02
		2	1.042	25.37	1.3E-05	1.2E-11	2.2E-01
		3.5	5.244	26.74			
7/26/07	2267	0.2	1.151	27.09	1.4E-05	1.1E-12	2.1E-02
		1.5	1.499	27.19	1.4E-05	1.6E-12	3.0E-02
		2.5	1.874	27.45	1.4E-05	9.0E-12	1.7E-01
		3.5	3.964	27.67			
7/27/07	2565	0.2	0.1	27.67	1.4E-05	3.3E-12	6.0E-02
		3	2.2	27.14	1.4E-05	1.2E-11	2.2E-01
		5	7.7	27.06	1.3E-05	1.6E-11	2.9E-01
		6.5	13.3	26.02			
8/30/07	3510	0.2	3.4	27.67	1.4E-05	1.0E-11	1.9E-01
		3	10.0	27.14	1.4E-05	1.7E-11	3.1E-01
		5	17.8	27.06			
Average					1.2E-05	3.9E-12	7.3E-02

Table 6a. Estimated water transfer velocities (k_w), volatile selenium fluxes, using an average volatile selenium concentration of 0.52 ng/L in water.

Estuarine model

Wind velocity: 5 miles/h (2.2 m/s)			
T(°C)	k_w (cm/h)	Flux (gSe/cm²/yr)	Flux (Kg Se/yr)
2	1.58	4.2E-08	766
6	1.77	4.6E-08	856
10	1.98	5.2E-08	956
17	2.38	6.2E-08	1150
28	3.06	8.0E-08	1480
Wind velocity: 25 miles/h (11.2 m/s)			
T(°C)	k_w (cm/h)	Flux (gSe/cm²/yr)	Flux (Kg Se/yr)
2	16.07	4.2E-07	7780
6	17.96	4.7E-07	8695
10	20.06	5.3E-07	9710
17	24.12	6.3E-07	11676
28	31.05	8.2E-07	15030

Modified Liss & Merlivat model

Wind velocity: 5 miles/h (2.2 m/s)			
T(°C)	k_w (cm/h)	Flux (gSe/cm²/yr)	Flux (Kg Se/yr)
2	2.05	2.4E-08	450
6	2.37	2.8E-08	522
10	2.75	3.3E-08	605
17	3.52	4.2E-08	774
28	4.92	5.9E-08	1083
Wind velocity: 25 miles/h (11.2 m/s)			
T(°C)	k_w (cm/h)	Flux (gSe/cm²/yr)	Flux (Kg Se/yr)
2	11.12	2.9E-07	5381
6	12.42	3.3E-07	6013
10	13.87	3.6E-07	6715
17	16.68	4.4E-07	8076
28	21.47	5.6E-07	10395

Table 6b. Results of measured volatile Se fluxes compared to Estuarine model predicted fluxes with environmental parameters used in calculations.

Sample ID	Site	Date	Avg. Wind Vel.	Surface Temp.	Vol Se Conc.	Measured Flux	Estuarine Pred. Flux
			m/s	°C	ng/L	ng/m²h	ng/m²h
1B	3510	6/1/07	2.63	20.55	0.21	11.12	6.20
1C	3510	6/27/07	3.74	24.71	0.04	2.08	2.00
2C	2267	7/2/07	1.25	25.53	1.82	20.13	39.64
3C	2267	7/26/07	1.34	27.09	4.59	9.38	105.89
4C	2565	7/27/07	1.86	27.67	0.37	3.23	10.12
1E	2267	9/27/07	3.43	12.00	0.62	7.85	19.75
2E	2267	9/27/07	1.58	12.00	0.33	3.30	5.68

Table 6c. Results of attempted flux recovery test showing significant partitioning of volatilized Se to surfaces of the measurement system.

Sample ID	Mass Added (µg)	Mass Recovered (µg)	Percent Recovery
SR1	0.0075	0.0018	24.3%
SR2	0.0119	0.0008	7.0%
SR3	0.0163	0.0022	13.5%

Table 6d. Summary of errors associated to different parameters used to calculate the volatilization flux of Se to the atmosphere.

Parameter	Error	Reference
Temperature (°C)	+/- 0.5	Crosman & Horel, 2006
Wind velocity (m/s)	+/- 2.5	Horel, 2007
$C_{water}^{1/Se}$ (ng/L)	x/ \div 5.9	Geometric standard deviation
Area Great Salt Lake (acres)	+/- 427.2	Average of calculated area difference per 0.1 foot in depth

Table 7a Results of shallow (only) sediment trap analyses at site 2267

Average month	Days acum.	Average sediment weight (g)	Downward flux (g/cm²/year)	[Se] (mg/Kg)	Se downward flux (gSe/cm²/yr)
Apr-06	64	18.22	2.55	0.27	6.76E-07
Jun-06	24	8.81	3.29	1.54	5.07E-06
Jul-06	39	18.21	4.19	0.31	1.30E-06
Jul-06	32	9.96	2.79	0.20	5.58E-07
Sep-06	64	24.76	3.47	0.33	1.13E-06
Nov-06	36	8.49	2.12	0.20	4.23E-07
Jan-07	103	8.82	0.77	1.16	8.94E-07
Apr-07	37	21.65	5.25		
Jun-07	34	8.13	2.14		
Average			2.95	0.57	1.44E-06
Accumulative	433	127.06	2.63		

n/a – not available

Table 7b Results of deep sediment trap analyses at site 2565

Average month	Days acum.	Average sediment weight (g)	Downward flux (g/cm²/year)	[Se] (mg/Kg)	Se downward flux (gSe/cm²/yr)
Apr-06	64	14.29	2.00	0.02	3.00E-08
Jun-06	24	0.86	0.32	1.70	5.48E-07
Jul-06	39	0.00	0.00	n/a	n/a
Aug-06	45	0.55	0.11	1.67	1.83E-07
Oct-06	51	1.26	0.22	0.23	5.09E-08
Jan-07	139	1.24	0.08	0.51	4.04E-08
Apr-07	37	1.79	0.43	0.15	6.50E-08
Jun-07	42	5.02	1.07		
Average			0.53	0.71	1.53E-07
Accumulative	441	25.01	0.51		

n/a – not available

Table 7c Results of shallow sediment trap analyses at site 2565

Average month	Days acum.	Average sediment weight (g)	Downward flux (g/cm²/year)	[Se] (mg/Kg)	Se downward flux (gSe/cm²/yr)
Apr-06	64	0.000	0.000	n/a	n/a
Jun-06	24	0.000	0.000	n/a	n/a
Jul-06	39	0.000	0.000	n/a	n/a
Aug-06	45	0.169	0.034	1.279	4.30E-08
Oct-06	51	0.000	0.000	n/a	n/a
Jan-07	139	0.853	0.055	0.558	3.07E-08
Apr-07	37	0.512	0.124	0.445	5.52E-08
Jun-07	42	0.301	0.064		
Average			0.035	0.761	4.30E-08
Accumulative	441	1.834	0.037		

n/a – not available

Table 7d Results of deep sediment trap analyses at site 3510

Average month	Days acum.	Average sediment weight (g)	Downward flux (g/cm²/year)	[Se] (mg/Kg)	Se downward flux (gSe/cm²/yr)
Jul-06	30	3.61	1.08	0.01	1.08E-08
Aug-06	47	0.08	0.02	0.87	1.41E-08
Oct-06	52	0.85	0.15	0.18	2.55E-08
Nov-06	34	0.00	0.00	n/a	n/a
Jan-07	101	1.09	0.10	0.70	6.82E-08
Jun-07	28	2.35	0.75	0.10	7.52E-08
Average			0.35	0.31	3.88E-08
Accumulative	292	7.98	0.25		

n/a – not available

Table 7e Results of shallow sediment trap analyses at site 3510

Average month	Days acum.	Average sediment weight (g)	Downward flux (g/cm²/year)	[Se] (mg/Kg)	Se downward flux (gSe/cm²/yr)
Jul-06	30	0.00	0.000	n/a	n/a
Aug-06	47	0.10	0.020	1.44	2.85E-08
Oct-06	52	0.35	0.061	0.20	1.19E-08
Nov-06	34	0.00	0.000	n/a	n/a
Jan-07	101	0.82	0.072	0.76	5.50E-08
Jun-07	28	0.79	0.252	< 0.01	< 2.52E-09
Average			0.068	0.40	3.18E-08
Accumulative	292	2.06	0.063		

n/a – not available

Table 8. Average Se concentration between 0 and 2 cm. in cores and their corresponding sedimentation region

CoreID	Sed Region	Sed Se Conc. (µg/L)
DD-C	High	3.02
2267-2	Low	1.03
DD-Q	Low	3.12
DD-I	Very High NW	1.70
3510-BOX	Low	2.35
DD-L	Medium	2.44
DD-R	Medium	1.65
2565-3	Very Low	0.79
	Average	2.01
	St. Dev.	0.86

Table 9. Average mass accumulation rate (MAR) in each core

CoreID	MAR (g/cm ² /yr)
DD-C	0.036
2267-2	0.000
DD-Q	0.010
DD-I	0.049
3510-BOX	0.043
DD-L	0.025
DD-R	0.027
2565-3	0.000
Average	0.024
St. Dev.	0.019

Table 10. Average 0-2 cm Se concentration, MAR, area, and calculated mass of selenium removed annually within each sedimentation zone

Sed Region	Area of Zone (Km²)	Avg. [Se] 0-2 cm (µg/g)	MAR (g/cm2/yr)	Mass of Se Removed (Kg/yr)
Very Low	1233.2	0.79	0.009	86.06
Low	404.6	2.16	0.018	154.63
Medium	358.5	2.04	0.026	190.15
High	47.9	3.02	0.036	52.08
Very High SE	4.6	3.02	0.045	6.25
Very High NW	34.3	1.70	0.049	28.49
			Total	517.65

Table 11a. Relative standard deviation (RSD) for Se concentration, area, and mass accumulation rate (MAR) propagated through to a relative standard deviation for each sedimentation region

Sed Region	RSD [Se]	RSD Area	RSD MAR	Total Zone RSD
Very Low	2.27	0.00083	3.89	4.51
Low	0.73	0.00083	0.70	1.01
Medium	0.49	0.00083	1.03	1.14
High	0.20	0.00083	0.19	0.28
Very High SE	0.20	0.00083	0.19	0.28
Very High NW	0.34	0.00083	0.17	0.38

Table 11b. Estimation of total uncertainty and range of Se removal by sedimentation based on a mean removal of 517.65 Kg_{Se}/yr

Sed Region	Total Zone RSD	Mass of Se Removed (Kg/yr)	Total Zone Uncertainty (Kg/yr)
Very Low	4.51	86.06	387.69
Low	1.01	154.63	156.38
Medium	1.14	190.15	217.55
High	0.28	52.08	14.57
Very High SE	0.28	6.25	1.75
Very High NW	0.38	28.49	10.82
	Total	517.65	471.61
	Range of Removal	46.05	989.26

Table 12. Change in elevation of the deep brine layer (DBL) corresponds to change in lake surface elevation, site 2565. Depth measurement determined from monthly water column profile.

Date	Depth to DBL (m.)	Saltair lake elevation (ft.)	Elevation of DBL (ft.)
6/19/06	6.5	4198.0	4176.7
7/28/06	6.5	4197.2	4175.9
9/28/06	6.5	4196.4	4175.1
11/1/06	6.5	4196.5	4175.2
11/21/06	6.5	4196.5	4175.2
12/6/06	6.5	4196.6	4175.3
3/20/07	6.5	4197.5	4176.2
4/26/07	6.5	4197.5	4176.2
5/10/07	6.5	4197.4	4176.1
5/23/07	6.5	4197.3	4176.0
6/26/07	6.5	4196.9	4175.6
7/25/07	6.5	4196.3	4175.0

Table 13. Arithmetic average values of batch test results for selenium and other trace metals given as percent solubilized (of extractible). Negative values indicate a decrease in water concentration compared to the shallow brine water used in the experiment.

Element	24 hour (air headspace)	Week	Month
Se	1.16 ± 1.36 %	2.40 ± 1.09 %	3.01 ± 1.06 %
As	2.04 ± 2.60 %	6.53 ± 4.19 %	-0.85 ± 3.40 %
Cd	0.58 ± 0.64 %	1.25 ± 1.38 %	2.05 ± 2.88 %
Co	0.62 ± 0.57 %	0.12 ± 0.10 %	1.13 ± 1.14 %
Cu	0.37 ± 0.57 %	-0.07 ± 0.08 %	0.70 ± 0.95 %
Mn	0.86 ± 0.64 %	0.76 ± 0.33 %	0.98 ± 0.85 %
Ni	0.49 ± 0.50 %	0.26 ± 0.08 %	0.74 ± 0.59 %
Pb	0.69 ± 0.74 %	-0.05 ± 0.04 %	1.04 ± 1.57 %
Sb	2.07 ± 5.82 %	5.85 ± 6.32 %	-4.01 ± 11.36 %
U	2.91 ± 2.05 %	4.99 ± 3.31 %	3.29 ± 4.26 %
Zn	1.00 ± 0.88 %	-0.04 ± 0.06 %	0.84 ± 0.98 %

Table 14a. Low, medium and high fluxes used in the removal processes distribution. Volatilization flux range was determined for 68% confidence interval (CI).

	LOW FLUXES (Kg/yr)	MEDIUM FLUXES (Kg/yr)	HIGH FLUXES (Kg/yr)
Volatilization (68% CI)	1380	2108	3210
Permanent sedimentation	45	520	990
Brine shrimp harvesting	28	28	28
TOTAL	1453	2656	4228

Table 14b. Low, medium and high fluxes used in the removal processes distribution. Volatilization flux range was determined for 95% confidence interval (CI).

	LOW FLUXES (Kg/yr)	MEDIUM FLUXES (Kg/yr)	HIGH FLUXES (Kg/yr)
Volatilization (95% CI)	820	2108	5450
Permanent sedimentation	45	520	990
Brine shrimp harvesting	28	28	28
TOTAL	893	2656	6468

Table 15. Estimated values for wet and dry Se atmospheric deposition flux at different locations.

	Estimated Se atmospheric deposition flux	Reference
Wet depositional flux, Bermuda ($\mu\text{mol}/\text{m}^2/\text{yr}$)	0.42	Cutter&Cutter, 1998
Wet depositional flux, Mace Head, Ireland ($\mu\text{mol}/\text{m}^2/\text{yr}$)	0.78	Cutter&Cutter, 1998
Total (wet+dry) deposition, Amazon River ($\text{nmol}/\text{m}^2/\text{yr}$)	1772	Cutter&Cutter, 2001
Wet deposition, Barbados ($\text{nmol}/\text{m}^2/\text{yr}$)	1440	Cutter&Cutter, 2001
Lake Superior, dry deposition ($\mu\text{g}/\text{m}^2/\text{yr}$)	52	Sweet et al, 1998
Lake Superior, wet deposition ($\mu\text{g}/\text{m}^2/\text{yr}$)	520	Sweet et al, 1998
Lake Michigan, dry deposition ($\mu\text{g}/\text{m}^2/\text{yr}$)	52	Sweet et al, 1998
Lake Michigan, wet deposition ($\mu\text{g}/\text{m}^2/\text{yr}$)	520	Sweet et al, 1998
Lake Erie, dry deposition ($\mu\text{g}/\text{m}^2/\text{yr}$)	95	Sweet et al, 1998
Lake Erie wet deposition ($\mu\text{g}/\text{m}^2/\text{yr}$)	630	Sweet et al, 1998
Chesapeake Bay- average, dry deposition ($\mu\text{g}/\text{m}^2/\text{yr}$)	259	Baker et al, 1994
Chesapeake Bay- average, wet deposition ($\mu\text{g}/\text{m}^2/\text{yr}$)	130	Baker et al, 1994
Chesapeake Bay- average- total deposition ($\mu\text{g}/\text{m}^2/\text{yr}$)	389	Baker et al, 1994

FIGURES

Figure 1. Great Salt Lake sampling locations. GS sites are located within the 6-m-depth boundary (in red) (Map courtesy of the USGS)

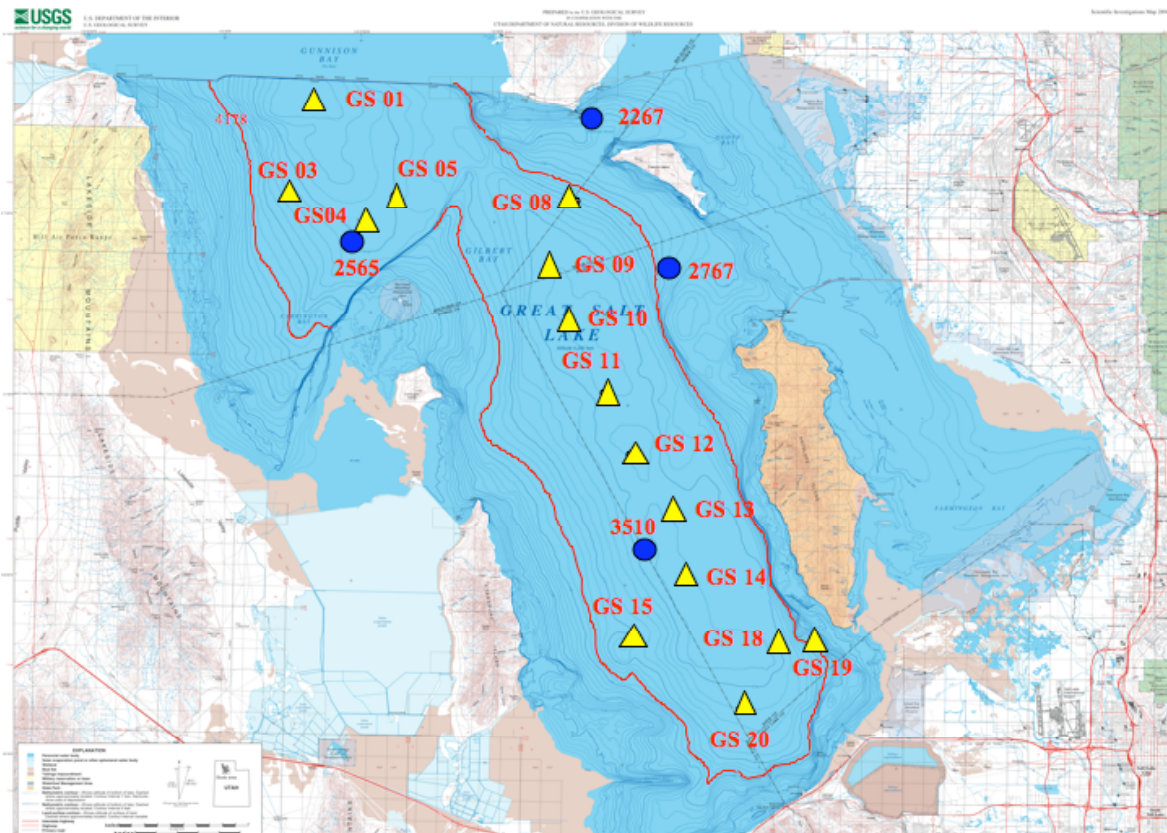


Figure 2a. Schematic representation of thermistor positions in sediment traps.

**2565 and 3510
Thermistor
Locations**

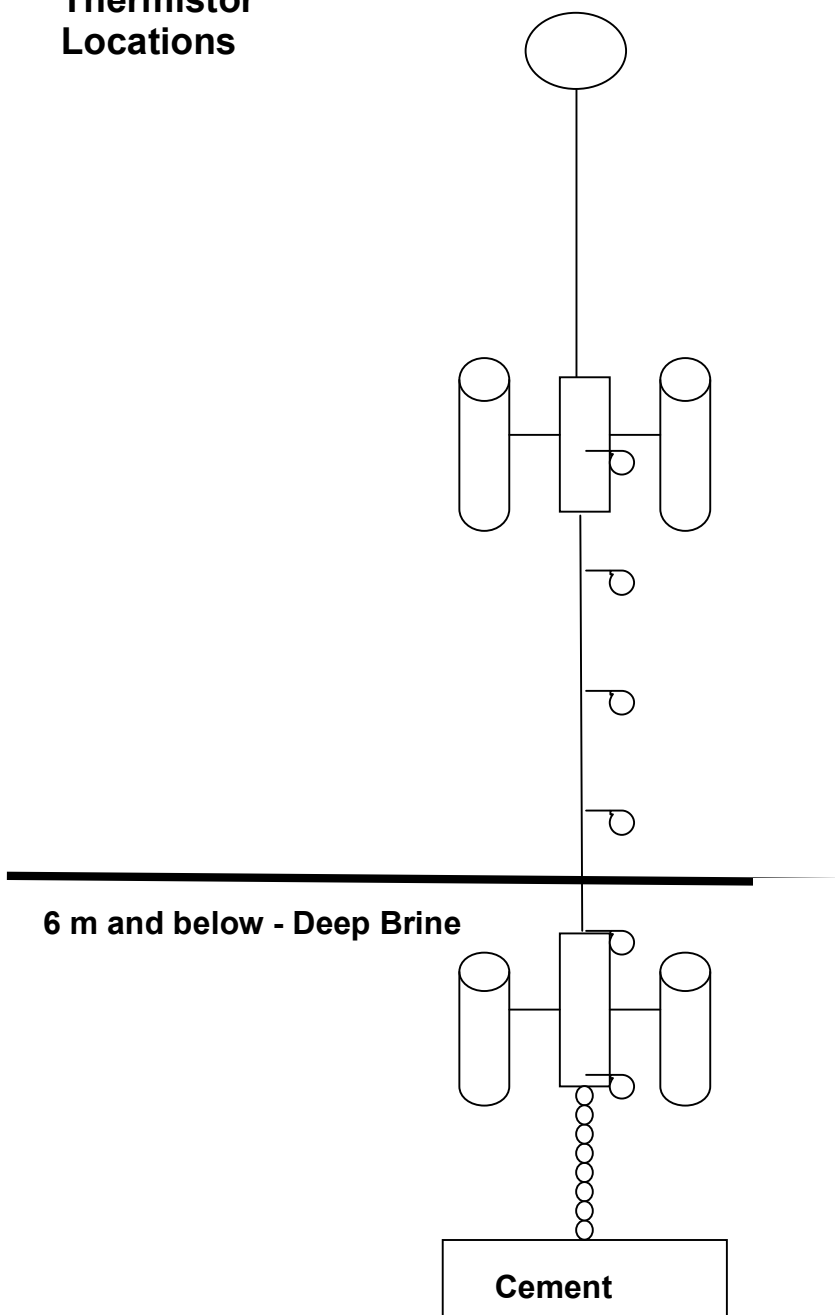


Figure 2b. Schematic of sediment traps for shallow site (2267)

**Shallow Sediment Trap
TD 4.1 m**

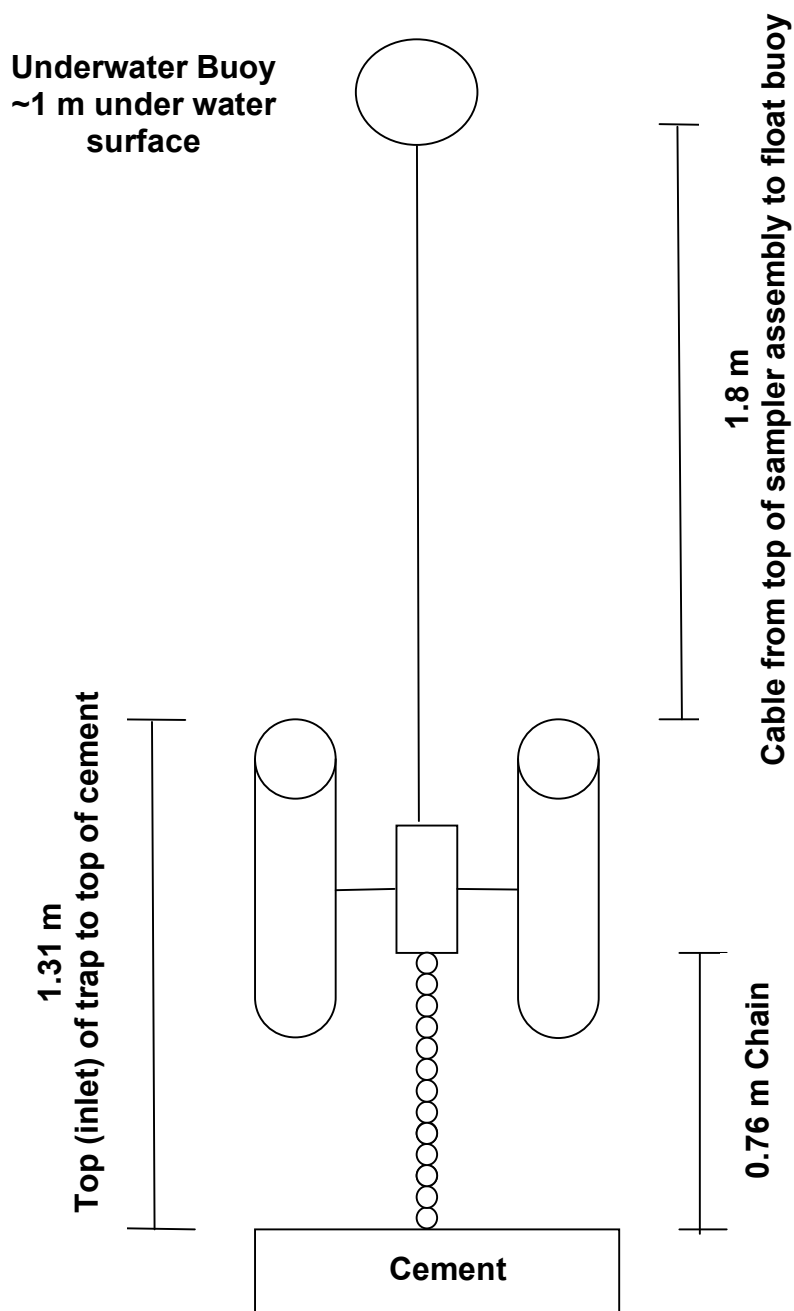


Figure 2c. Schematic of sediment traps for deep sites (2565 and 3510)

Deep site Sediment Trap
TD 8.1 m (2565) or 8.4 m (3510)

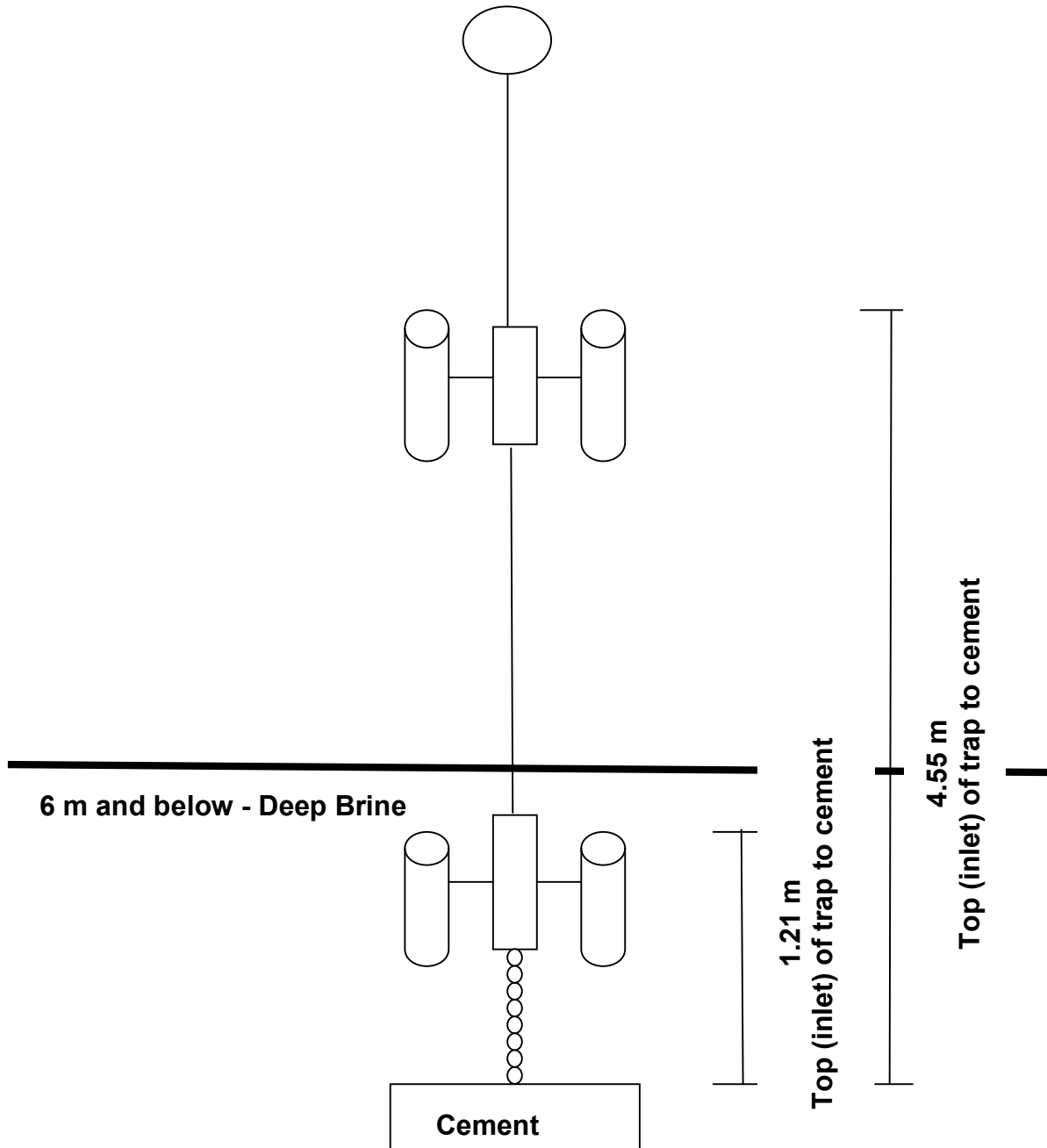


Figure 2d. Long core sampling locations

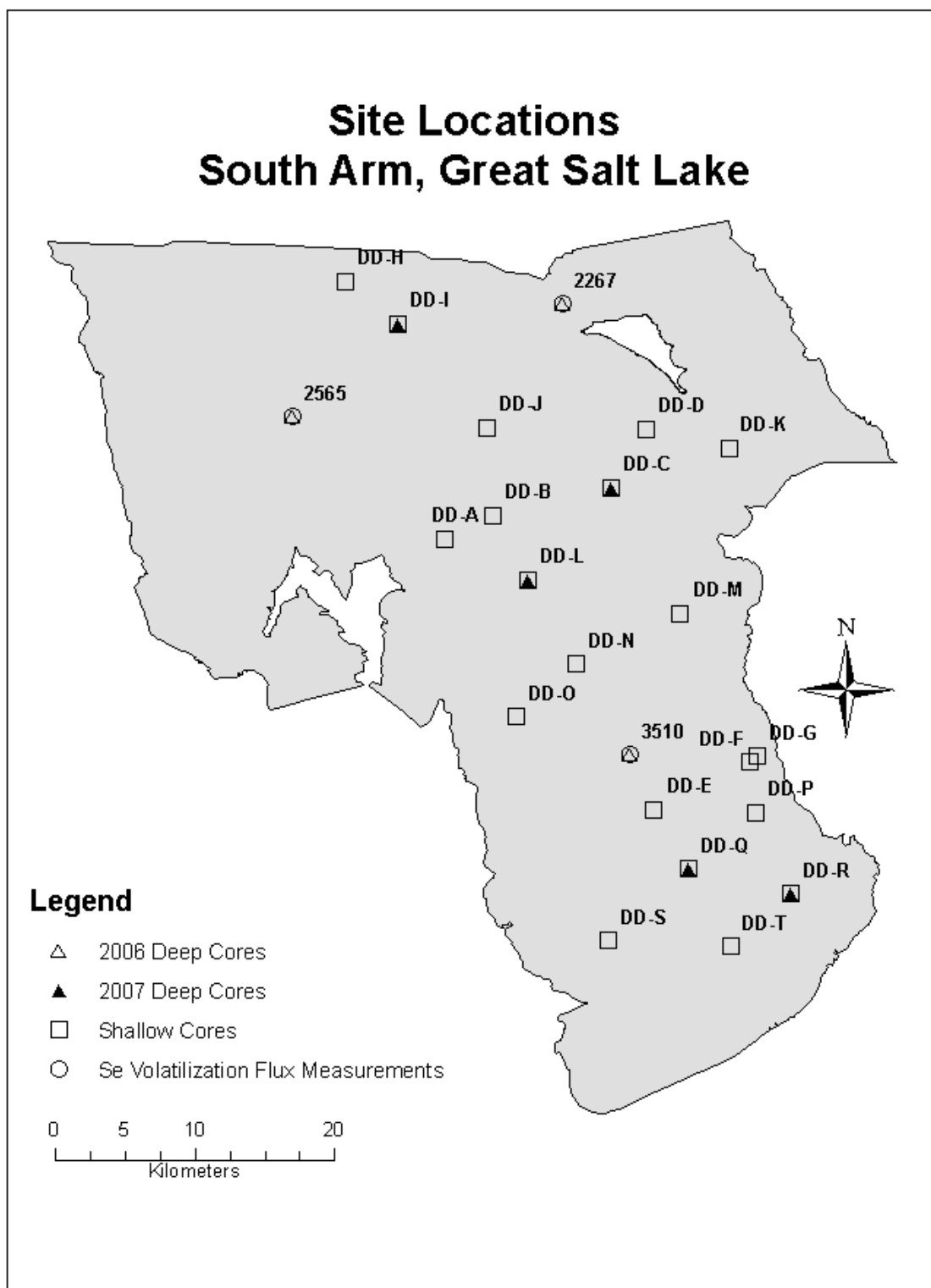


Figure 3a. Schematic representation of the volatile selenium cryo-focusing trap collection system

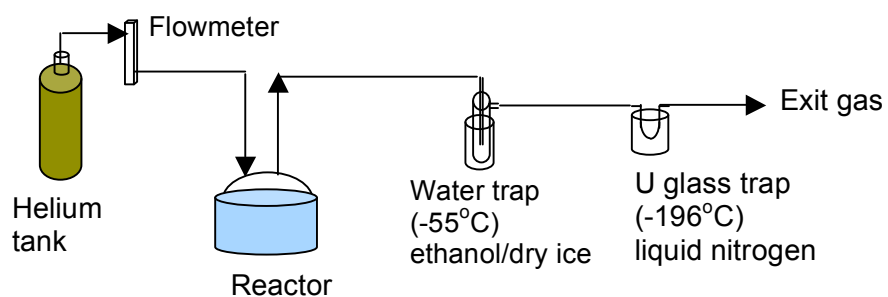


Figure 3b. Calibration curve for dimethyl selenide using the purge and trap system.

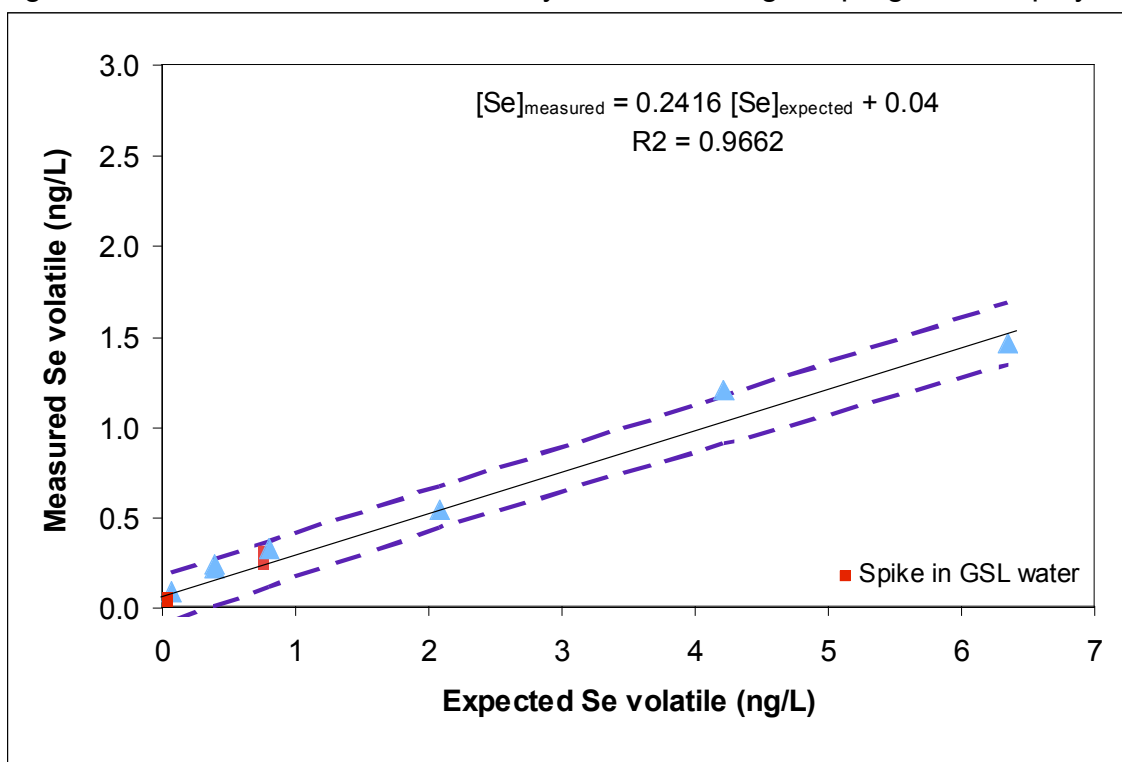


Figure 3c. AVHRR temperature compared with measured temperature at Gunnison Island weather station from January to December 2006 (top). Same comparison for Gunnison Island temperatures from September 2006 to August 2007 (bottom) with the AVHRR data from 2006.

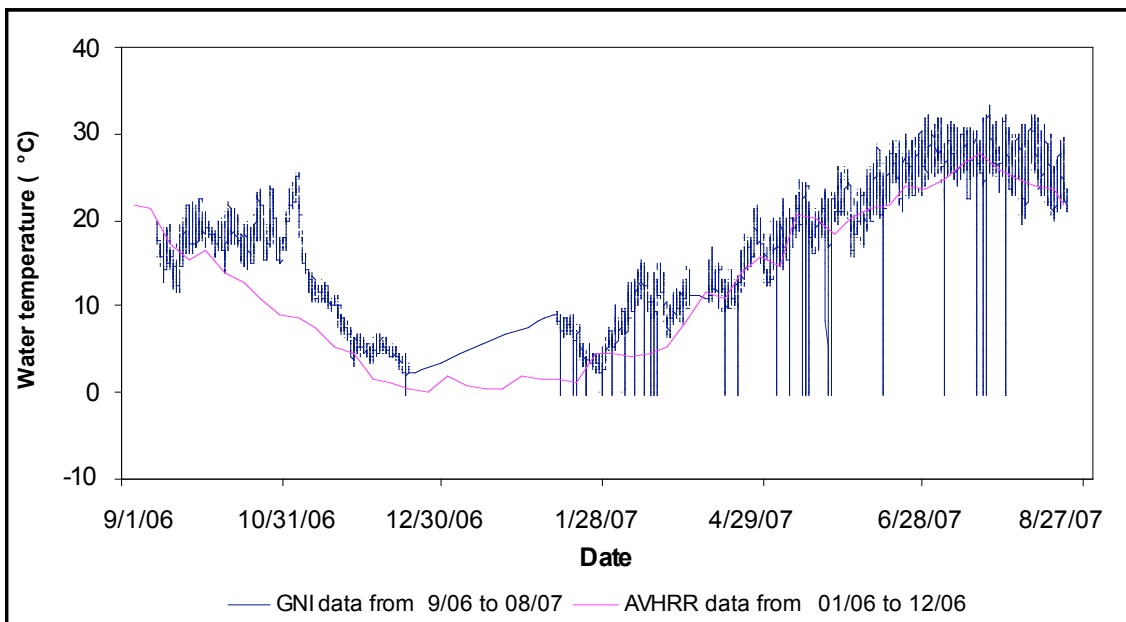
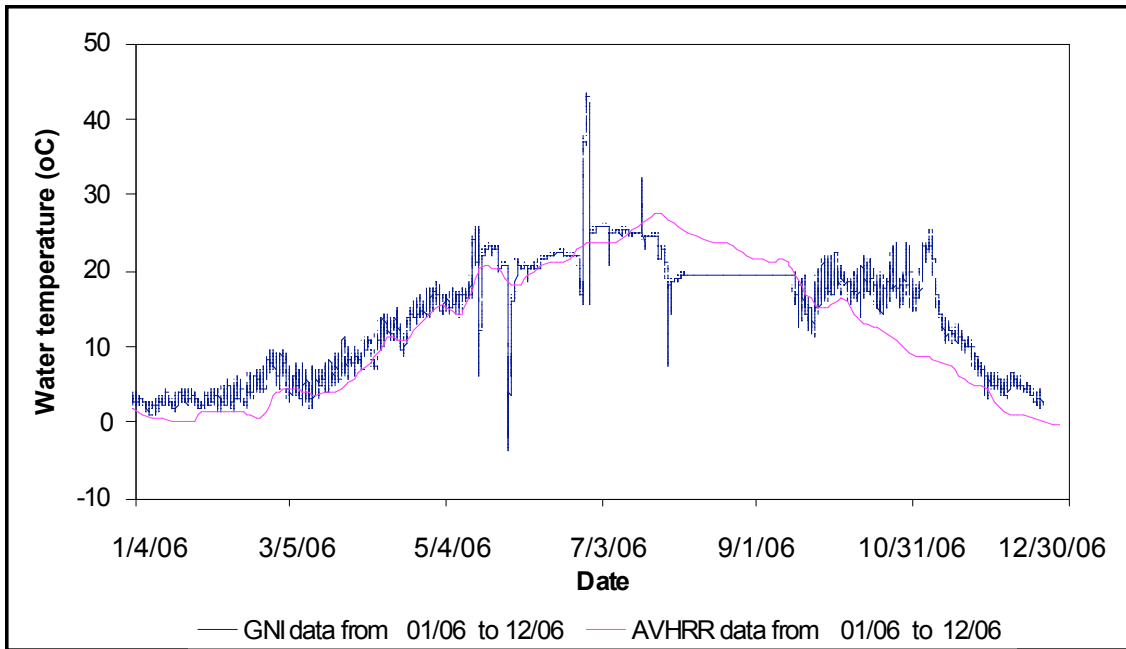


Figure 4a. St Croix Sensory, Inc. Emission Isolation Flux Chamber during sample collection on calm day.

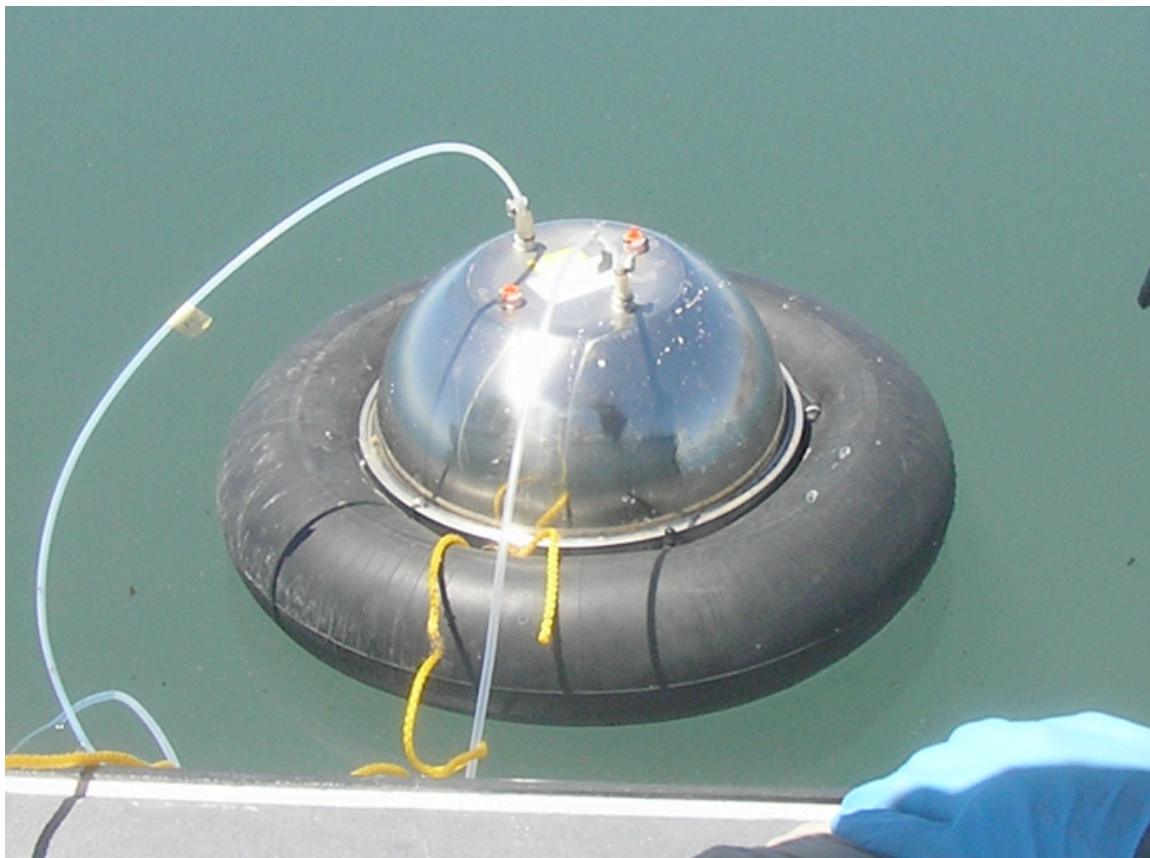


Figure 4b. Diagram of temperature-controlled cryo-focusing system for collection of volatilized selenium from GSL.

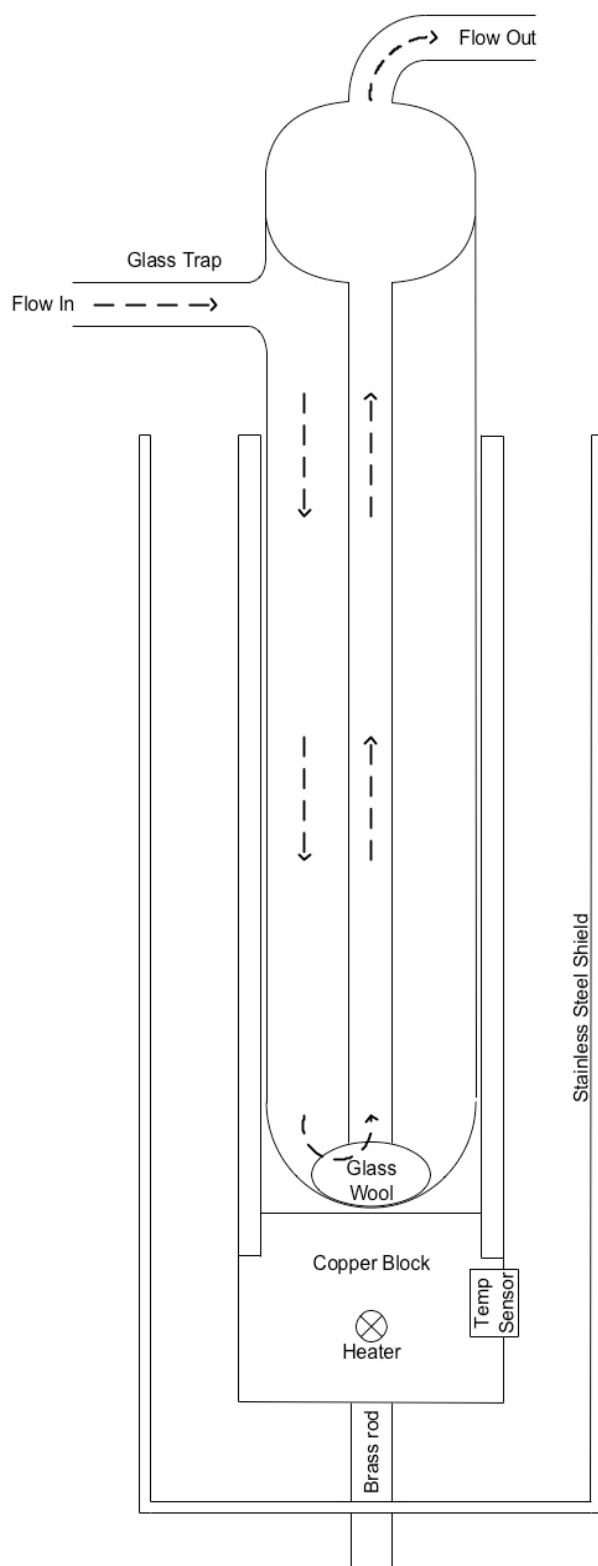
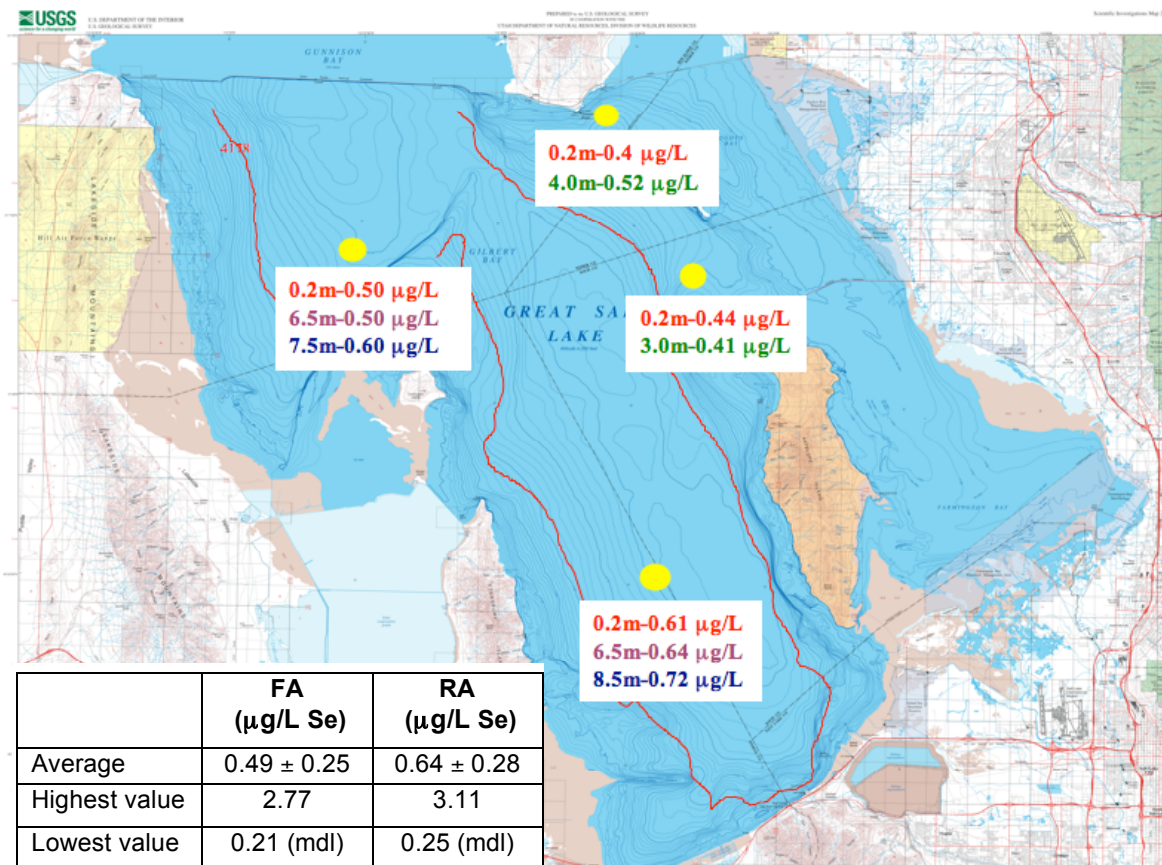


Figure 5. Spatial distribution of total (RA) aqueous selenium concentrations from May 2006. Average, high, and low concentrations (n = 128) for period from May 2006 to July, 2007. RA refers to “raw acidified”, FA refers to “filtered acidified”. (Map courtesy of the USGS).



mdl: method detection limit

Figure 6a. Dissolved oxygen (DO) profiles.

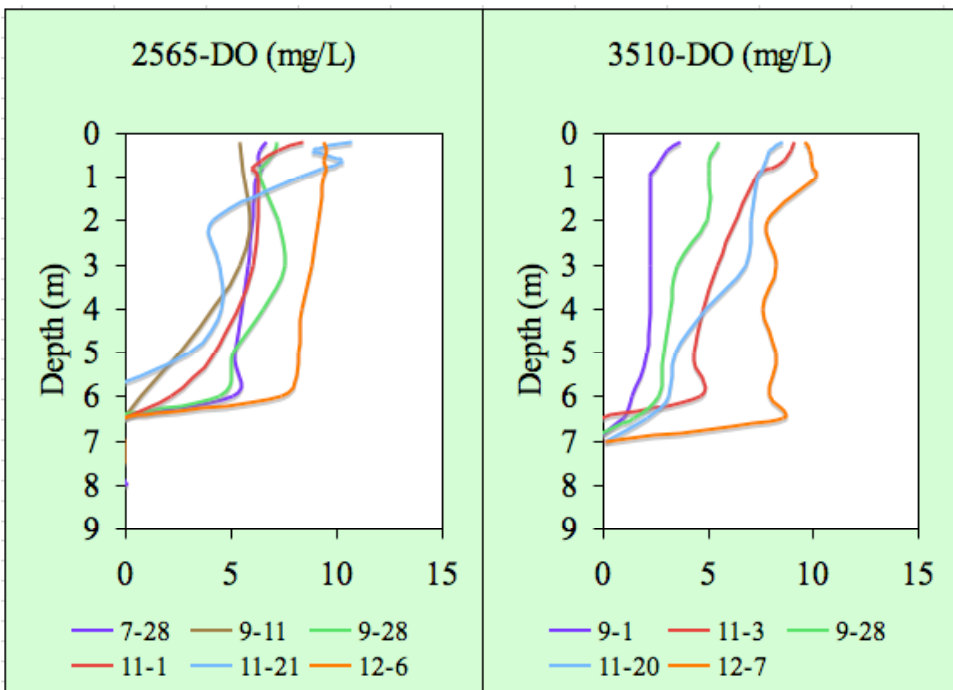
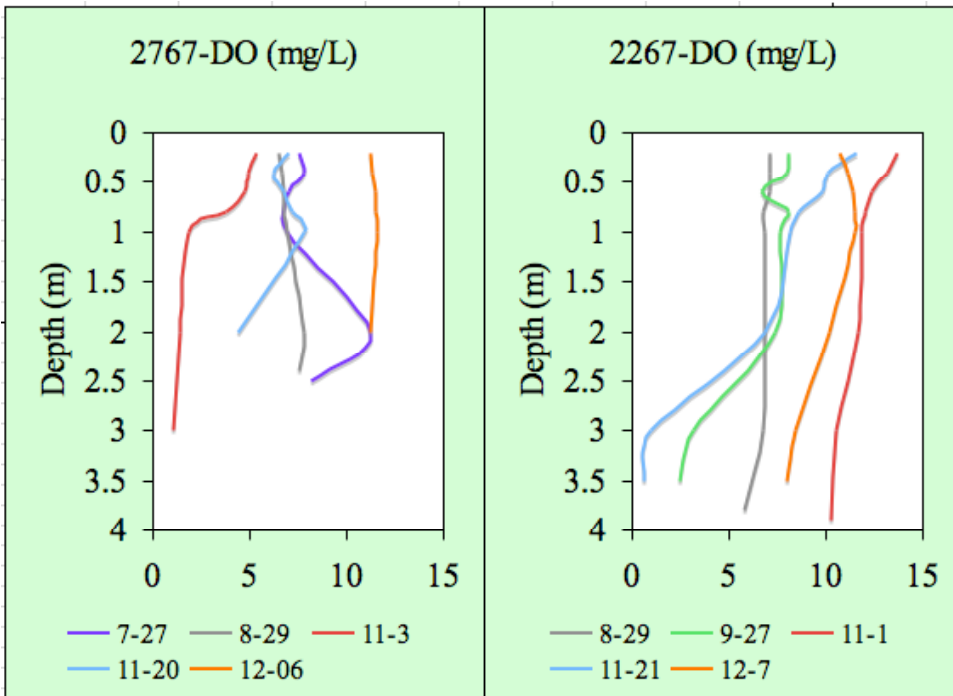


Figure 6b. Oxidation reduction potential (ORP) profiles.

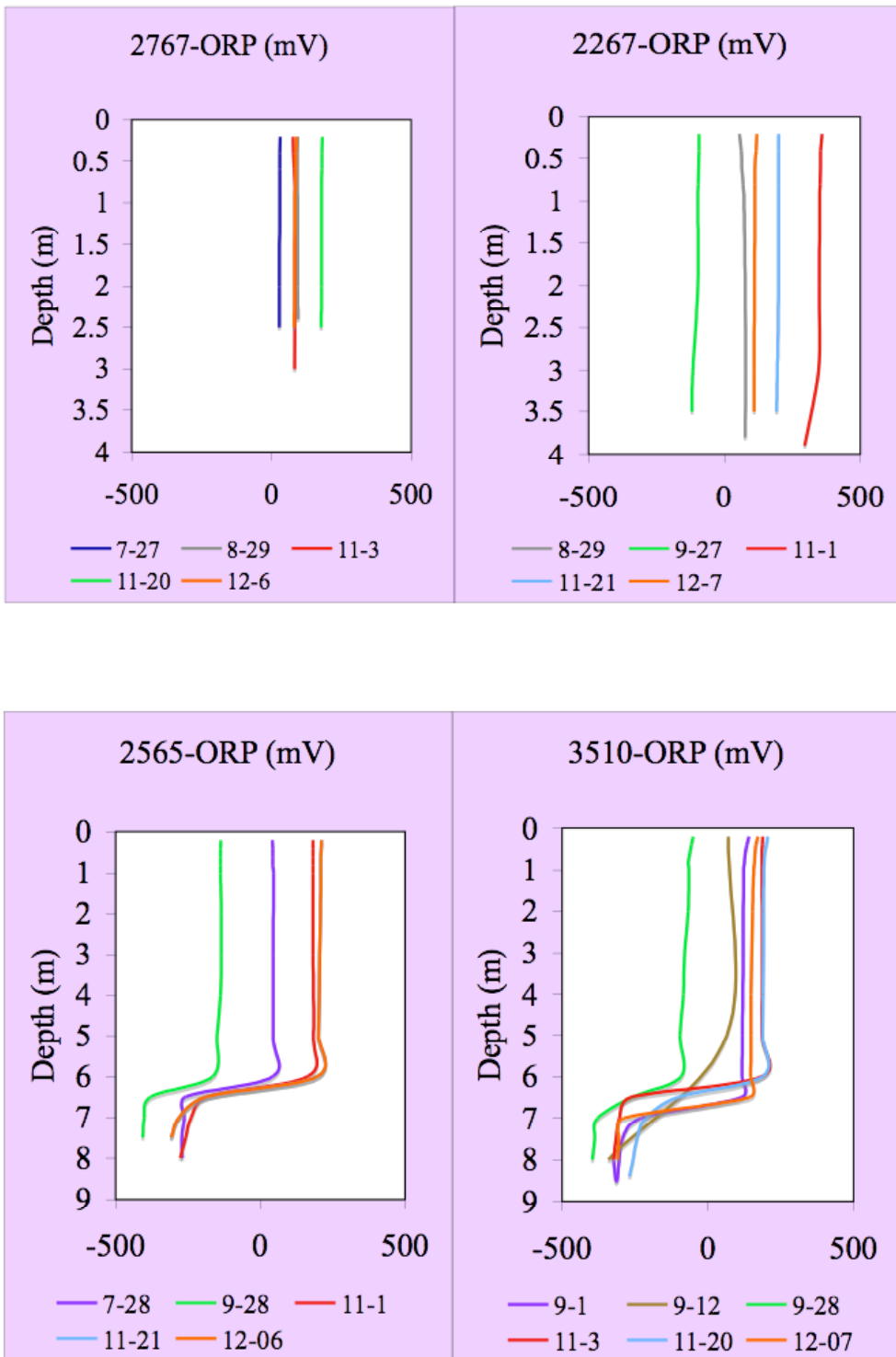


Figure 6c. Conductivity profiles.

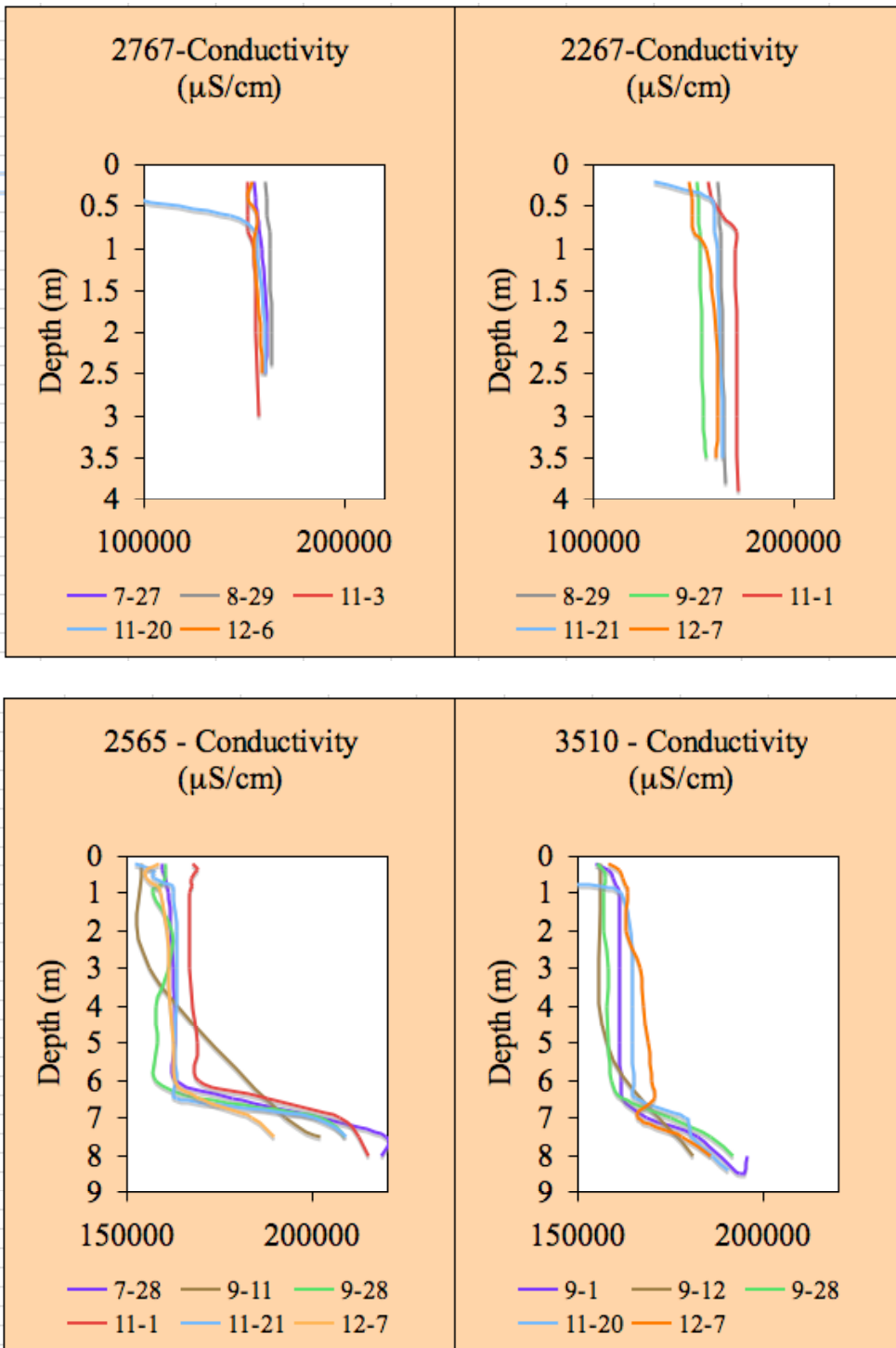


Figure 6d. pH profiles.

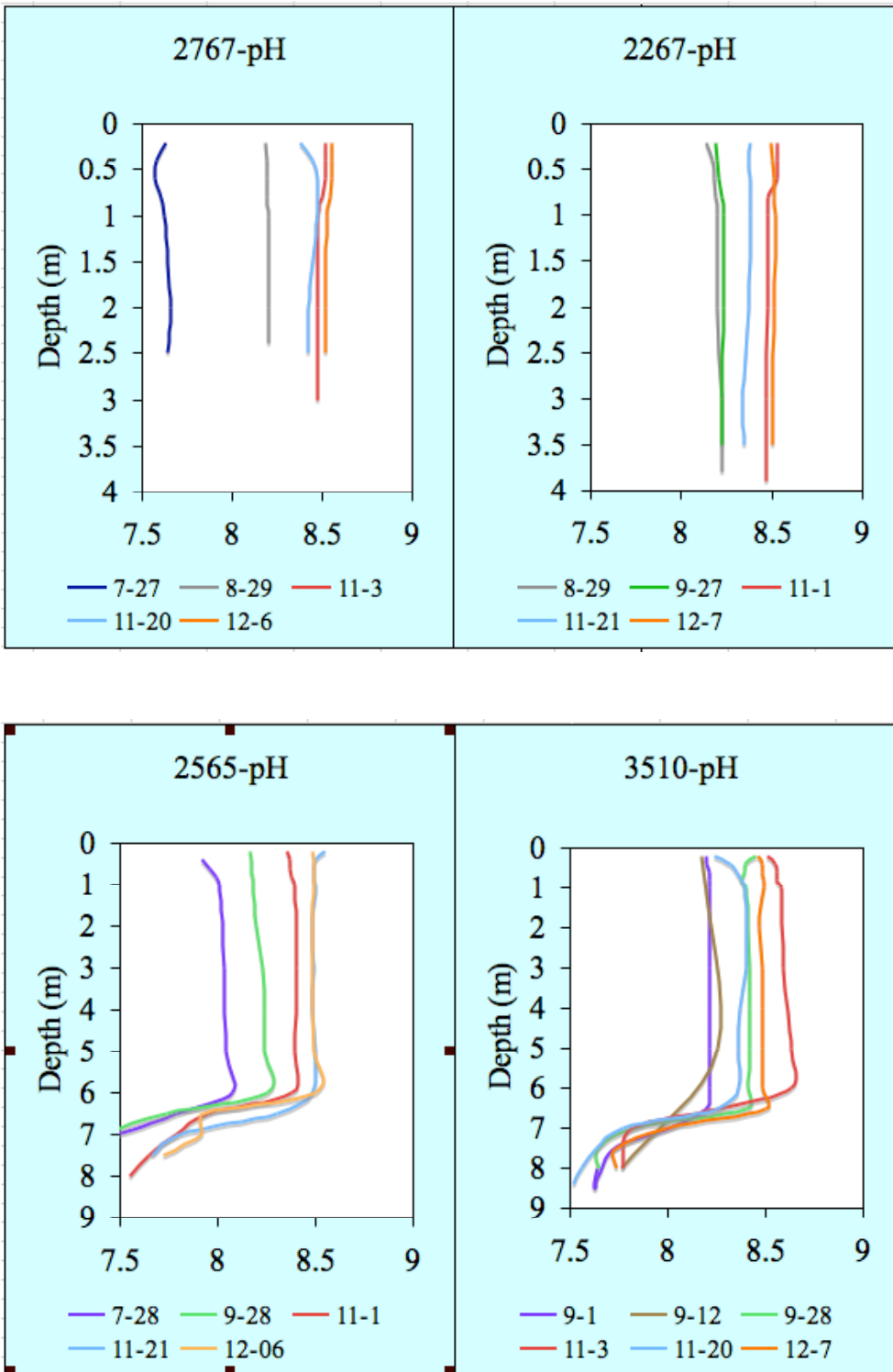


Figure 6e. Temperature profiles.

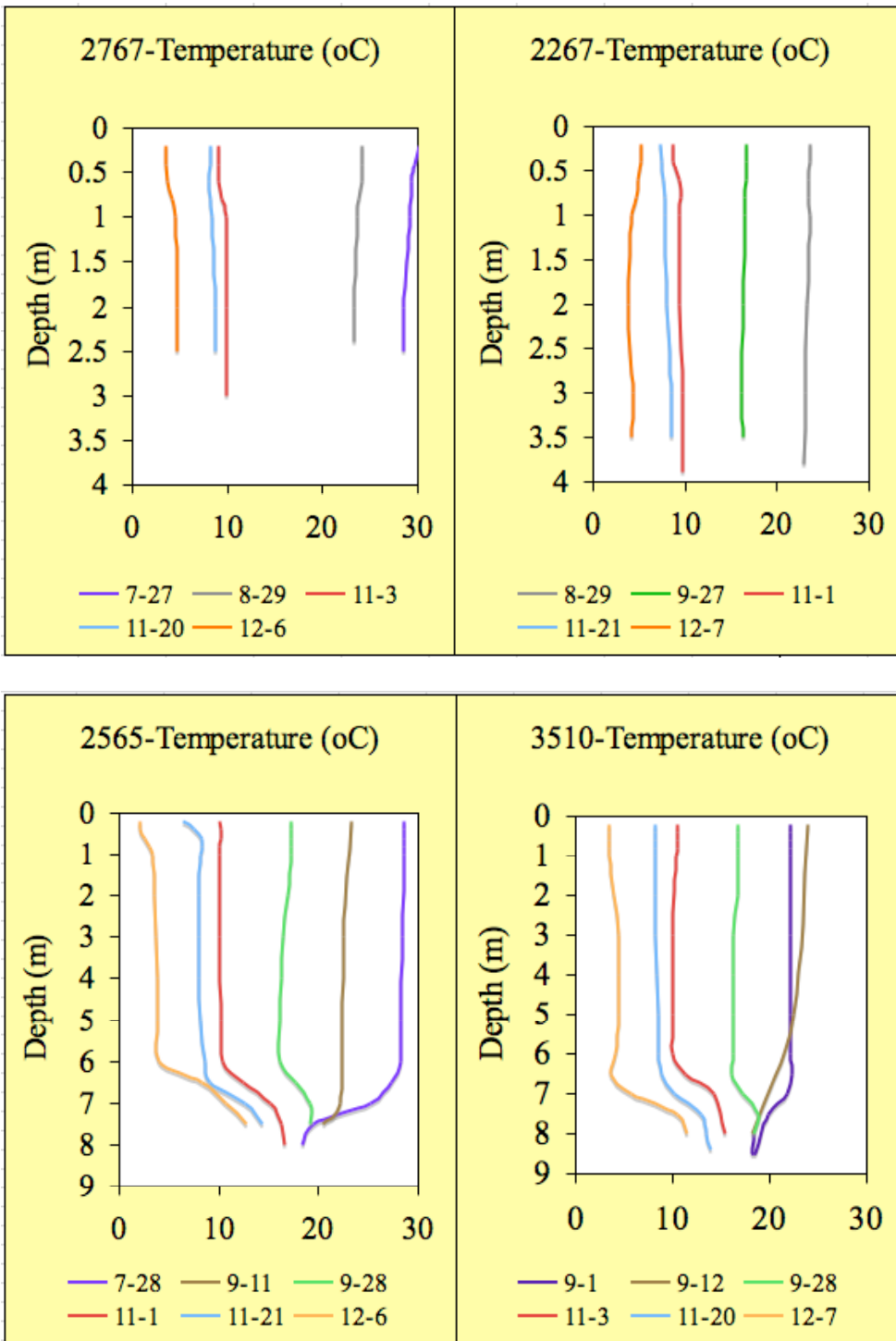


Figure 7a. Total (RA) and dissolved (FA) selenium aqueous concentrations at site 2267.

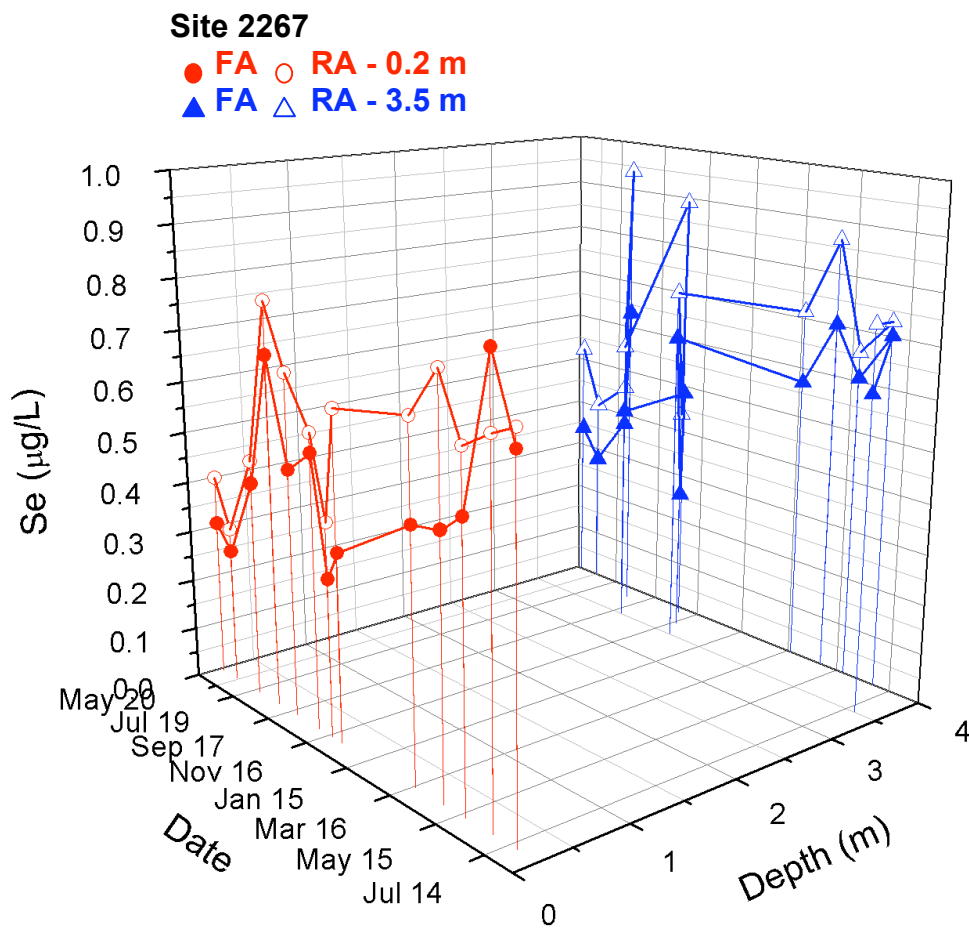


Figure 7b. Total (RA) and dissolved (FA) aqueous selenium concentrations at site 2767.

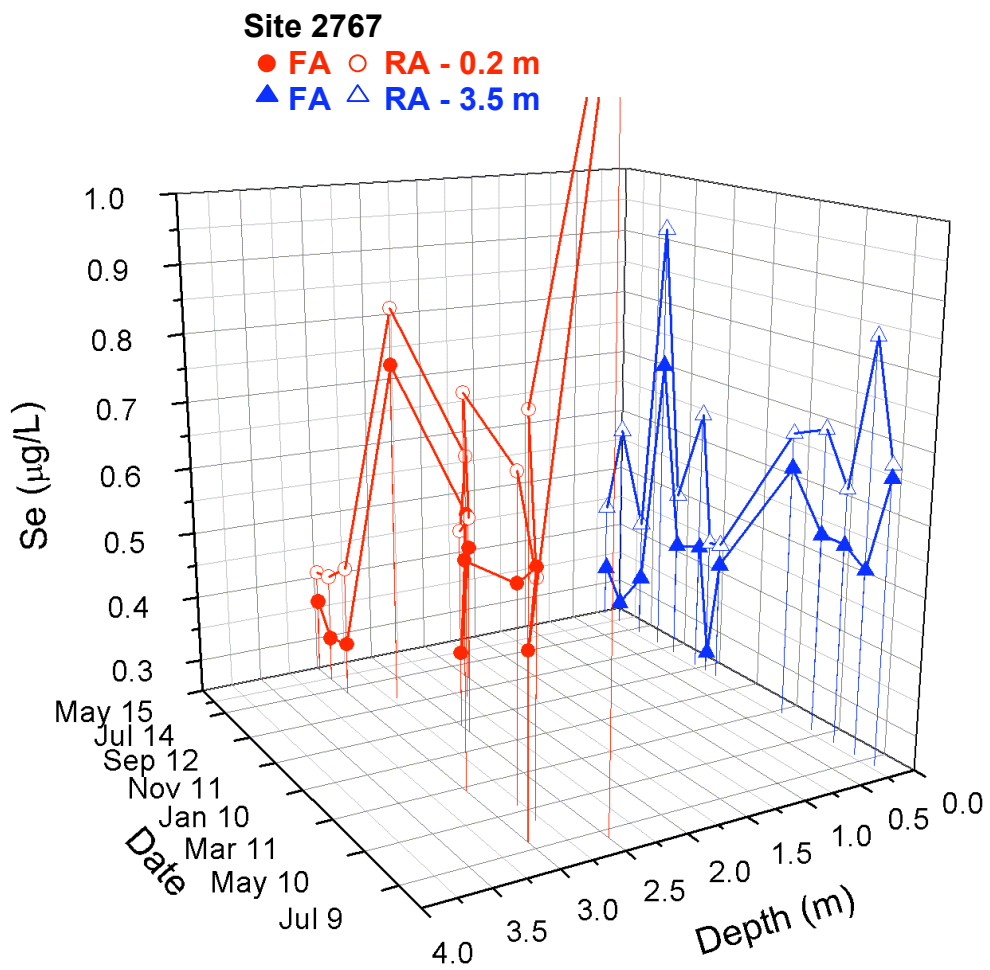


Figure 7e. Total Se concentration trend in water samples analyzed at the U of Utah via ICP-MS

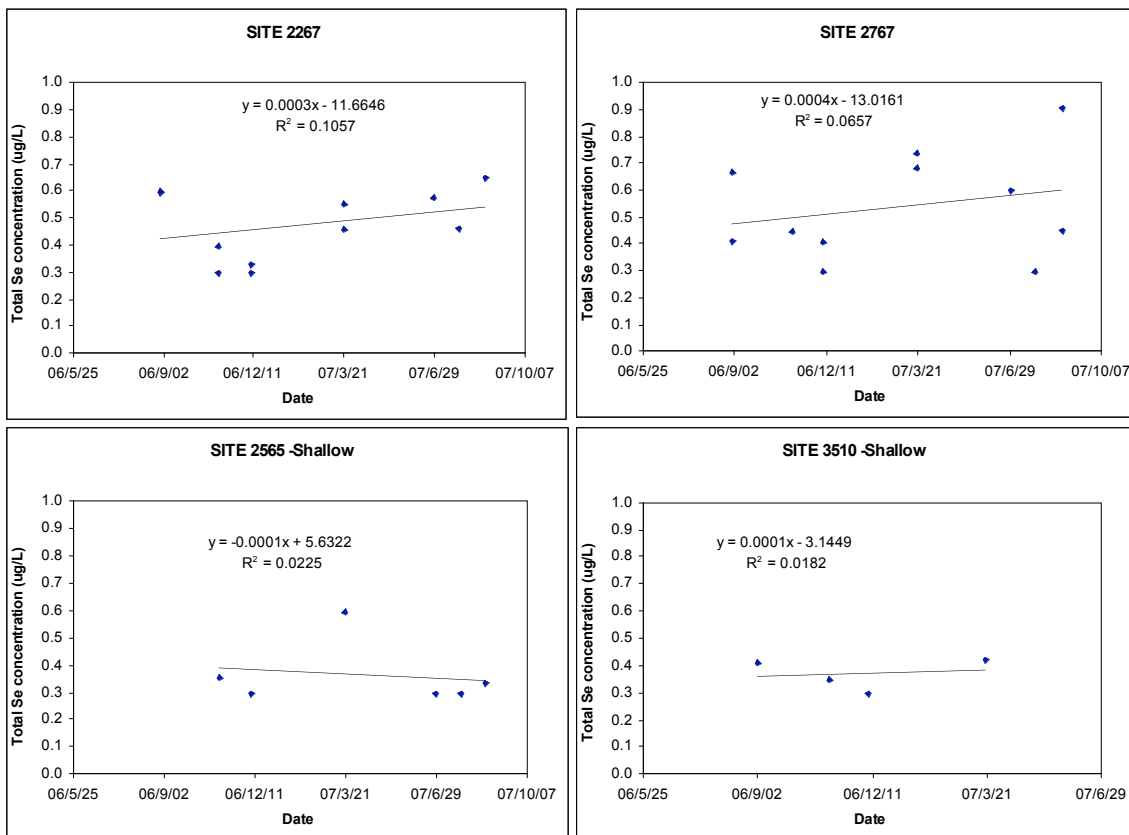


Figure 7f. Dissolved Se concentration trend in water samples analyzed at the U of Utah via ICP-MS.

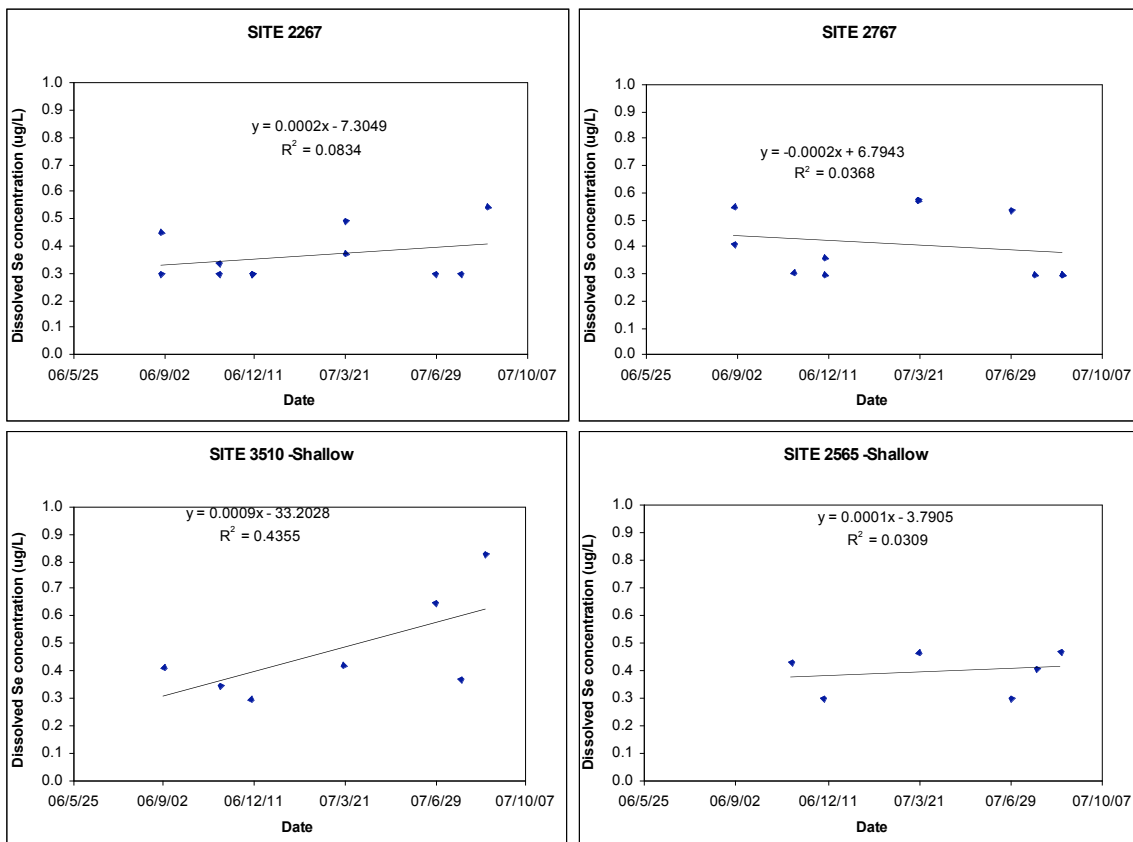


Figure 8a. Average values of dissolved trace elements in shallow and deep brine layers.

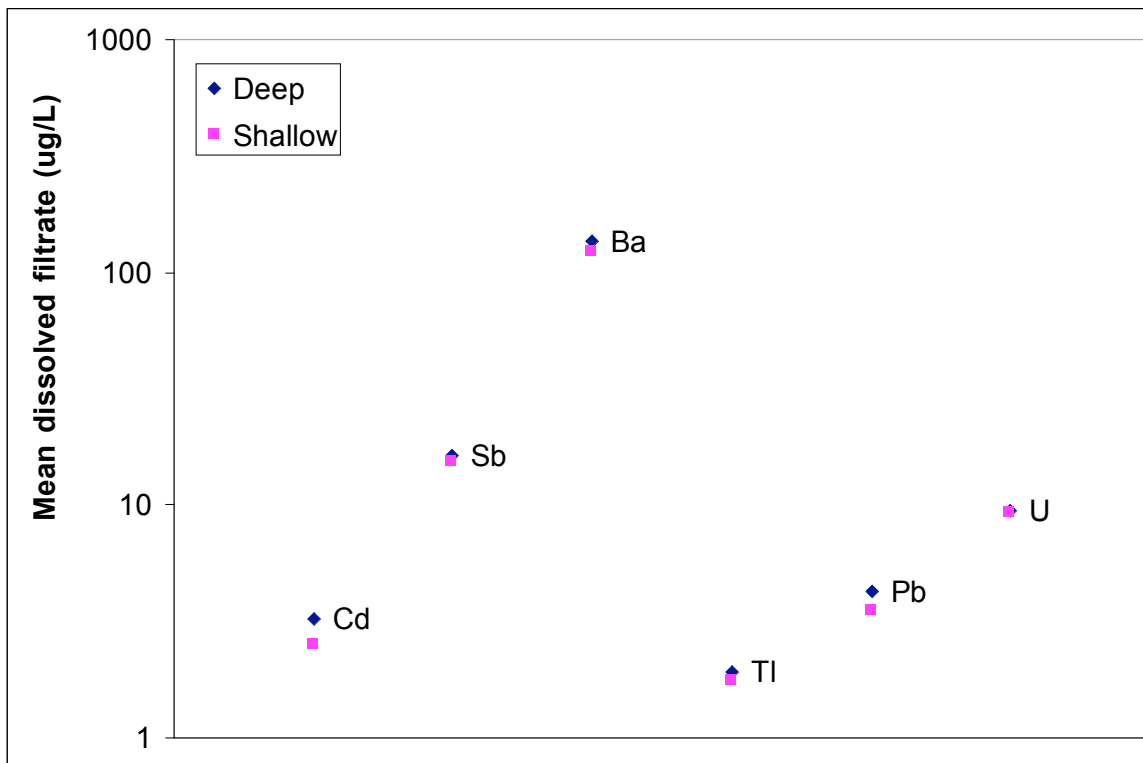


Figure 8b. Average values of dissolved trace elements in shallow and deep brine layers.

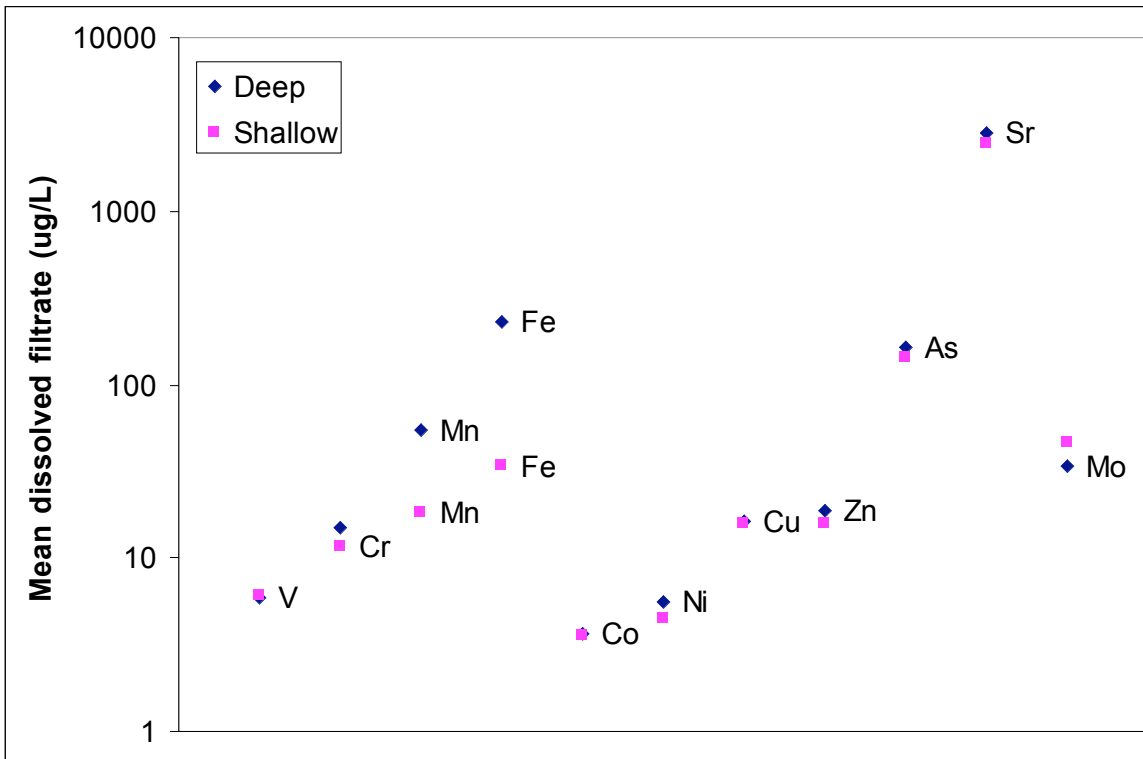


Figure 8c. Average values of dissolved major elements in shallow and deep brine layers.

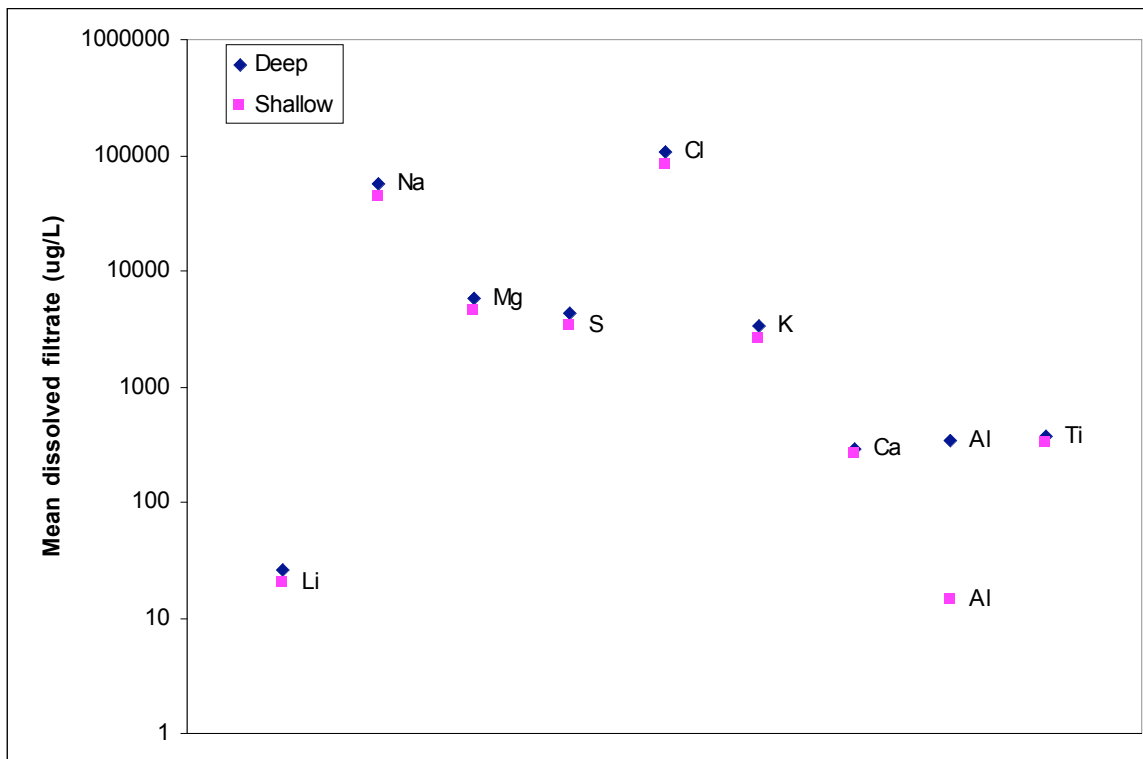


Figure 9a. Percentage of trace element concentration found to be associated with particulates

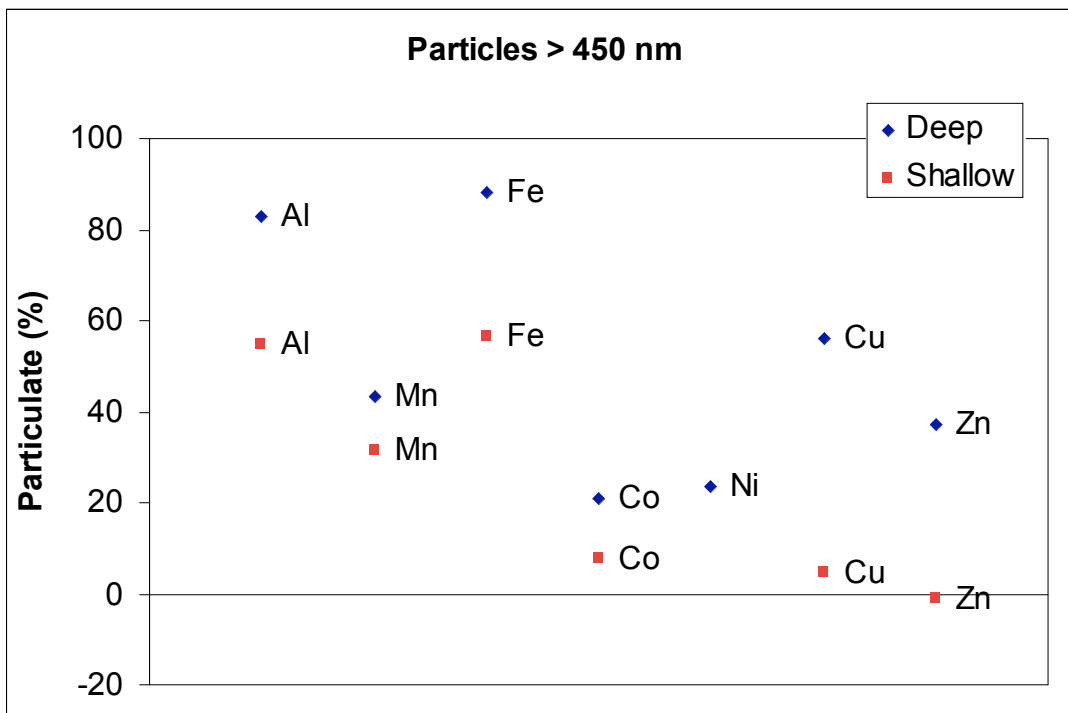


Figure 9b. Percentage of trace element concentration found to be associated with particulates

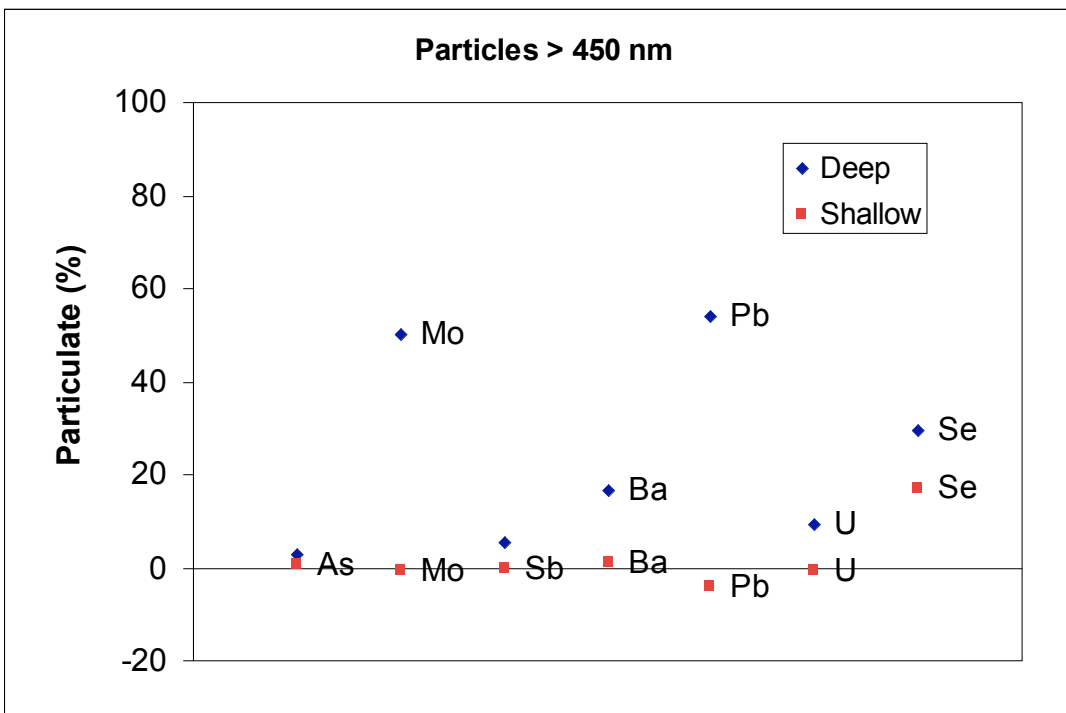


Figure 9c. Percentage of major element concentration found to be associated with particulates

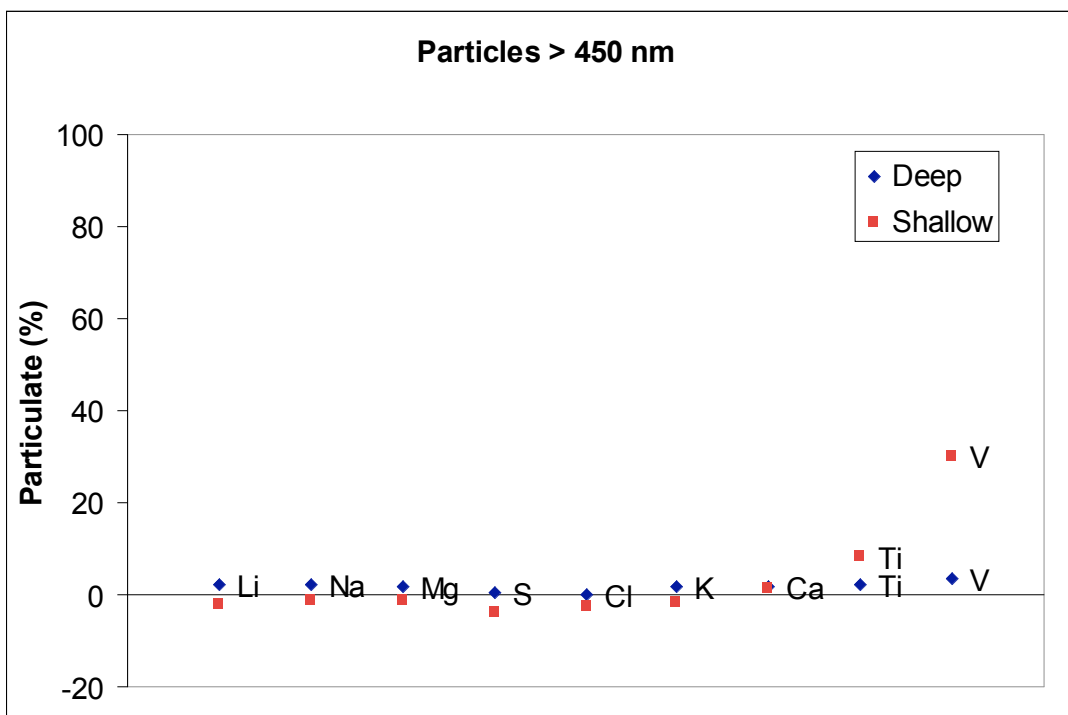
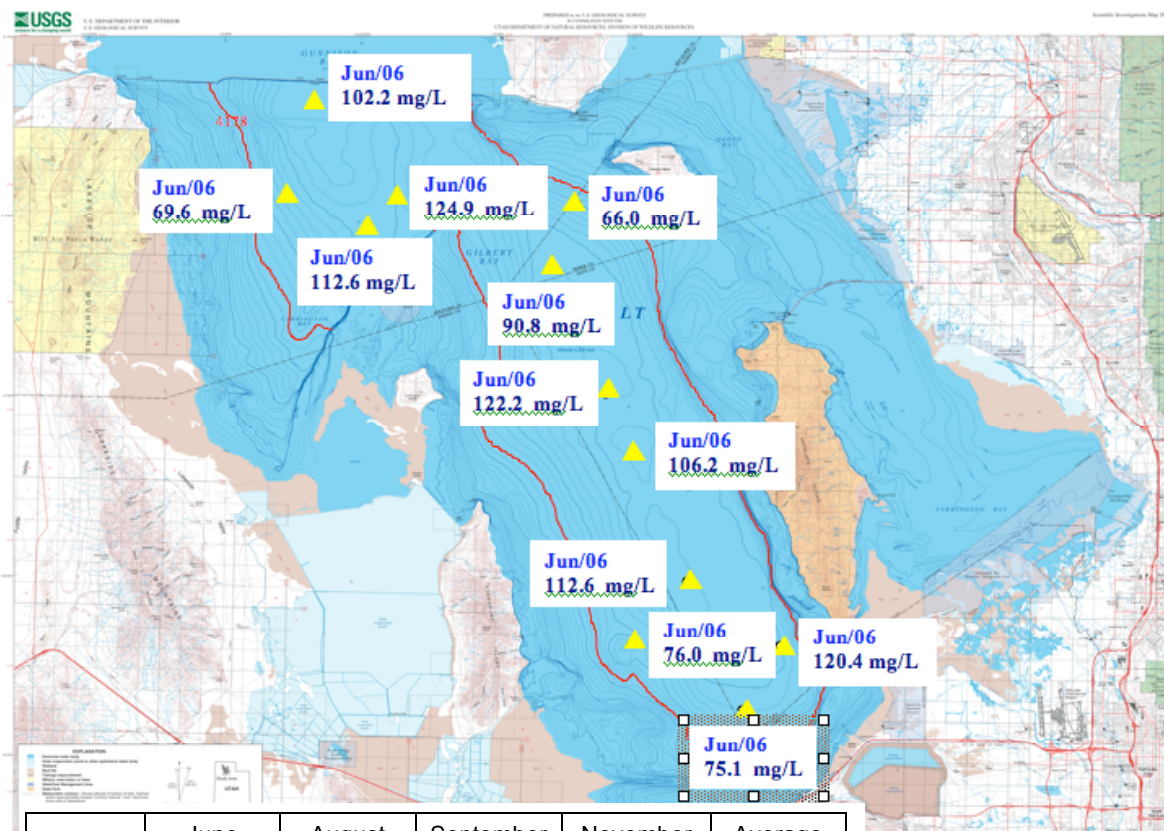


Figure 10. Spatial variation of TOC in deep brine waters (June used as an example). Average concentration of TOC by temporal variation showed in table. (Map courtesy of the USGS)



	June (mg/L)	August (mg/L)	September (mg/L)	November (mg/L)	Average (mg/L)
Average	96.1±21.5	84.4±14.4	86.8±16.3	101.9±25.1	92.3±19.3
Highest	124.9	104.2	100.6	138.7	124.9
Lowest	56	51.7	50.9	58.7	50.9

Figure 11. Selenium concentrations (mg/Kg) in bed sediments (Map courtesy of the USGS).

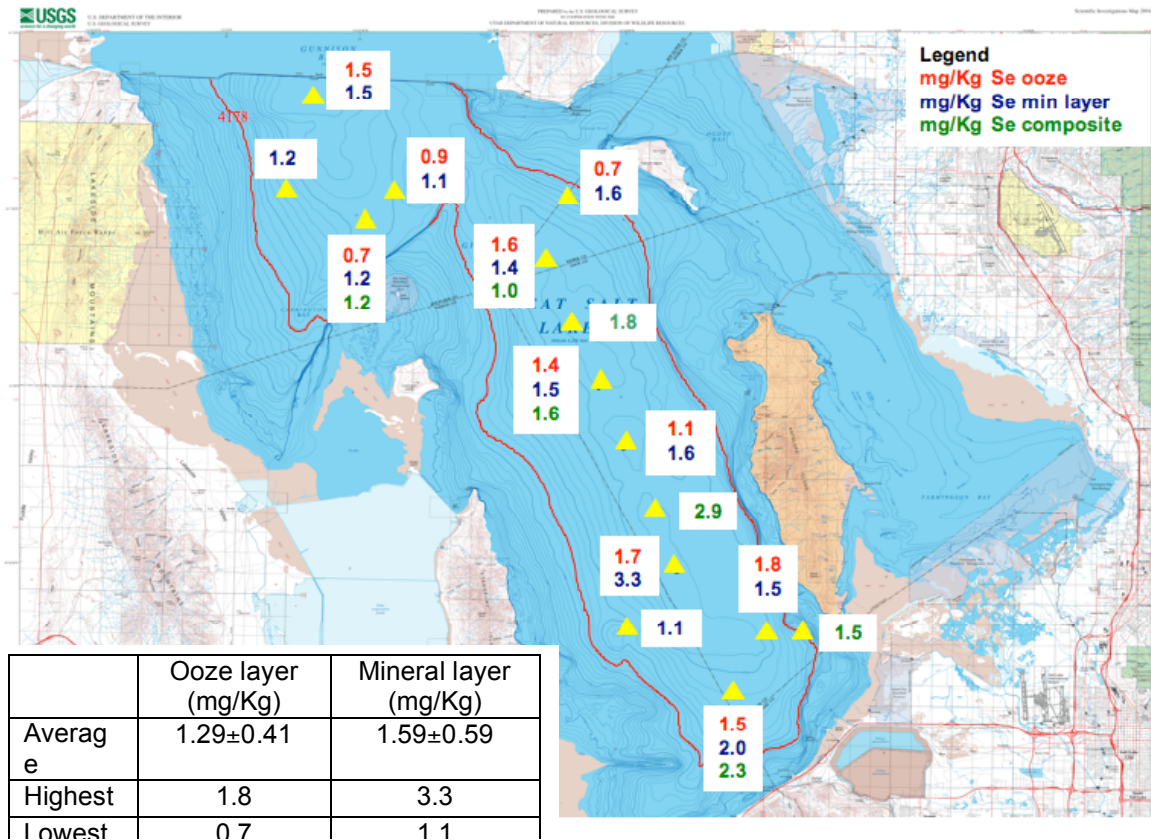


Figure 12. Concentrations of total organic carbon (TOC) in bed sediments corrected for salinity. (Map courtesy of the USGS).

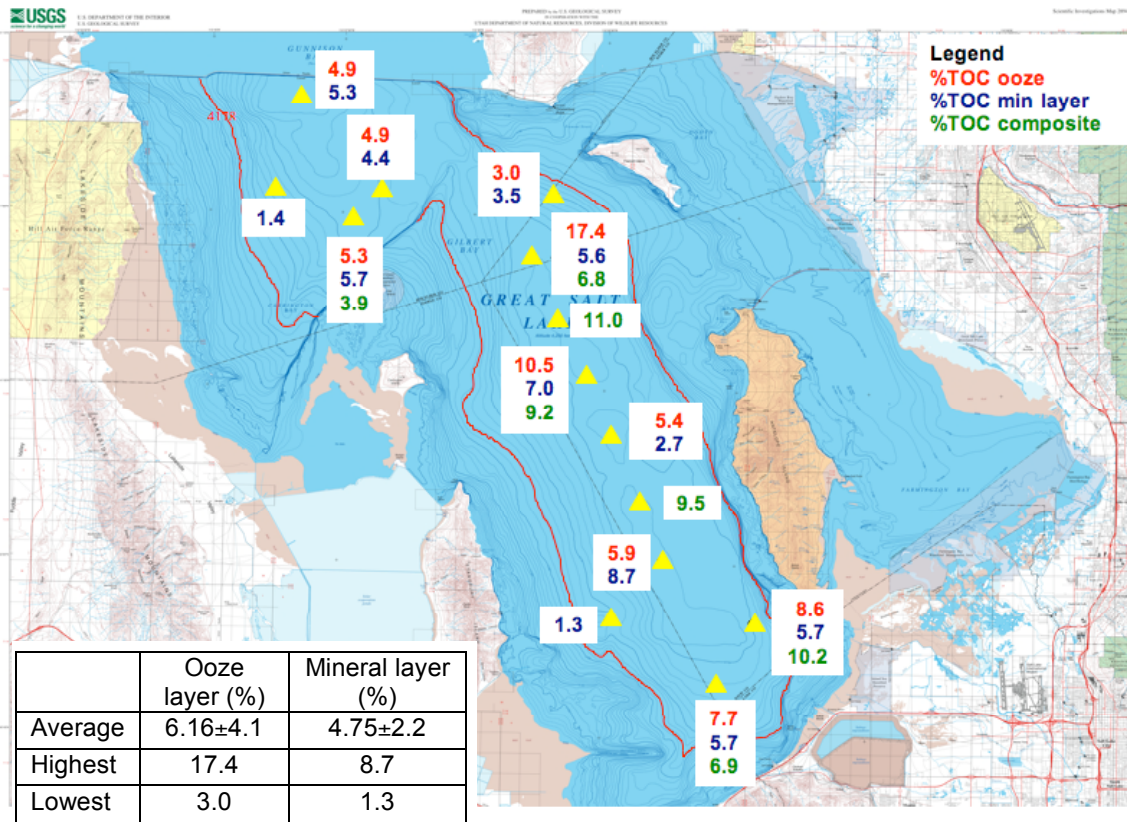


Figure 13. Selenium concentrations in the bed sediments versus TOC in bed sediments. Trendline determined for the mineral layer samples.

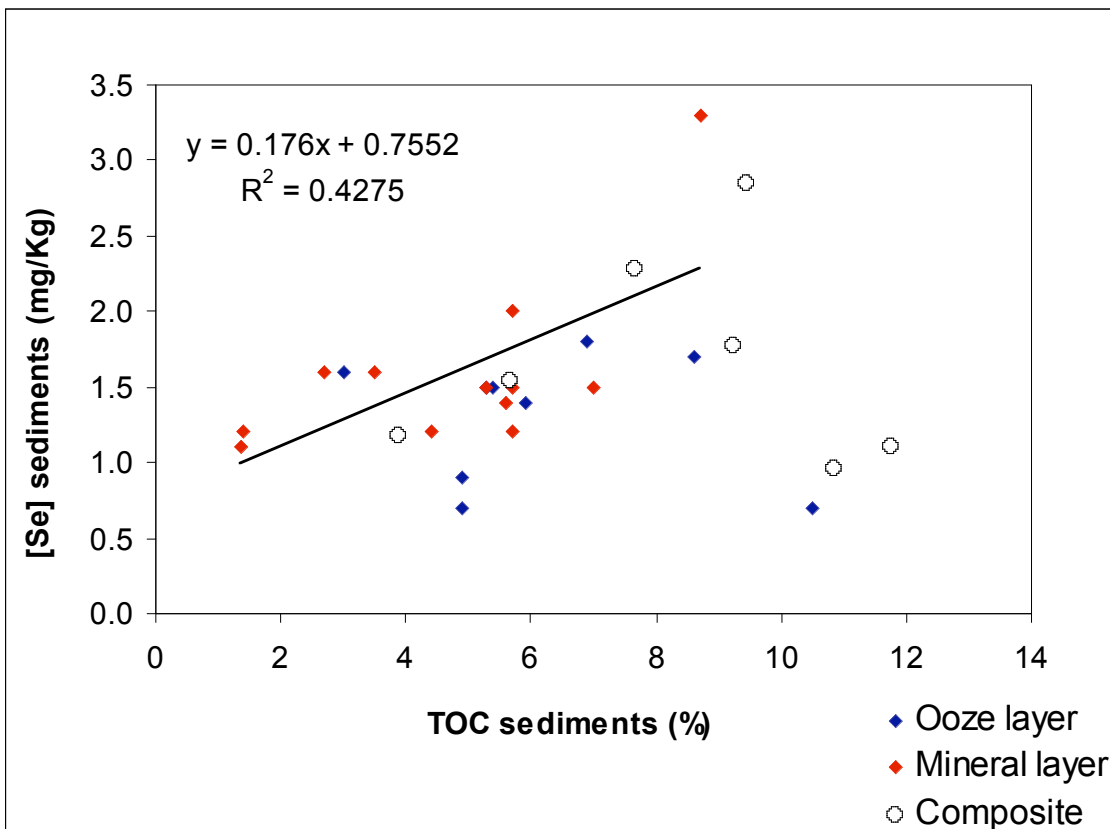
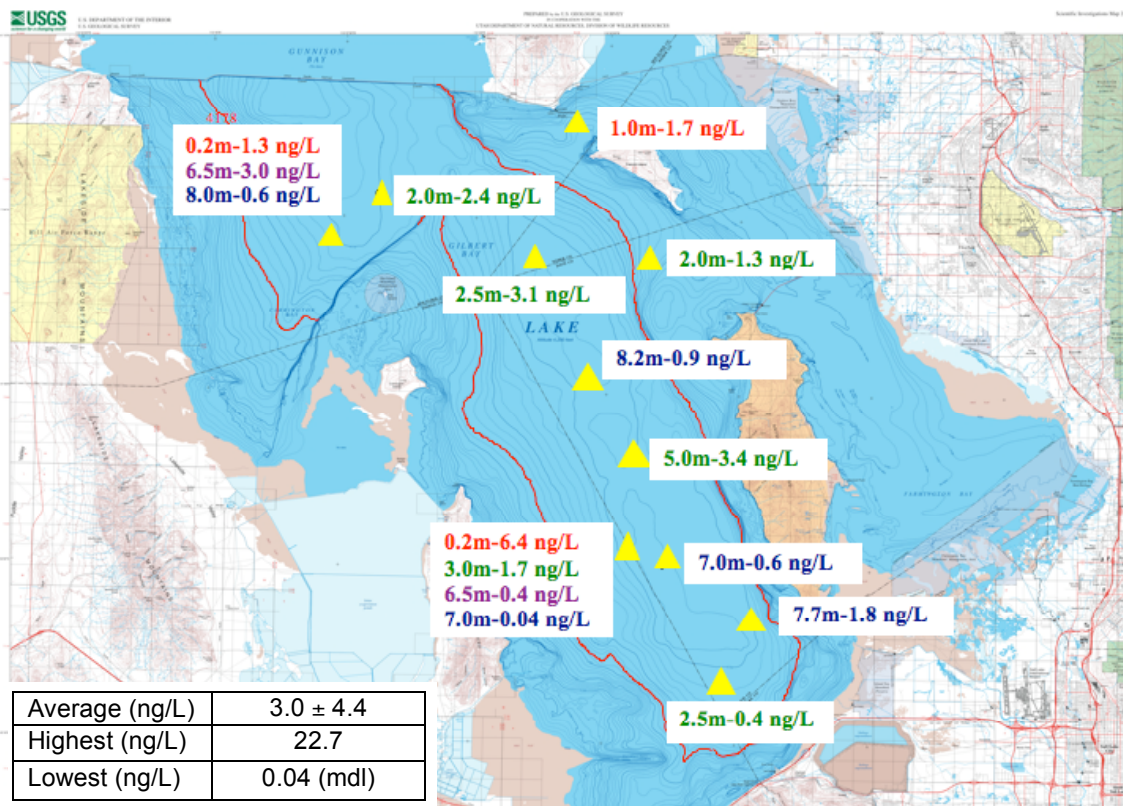


Figure 14. Volatile selenium concentrations (ng/L) in shallow and deep brine layers. (November, 2006 used as an example). (Map courtesy of the USGS).



mdl: method detection limit

Figure 15a. Volatile selenium concentrations in the shallow brine layer. For any given site, the data shows same-day measurements at different depths.

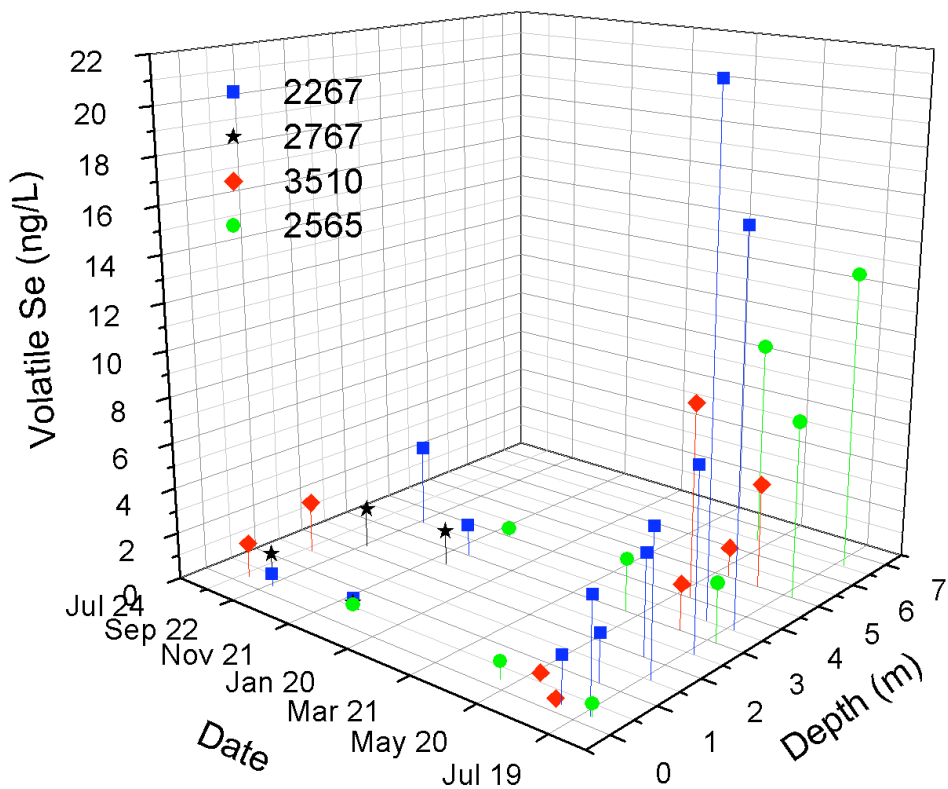


Figure 15b. Volatile selenium concentrations including deep brine layer (depths below 6.5 m). For any given site, the data shows same-day measurements at different depths.

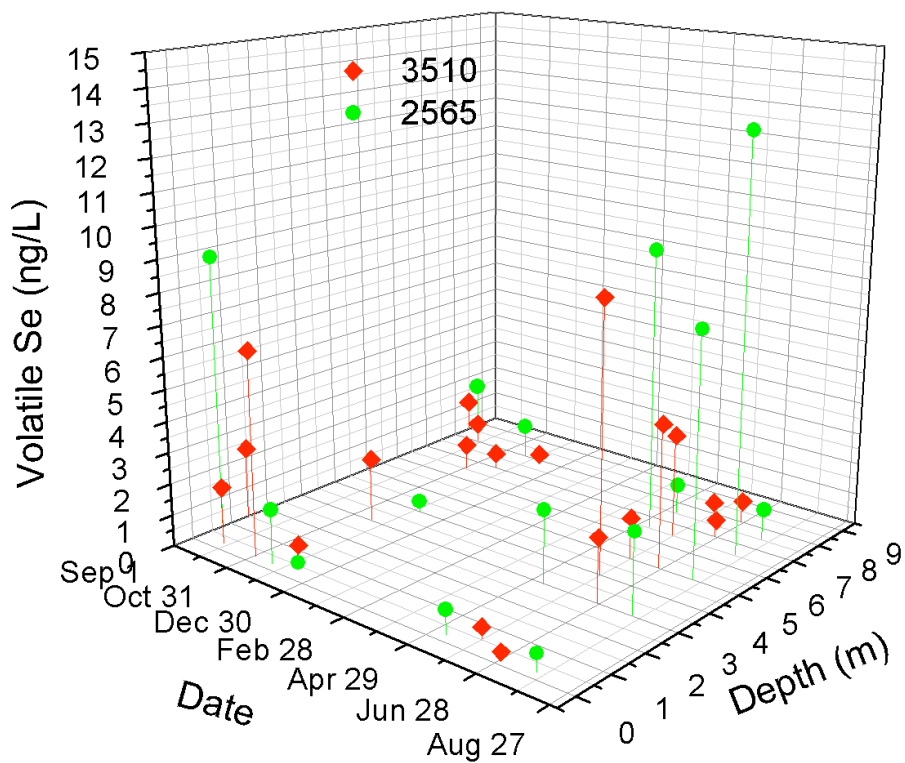
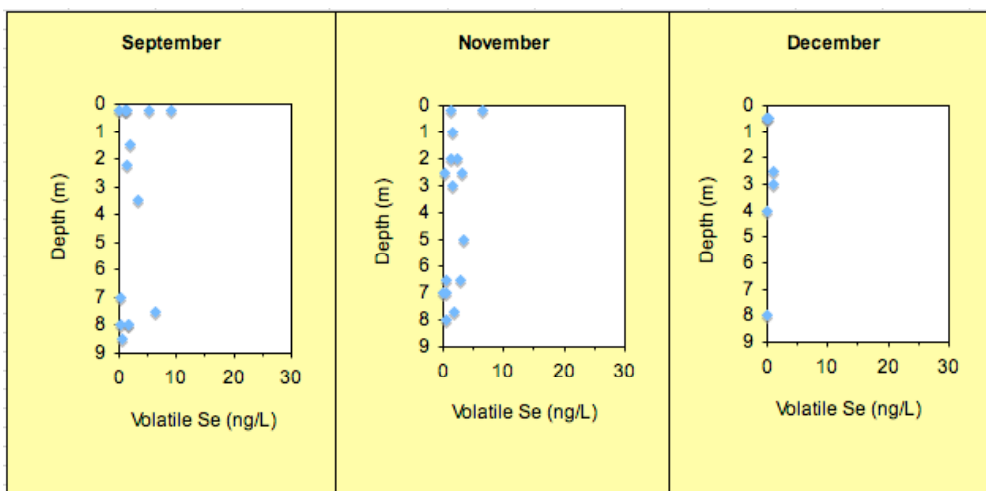


Figure 16a. Temporal variation of volatile selenium.

2006



2007

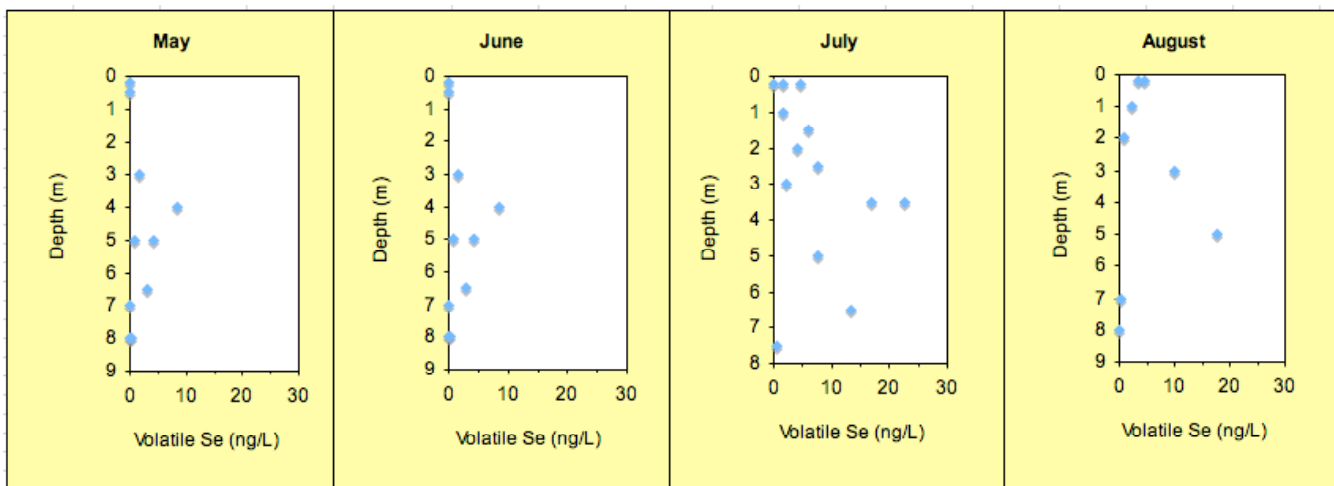


Figure 16b. Relationship between Estuarine model-predicted volatilization rates to measured volatilization rates after subtraction of average background flux of 1.6 ng/m²h. Top: log axes. Bottom: linear axes.

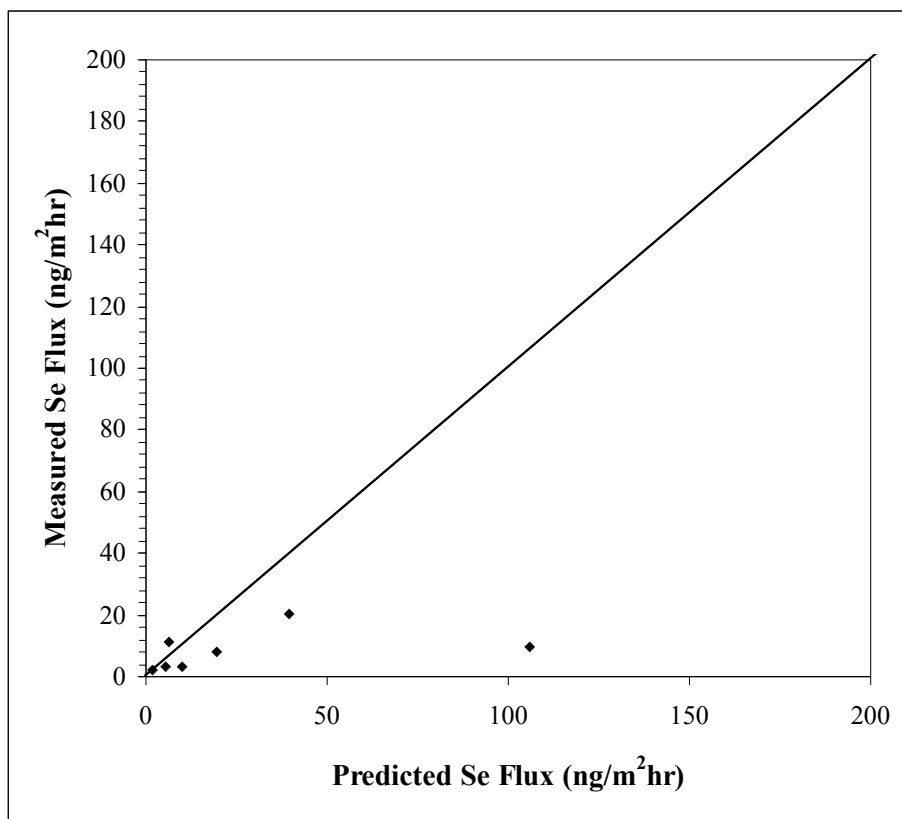
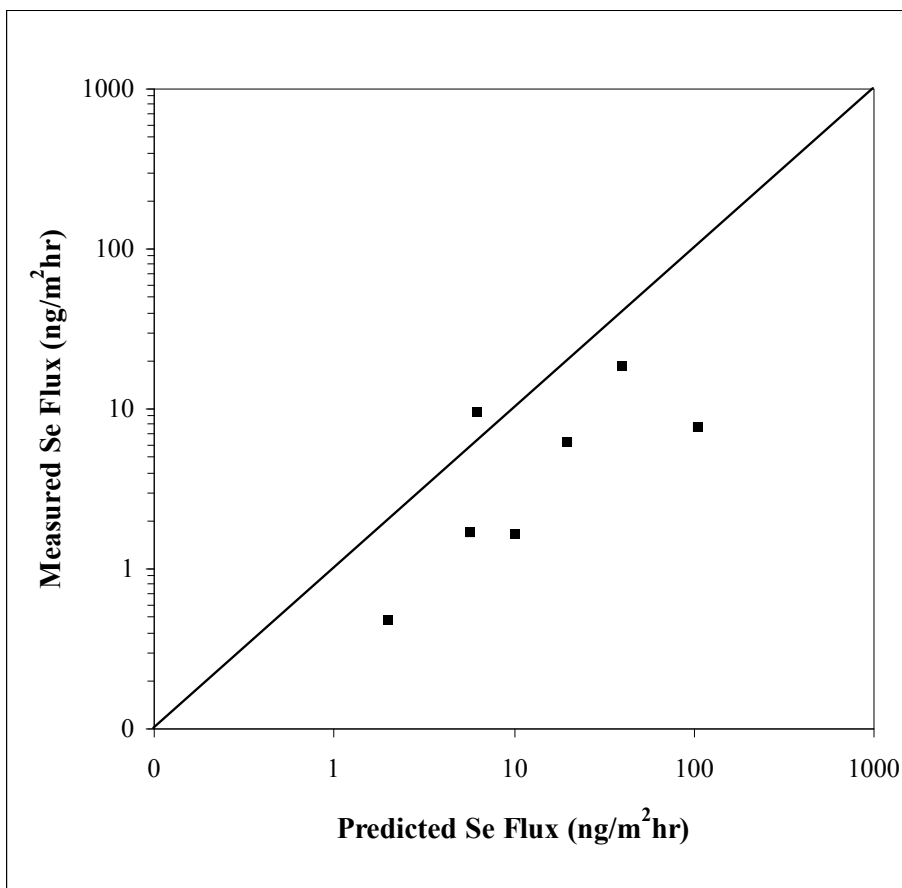


Figure 16c. Relationship between observed and Estuarine model-predicted Se fluxes under controlled laboratory conditions. Line represents the linear fit to controlled laboratory conditions.

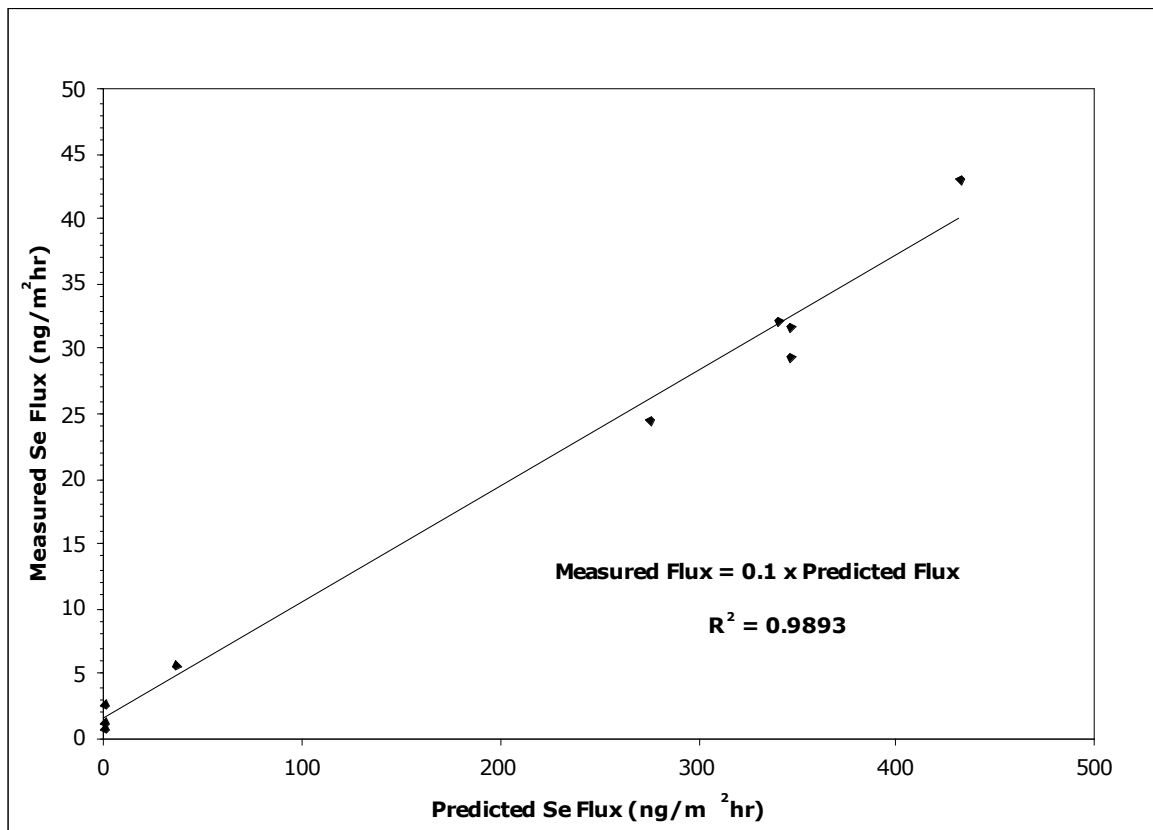


Figure 16d. Relationship between Estuarine model predicted volatilization rates to measured volatilization rates after corrections for background and measurement inefficiency. Top: log axes. Bottom: linear axes

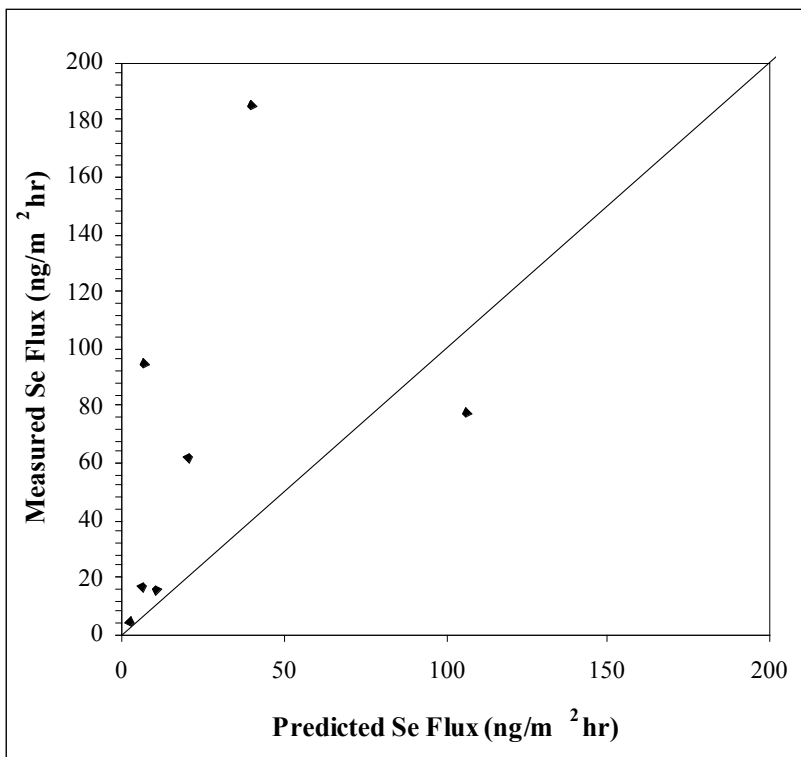
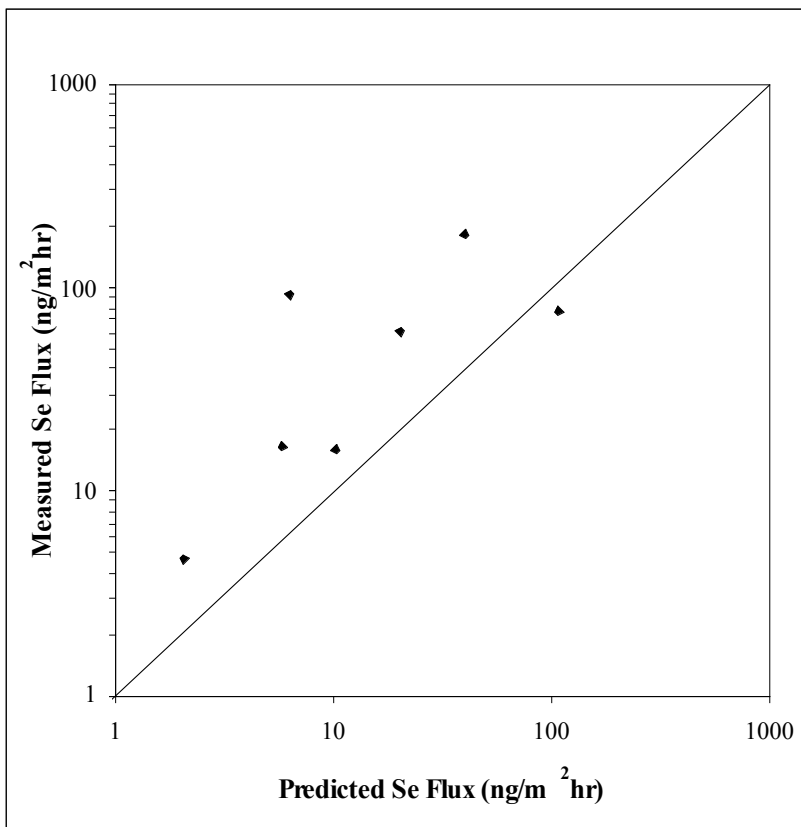


Figure 17a. Wind velocity, atmospheric temperature and lake elevation from January to December 2006.

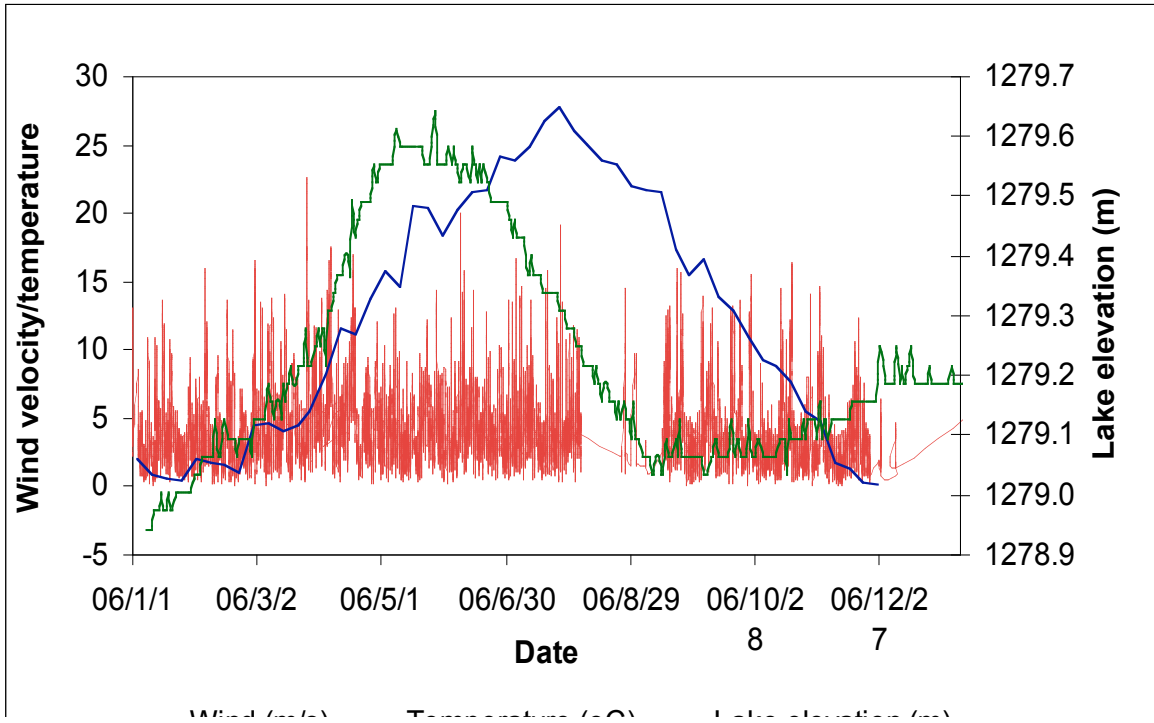


Figure 17b. Concentration of volatile Se collected at 0.2 – 0.5 m from September 2006 to August 2007. Blue trendline shows sinusoidal fit to data. Orange trendlines show the 95% confidence interval. Lower quantification limit of 0.04 ng/L is shown as dashed horizontal line.

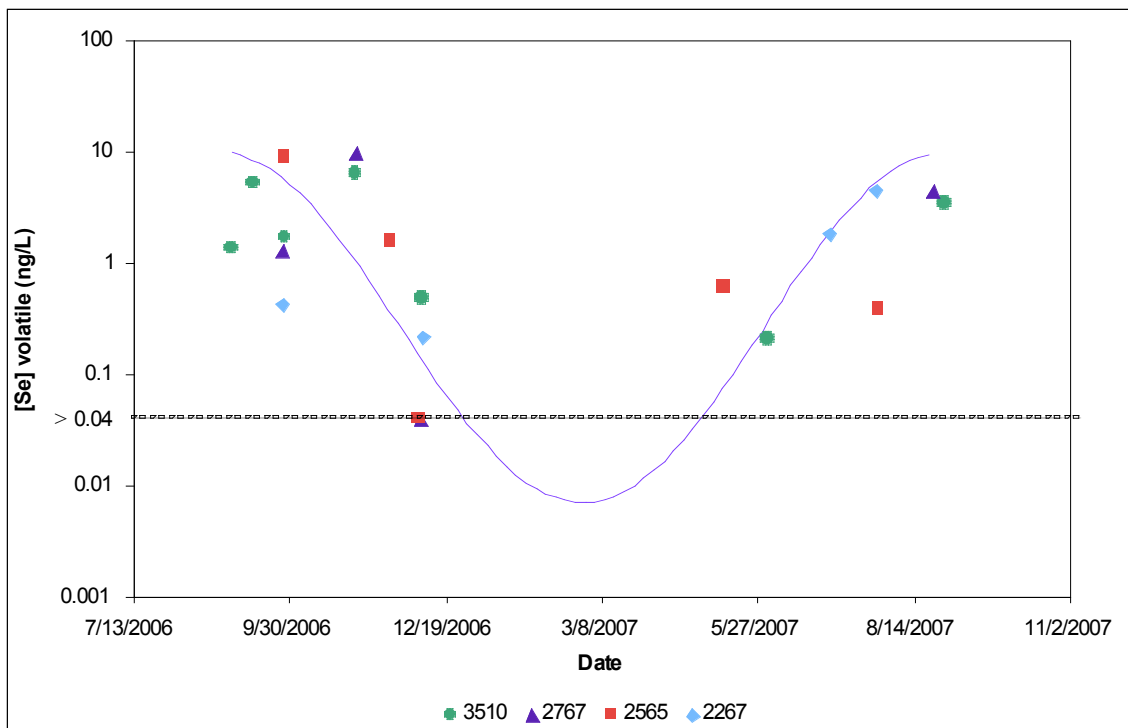


Figure 17c. Integration of annual volatile Se flux using temperature and wind data from January to December 2006, and measured volatile Se concentrations 2006-2007 (Figure 17b).

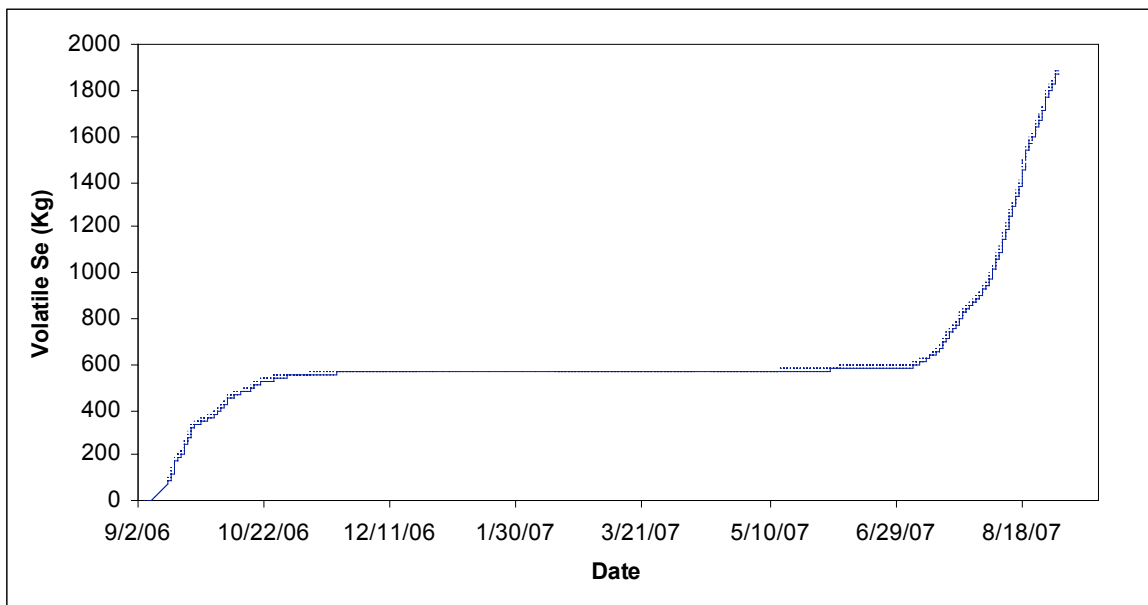


Figure 17d. Determination of the 95% confidence interval using expected vs. measured data of near surface volatile Se concentrations. Expected values obtained from the sinusoidal function. Top: log values in a normal scale. Bottom: Arithmetic values in a log scale.

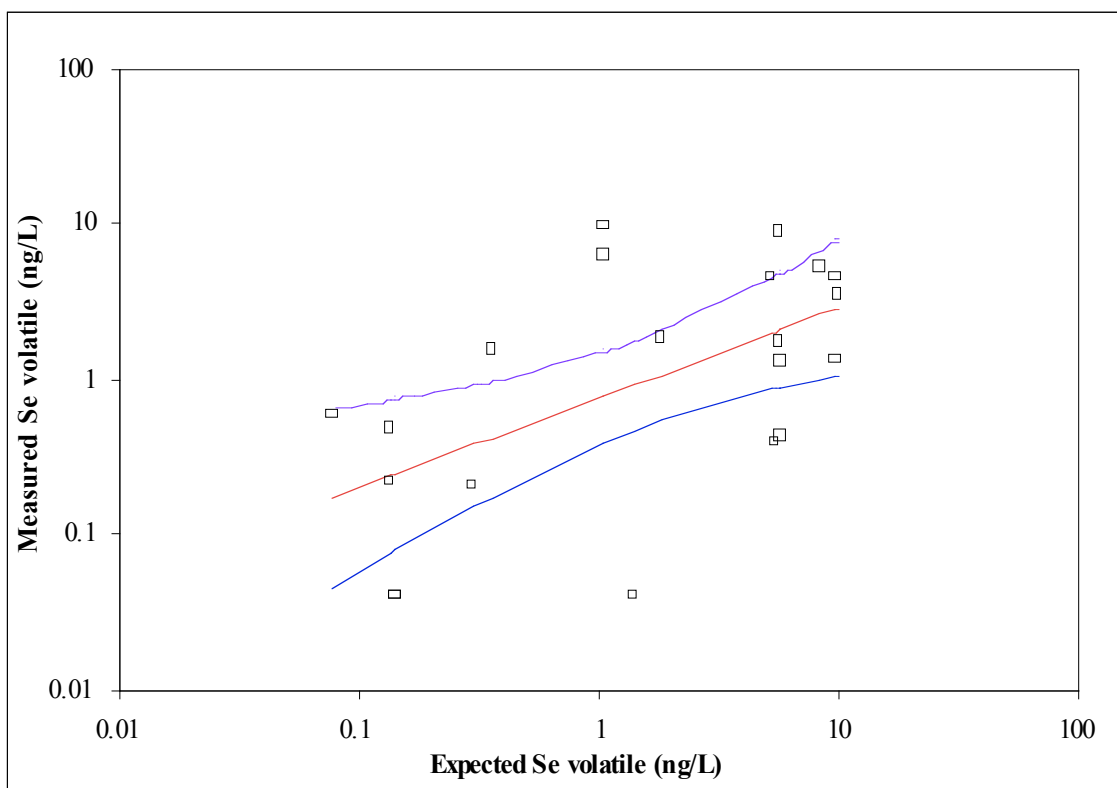
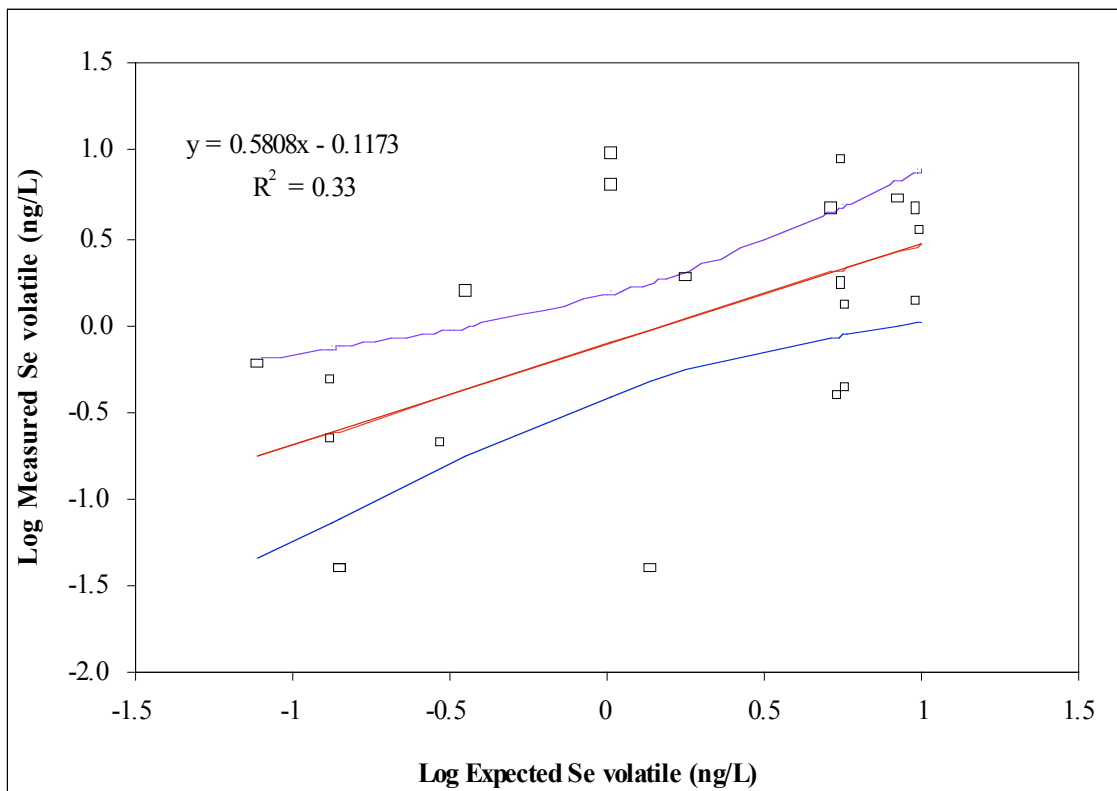


Figure 17e. Determination of the 68% confidence interval using expected vs. measured data of near surface volatile Se concentrations. Expected values obtained from the sinusoidal function. Top: log values in a normal scale. Bottom: Arithmetic values in a log scale.

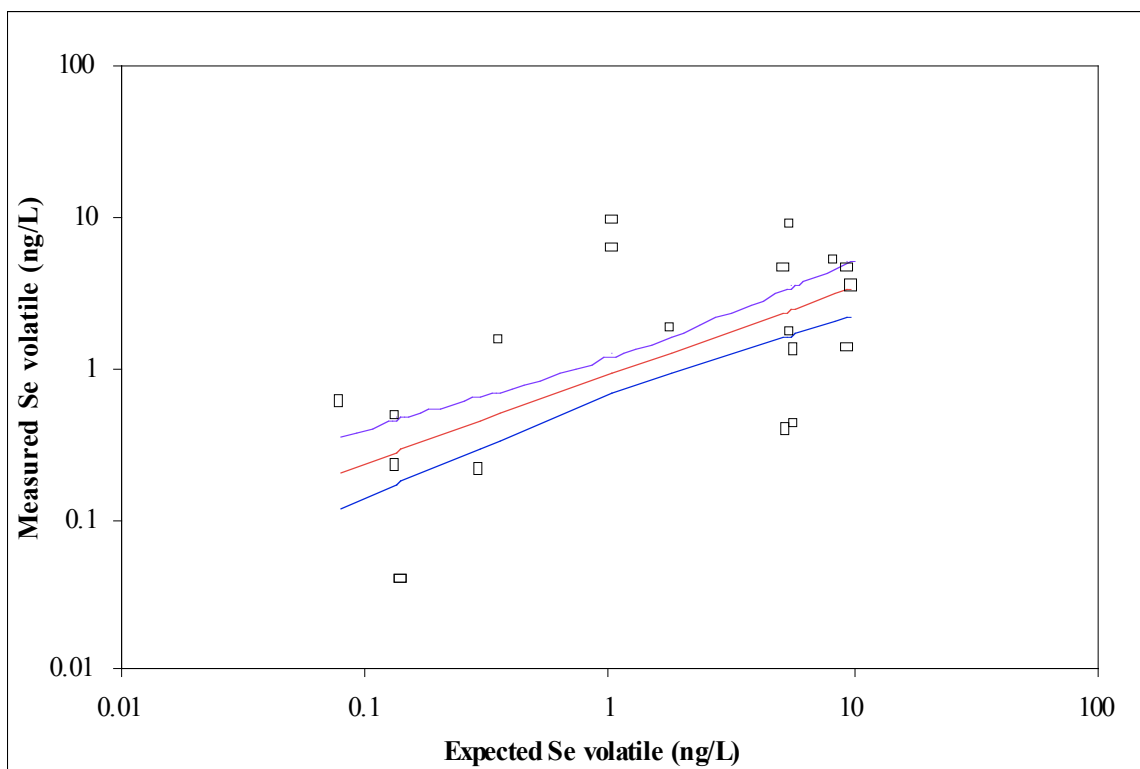
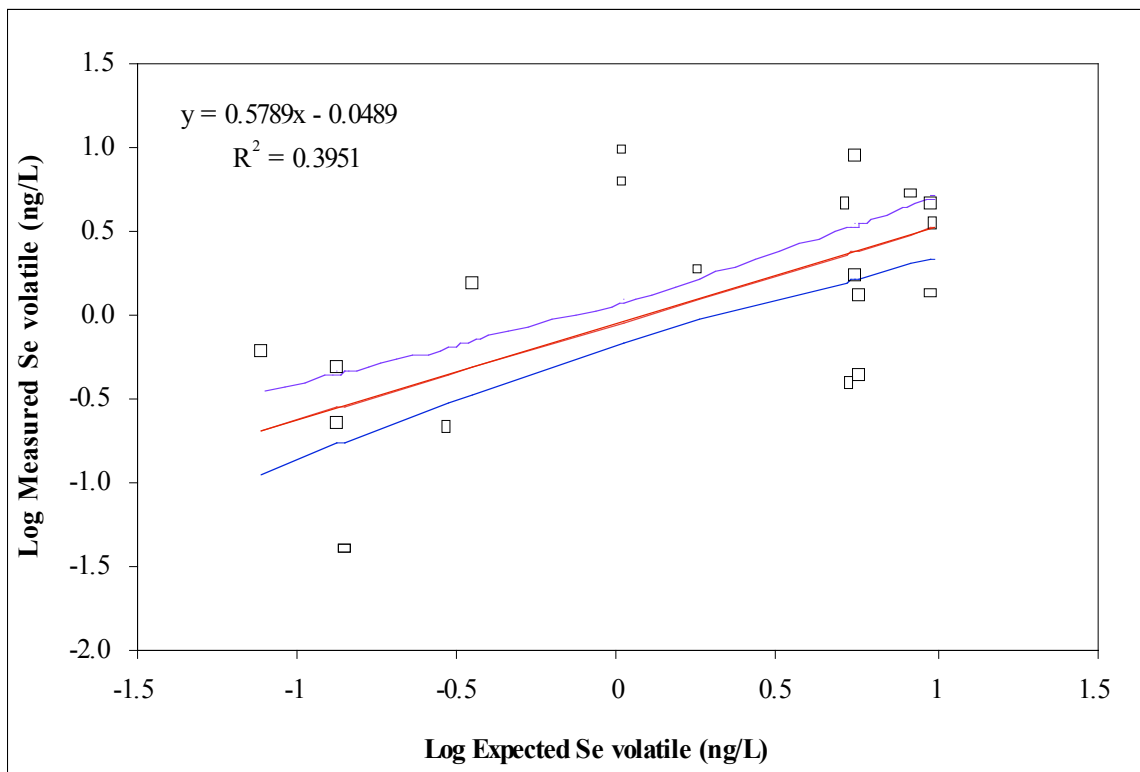


Figure 18a. Sedimentation flux and Se sedimentation flux at site 2267 (shallow site). The Se flux values plotted were multiplied by 10^6 . To obtain the actual values, multiply by 10^{-6} . Period of measurement was February 2006 to July 2007.

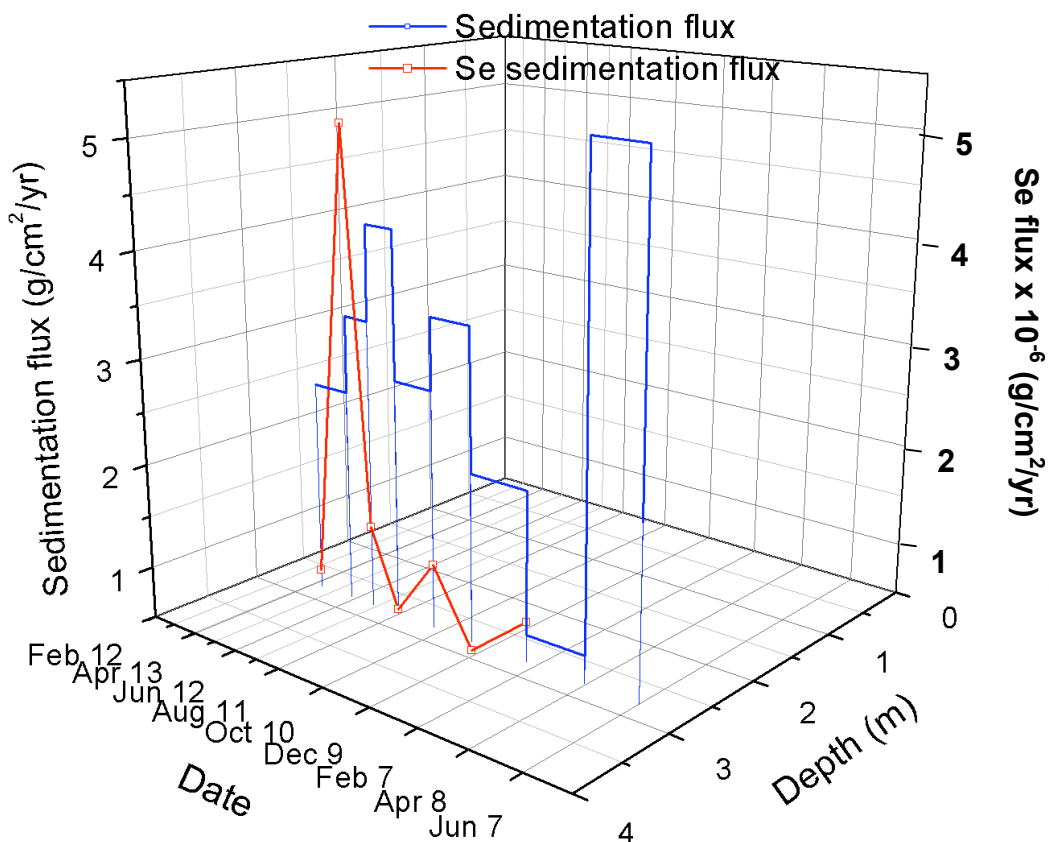


Figure 18b. Sedimentation flux and Se sedimentation flux at site 2565 (deep site). The Se flux values plotted were multiplied by 10^7 . To obtain the actual values, multiply by 10^{-7} . Period of measurement was February 2006 to July 2007.

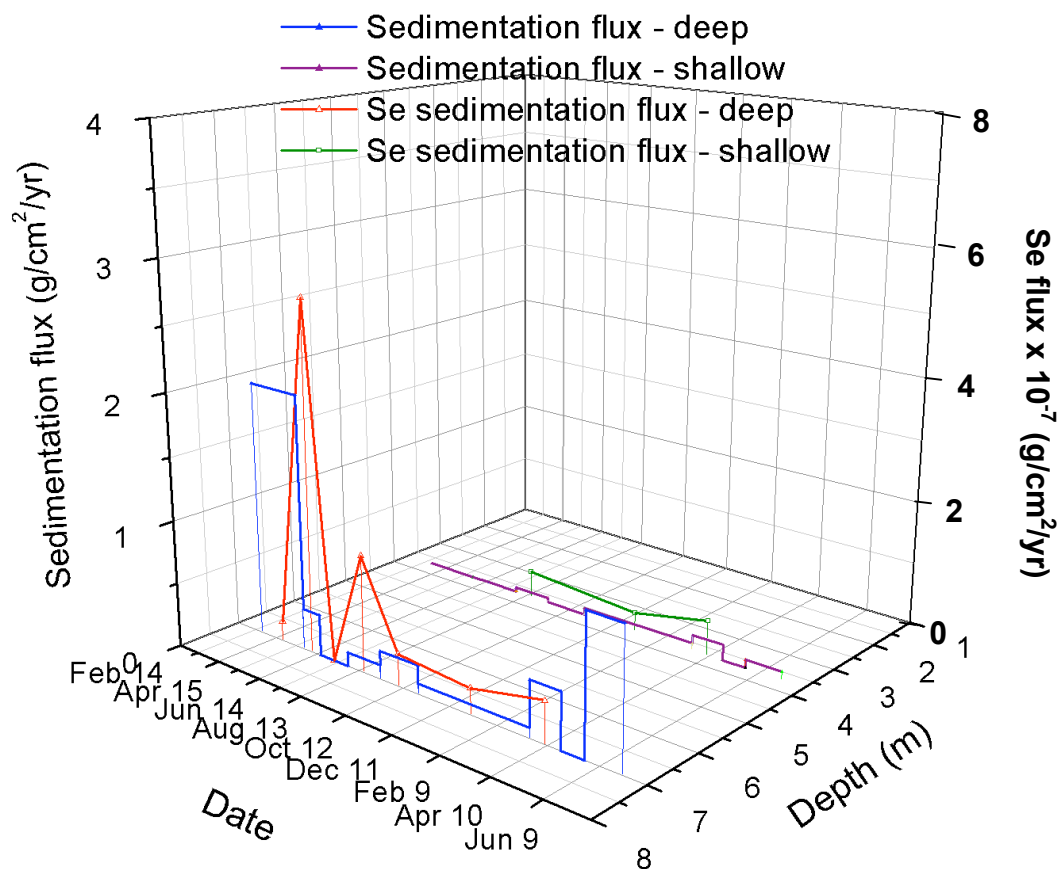


Figure 18c. Sedimentation flux and Se sedimentation flux at site 3510 (deep site). The Se flux values plotted were multiplied by 10^8 . To obtain the actual values, multiply by 10^{-8} . Period of measurement was February 2006 to July 2007.

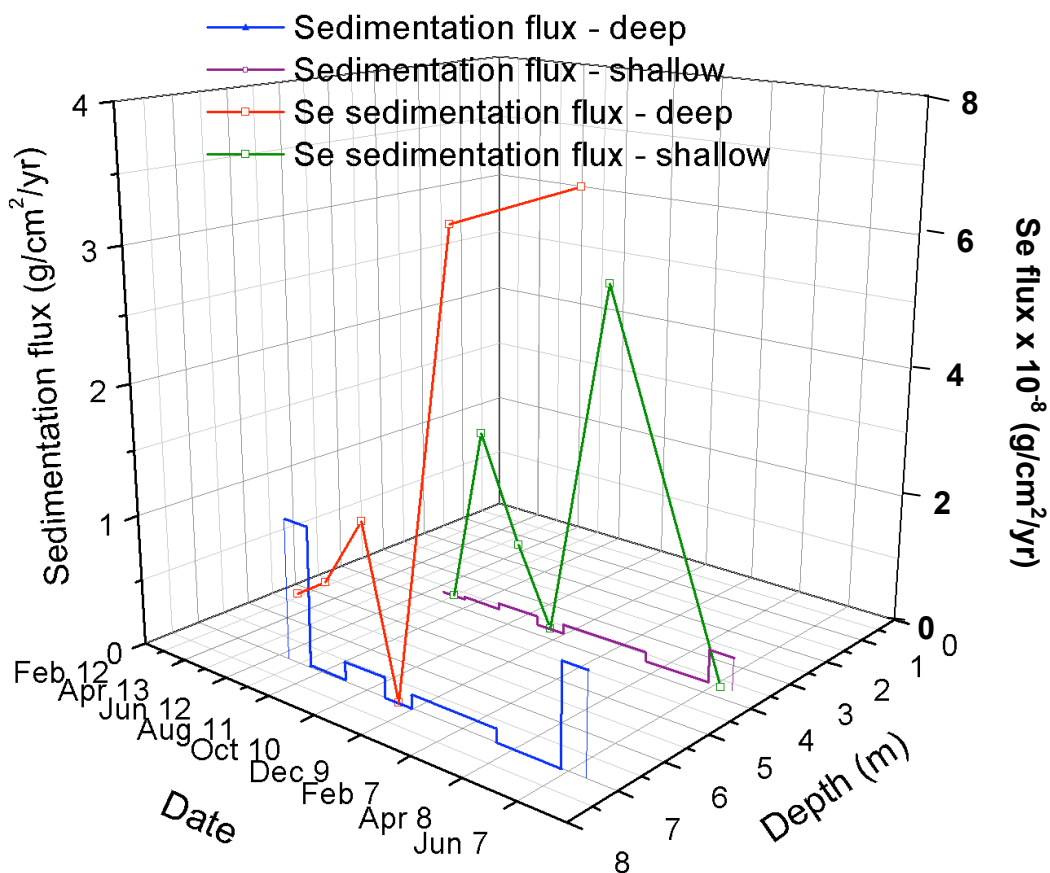


Figure 19. Total ^{210}Pb and ^{226}Ra activity, in disintegrations per minute per gram, versus depth in sediment core 3510 BOX. Horizontal error bars depict 1 sigma uncertainty in measured activity based on counting statistics.

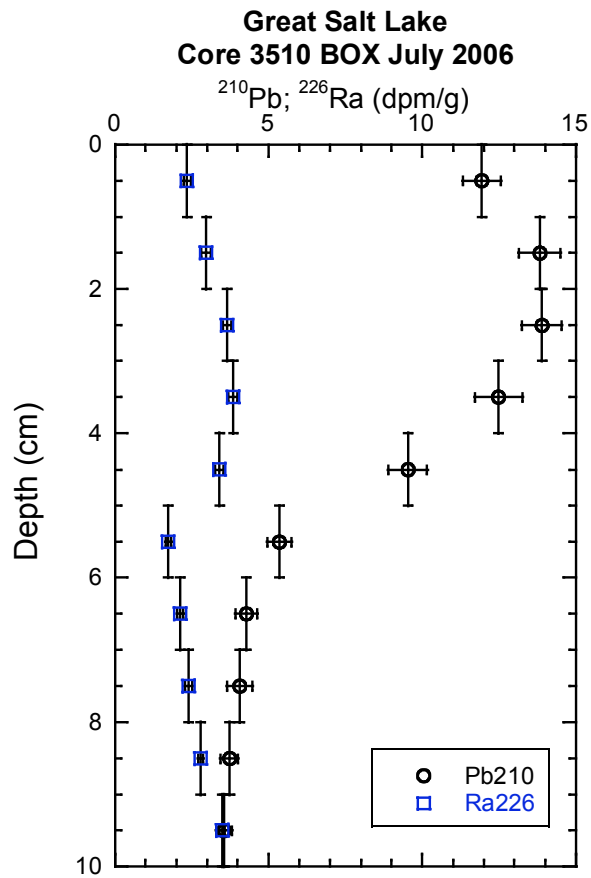


Figure 20. Natural logarithm of unsupported ^{210}Pb activity versus cumulative dry sediment mass in sediment core 3510 BOX. Unsupported ^{210}Pb is the difference between total ^{210}Pb and its long-lived progenitor, ^{226}Ra . Only data with measurable unsupported ^{210}Pb are presented. Solid line represents linear regression of the data used to derive sediment mass accumulation rate

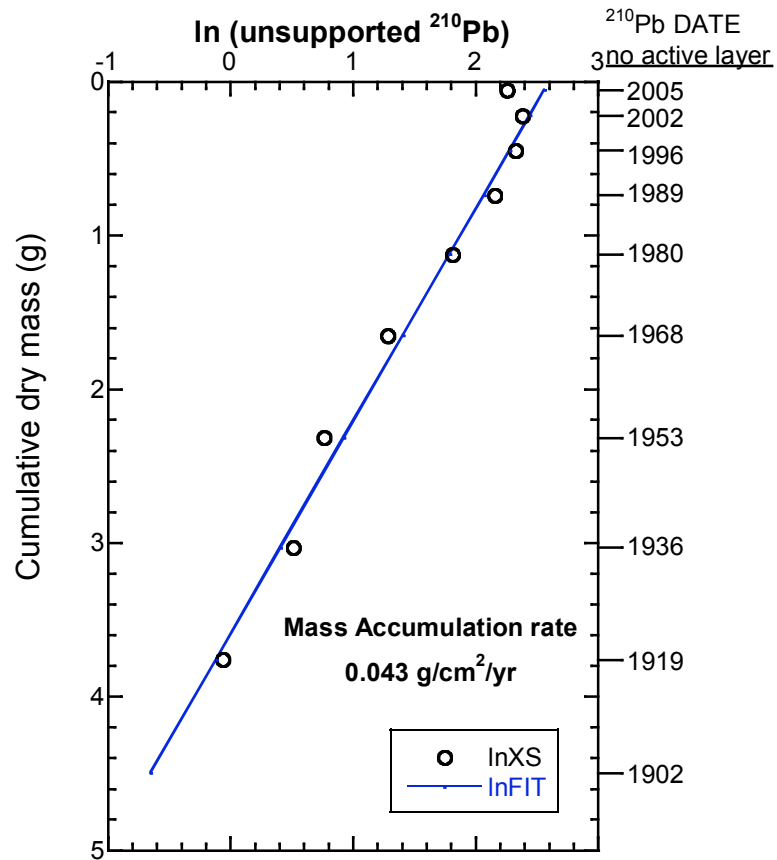


Figure 21a. Sediment deposition date as function of depth based on the sediment mass accumulations estimated from ^{210}Pb using the CF-CS method, with and without correction for 2-cm active layer. Non-linearity in deposition date versus depth is the result of sediment compaction.

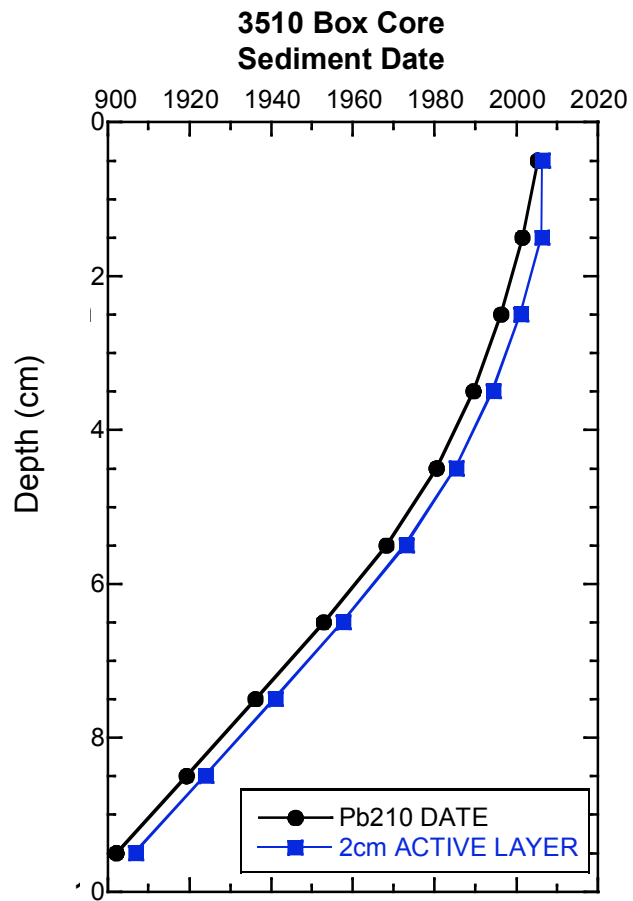


Figure 21b. ^7Be activity, in disintegrations per minute per gram, versus depth in sediment core 3510-BOX. Horizontal error bars depict 1 sigma uncertainty in measured activity based on counting statistics.

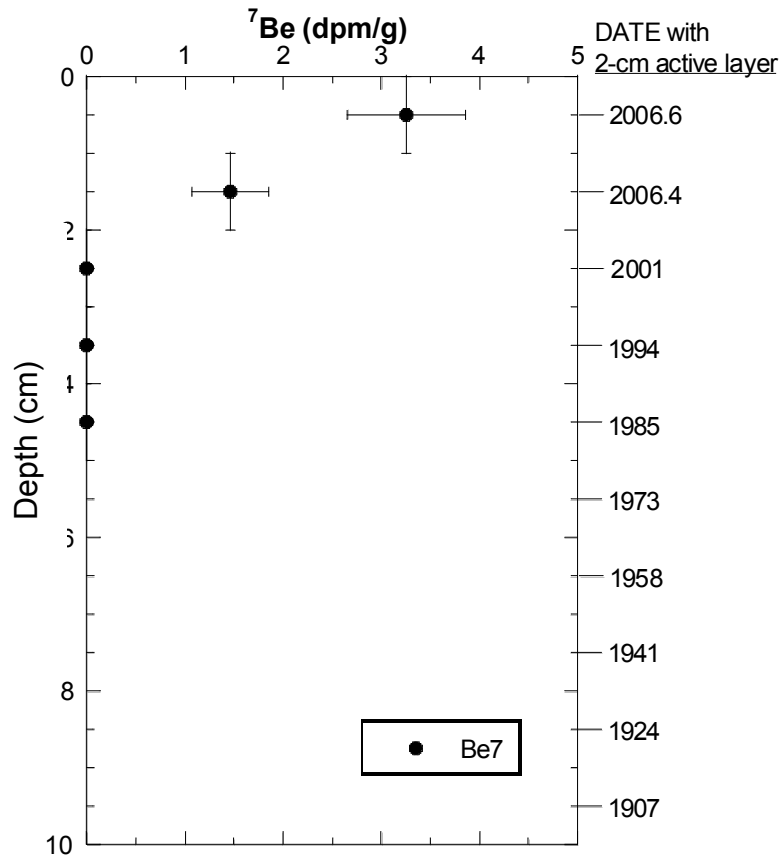


Figure 22. ^{137}Cs activities with depth in sediment core 3510-BOX.

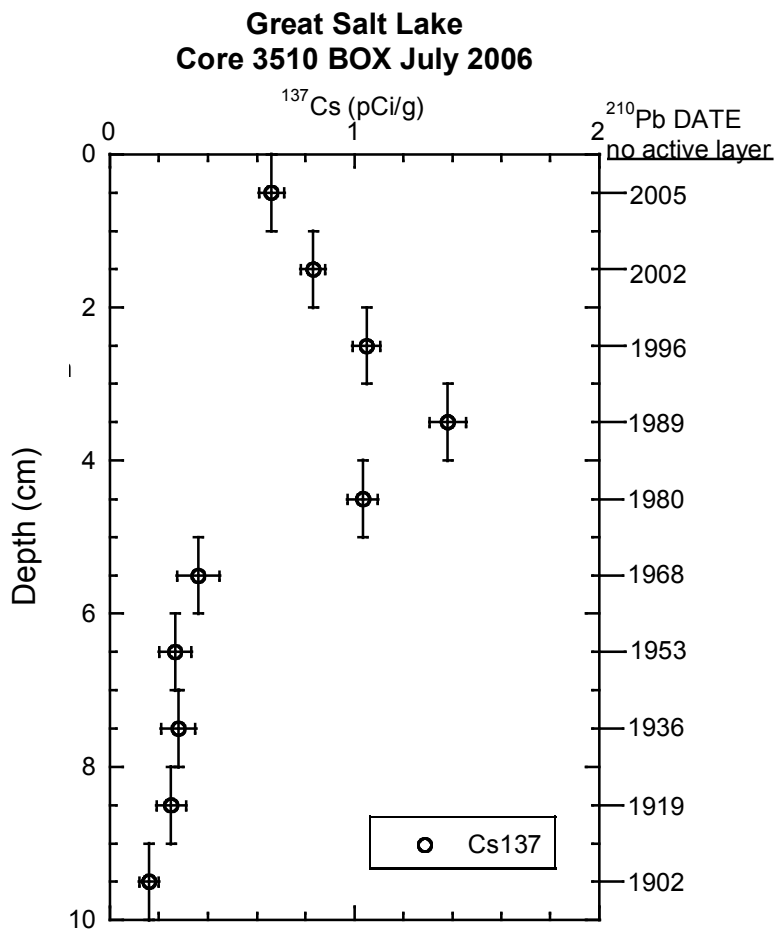


Figure 23. Total ^{210}Pb and ^{226}Ra activity, in disintegrations per minute per gram, versus depth in sediment core 2267. Horizontal error bars depict 1 sigma uncertainty in measured activity based on counting statistics.

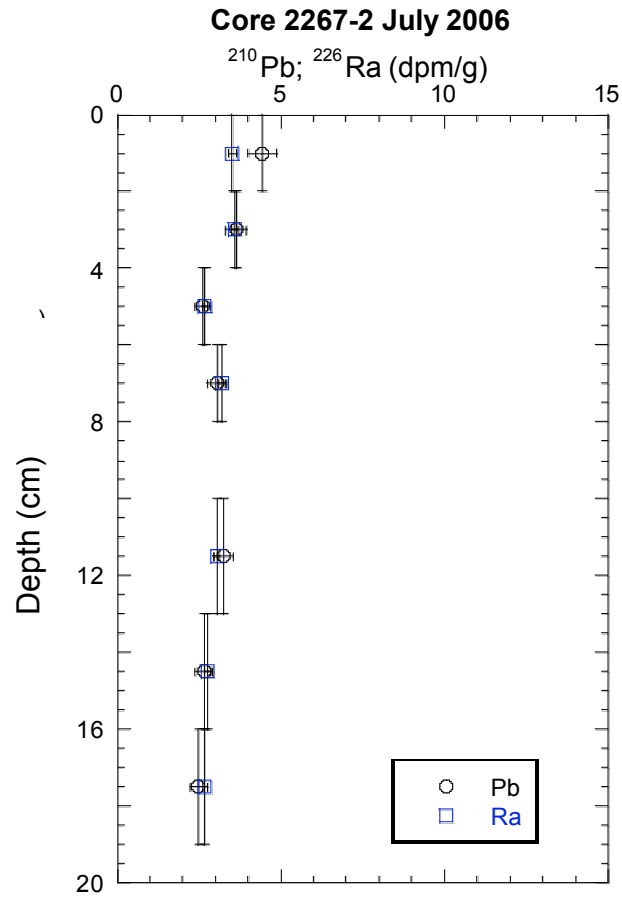


Figure 24. Total ^{210}Pb and ^{226}Ra activity, in disintegrations per minute per gram, versus depth in sediment core 2565. Horizontal error bars depict 1 sigma uncertainty in measured activity based on counting statistics.

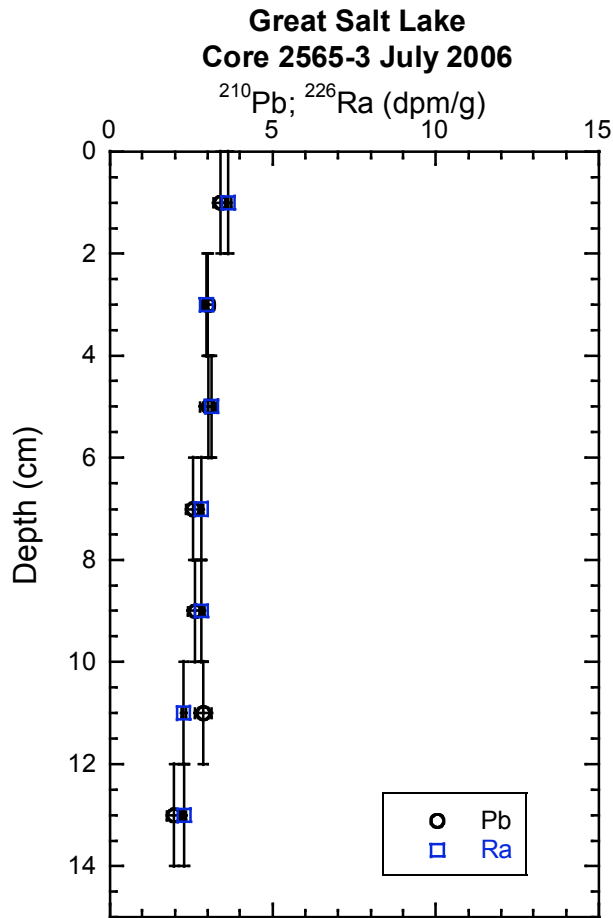


Figure 25. ^{137}Cs activity, in picoCuries per gram, and ^7Be , in disintegrations per minute per gram, versus sediment depth in sediment cores 2267.

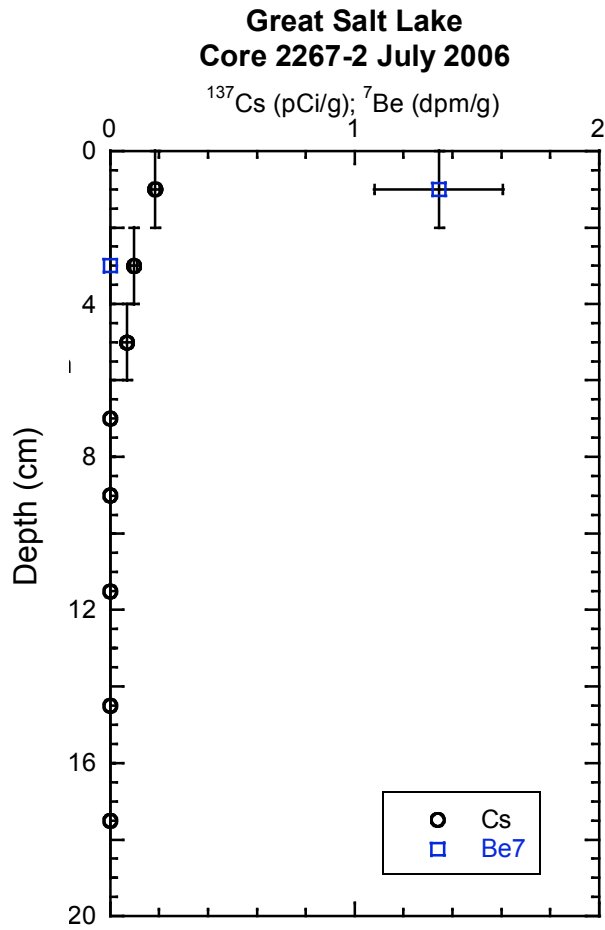


Figure 26. ^{137}Cs activity, in picoCuries per gram, and ^7Be , in disintegrations per minute per gram, versus sediment depth in sediment cores 2565.

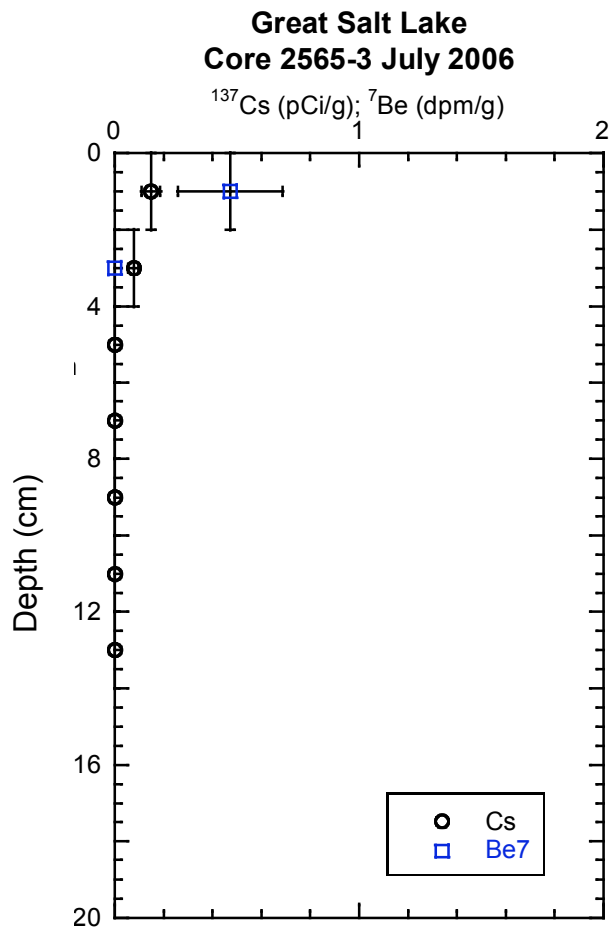


Figure 27a. Shallow core results and Holocene thickness contours

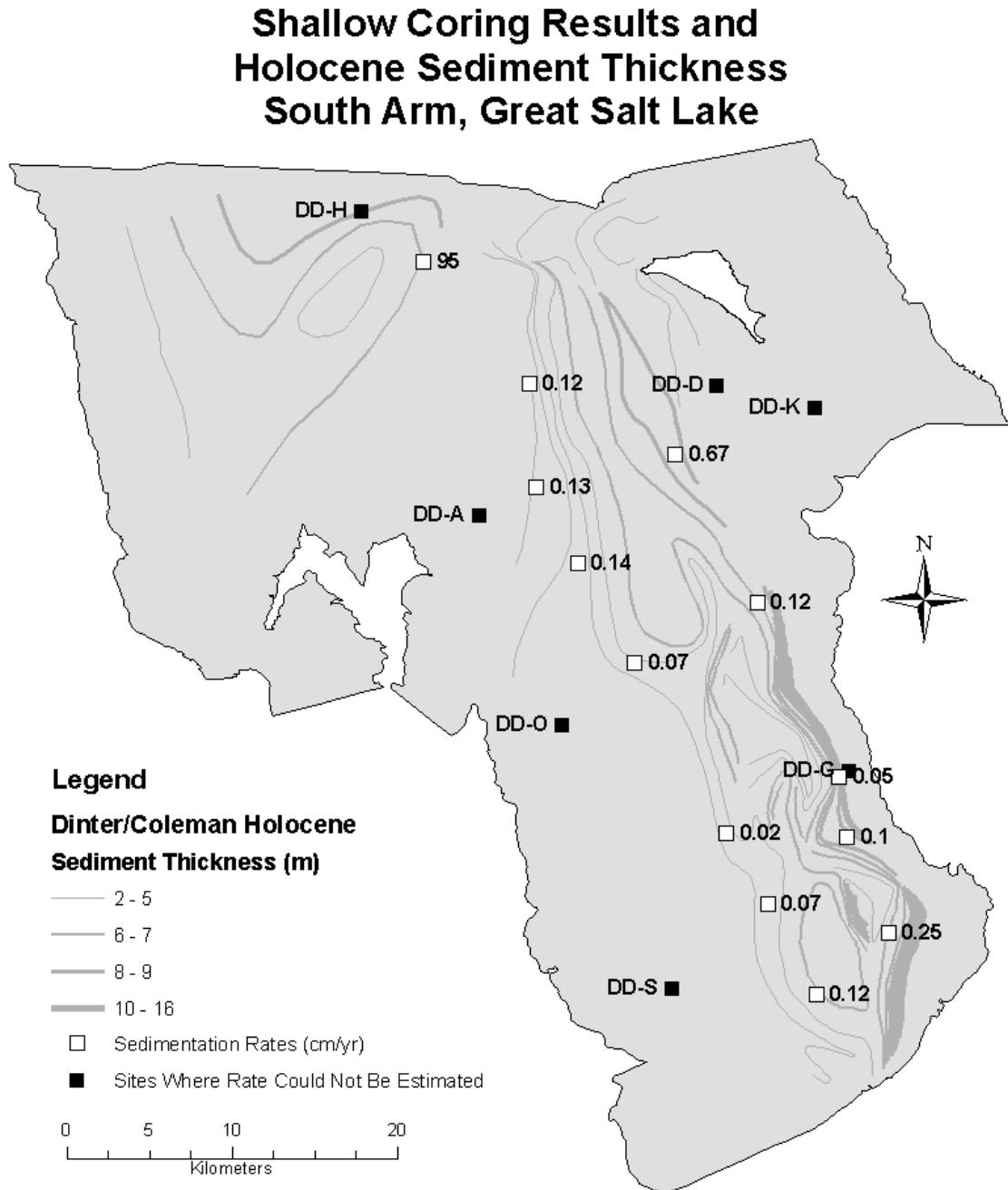


Figure 27b. Qualitative Sedimentation Zones

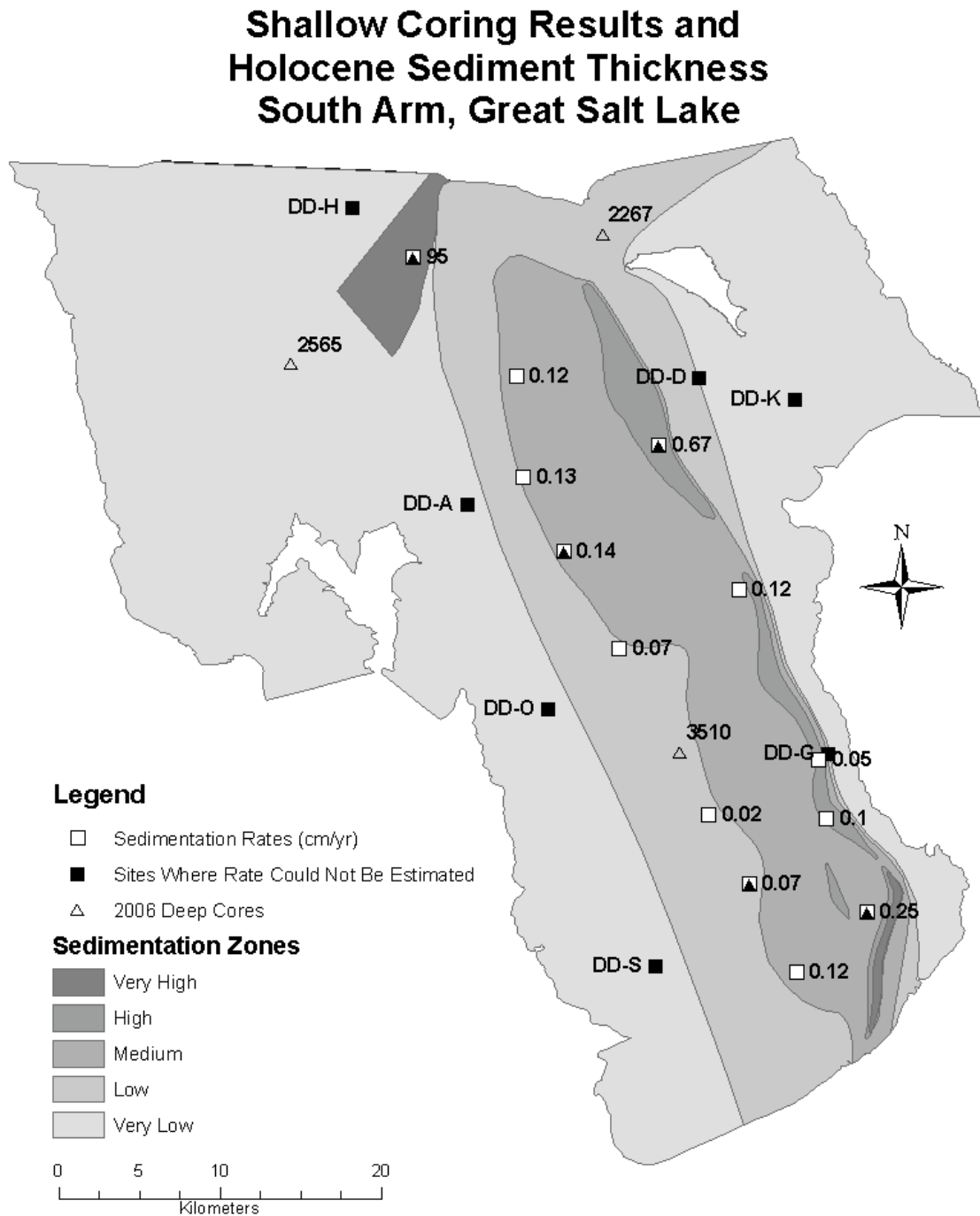


Figure 27c. Se concentration profile in cores from site 3510.

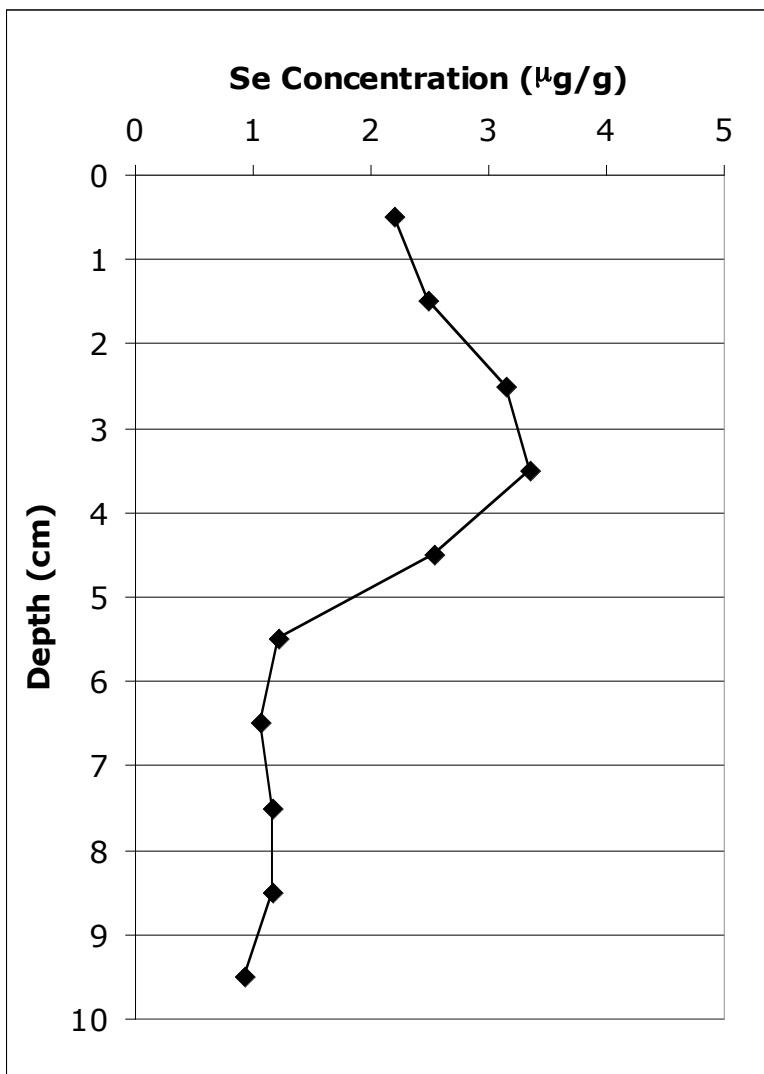


Figure 27d. Standard deviations as a function of the number of randomized MAR values assessed.

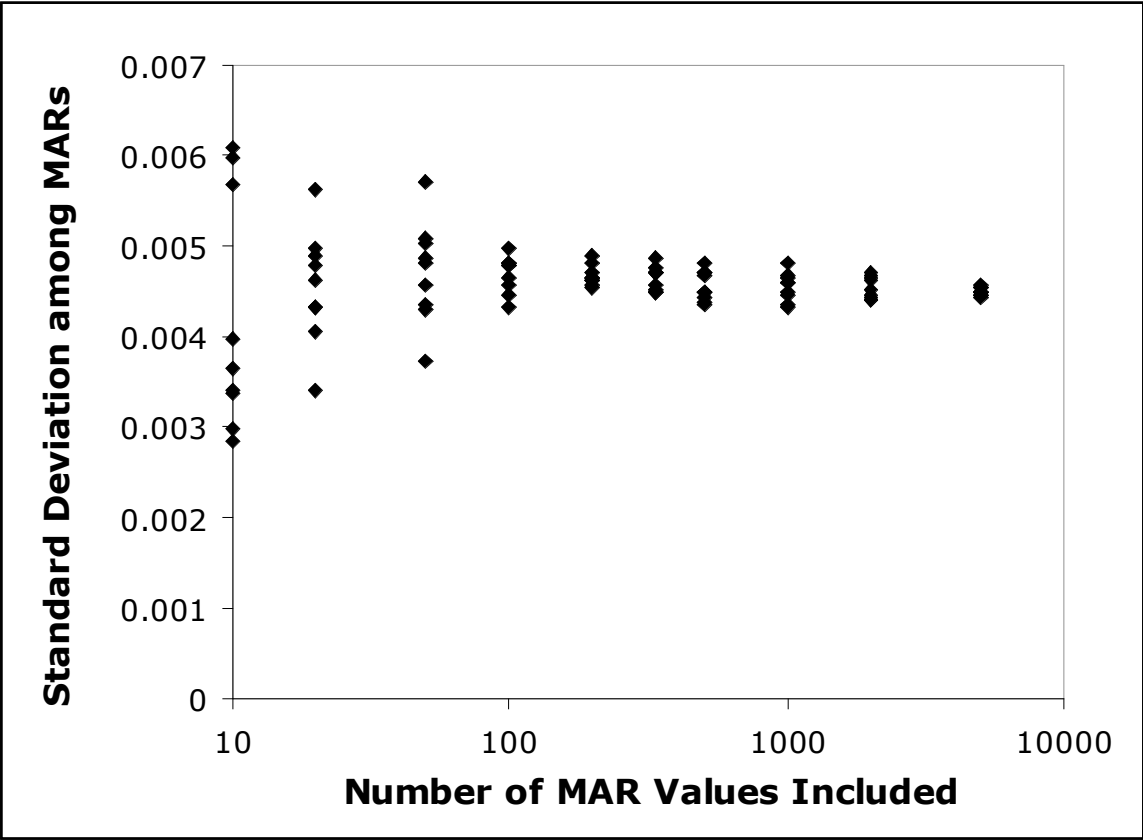


Figure 28. Major and minor elements distribution chronologically at site 3510 core

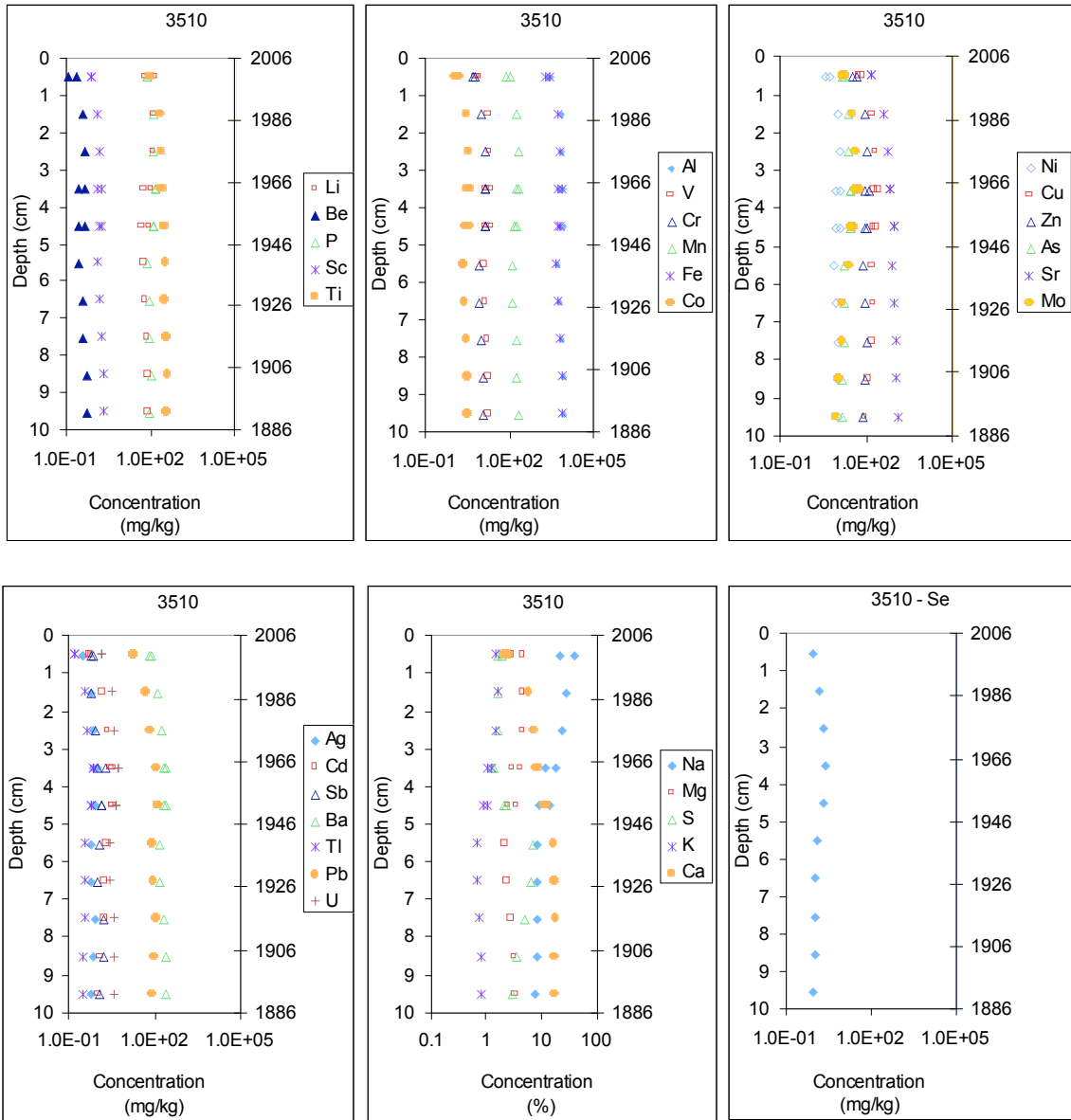


Figure 29. Major and minor elements distribution at site 2565 core

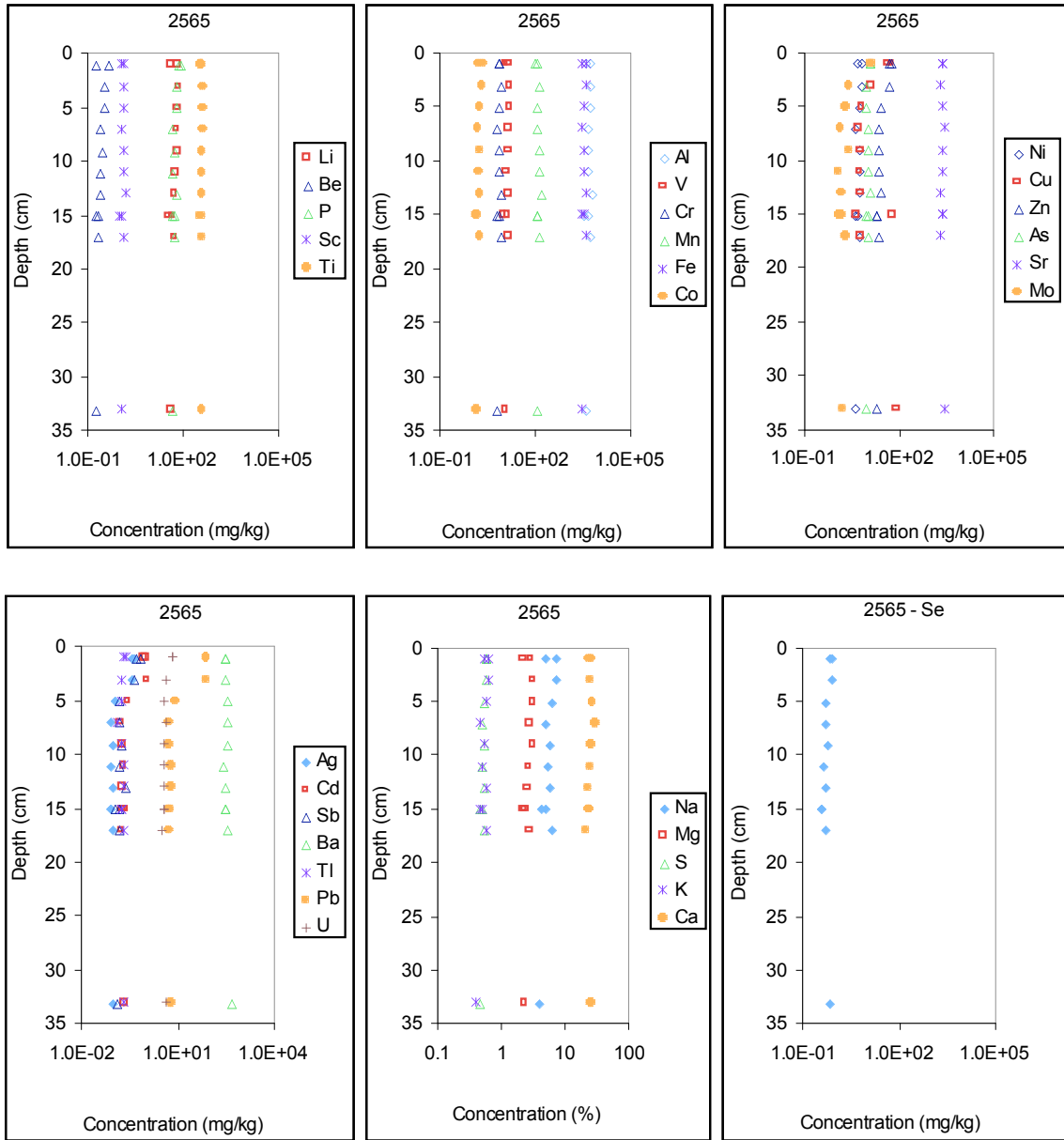


Figure 30. Major and minor elements distribution at site 2267 core

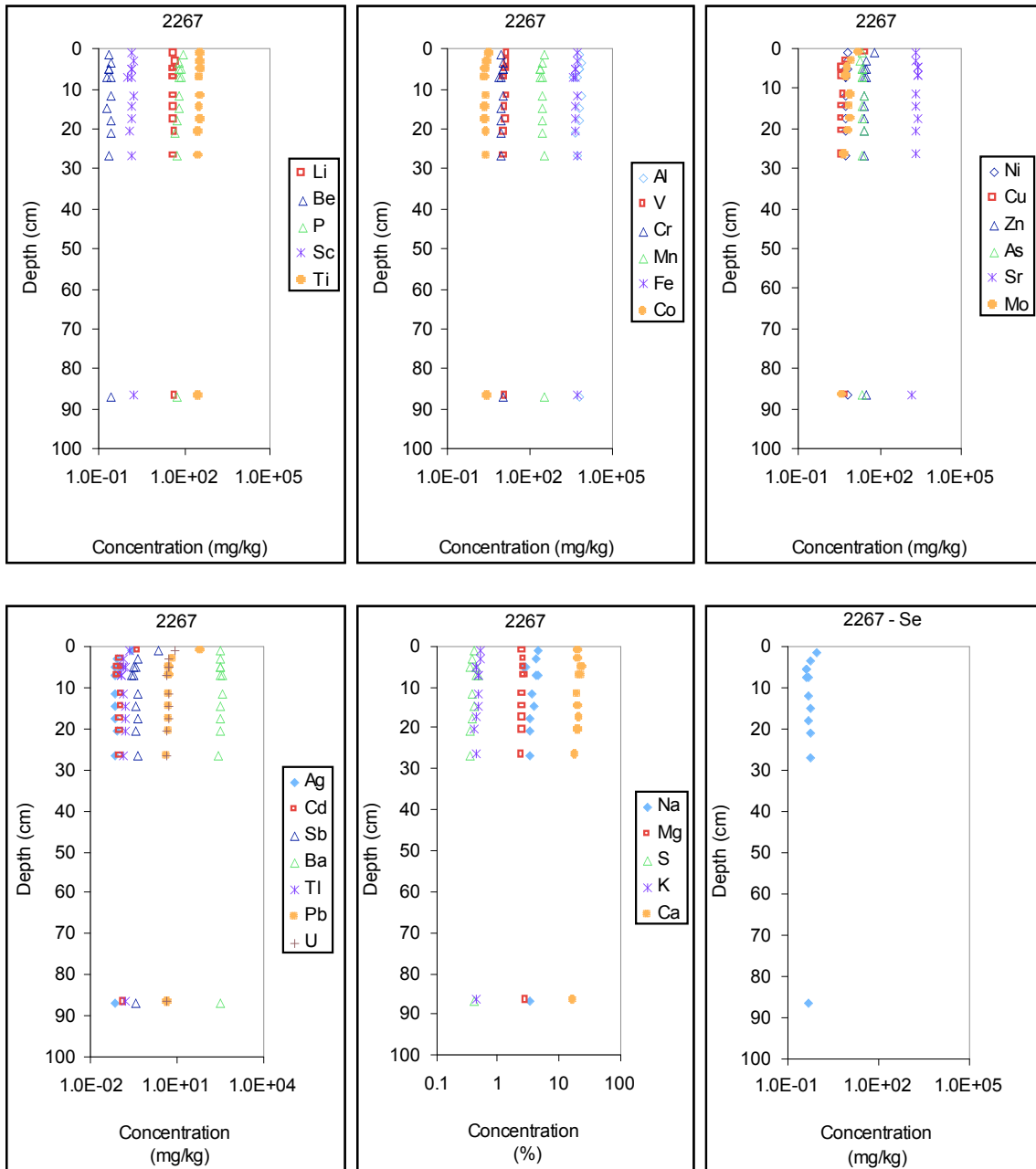


Figure 31a. Temperature variations at site 2565 during summer and fall, 2006. Warmer colors indicate shallow thermistors and cooler colors indicate deeper thermistors.

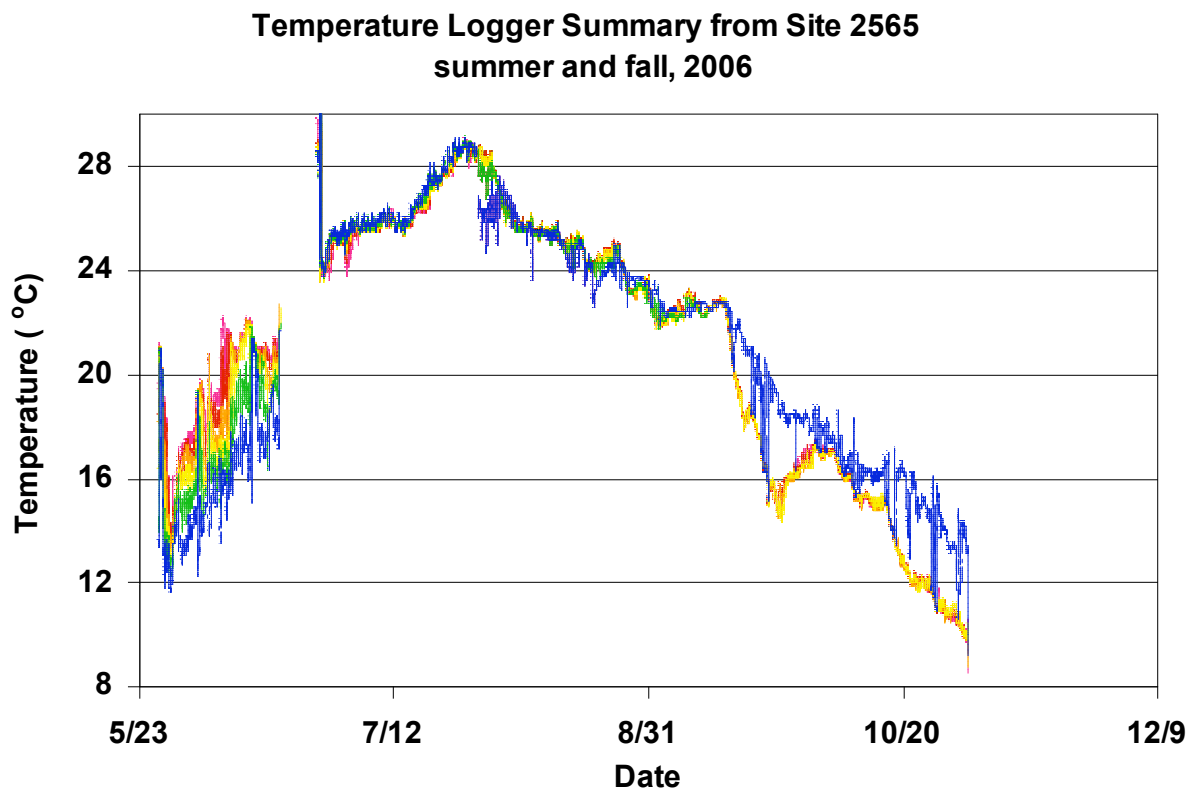


Figure 31b. Temperature variations at site 3510 during summer and fall, 2006. Warmer colors indicate shallow thermistors and cooler colors indicate deeper thermistors.

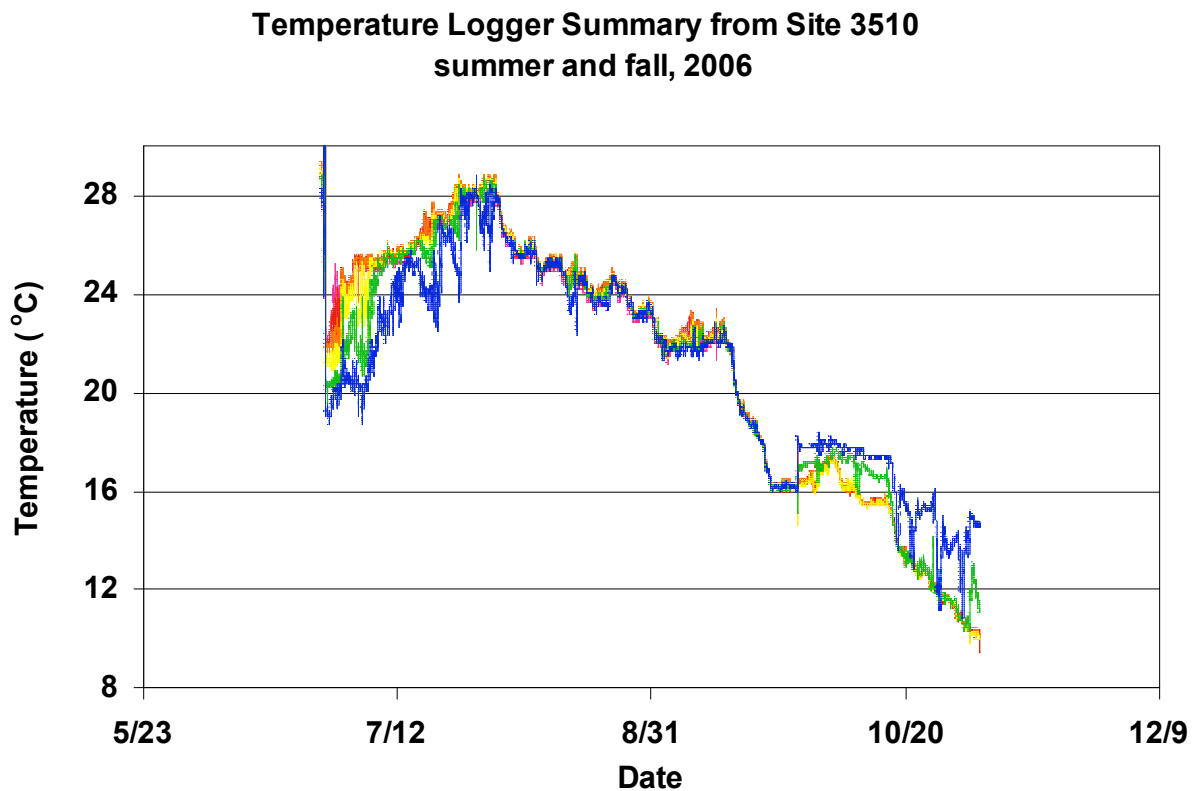


Figure 31c. Multiple temperature equilibration events at site 2565 during April, 2007 correlate with lake level fluctuations at Saltair Gauge (bottom series in plot).

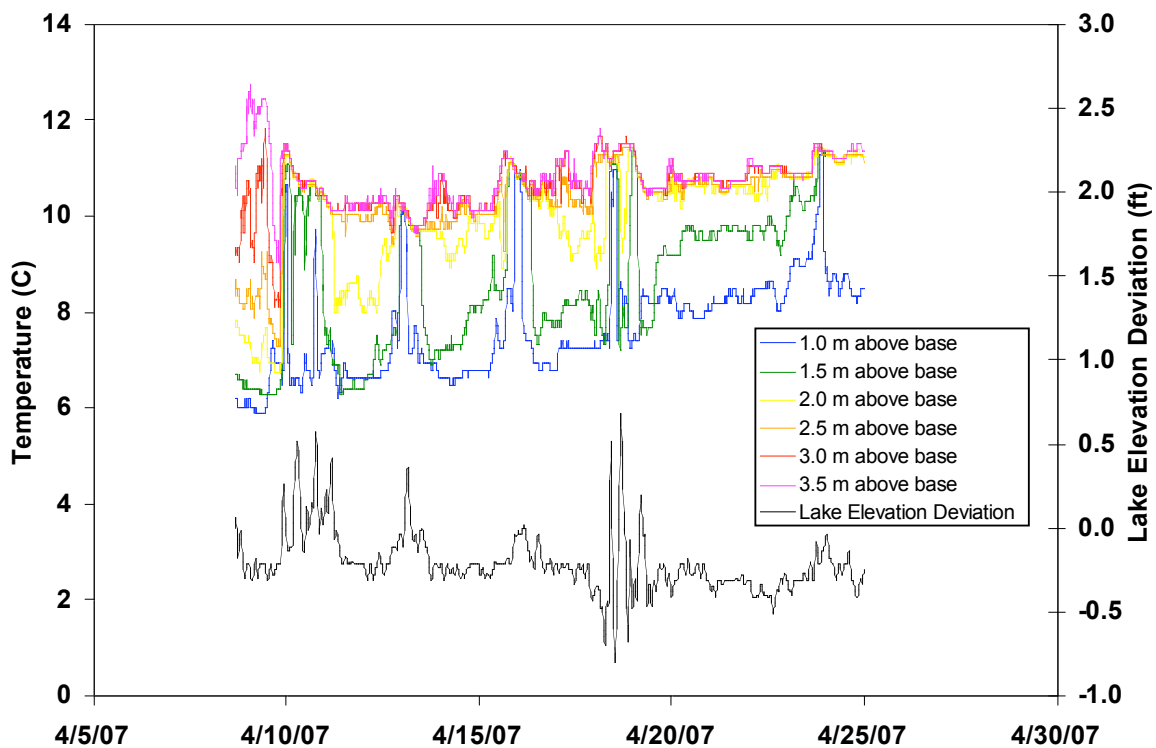


Figure 32a. June temperature record from site 2565, tick marks represent midnight (MDT) and values represent distance above lake bottom. Lowest figure shows wind speed (black) and wind direction (orange) at Hat Island.

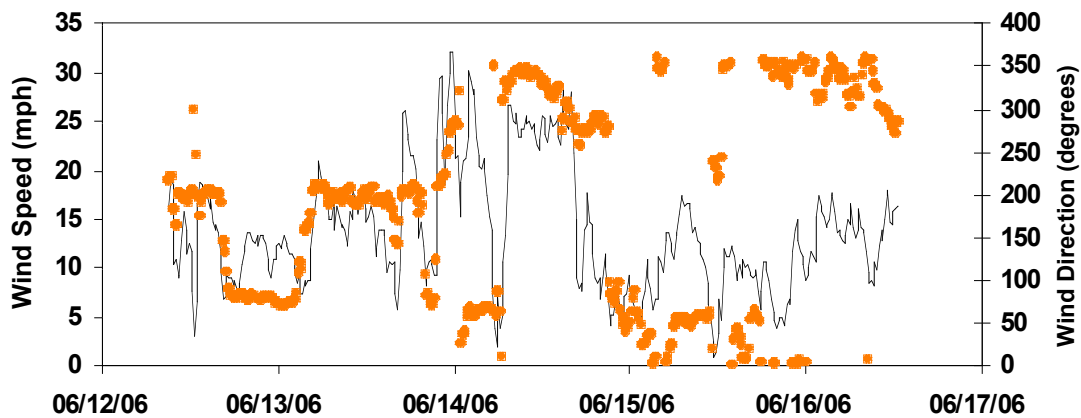
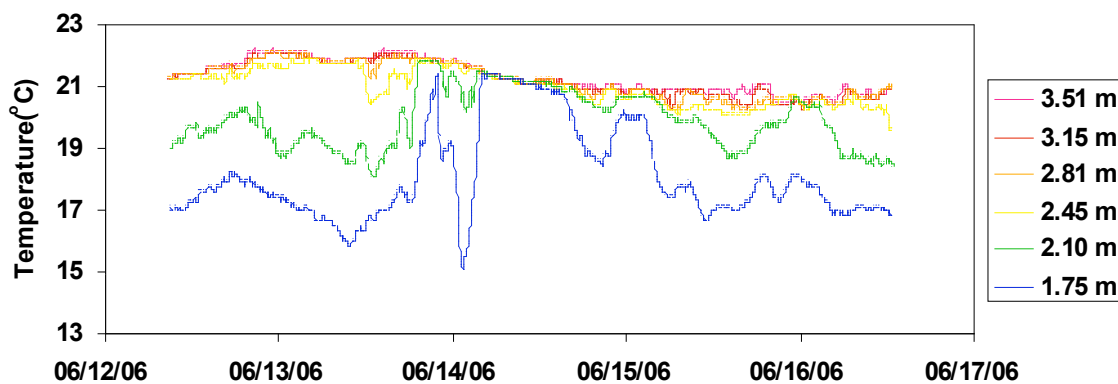


Figure 32b. October temperature records 3510 (top) and 2565 (middle). Tick marks represent midnight (MDT) and values represent distance above lake bottom. Lowest figure shows wind speed (black) and wind direction (orange) at Hat Island.

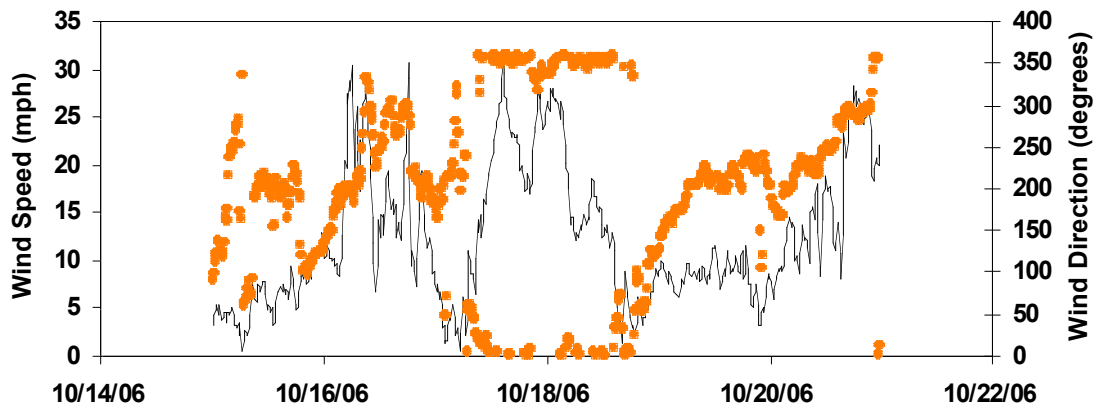
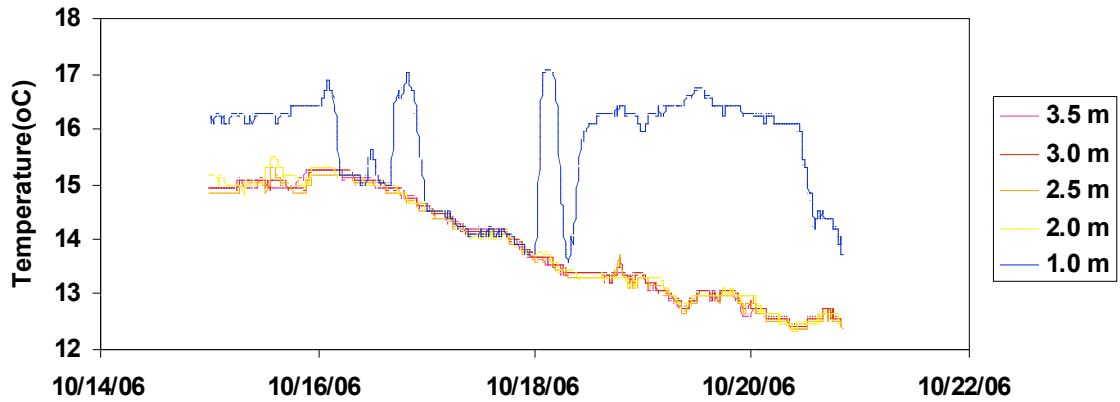
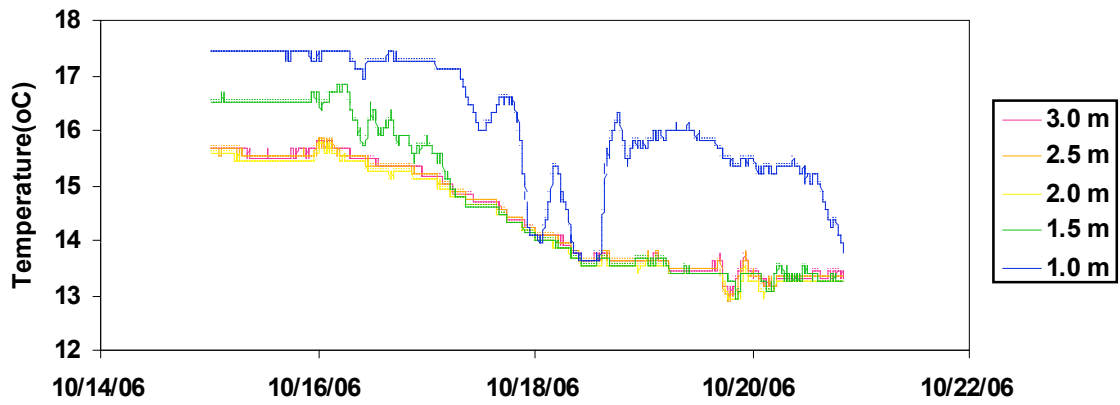


Figure 33a. Lake level oscillation as a result of a strong wind event. Note the inverse correlation between the lake level at opposite ends of the lake (Lin, 1977).

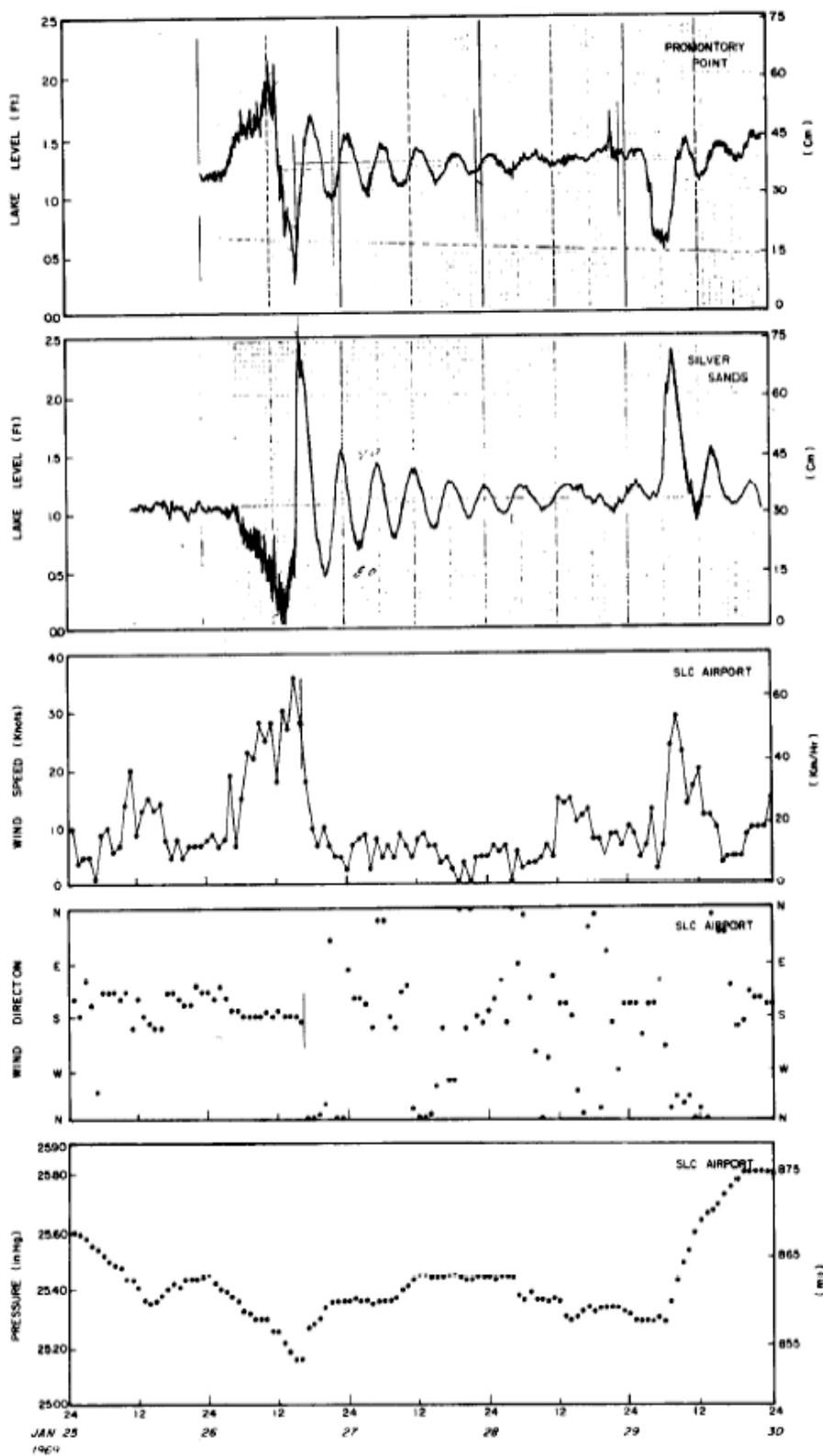


Figure 33b. Magnitude of seiche across the Great Salt Lake (Lin, 1977).

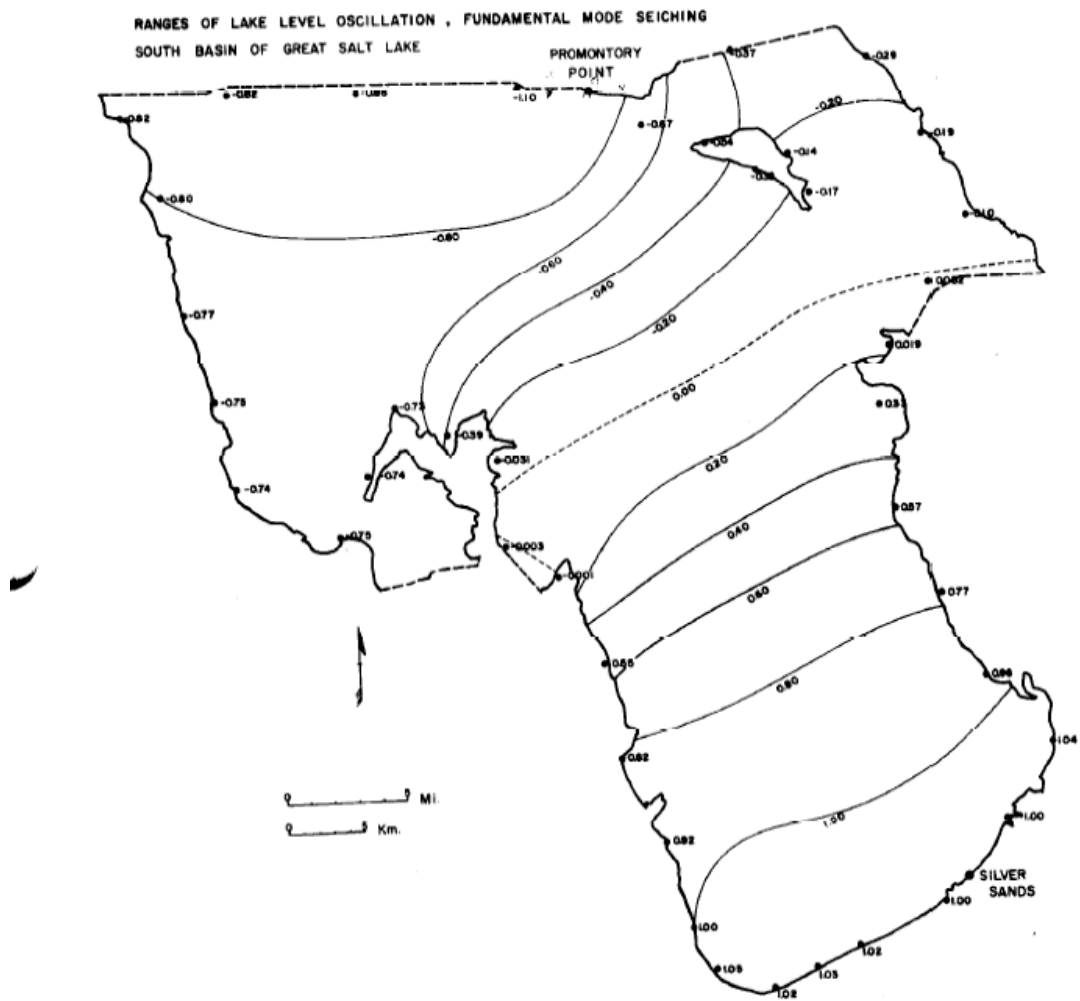


Figure 34a. Initiation of site 2565 temperature equilibration event in June, 2006 corresponds to fluctuations at USGS Saltair Gauge Station. Values on legend are distance above the bottom of the lake.

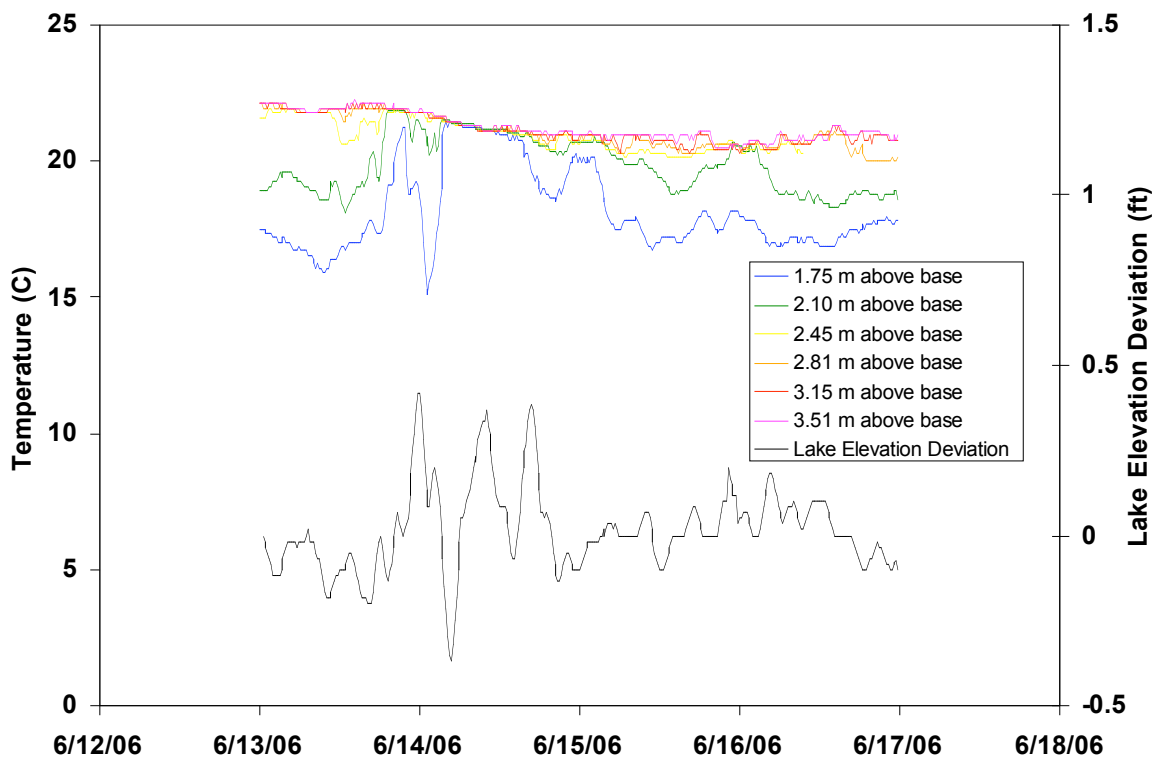


Figure 34b. Initiation of the October, 2006 temperature equilibration event at site 3510 occurred hours after rise in lake elevation at Saltair Gauge. Values on legend are distance above the bottom of the lake.

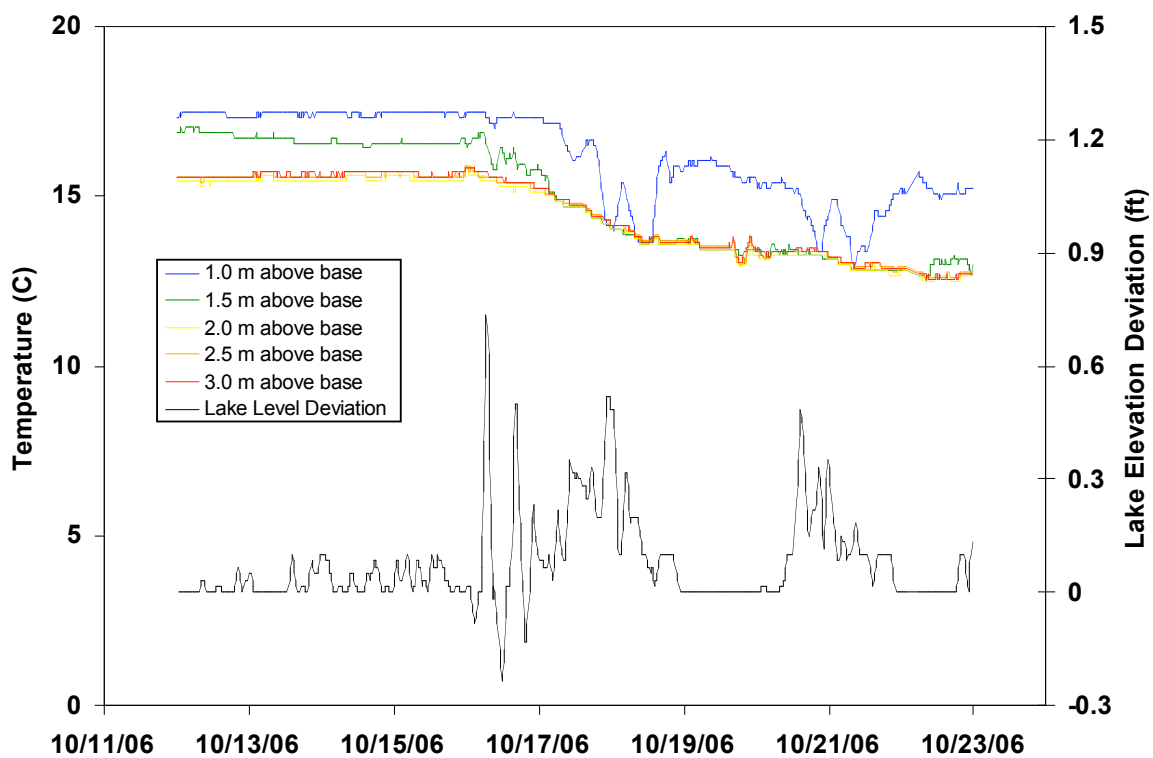


Figure 35a. Selenium concentration in the bed sediments beneath the deep brine layer as analyzed by contract lab (LET) and University of Utah ICP-MS lab.

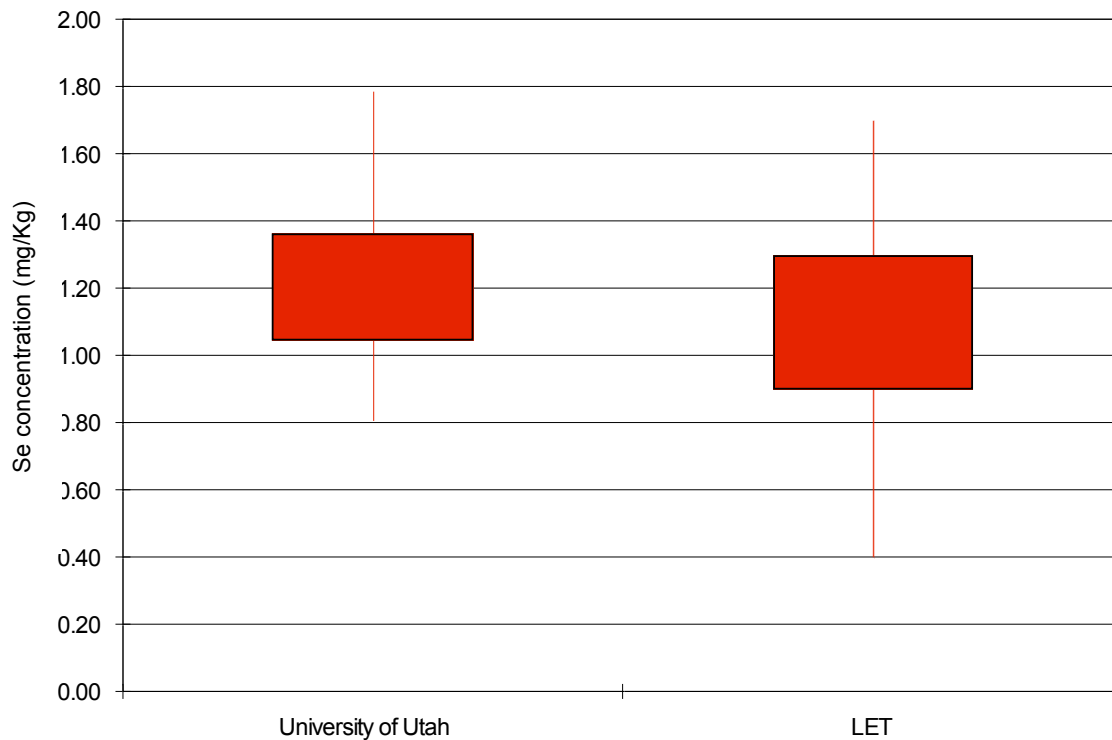


Figure 35b. Se solubilized into the shallow brine water during 24 hour duration batch equilibration experiments as a percent of Se extracted from the bed sediment using HCL/HNO₃.

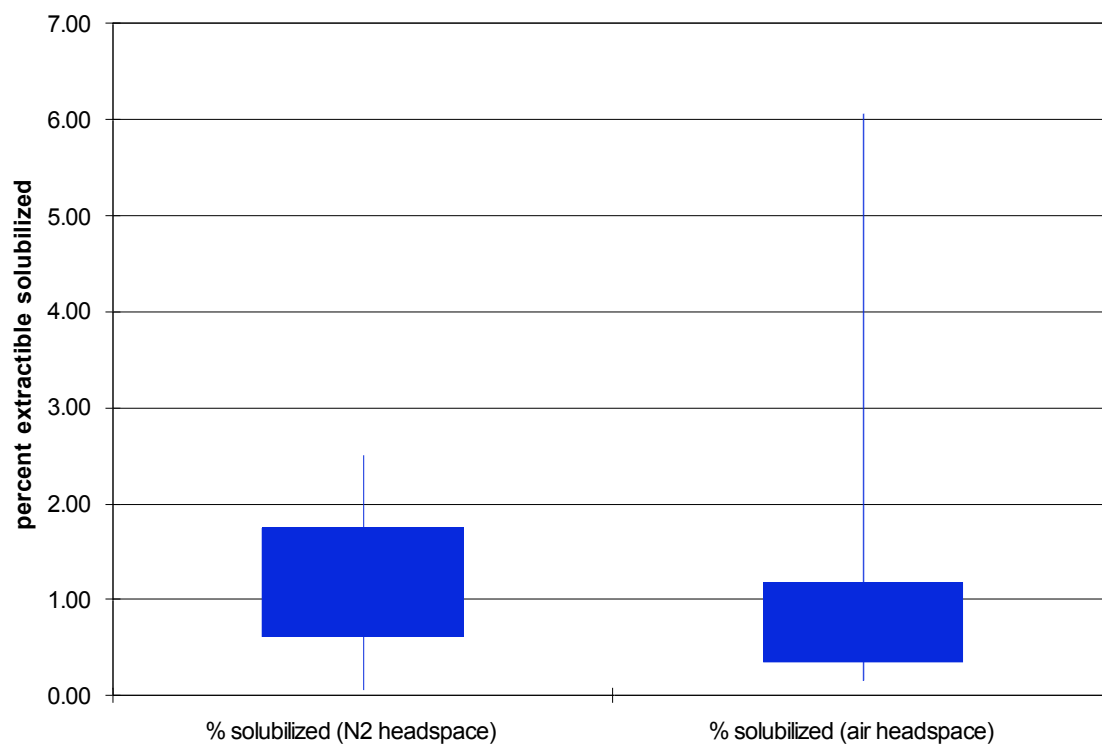


Figure 36. Resultant additional selenium concentration to 4 m of the water column after mixing event determined from results of the 24 hour duration batch test. Note the variability between samples and differences based on headspace gas.

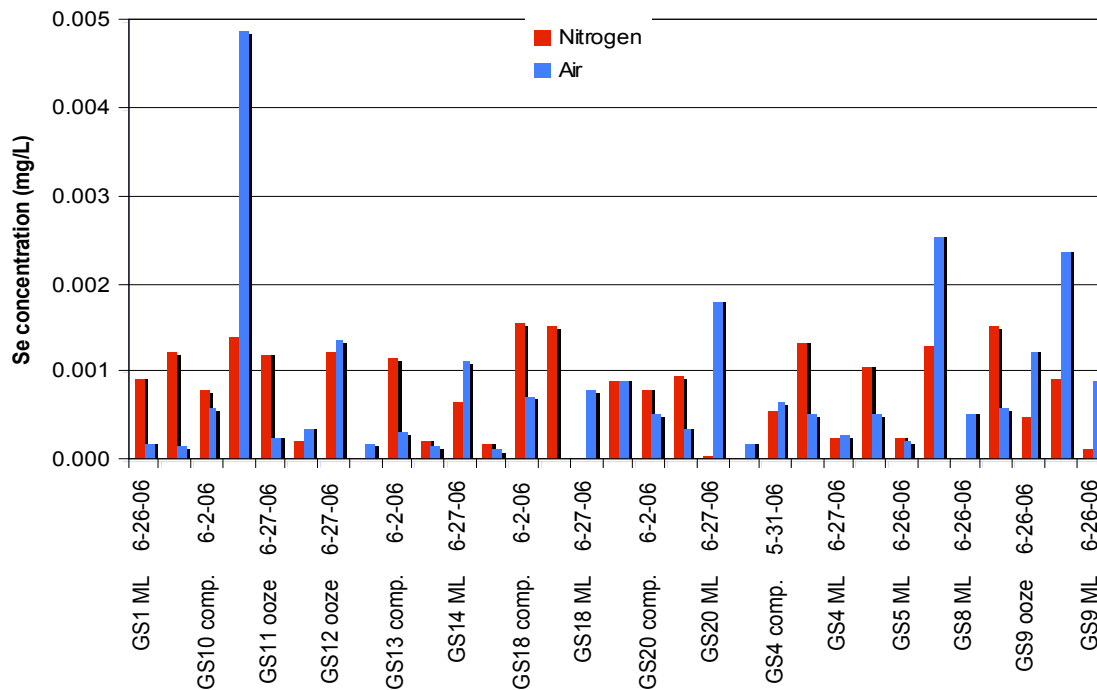


Figure 37a. Se mass (μg) released during week and month batch equilibration experiment.

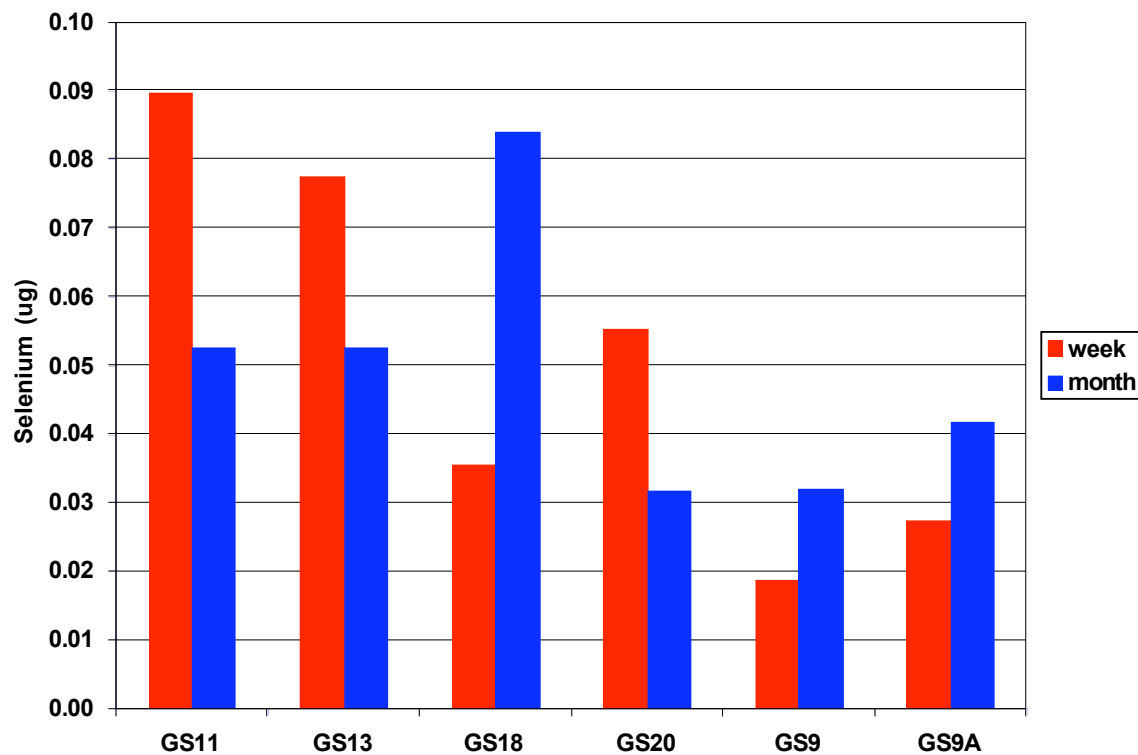


Figure 37b. Time series variation of average percent Se solubilized (of extractable) from all batch equilibration experiments. Bars represent one standard deviation on both sides of the average value.

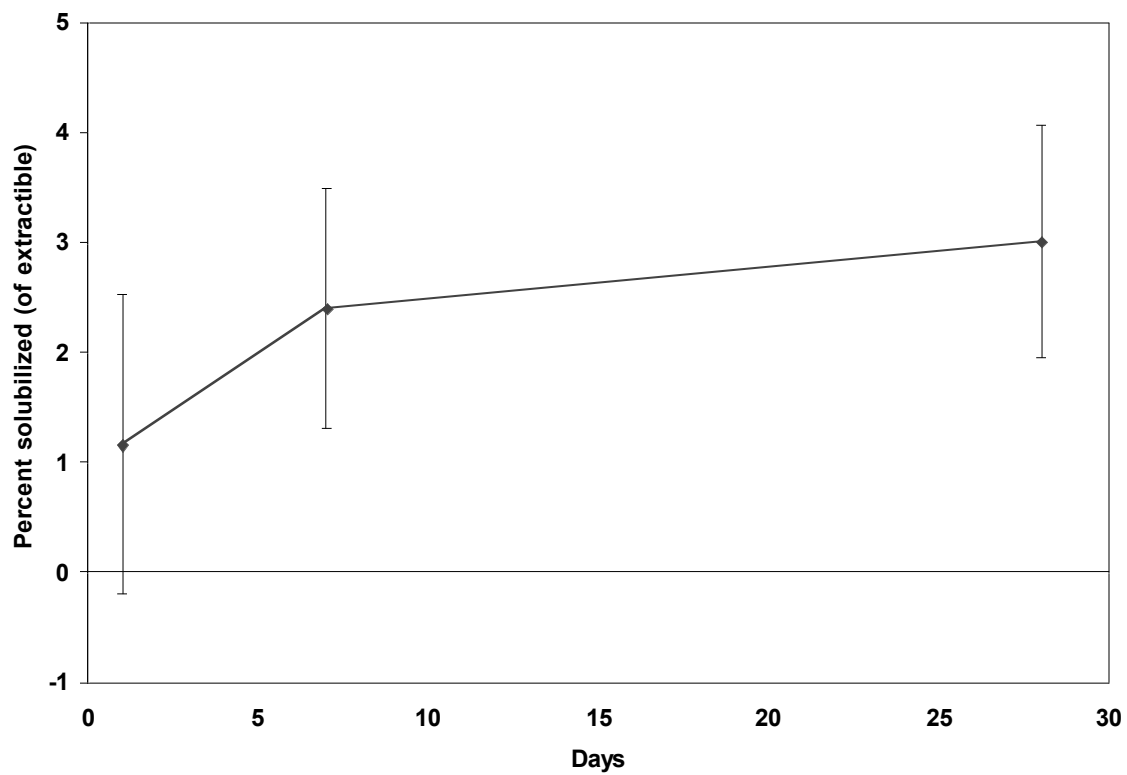
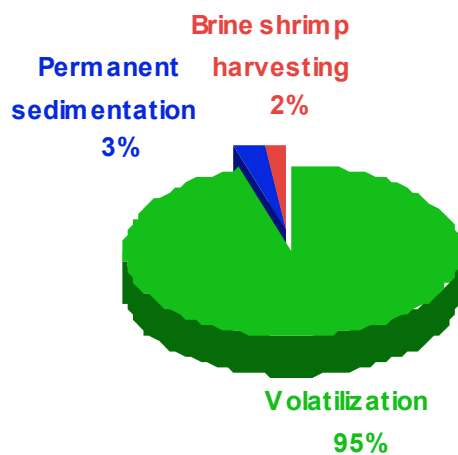
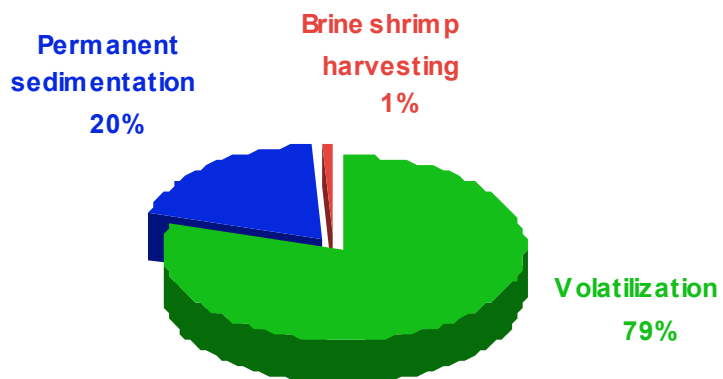


Figure 38. Selenium removal fluxes from volatilization, permanent sedimentation and brine shrimp harvesting.

Low Fluxes



Medium Fluxes



High Fluxes

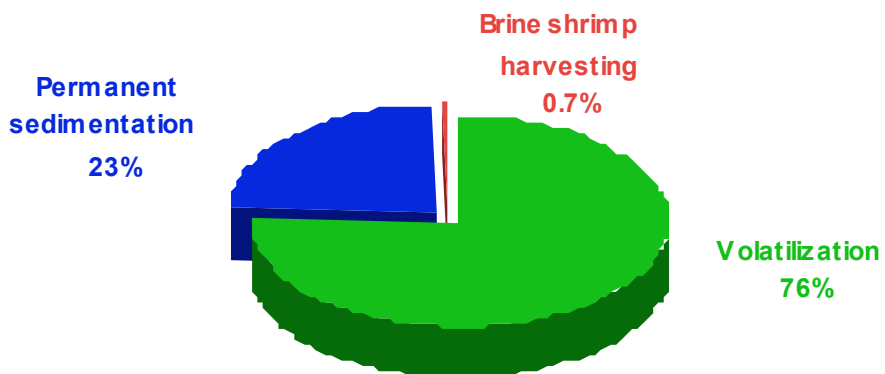


Figure 39. Top: Mass balance integration of Se concentration in the GSL without atmospheric deposition. Blue diamond represents measured final total Se concentration (average of the four sites). Bottom: Daily fluxes used in the mass balance integration.

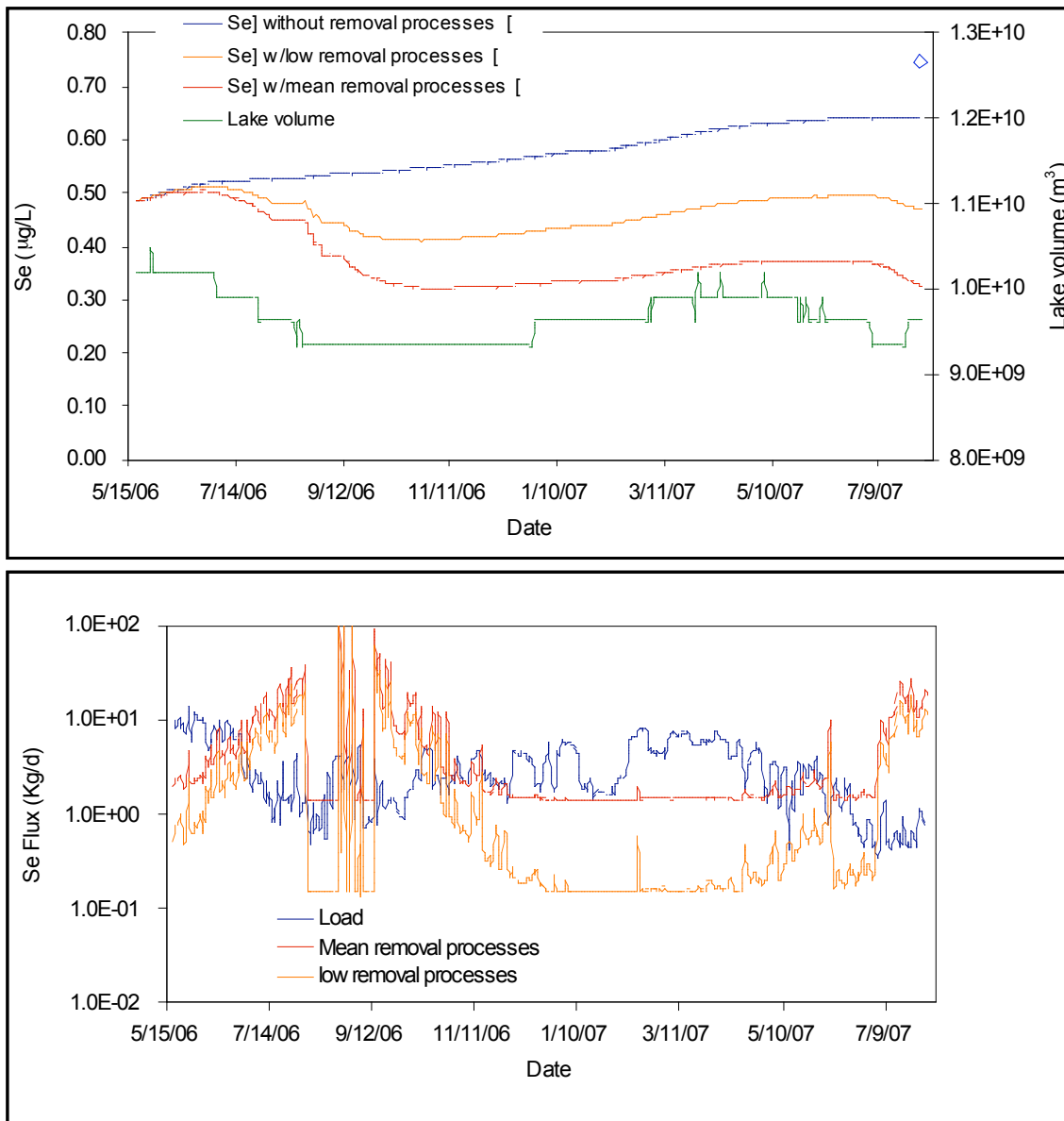


Figure 40. Top: Mass balance integration of Se concentration in the GSL with atmospheric deposition. Blue diamond represents measured final total Se concentration (average of the four sites). Bottom: Daily fluxes used in the mass balance integration.

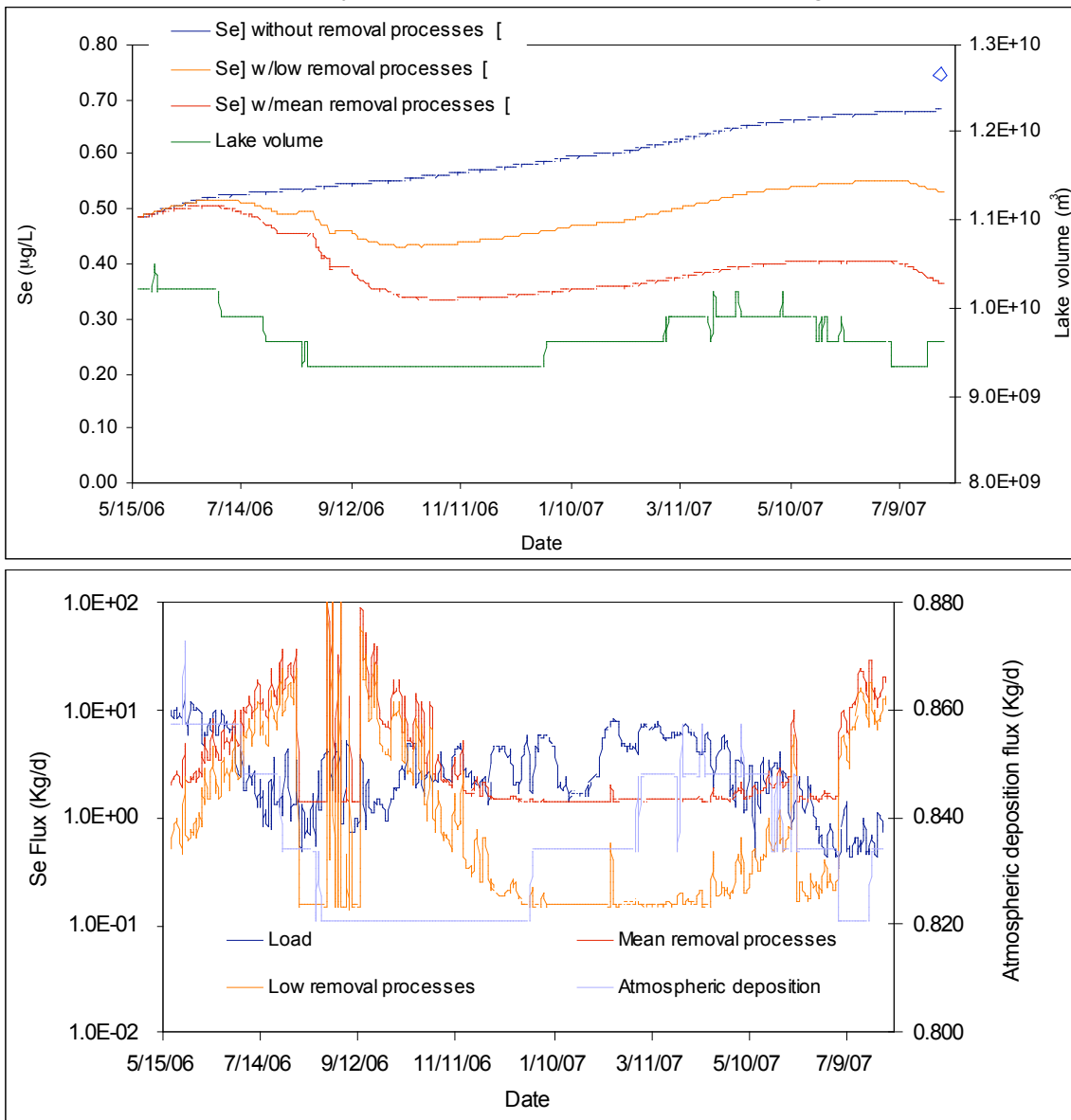


Figure 41a. Dissolved Se concentration trajectories (data from Frontier Geosciences).

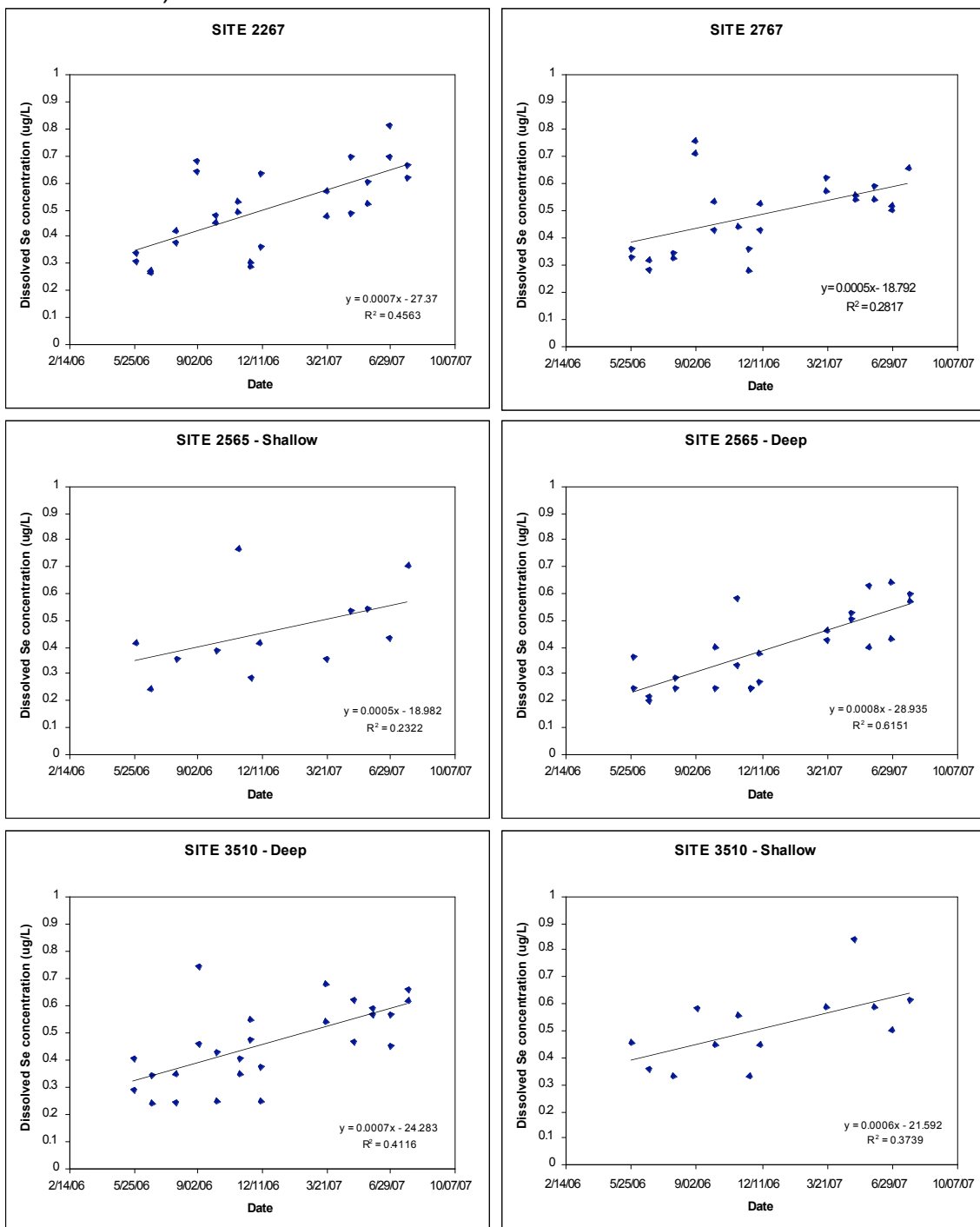


Figure 41b. Se concentration trajectories (associated with particulates) (data from Frontier Geosciences).

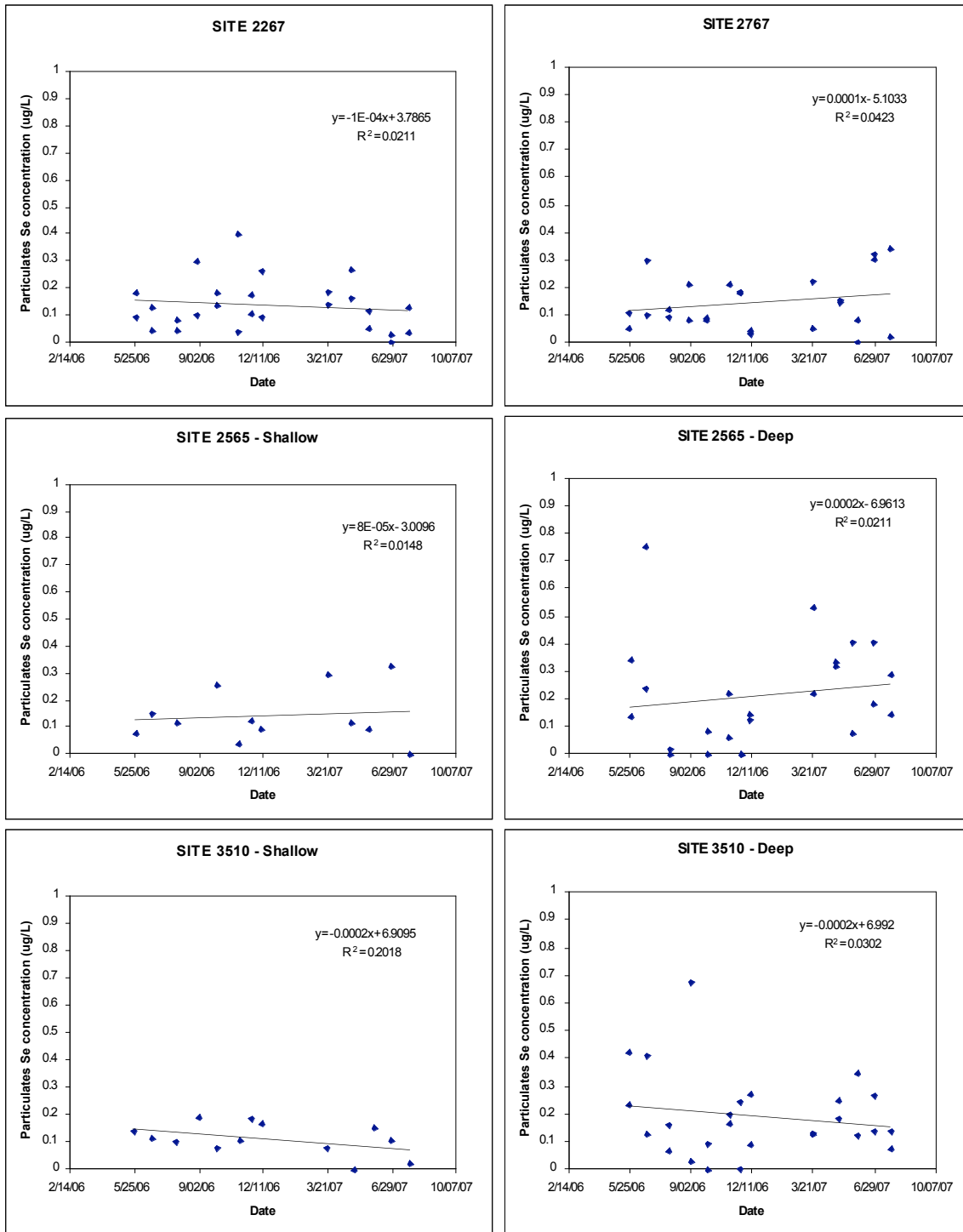


Figure 42. Quality control and quality assurance data for Se analyses by HG-AFS and ICP-MS.

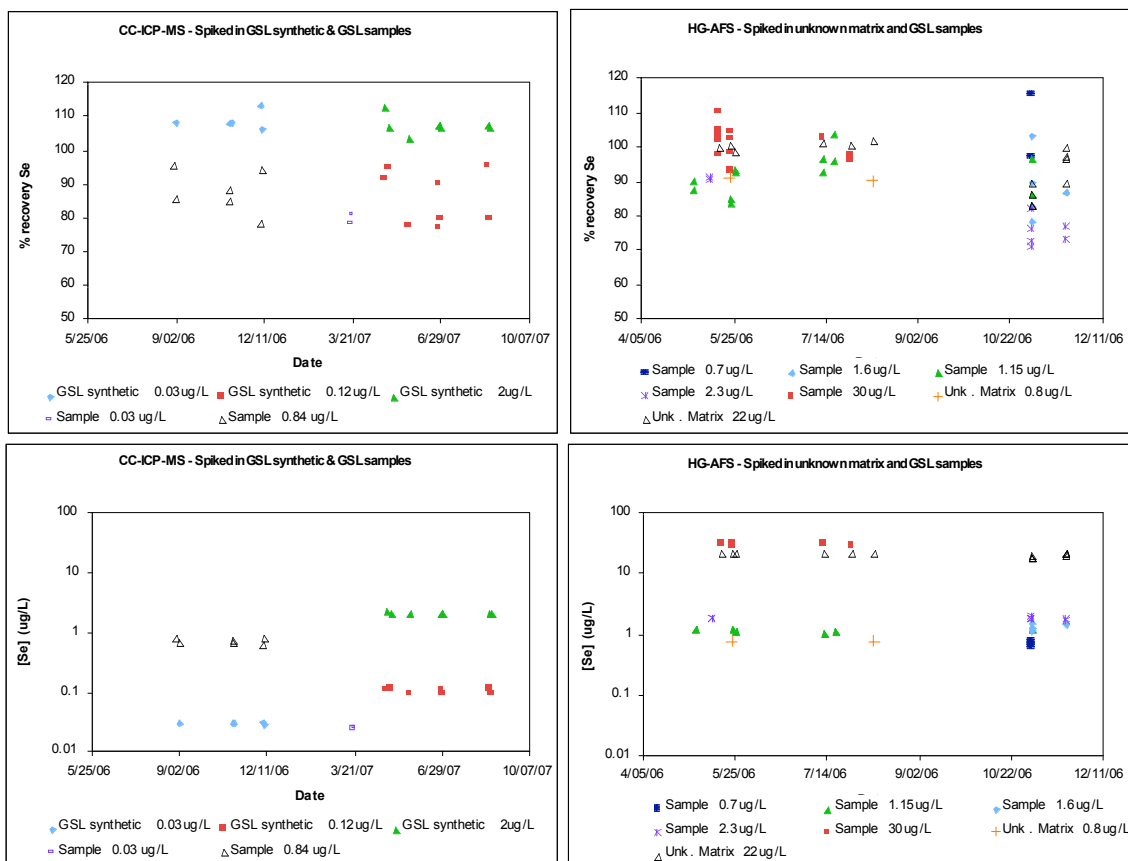


Figure 43. Multielement concentration trajectories (via ICP-MS) from site 2565 during the course of the study.

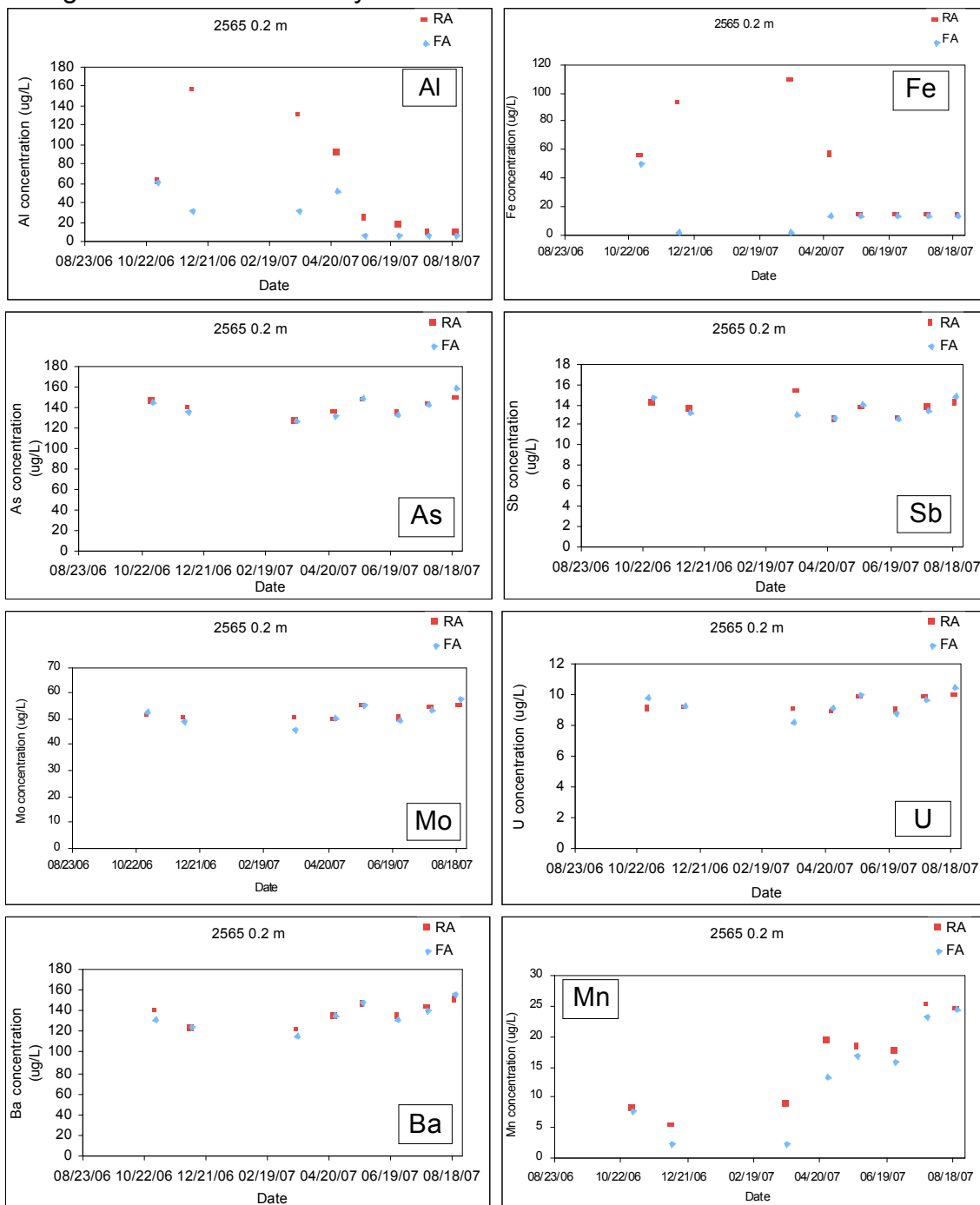


Figure 44. Multielement concentration trajectories (via ICP-MS) from site 2565 during the course of the study.

